A REDUCED MODEL OF BOREHOLE THERMAL

ENERGY STORAGE THERMAL RESPONSE

A REDUCED MODEL OF BOREHOLE THERMAL

ENERGY STORAGE THERMAL RESPONSE

By JACOB DUDALSKI, B.Eng.

A Thesis Submitted to the School of Graduate Studies in Partial Fulfilment of the Requirements
for the Degree Master of Applied Science

Master of Applied Science 2023   McMaster University

Mechanical Engineering   Hamilton, Ontario, Canada

TITLE: A REDUCED MODEL OF BOREHOLE THERMAL ENERGY

                STORAGE THERMAL RESPONSE

AUTHOR: Jacob Dudalski

                B.Eng. (Mechanical Engineering)

                McMaster University, Hamilton, Ontario, Canada

SUPERVISORS: Dr. James Cotton and Dr. Marilyn Lightstone

NUMBER OF PAGES: 118

Abstract

In Canada 15% of greenhouse gas (GHG) emissions are produced by the residential sector's energy demand. The majority of the energy demand is space heating which is primarily met with natural gas combustion. Motivation exists to reduce GHG emissions due to their contribution to climate change. Integrated Community Energy Harvesting (ICE-Harvest) systems seek to integrate thermal and electrical energy production, storage, redistribution, and consumption in a way that reduces GHG emissions. Borehole thermal energy storage (BTES) is implemented in ICE-Harvest systems as seasonal thermal energy storage.

This thesis presents a novel model of BTES thermal response with reduced complexity to aid in early siting, design, optimization, and control systems development work for ICE-Harvest systems. The reduced model can be used to approximate periodic steady state BTES thermal response. The model provides information on average ground storage volume temperature, outlet fluid temperature, heat exchanger fluid to storage volume heat transfer rate, storage volume top loss heat transfer rate, storage volume side and bottom loss heat transfer rate, and annual thermal energy storage efficiency which aids system modelling efforts for BTES in solar thermal and ICE-Harvest systems.

The reduced model is formed from a solution of the thermal energy balance equations for the BTES ground storage volume and heat exchanger fluid with simplified operating conditions for a yearly BTES charging and discharging cycle. Ground storage volume temperature is lumped as a single value. Heat transfer rates between the storage volume and the heat exchanger fluid and the storage volume and its surroundings are modelled with periodic steady state thermal resistance values for the charging and discharging timesteps. A TRNSYS DST simulation of BTES is validated against measurements from a BTES installation and TRNSYS DST is used to

generate the periodic steady state thermal resistance values the reduced model requires. The periodic steady state thermal resistance values of BTES charging and discharging are dependent on BTES design parameters (spacing between boreholes, number of boreholes, borehole depth, and storage volume size) and ground thermal properties (thermal capacity and thermal conductivity) which is presented in a series of parameter sweeps with respect to a reference simulation.

The reduced model predicts periodic steady state average storage volume temperature with a RMSD of 0.96°C for charging and 1.3°C for discharging when compared to the TRNSYS DST reference simulation. The reduced model predicts the periodic steady state heat exchanger total energy transfer within 1.8% for the charging timestep and 2.8% for the discharging timestep when compared to the TRNSYS DST reference simulation. The reduced model's periodic steady state thermal resistance values are demonstrated to be independent of heat exchanger fluid inlet temperature except for the side and bottom loss thermal resistance during discharging. The reduced model cannot replicate the change in heat transfer direction that occurs during BTES discharging when the temperature of the storage volume decreases below the temperature of the surrounding ground, however, the magnitude of the energy transfer that would occur is negligible compared to the magnitude of the BTES heat exchanger total energy transfer.

Acknowledgments

I would like to express my gratitude to the following people without whom this thesis would not be possible.

My sincerest gratitude goes to:

- Dr. James Cotton

- Dr. Marilyn Lightstone

- Dr. Yasser Abdelsalam

- Chantel Millar

- My parents: Vick and Monika Dudalski and siblings: Nicholas and Dalia

Thank you for your support, guidance, encouragement, and patience during all stages of research and writing.

Jacob Dudalski

Table of Contents

Notations and Abbreviations

<u>Nomenclature</u>

#BH	Number of Boreholes
A	Area [m^2]
c_p	Specific Heat Capacity [J/kgK]
D	Diameter [m]
E	Energy [J]
H	Depth [m]
k	Thermal Conductivity [W/mK]
M	Mass [kg]
$\dot{m}$	Mass Flow Rate [kg/s]
Q	Heat Flow Rate [W]
r	Radius [m]
R	Thermal Resistance [°Cm^2/W]
Spacing	Borehole Spacing [m]
T	Temperature [°C]
$\widetilde{T}$	Average Temperature [°C]
t	Time [s], [hr], or [day]
V	Volume [m^3]
ρ	Density [kg/m^3]

<u>Subscripts</u>

∞	Infinite

∞_amb	Ambient Air (Temperature)
∞_ground	Undisturbed Ground (Temperature)
f	Fluid
g	Ground
hx	Heat Exchanger
i	Initial
in	Fluid Inlet
loss	Energy Loss
loss_s,b	Energy Loss via the Side and Bottom Surfaces of the Storage Volume
loss_t	Energy Loss via the Top Surface of the Storage Volume
out	Fluid Outlet
outer,BHE	Outer (Diameter) for a Borehole Heat Exchanger
SV	Storage Volume
SV_s,b	Side and Bottom Surfaces of the Storage Volume
SV_t	Top Surface of the Storage Volume
TBA	Total Borehole Area

Abbreviations

BHE	Borehole Heat Exchanger
BTES	Borehole Thermal Energy Storage
CFD	Computational Fluid Dynamics
CHP	Combined Heat and Power
DST	Duct Storage
GHG	Greenhouse Gases

ICE-Harvest	Integrated Community Energy Harvesting
ODE	Ordinary Differential Equation
RMSD	Root Mean Square Difference
TRNSYS	Transient System Simulation Tool

List of Tables

List of Figures

1   Introduction and Problem Statement

In Canada space heating accounts for 63% of the average household's energy demand [1]. The demand is primarily met with natural gas combustion which contributes to 15% of all Canadian greenhouse gas (GHG) emissions being produced by the residential sector [1]. In cold climates there is a seasonal imbalance between the average household's thermal energy demand and the availability of sustainable energy sources [2]. Sustainable energy sources available in the summer include thermal energy from solar collectors and waste heat that is generated from the power plants and refrigeration processes, while space heating demand is greatest in the winter [2]. Utilizing seasonal storage to meet space heating demand with sustainable energy sources has the potential to significantly reduce GHG emissions from the residential sector.

Thermal waste energy from electrical power generation and refrigeration cycles is underutilized by being emitted to the environment. Each system's total energy efficiency is reduced because there is residual energy loss to the environment. Utilizing thermal waste energy for space heating instead of expelling it to the environment would increase each system's total energy efficiency and reduce the amount of GHG emissions needed to meet the reduced heating demand.

Integrated Community Energy and Harvesting (ICE-Harvest) systems seek to integrate thermal and electrical energy production, energy storage, redistribution, and consumption in a way that significantly reduces GHG emissions [3]. The ICE-Harvest system uses a decentralized combined heat and power peaking plant to supply electricity to multiple households. A thermal network is used to distribute the thermal energy produced by the CHP unit for the community. Individual units that are a part of the ICE-Harvest thermal network can either supply

1

refrigeration by-product thermal energy to the thermal network or take heat from the network for space heating.

The ICE-Harvest system bridges the gap between thermal energy demand and sustainable thermal energy source production using short term thermal storage for hourly control and borehole thermal energy storage (BTES) for seasonal thermal energy storage. To maximize the GHG emission offset an ICE-Harvest community can provide, energy efficient components, that scale with community demand, must be designed. Effective thermal storage design reduces thermal losses while maximizing capacity.

For effective design of an ICE-Harvest system, a "digital twin" must be developed in transient system solvers which approximate the system's component specifications, controls, and operation. There is a need for a simplified model of BTES operation, which can approximate annual steady state BTES storage efficiency, and thermal response of BTES installations depending on their thermal properties and design parameters. The reduced model can be used to aid in early ICE-Harvest controls development, and site specific BTES design.

This thesis uses the University of Wisconsin's TRNSYS [12], a transient system simulation program, to study the impact BTES design parameters and thermal properties have on the periodic steady state thermal response and annual thermal storage efficiency of BTES systems. A reduced model representing BTES thermal response is developed for a range of field configurations, thermal properties, and operating conditions.

The following chapters will focus on the fundamental components of the research and development of the reduced model. Chapter 2 is the literature review, which covers BTES design and operation fundamentals, borehole thermal energy storage modelling techniques, and the state

of BTES parameter dependence studies. Chapter 3 focusses on the numerical methods used by the BTES model included in the TRNSYS simulation suite, and the validation of the model against borehole operation and thermal response data from an active BTES installation. Chapter 4 describes BTES thermal response outputs and outlines a "base case" of simplified BTES operation conditions based on the validated BTES design parameters and thermal properties from Chapter 3. Chapter 5 presents the reduced model derivation and verification. It also presents the results of the BTES parameter sweeps simulated in TRNSYS. Chapter 6 includes conclusions and recommendations for future work.

2 Literature Review

2.1 Introduction

This literature review summarizes relevant work that pertains to BTES design and operation fundamentals, modelling techniques, and parameter dependence investigations. The research space for the BTES reduced model is highlighted with respect to the needs of the Integrated Community Energy and Harvesting (ICE- Harvest) systems cooperative research project and the limitations of existing work.

2.2 Problem

In cold climate locations there is an annual mismatch between the winter period's peak heating demand and summer period's carbon free thermal energy sources [2], such as captured waste thermal energy and renewable energy sources. In Canadian cities space heating demand is largely met by natural gas furnaces which emit GHGs [1]. The implementation of seasonal thermal storage can "bridge the gap" between summer sustainable thermal energy sources and winter heating demand and reduce the heating load met by natural gas furnaces. The ICE-Harvest systems utilize seasonal thermal storage as a component in a distributed energy network which has the potential to significantly reduce GHG emissions.

2.3 ICE-Harvest

ICE-Harvest is a cooperative research project which seeks to create modelling, analysis, and design tools to site, design, optimize, and control community energy systems which integrates thermal and electrical energy production, storage, redistribution, and consumption to significantly reduce GHG emissions [3]. Peak community electricity demand is met by a combined heat and power plant (CHP) which harvests waste thermal energy produced by the

plant's electricity production to supply a thermal network. Community buildings with refrigeration dominated energy requirements can also contribute harvested waste heat to the thermal network. The thermal network supplies community buildings' heating demand or it can supply the short-term or seasonal thermal storage to meet future heating demand. Meeting community heating demand with thermal energy that is the by-product of other utility processes rather than using natural gas furnaces reduces GHG emissions.

The development of modelling, analysis, and design tools for site identification, system design and optimization, storage design and optimization, and controls development are interdependent components of developing "digital twins" of ICE-Harvest systems. "Digital twins" are site specific simulations of predicted electrical and thermal load demand and response. They prove ICE-Harvest systems physical feasibility, economic viability, and ability to reduce GHG emissions compared to business-as-usual. The development of a "digital twin" with the modelling, analysis, and design tools developed from the cooperative research project is a critical step towards the installation of a pilot ICE-Harvest system.

The effectiveness of ICE-Harvest systems depends on the design of cost effective and thermally efficient seasonal thermal energy storage and the ability of control systems to accurately predict seasonal thermal storage state-of-charge and thermal response.

2.4   Seasonal Thermal Storage

Seasonal thermal storage utilizes closed loop fluid heat exchangers and storage volume material to inject thermal energy in the summer and extract thermal energy in the winter. Common storage volume materials include water, soil, gravel, or a combination of the three. Although the use of water-based thermal storage has benefits because of the high heat capacity

of water, soil-based systems are the most common seasonal thermal storage installations used in community energy projects [4]. Soil-based systems feature low manufacturing and maintenance costs while allowing modular and scalable construction [4]. ICE-Harvest systems use borehole thermal energy storage (BTES) as soil-based seasonal thermal energy storage.

2.5   Borehole Thermal Energy Storage

BTES uses soil volume as a thermal storage medium and an array of interconnected borehole heat exchangers (BHE) to inject and extract thermal energy. A BHE consists of polyethylene piping encased in grout which transports heat exchanger fluid and induces thermal energy exchange between the fluid and the soil [5]. For BTES applications the orientation of the BHEs is vertical to reduce thermal losses to ambient air and increase thermal storage efficiency. The types of BHE piping are single U-tube, double U-tube, and coaxial [5]. Typical BHE have diameters of 60 – 340mm and extend to a depth of 30 – 300m below ground [6]. BTES installation cost is primarily a function of bore depth and number of bores due to drilling costs [4]. Typical BTES have 20 – 500 BHE [4] with spacing of 1.5 – 3m between them [5]. Installed BTES can have their capacity increased by drilling and connecting more BHE if the BTES is surrounded by sufficient suitable area for drilling. The modularity and scalability of BTES construction makes it the ideal seasonal thermal storage solution to implement into the modular and scalable ICE-Harvest system.
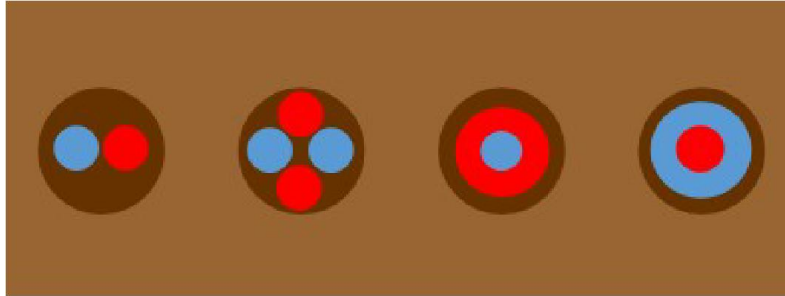
Figure 2.1: From Left to Right: U-tube, Double U-tube, Coaxial Cold Internal, Coaxial Hot Internal [6].

BTES efficiency is defined as the annual ratio of total energy extracted from the ground storage volume to total energy injected to the ground storage volume [7]. As BTES installations operate, their BTES efficiency increases to a maximum of around 40-60% [7]. Calculating BTES efficiency is a transient multivariable multidomain problem. It is dependent on the thermal properties (k, ρ, c_p) of the soil, solid BHE components, and working fluid. It is dependent on BTES design parameters including number of boreholes, depth per borehole, borehole spacing, and borehole diameter. Finally, BTES operation information such as inlet fluid temperature and mass flow rate with respect to time substantially effects BTES efficiency.

Simulations of BTES operation are transient, multidomain, and have multivariable dependencies making traditional fluid dynamics solutions restrictively computationally expensive and impractical for system optimization and control. Reduced models of BTES thermal response are critical tools used by system optimization and controls engineers to reduce both simulation time and total system design time.

2.6 Modelling BTES

Modelling techniques are presented from highest to lowest fidelity and their strengths and weaknesses are addressed regarding the needs of engineers working on ICE-Harvest system design and controls development.

2.6.1 CFD

Computational fluid dynamics (CFD) uses numerical analysis to solve the three-dimensional conservation of momentum and energy equations for fluid and solid domains. The simulation domain and governing equations are discretized into smaller control volumes and are each solved numerically to determine the total domain solution. CFD can provide high-fidelity predictions of BTES heat transfer and temperature distribution if material properties, initial conditions, and boundary conditions are accurately input. BTES operation simulations are, however, 3-dimensional, multidomain, feature long total simulation times, and typically a discrete (on/off) loading cycle. These factors contribute to order of magnitude variances for both the time and length scales adding discretization complexity.

CFD simulations of BTES operation can have their complexity reduced by simplifying the internal BHE domains and approximating the heat exchange between the BHE outer diameter and the ground volume it touches. BHE can be simulated as a 1-dimensional fluid flow acting on a cylindrically coordinated 2-dimensional solid [8], however, this simplification is not suitable for BTES simulations as BTES operation involves multiple BHE installed in thermally interactive proximity to each other. TOUGH2 [9] and COMSOL [10] use approximations of the heat flow between the BHE outer diameters and the ground storage volume resulting from BHE operation to predict temperature distributions for the soil in and around a BTES installation. CFD simulations of BTES can be simplified by applying a time-varying temperature boundary

8

condition at the BHE outer diameters that reflects the overall borehole temperatures to predict BHE heat flow and the resulting soil temperature distributions [11].

Even with BHE simulation simplifications, CFD computational cost is prohibitively high which excludes it from useful application in the early stages of BTES design, and controls development in ICE-Harvest systems. Simulating BTES with varying design parameters and thermal properties requires domain, mesh, and timestep independence tests for every BTES installation variant. CFD independence testing adds computational cost and further excludes CFD simulations from usefulness in initial BTES design, optimization, and operational control.

2.6.2 TRNSYS DST

Transient system solvers use simplified BTES operation models that still provide realistic representations of BTES thermal response. TRNSYS [12] is a popular transient simulation software which integrates the Duct Ground Heat Storage Model (DST) [13] to simulate BTES thermal response to be a component of transient sustainable energy systems simulations. DST superposes a 1-dimensional "local" ground temperature solution with a 2-dimensional "global" ground temperature solution to provide BTES thermal response outputs to the user [14]. The model's simplifications result in DST simulations having a lower computational cost than CFD in exchange for some simulation constraints. DST model constraints include that DST can only simulate axisymmetric and uniformly distributed BHE configurations, borehole thermal capacity is not considered, and borehole thermal resistance remains constant throughout the DST simulation [15]. If realistic thermal properties and operation conditions are set as inputs, DST can accurately represent BTES thermal response for longer simulations as they reduce the influence of borehole thermal capacity.

TRNSYS and DST are used in BTES design by inputting thermal system operation information into TRNSYS, inputting BTES design parameter information, and applying a generational optimizer to the desired design parameters. To use a generational optimizer, site specific operational data is required. Early stages of BTES design and controls development for ICE-Harvest systems require knowledge of BTES thermal response and storage efficiency before site specific operation data is available, which highlights the research space of the reduced model of BTES response.

2.6.3 G-Functions

G-functions are step-response functions that give the relation between the heat flow rate through the BHE outer diameters and the temperature of the BHE outer diameters [16]. The solution of borehole thermal response using g-functions sets all BHE outer diameters to be a uniform temperature. This condition is based on the assumptions that the borehole thermal resistance is low enough that the BHE outer diameter temperature is close to the heat exchanger fluid temperature and that the mass flow rate of the heat exchanger fluid is high enough that temperature variations in the heat exchanger fluid are minimal. These assumptions allow the thermal response of a borehole installation to be approximated by the temporal superposition of heat transfer for a cylinder at uniform temperature and a characteristic g-function solution dependent on borehole configurations [16].

G-functions depend on the number of BHE and their installation configuration (e.g. a line, L-shape, U-shape, or rectangular array) as well as the installation's borehole radius, borehole spacing, buried depth, and operation time which have been nondimensionalized with respect to the length of each BHE in the borehole field (and soil thermal diffusivity in the case of the nondimensional time constant) [16]. G-functions were initially obtained numerically using

10

finite differentiation, however, for large borehole fields this is too computationally expensive so analytical and semi-analytical methods for generating g-functions have been developed [17].

G-functions are implemented in ground heat exchanger design software such as EED, GLHEPRO, and EnergyPlus with pre-calculated g-functions for different configurations [18]. G-functions are only available for tabulated and predefined BTES design parameter geometries and users are restricted to these configurations for their simulations. G-Function borehole field sizing techniques also require site specific load data and g-functions are primarily developed for borehole configurations set up for geo-exchange operation [15]. Early stages of BTES design and controls in ICE-Harvest systems development require knowledge of the thermal response and storage efficiency for borehole fields in BTES configurations before site specific operation data is available. Thermal response information for BTES configurations that do not have g-functions calculated for them may be required for BTES design and controls development and calculating g-functions for every BTES design parameter iteration would prove too computationally expensive, which highlights the research space of the reduced model of BTES response.

2.7 ICE-Harvest BTES Reduced Model

ICE-Harvest controls and system design in early stages of development require a simple model of BTES thermal response and a pre-feasibility level calculation of steady state thermal efficiency for a wide array of BTES design parameters, soil thermal properties, and inlet fluid temperatures. The BTES design parameters which effected storage efficiency the greatest in the TRNSYS sensitivity study of a BTES in Filborna, Sweden are number of boreholes, borehole depth, and borehole spacing [19]. The reduced model aims to identify the effect these parameters and soil thermal properties have on thermal response and energy storage efficiency.

11

2.8 Summary & Objectives

This chapter presents a literature review of ICE-Harvest systems, the role of BTES as seasonal storage, important BTES design parameters and thermal properties, BTES modelling, and ICE-Harvest requirements for early stage BTES design and controls development.

BTES is an important technology for meeting seasonal heating demand while reducing GHG emissions and it is an integral part of ICE-Harvest systems because of its modular and scalable construction. When siting, designing, optimizing, and developing controls for ICE-Harvest systems, an approximation of periodic steady state BTES thermal response and storage efficiency with respect to design parameters and thermal properties is needed before site specific thermal load data is available. CFD, TRNSYS DST, and g-function simulations of BTES are too computationally expensive for the requirements of early BTES design and controls development for ICE-Harvest systems.

This work will use a periodic steady state energy balance ODE solution and a dataset of periodic steady state thermal resistances to solve BTES thermal response and storage efficiency for use in controls development and design of BTES installations in ICE-Harvest systems. The thermal resistance dataset will be generated with respect to varying number boreholes, borehole spacing, and borehole depth as well as varying soil thermal conductivity and thermal capacity.

3 Numerical Modelling and Validation

3.1 Introduction

The following chapter presents details on the mathematical modelling of borehole fields within the system simulation code TRNSYS. Validation of the Duct Storage Model (DST) in TRNSYS against experimental data is also presented. The validated model is then used to simulate borehole thermal energy storage (BTES) thermal response for analysis and implementation into the BTES reduced model which is presented in Chapter 5. The numerical methods and limitations of the DST model are outlined. DST is validated with measured operation data from a BTES installation. Finally, the validation simulation is confirmed to be mesh and timestep independent.

3.2 TRNSYS

The development of a new reduced model of BTES thermal response, the focus of the current thesis, requires the simulation of a range of BTES configurations, therefore, CFD is too computationally expensive for the requirements. A simpler model is preferred for simulating BTES configurations because of the time associated with control volume definition, computation, and numerical independence verification each configuration's CFD simulation would require. The DST model implemented in TRNSYS is chosen for simulating BTES configurations due to the ease at which BTES design parameters can be changed, relative to CFD simulations.

TRNSYS is a transient system simulation environment commonly used for calculating the performance of time dependent thermal and electrical energy systems [12]. The DST model is implemented in the TRNSYS library of energy system components by way of the module

"type 557" to simulate BTES thermal response. DST calculates heat transfer between the circulating fluid within the borehole heat exchangers and the ground volume used for energy storage and it is often used as a benchmark for evaluating the accuracy of other BTES simulation software [20].

3.3   DST

DST inputs transient BTES operation data and constant BTES design parameters to calculate transient heat transfer outputs. DST reads input values at a user defined timestep (usually hourly) for borehole fluid inlet temperature, total borehole fluid mass flow rate, and ambient air temperature above the storage volume. The BTES design parameters are set by the user to provide information about the geometry and thermal properties of the borehole heat exchanger field and the ground storage volume. The fluid inlet data and the BTES design parameters are used by the DST model in the calculation of borehole fluid outlet temperature, fluid to ground heat transfer rate, and ground volume average temperature outputs at the timestep of the input data. The DST model also calculates conductive energy losses through the top, side, and bottom surfaces of the ground storage volume and provides energy loss rate outputs at a larger timestep than the input data timestep.

DST calculates the amount of heat transferred from the borehole fluid to the ground by splitting the problem into simpler components and superposing the component solutions to calculate the final solution. The simplified components include the local and global problems, which are solved with explicit forward finite differentiation, and the steady flux problem, which is solved analytically. The local problem models heat transfer between the heat exchanger fluid and the ground surrounding each borehole heat exchanger, where the ground volume is modelled with a one-dimensional radial mesh network. The global problem models heat transfer within the

14

BTES volume and between the BTES volume and the surrounding ground. The global problem is solved with a two-dimensional mesh simulating axial and radial heat conduction for the storage volume and the surrounding ground volume. The steady flux problem simulates the slow redistribution of heat within the BTES ground volume, modelled by the two-dimensional global mesh, due to the circulation of the heat carrier fluid [14].

The local and global meshes are connected by the subregion mesh. The subregion mesh sets the number of local problems to be solved and the locations within the global mesh each local problem interacts with. The subregion mesh overlaps with the BTES volume of the two-dimensional global mesh. The subregion mesh allows the modelling of heat transfer between the heat exchanger fluid and the ground storage volume calculated by the local problem to connect to the global problem's modelling of the dissipation and redistribution of thermal energy within the BTES volume and the surrounding ground. The combination of the two meshes creates a quasi-three-dimensional solution which allows for accurate modelling of BTES thermal response. The dimensions of the local and global mesh networks are calculated by the DST model using the dimensions and thermal properties of the heat carrier fluid, borehole heat exchanger and the BTES ground volume.

Figure 3.1: Example of local, global, and subregion mesh networks used in the DST model, and the relationship between the meshes and BTES volume (not to scale) [21].

The DST model's finite differentiation operates on two timesteps. The local problem is simulated on a short timestep, and it is solved multiple times per hour (the most common TRNSYS timestep). The global problem is simulated on a long timestep, where finite

differentiation is solved at a timestep longer than the TRNSYS timestep. An example of the difference in timestep magnitudes is provided by Chapuis and Bernier (2009) where the timestep for local finite differentiation is 6 minutes, and the global timestep is 59 hours [21]. Local heat transfer from the borehole heat exchanger outer diameter through the local mesh is therefore calculated multiple times per TRNSYS timestep. The energy interaction between the local and global meshes, the redistribution of energy from the steady flux problem, and the conductive thermal diffusion in the global mesh are calculated for multiple TRNSYS timesteps simultaneously. The result of the DST model's numerical methods is that TRNSYS provides output data for fluid heat exchange at every user defined timestep from the integration of the local timesteps, and conductive energy loss data is only available at the long timestep of the global problem.

3.4   Limitations

The limitations of DST reduce its ability to realistically simulate BTES thermal response and, since DST is the basis of the reduced model, become limitations present within the reduced model. DST does not simulate convective heat transfer within the storage volume ground water content of a BTES or its surrounding ground volume. DST can only simulate axisymmetric and uniformly distributed BTES configurations. Finally, DST does not consider the thermal capacity of the borehole heat exchangers in its simulation. The magnitude of total ground storage volume thermal capacity is greater than borehole heat exchangers' total thermal capacity so the influence of this decreases as total simulation time increases [15].

3.5   Validation

To use TRNSYS simulation results as the basis of the reduced model of BTES thermal response, the simulation's outputs must be validated against measurements from an operational

17

BTES installation. Validation requires the TRNSYS simulation's DST parameters be set corresponding to the geometry and thermal properties of the installed borehole field, and that the dynamic inlet mass flow rate and fluid temperature profiles measured from the installed field be set as inputs to the DST simulation. The DST outputs of fluid outlet temperature and average storage volume temperature are compared to BTES installation measurements for the same parameters to determine if the DST model can accurately simulate energy exchange between the heat carrier fluid and the ground storage volume. A borehole thermal energy storage installation with accessible data that is required for validation exists in Brædstrup, Denmark at the Brædstrup Total Energy Plant.

The Brædstrup Total Energy Plant is a production plant for district heating in Brædstrup, Denmark installed by PlanEnergi [22]. The plant includes a BTES installation with a reported soil storage volume of 19 000 m^3, 18 600 m^2 of solar thermal collectors, a 1.2 MW electrical heat pump, a 10 MW electric boiler, a natural gas-powered combined heat and power unit, and 2 heat accumulation tanks of 2 000 m^3 and 5 500 m^3 [22]. The Brædstrup Total Energy Plant is installed in phases with increasing solar collector area, borehole storage volume, and heat pump capacity planned during its operation lifecycle. The objective of the plant's installation phases is to eventually meet the community's natural gas combined heat and power requirement with solar thermal energy.
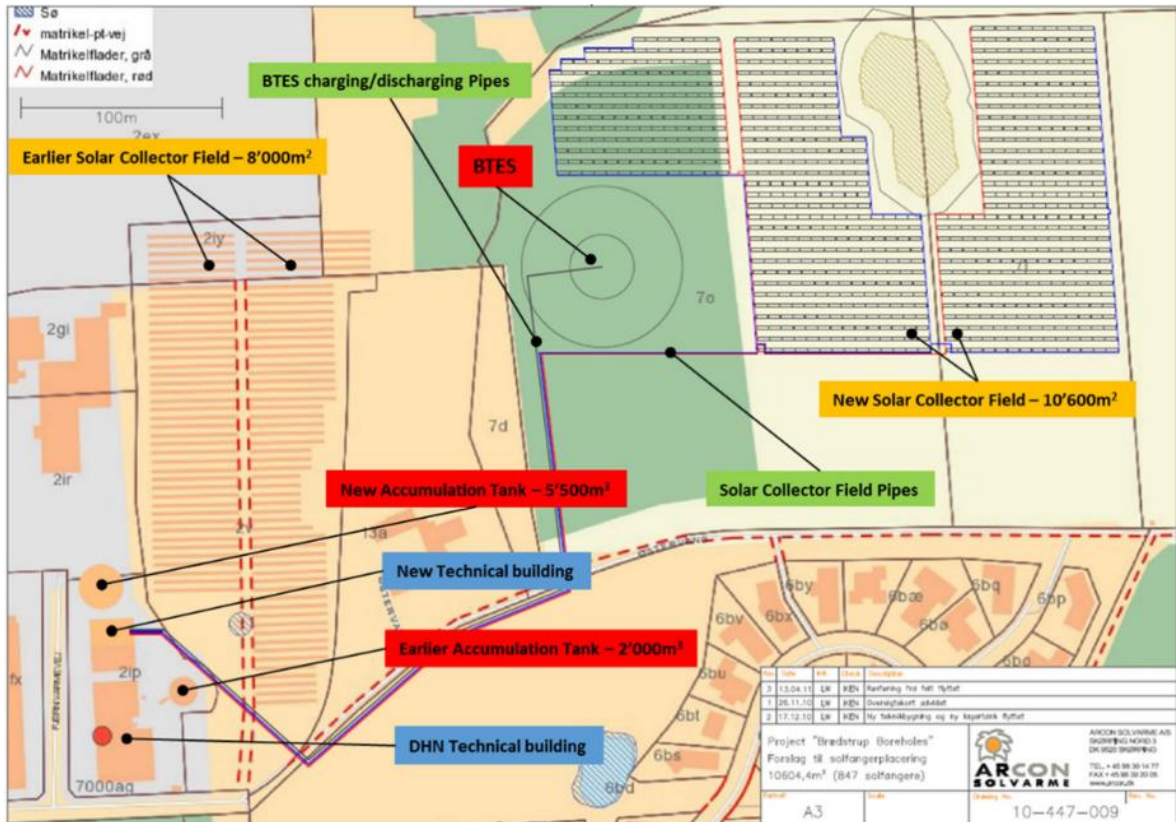
Figure 3.2: Schematic of Brædstrup Total Energy Plant [23].

The 19 000 m^3 storage volume BTES in Brædstrup consists of 48 borehole heat

exchangers which each span a depth of 45 metres and are spaced 3 metres from each other within

a hexagonal borehole array. The BTES consists of 2 sets of 8 strings with 6 single U-tubes

connected in series per string. Each string transports the working fluid outwards from the centre

of the array. During BTES charging hot water flows through the boreholes from the centre of the

array outwards, and during BTES discharging cold water flows in the opposite direction. Each

BHE has a diameter of 15 centimetres and contains 2 U-tubes. The top-down borehole field

layout and one set of borehole string connections are displayed in Figure 3.3. The second set of 8

strings are connected in an arrangement which mirrors the U-tube connections shown in Figure

3.3 about a central vertical axis. Due to limitations of TRNSYS DST, however, the field is

simulated as 1 set of 8 strings with each string connecting 6 double U-tube heat exchangers in series. The U-tube pipes are made of cross-linked polyethylene and have an internal diameter of 32 mm with a wall thickness of 2.9 mm. Water is the working fluid which flows through the 2 U-tubes in each borehole. The borehole field lies under 0.5 metres of insulation which lies under 0.5 metres of soil. The homogenous approximation of the soil thermal conductivity and volumetric heat capacity were determined by a thermal response test at the BTES site, and the thermal conductivities of the borehole components are provided in the project report. Finally, the undisturbed ground temperature was measured on site to be approximately 8°C. All the BTES configuration, geometry, and thermal property data is from the Brædstrup Total Energy Plant final report by PlanEnergi [22] and is interpreted into the TRNSYS DST parameters presented in Table 3.1 for the validation case with additional explanations when necessary.
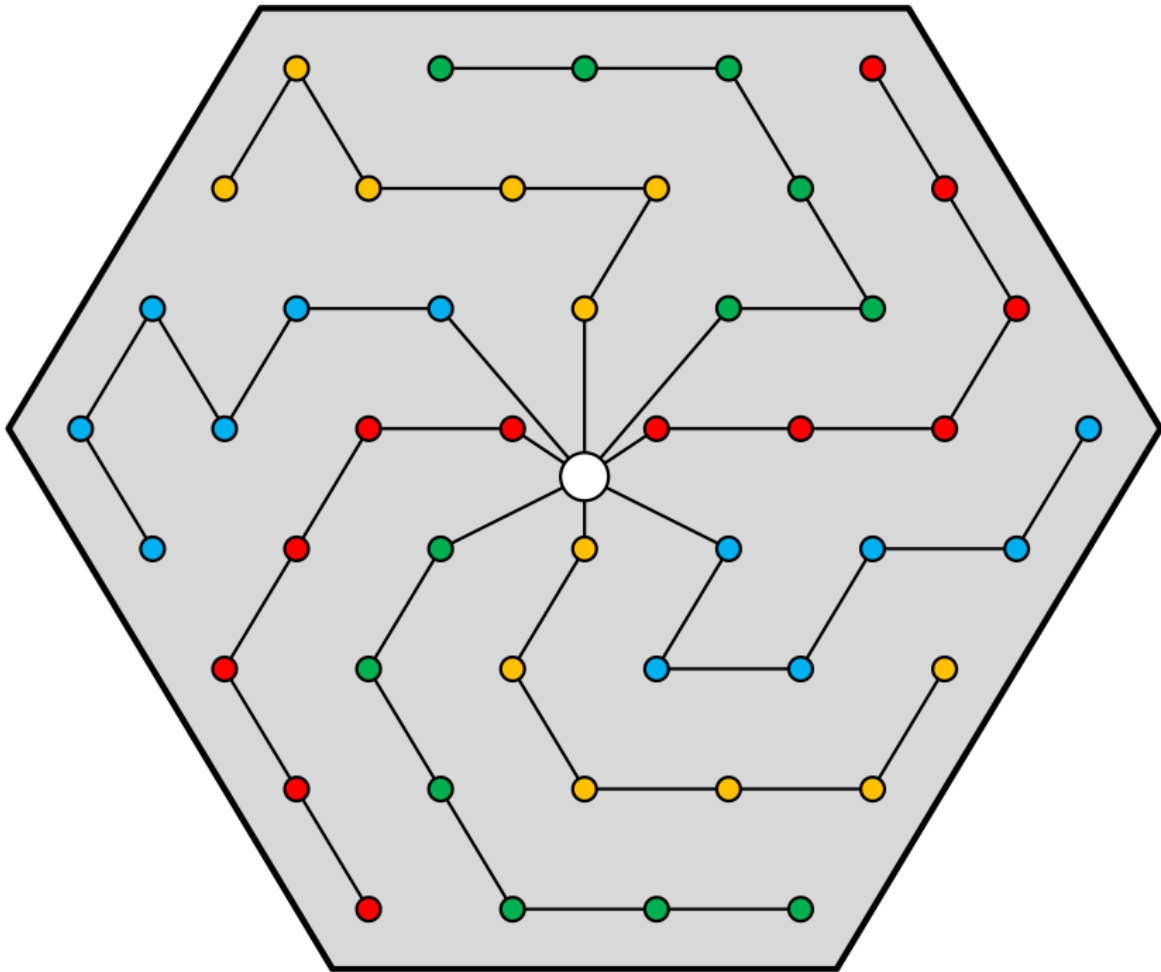
Figure 3.3: Borehole layout and borehole string connections for the Brædstrup Total Energy Plant BTES [22].

Parameter	Value	Units	Explanation
TRNSYS-DST Volume	16 833	m^3	Based on calculation of volume performed by DST: V=π(Number of boreholes)*(Borehole Depth)*(0.525*Borehole Spacing)^2, where number, depth, and spacing are known
Borehole Depth	45	m	
Header Depth	1	m	
Number of Boreholes	48	-	

Borehole Radius	0.075	m	
Number of Boreholes in Series	6	-	8 strings of double U-tube heat exchangers connected in parallel
Number of Radial Regions	20	-	Maximizes control volumes for subregion mesh. Effect investigated in mesh sensitivity
Number of Vertical Regions	20	-	Maximizes control volumes for subregion mesh. Effect investigated in mesh sensitivity
Storage Thermal Conductivity	1.42	W/(m*K)	Result of thermal response test
Storage Heat Capacity	1900	kJ/(m^3*K)	Result of thermal response test
U-tubes per bore	2	-	
Outer Radius of U-Tube Pipe	0.0189	m	DN 32×2.9 mm piping
Inner Radius of U-Tube Pipe	0.016	m	DN 32×2.9 mm piping
Centre to Centre Half Distance	0.375	m	
Fill Thermal Conductivity	1.44	W/(m*K)	Measured and presented in PlanEnergi final report
Pipe Thermal Conductivity	0.41	W/(m*K)	Measured and presented in PlanEnergi final report
Gap Thickness	0	m	
Reference Borehole Flow rate	33996	kg/hr	Maximum mass flow rate from Brædstrup operation
Reference Temperature	85	°C	Maximum Temperature from Brædstrup operation

Pipe to Pipe Heat Transfer	0	-	Ignore Heat Transfer between the upwards and downwards U-tubes within a borehole
Fluid Specific Heat	4.18	kJ/(kg*K)	Properties of water
Fluid Density	995	kg/m^3	Properties of water
Insulation Indicator	2	-	Insulation extends a user defined fraction of storage height horizontally beyond the top surface boundary
Insulation Height Fraction	0.067	-	0.067*(Borehole Depth)=(distance of insulation extension) 0.067*45m=3.015m 3m constant thickness provides the same volume of extra insulation as 6m length of reducing thickness insulation
Insulation Thickness	0.5	m	
Insulation Thermal Conductivity	0.121	W/(m*K)	Measured and presented in PlanEnergi final report
Number of DST Simulation Years	5	years	Sets the outer bounds of the global mesh far enough so TRNSYS does not crash with a 2 year preheat + 3 year simulation
Maximum Temperature of Storage Volume	99	°C	Set to an absolute maximum based on the boiling temperature of the heat exchange fluid
Initial Surface Temperature of Storage Volume	8	°C	Based on undisturbed ground temperature at the site
Initial Thermal Gradient	0	-	Ground temperature begins uniformly at 8°C
Number of Preheating Years	2	years	Preheating data from Gauthier [23] set so that when the simulation begins, average storage temperature in the DST model matches the average storage temperature at the beginning of the operation data from the installed field (27.8 °C)

Maximum Preheat Temperature	29	°C	
Minimum Preheat Temperature	12	°C	
Preheat Phase Delay	68	days	
Average Air Temperature for Preheat Years	9.2	°C	
Amplitude of Air Temperature for Preheat Years	6.6	Δ°C	
Air Temperature Phase Delay for Preheat Years	244	days	
Number of Ground Layers	1	-	Assume that the soil beyond the storage volume is homogenous with the same thermal properties as the storage volume discovered with the thermal response test
Thermal conductivity of Layer	1.42	W/(m*K)	
Heat Capacity of Layer	1900	kJ/(m^3*K)	
Thickness of Layer	90	m	Extends twice the borehole depth

Table 3.1: DST parameters representing the BTES of the Brædstrup Total Energy Plant for simulation in TRNSYS. The values are presented in and interpreted from the PlanEnergi final report on the site [22].

The BTES operation data spans from 1st January 2014 to 1st January 2017 and includes hourly site measurements of fluid inlet volumetric flow rate [m^3/hr], fluid inlet temperature [°C],

fluid outlet temperature [°C], average storage volume temperature [°C], and ambient air temperature [°C] [24]. Validation, mesh independence, and timestep independence tests use fluid inlet volumetric flow rate, fluid inlet temperature, and ambient air temperature as inputs for the DST model and the DST outputs are plotted against fluid outlet temperature and average storage volume temperature. Each parameter is plotted with respect to time over the 3-year simulation. The following figures display the site measurements used as DST model inputs and the DST model outputs compared to their corresponding site measurements to validate the DST model's simulation of BTES thermal response.

3.6 Validation Inputs
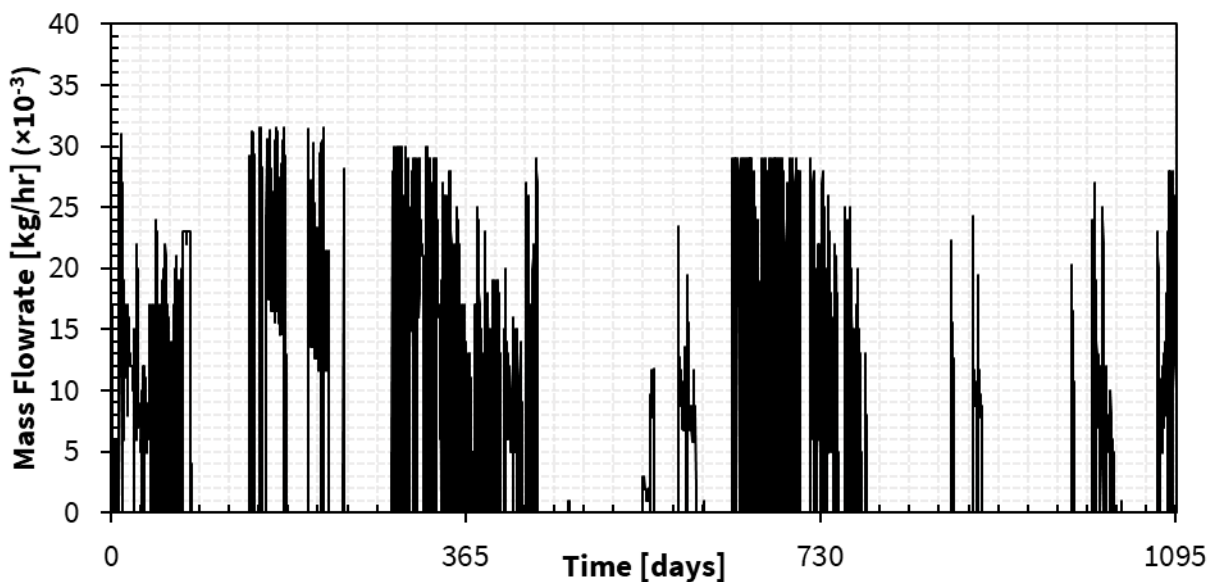
Figure 3.4: Hourly mass flow rate control of the BTES installed in Brædstrup, Denmark from 1 January 2014 to 1 January 2017. Values displayed have been reduced by a factor of 10^3.
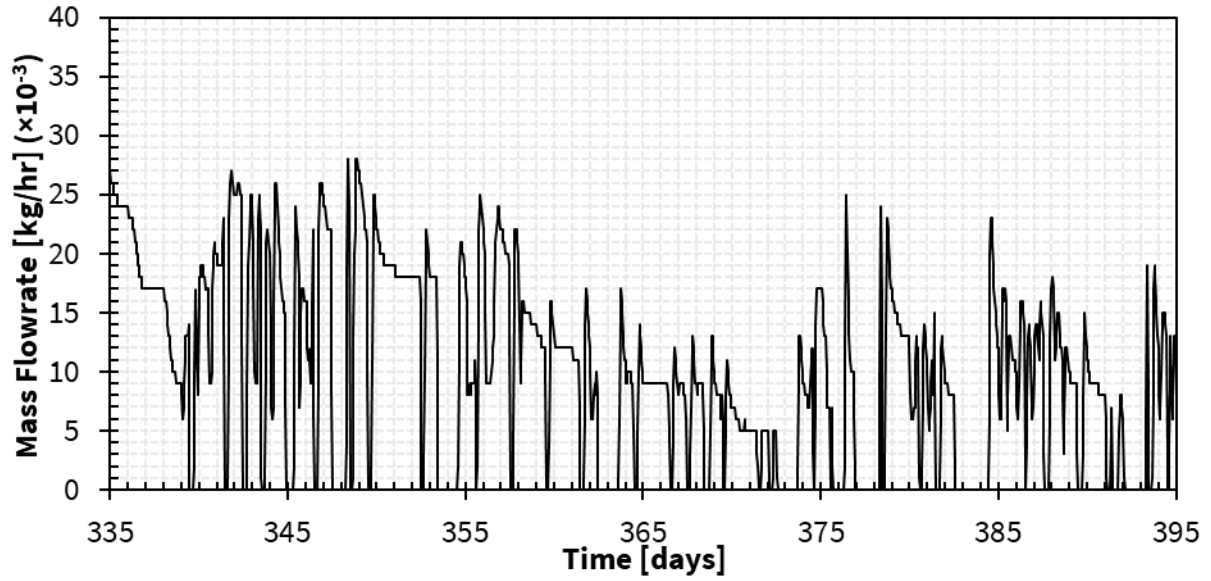
Figure 3.5: Hourly mass flow rate control of the BTES installed in Brædstrup, Denmark from 2 December 2014 to 30 January 2015. Shows the dynamic on/off behavior for a portion of Figure 3.4. Values displayed have been reduced by a factor of 10^3.
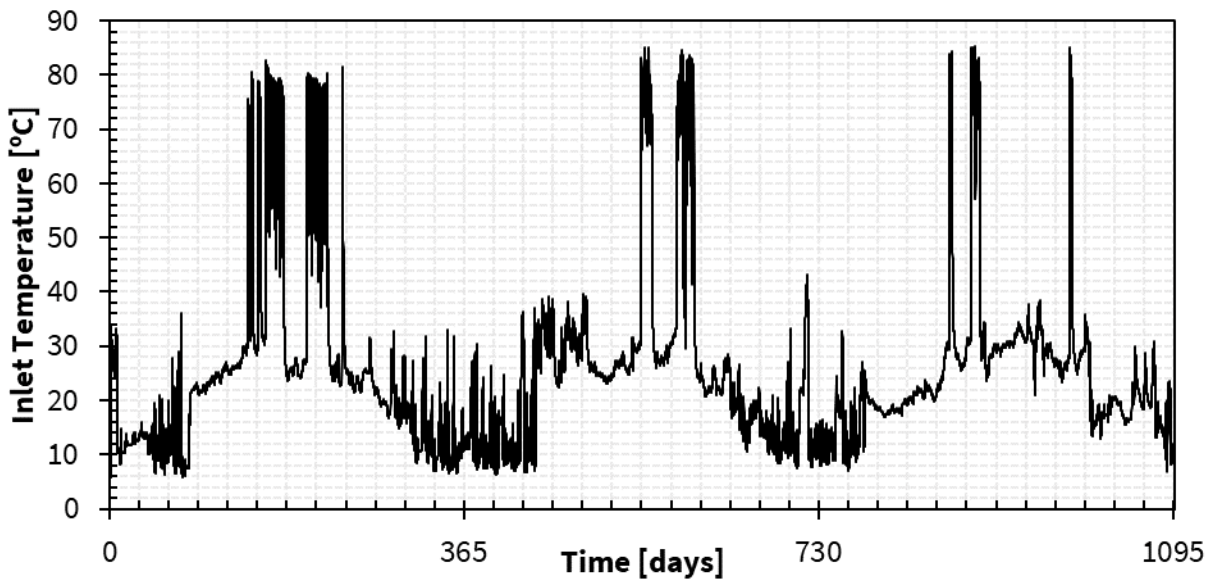
Figure 3.6: Hourly inlet temperature control of the BTES installed in Brædstrup, Denmark from 1 January 2014 to 1 January 2017.
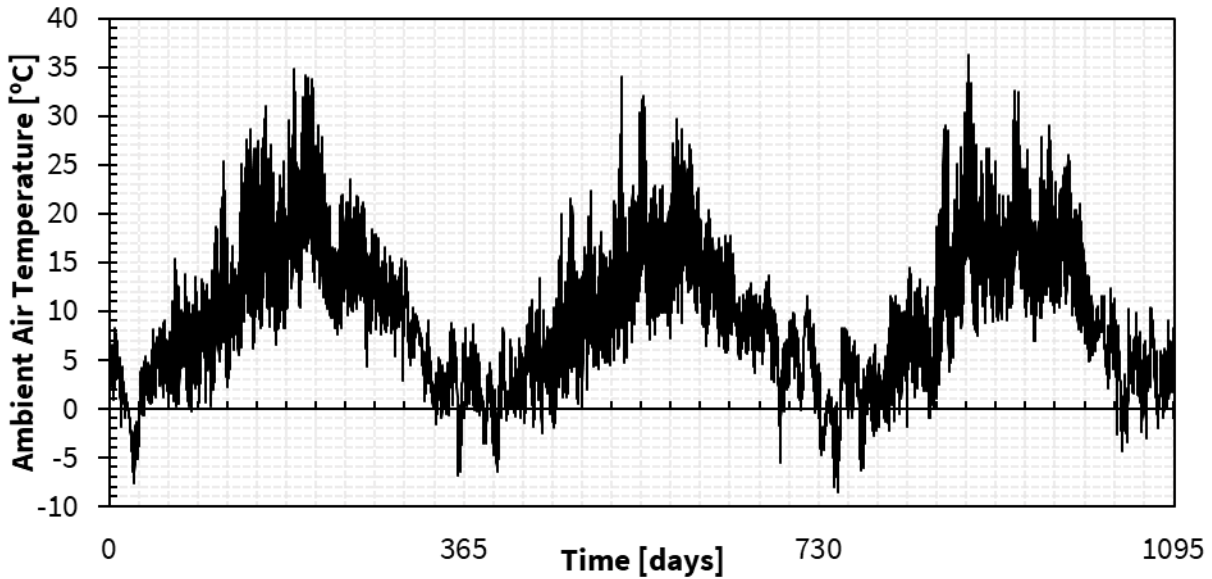
Figure 3.7: Hourly ambient air temperature measurements above the BTES installed in Brædstrup, Denmark from 1 January 2014 to 1 January 2017.

3.7 Validation Outputs

The validation figures show agreement between the TRNSYS DST output parameters and their corresponding BTES site measurements. Figure 3.8 shows the simulated and measured outlet fluid temperature for the period of January 2014 to January 2017. The outlet temperatures vary from about 9°C to 67°C depending on whether the BTES is being charged or discharged and depending on the inlet fluid temperature during charging or discharging. The overall root mean square difference between the site measurements and simulated values of fluid outlet temperature is 5.93°C. Figure 3.11 shows the simulated and measured average storage volume temperature for the period of January 2014 to January 2017. The average storage temperatures vary from about 15°C to 43°C depending on the heat transfer induced from the heat exchanger fluid while the BTES is charging or discharging. The overall root mean square difference between the site measurements and simulated values of average storage volume temperature is 1.09°C. When the TRNSYS DST model is provided the dynamic inlet temperature and mass

27

flow rate from the BTES site and the constant DST parameters are set according to the BTES site's geometry and thermal properties, TRNSYS DST can accurately simulate the site's BTES thermal response.

The only significant deviation between the site measurements and TRNSYS DST outputs of outlet temperature and average field temperature occurs halfway through year 2 around day 545. This occurs because the low mass flow rate measurement set as an input during that time causes the model to overestimate the temperature drop for the working fluid and underestimate the energy gained by the field due to the low total energy capacity associated with the low mass flow rate. The discrepancy occurs because TRNSYS calculates the local borehole solution with a constant thermal resistance based on a reference mass flow rate. The reference mass flow rate is set as the maximum mass flow rate of the validation, therefore, lowering the dynamic mass flow rate increases the difference between it and the reference mass flow rate. The DST model implemented in TRNSYS displays its ability to accurately simulate BTES thermal response for the requirements of the reduced model, regardless of the discrepancies in the validation caused by low mass flow rate.
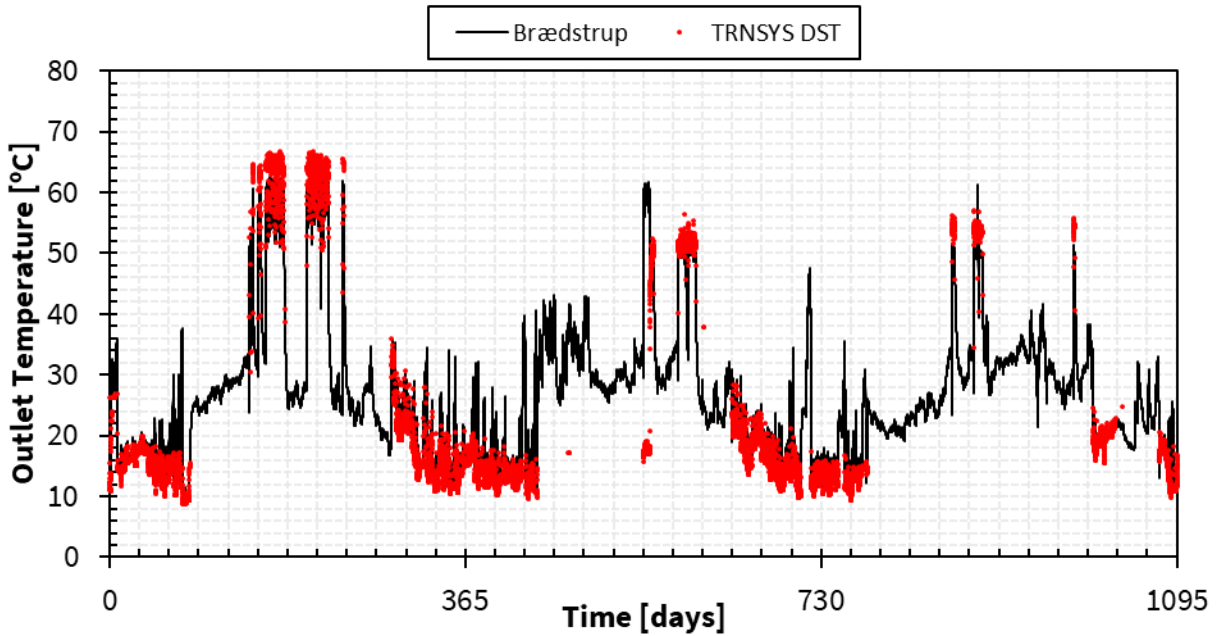
Figure 3.8: Hourly outlet temperature measurements of the BTES installed in Brædstrup, Denmark from 1 January 2014 to 1 January 2017 overlayed with hourly outlet temperature simulated by TRNSYS DST when the mass flow rate is greater than 0. RMSD=5.93°C
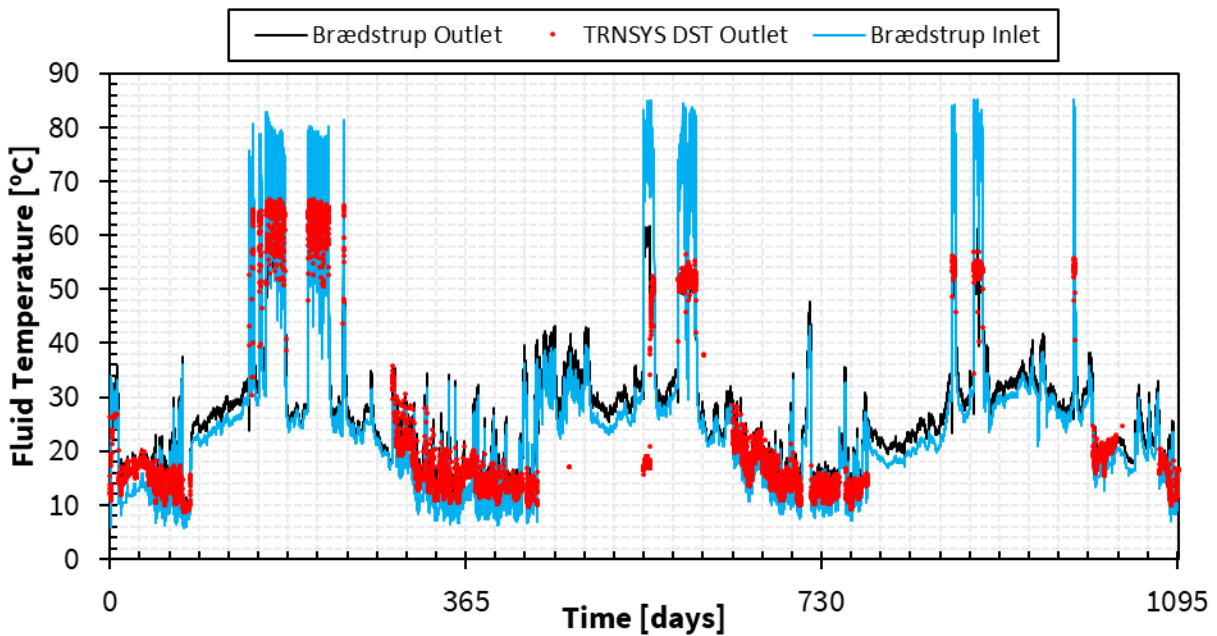
Figure 3.9: Hourly outlet temperature measurements of the BTES installed in Brædstrup, Denmark from 1 January 2014 to 1 January 2017 overlayed with hourly outlet temperature

simulated by TRNSYS DST when the mass flow rate is greater than 0 and hourly inlet temperature control of the BTES. Outlet RMSD=5.93°C
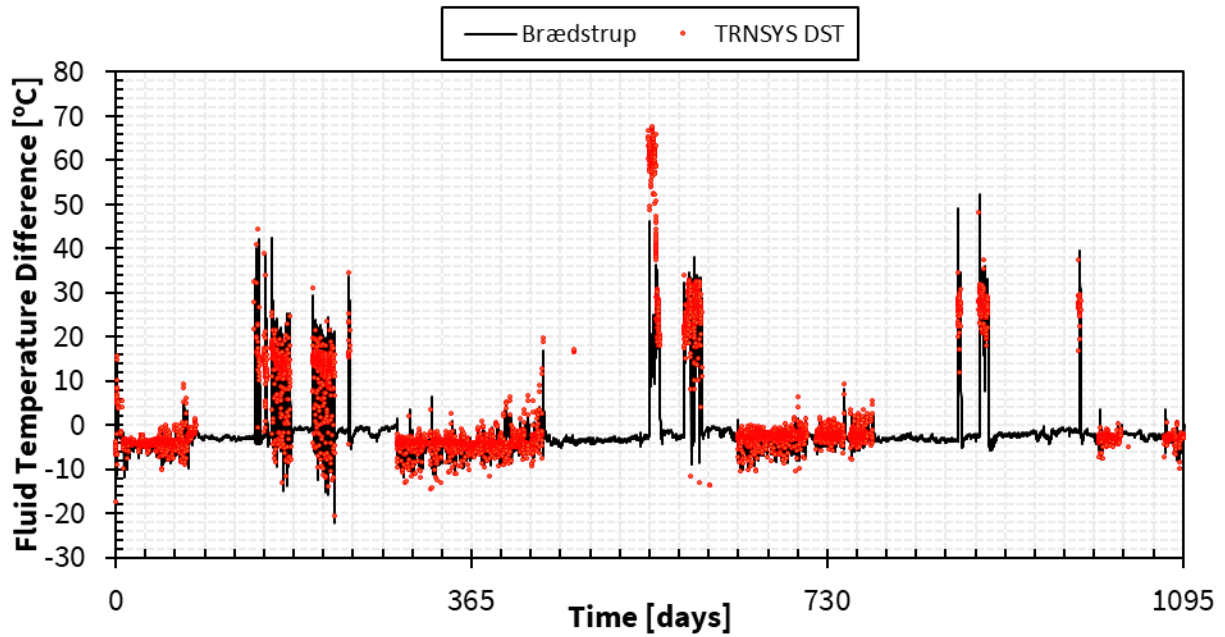
Figure 3.10: Hourly difference between inlet and outlet temperature measurements of the BTES installed in Brædstrup, Denmark from 1 January 2014 to 1 January 2017 overlayed with hourly difference between fluid inlet and outlet temperatures simulated by TRNSYS DST when the mass flow rate is greater than 0. RMSD=5.93°C
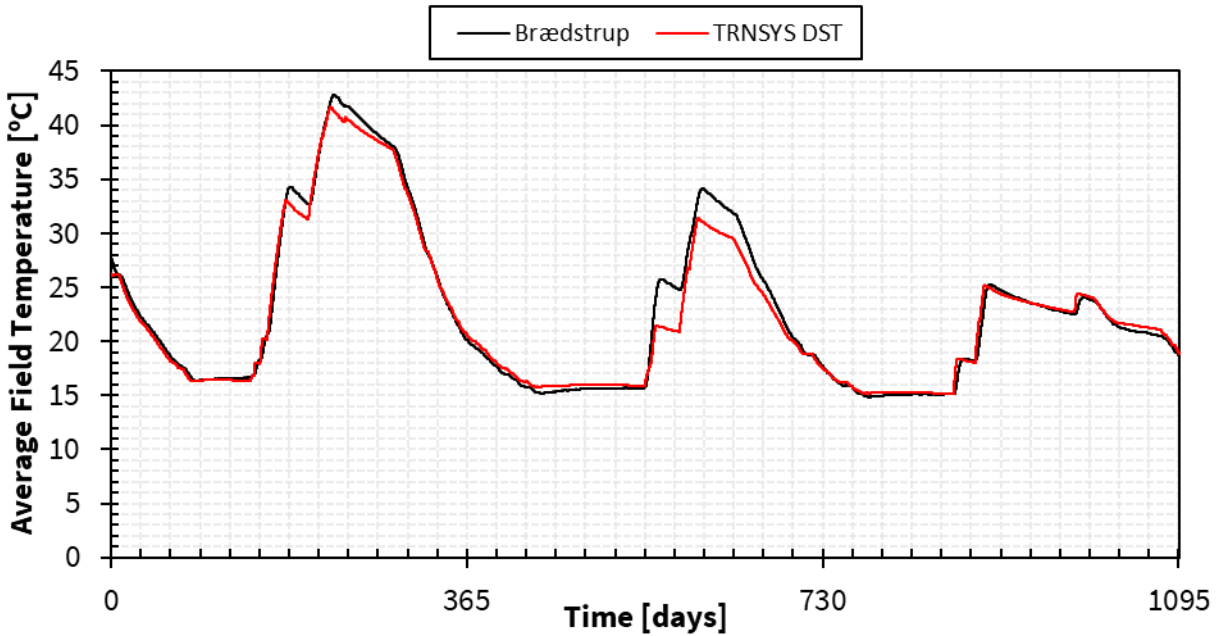
Figure 3.11: Hourly average storage volume temperature measurements of the BTES installed in Brædstrup, Denmark from 1 January 2014 to 1 January 2017 overlayed with hourly average storage temperature simulated by TRNSYS DST. RMSD=1.09°C

3.8   Numerical Independence

The TRNSYS DST domain discretization mesh and timestep independence is tested by varying the number of radial subregions, the number of vertical subregions, and timestep length to see the effect each has on the fluid side thermal exchange solution and simulation computational requirements.
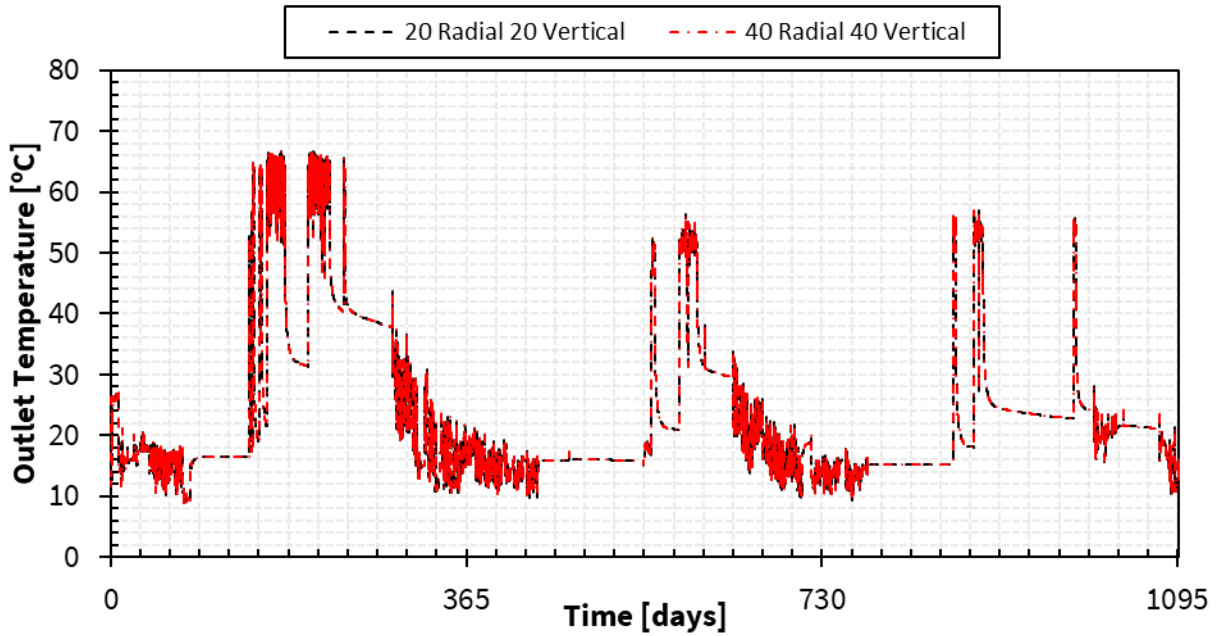
Figure 3.12: Hourly TRNSYS simulated values for outlet temperature comparing the outputs dependency to the number of radial and vertical subregions. The simulation with 20 radial and 20 vertical subregions is shown to be independent to an increase in the number of subregions. Both simulations took 14 seconds wall clock time to complete. RMSD=0.00°C
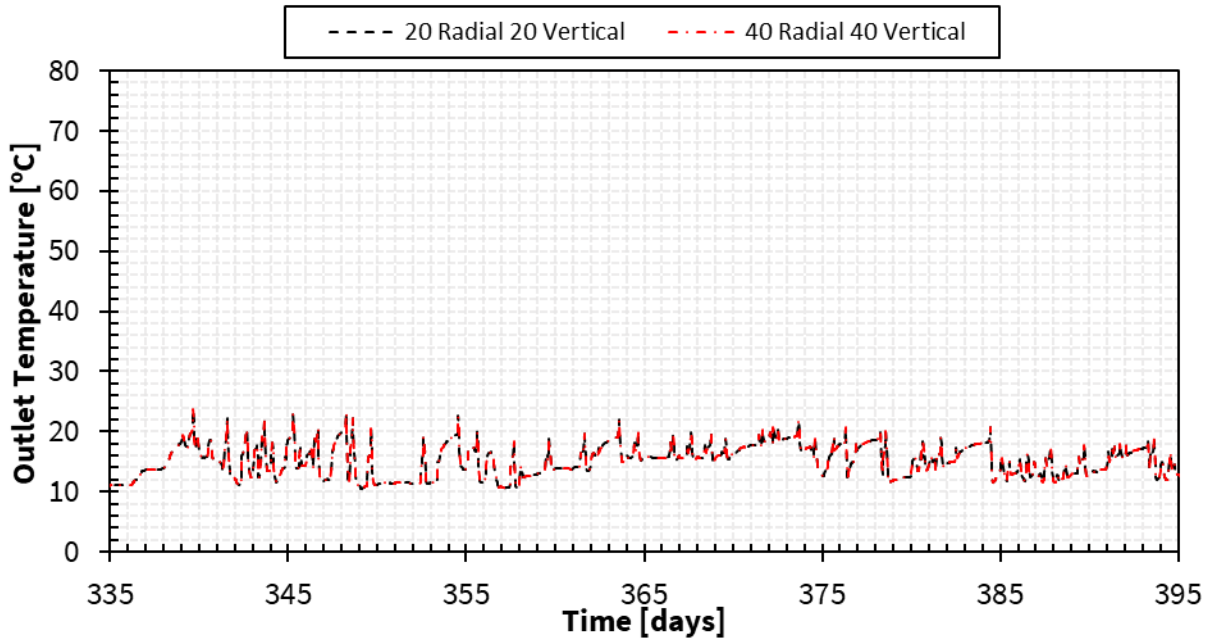
Figure 3.13: Displays the independence of fluid outlet temperature to doubling the number of radial and vertical subregions from 335 days to 395 days. RMSD=0.00°C
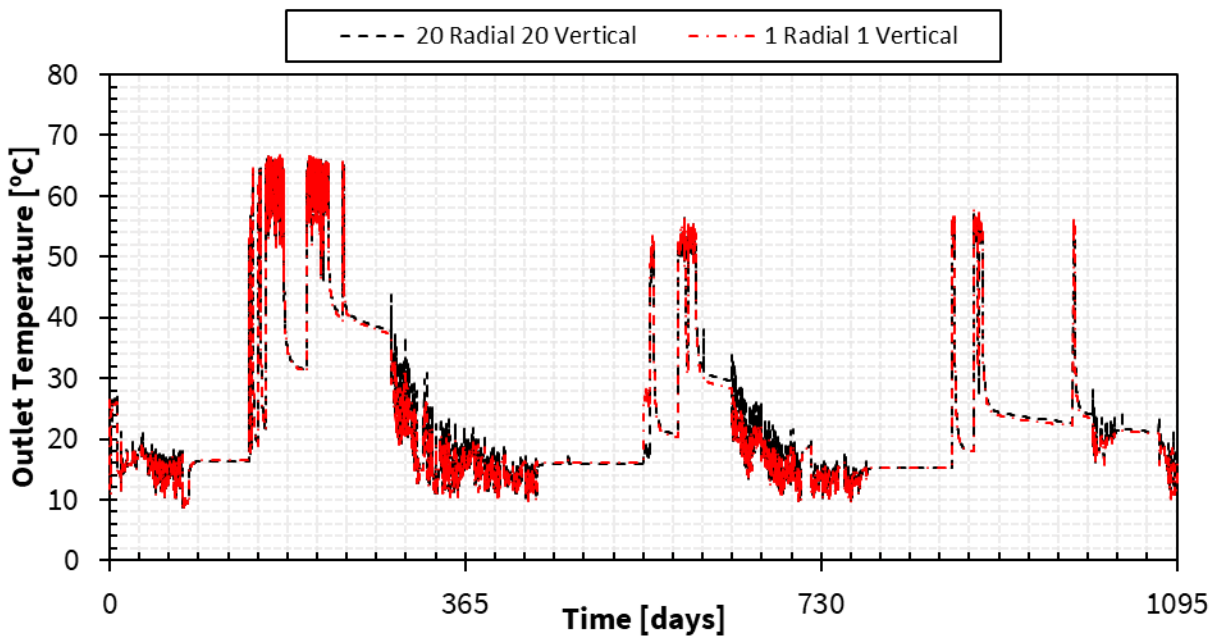
Figure 3.14: Hourly TRNSYS simulated values for outlet temperature comparing the outputs dependency to the number of radial and vertical subregions. The simulation with 1 radial and 1 vertical subregion shows the maximum instantaneous simulation error due to the subregion mesh

33

dependence. The coarse mesh simulation took 7 seconds wall clock time to complete, compared to the fine mesh simulation's 14 seconds. RMSD=0.95°C

Doubling the number of radial and vertical subregions does not influence the calculation of fluid outlet temperature as TRNSYS DST decides the number of vertical and radial subregions depending on the geometry of the BTES. 20 radial and 20 vertical subregions already maximizes the number of subregions so there is no difference in the simulation when the number of radial and vertical subregions are increased to 40. Reducing the subregion count to 1 radial and 1 vertical reduces the complexity of the simulation but it does not save significant computational resources. The root mean square difference between the simulations maximizing and minimizing the number of subregions is 0.95°C, but the simulation time only decreases from 14 seconds to 7 seconds. Maximizing the number of subregions (which can be achieved with a setting of 20 radial and 20 vertical subregions) is preferable as it increases the accuracy of the DST model and does not significantly increase computation time.
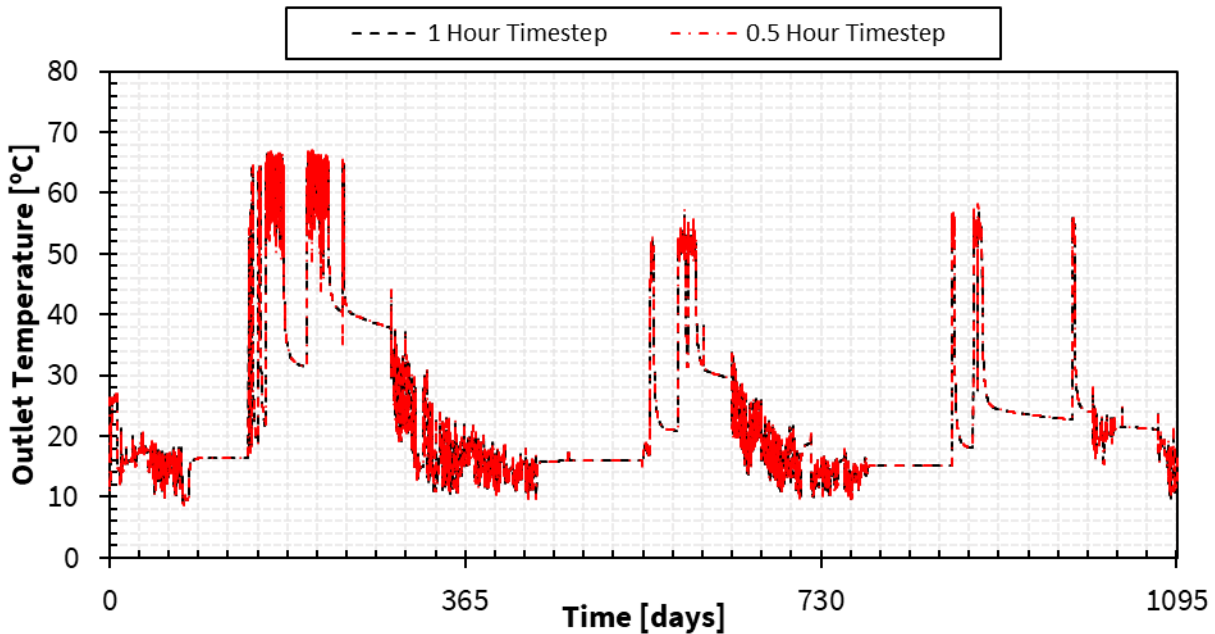
Figure 3.15: Timestep dependency test comparing the fluid outlet temperature simulated by TRNSYS with a half-hour timestep to the TRNSYS simulation output with an hour timestep. The results show low variation between the coarse and fine timesteps, and therefore, timestep independence. The half-hour timestep simulation took 20 seconds wall clock time to complete; compared to the hour timestep's 14 seconds. RMSD=0.075°C

Changing the timestep from 1 hour to 0.5 hour does not significantly change the outlet temperature profile and provides no advantages to the simulation. Comparing half hour timestep simulations to hour timestep simulations results in a root mean square difference of only 0.075°C. BTES simulations and data measurements are usually taken at an hourly timestep, so the simulations required for the reduced model will use an hourly timestep.

3.9   Conclusion

Comparing BTES site measurements and simulation outputs for fluid outlet temperature and average storage volume temperature shows that the DST model implemented in TRNSYS can accurately simulate BTES thermal response and is a suitable model to use as the basis of the

new reduced model of BTES thermal response. The effect that the number of subregions has on the simulation was investigated and it was determined that maximizing the number of subregions is most suitable for the basis of the reduced model. Setting 20 radial subregions and 20 vertical subregions allows DST to maximize the number of subregions in the simulation. The effect of timestep length was investigated, and it was determined that hourly inputs is most suitable for DST simulations for the reduced model.

4 BTES Reference Simulation Thermal Response

4.1 Introduction

To develop the reduced model of BTES thermal response and study the effects of BTES design parameters, a reference simulation requires definition and analysis. The reference simulation uses BTES design parameters and operating conditions consistent with the reduced model parameter sensitivity study which will be presented in Chapter 5. The design parameter sensitivity study for the reduced model uses the reference simulation's design parameters as the base case and presents the effects that changing BTES design parameters has on thermal response, while operation conditions for each simulation remain constant.

4.2 Reference Simulation Definition

The BTES reference simulation is based on the design parameters and thermal properties of the validation BTES from Brædstrup, Denmark (Table 3.1). Differences between the validation and reference simulations' design parameters include the number of U-tubes per bore and the number of boreholes per string. Single U-tube borehole heat exchangers are more economical to produce and install than double U-tube or coaxial borehole heat exchangers, therefore, they are more commonly used in BTES installations and are the focus of ICE-Harvest BTES studies. The borehole heat exchangers are simulated with parallel fluid inlets (1 borehole per string) to simplify the reference simulation for the number of boreholes parameter sensitivity study.

The operation conditions of the reduced model are constant inlet temperature and mass flow rate, therefore, the reference simulation is a simplified yearly charging and discharging cycle. The fluid inlet temperature input for the BTES is 95°C for 6 months to simulate thermal

storage charging followed by a fluid inlet temperature setting of 20°C for 6 months to simulate thermal storage discharging. The charging inlet temperature setpoint is 95°C because it is the maximum operation temperature of liquid water in BTES systems [25]. The discharging inlet temperature setpoint is 20°C as it is approximately room temperature. The fluid inlet temperature setpoints for charging and discharging are chosen to maximize the temperature difference between the heat exchanger fluid and the ground storage volume so the parameter sweep also presents theoretical maximum steady state thermal storage efficiencies of BTES with respect to BTES design parameters. In Chapter 5 temperature independence testing checks if the reduced model accurately predicts thermal response for lower fluid inlet temperature setpoints. The ambient air temperature is changed from the dynamic site measurements in Brædstrup, Denmark to a constant 8°C, the undisturbed ground temperature at the site and in the reference simulation. Undisturbed ground temperature of a location provides an approximation of average ambient air temperature of the location. The reference simulation and parameter dependence simulations will use these temperature setpoints to develop the reduced model.

The mass flow rate of the reference simulation is 12 500 [kg/hr]. The mass flow rate is based on the validation's reference mass flow rate of 25 000 [kg/hr] for a double U-tube borehole system [22]. The number of U-tubes per bore from the validation to the reference simulation is halved, therefore, the mass flow rate is halved. To simplify the simulation, the mass flow rate is constant 12 500 [kg/hr] during both charging and discharging. The direction of flow is from the centre of the field to the periphery during charging and the opposite during discharging, however, the direction setting does not affect the simulation as all boreholes are arranged in parallel. The reference simulation has a duration of 5 years, or 5 charge-discharge cycles, for the BTES to reach an approximate periodic steady state operation. In the parameter sweep of

Chapter 5, the simulation is increased to 10 charge-discharge cycles to ensure periodic steady

state operation is approximately met for BTES installations larger than the reference simulation.

The fluid inlet temperature is set constant for 6-month intervals, but the fluid temperature

and mass flow rate inputs are read by the TRNSYS DST model at an hourly timestep. The DST

outputs of fluid outlet temperature, average storage volume temperature, and fluid to storage

volume heat transfer rate are written to the output file at an hourly timestep.

The DST model outputs heat loss through the top, side, and bottom boundaries of the

storage volume at the global solution timestep which is longer than 1 hour. For the reference

simulation, the storage volume heat loss timestep occurs 945 times over a 43 800-hour

simulation, or approximately once every 46.35 hours. For each heat loss timestep, DST outputs

the total energy loss at the timestep and the hours preceding it up to the hour of the previous heat

loss timestep. Each heat loss rate value represents approximately 46.35 hours of heat loss instead

of 1, therefore, to represent the transient heat loss rate the simulation outputs are scaled down by

46.35. The global solution timestep causes the transient heat loss graphs to begin at the first heat

loss timestep rather than hour 0, and to change function shape at the first heat loss timestep after

the BTES switches between the charging and discharging inlet temperature setpoints rather than

occurring every 6 months.
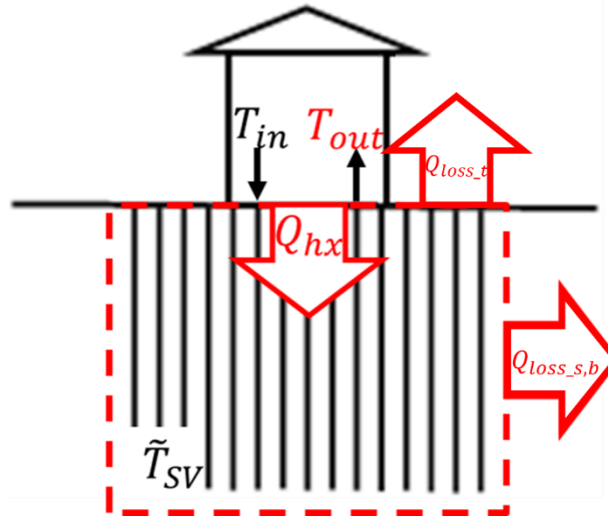
Figure 4.1: Schematic of the BTES with the ground storage volume highlighted with the red dashed lines. The schematic highlights the positive directions for the reference simulation's heat transfer rates of the heat exchanger, heat loss through the sides and bottom, and heat loss through the top. The heat exchanger heat transfer rate is the result of heat exchanger fluid circulating through the BHE represented by the parallel black lines and causes the temperature difference between the fluid inlet and outlet.

4.3 Reference Simulation Heat Exchanger Transient Results

The 6-month exponential function shape for fluid outlet temperature, average storage volume temperature, and fluid to storage volume heat transfer rate are consistent with the shape of a first-order ordinary differential equation solution. Fluid outlet temperature (Figure 4.2) and average storage volume temperature (Figure 4.3) have the function shape of $f(t)=-e^{-t}$ during BTES charging and $f(t)=e^{-t}$ during BTES discharging. Heat exchanger fluid to storage volume heat transfer rate (Figure 4.5) has the function shape of $f(t)=e^{-t}$ during BTES charging and $f(t)=-e^{-t}$ during BTES discharging. The outputs approach periodic steady state when the operating conditions are a constant yearly cycle. This justifies the creation of a reduced model to classify the periodic steady state thermal response between the heat exchanger fluid and storage volume of BTES systems. The constant operation and periodic steady state thermal response between the

40

heat exchanger fluid and the storage volume can be represented with thermal resistance values

for BTES charging and discharging profiles.
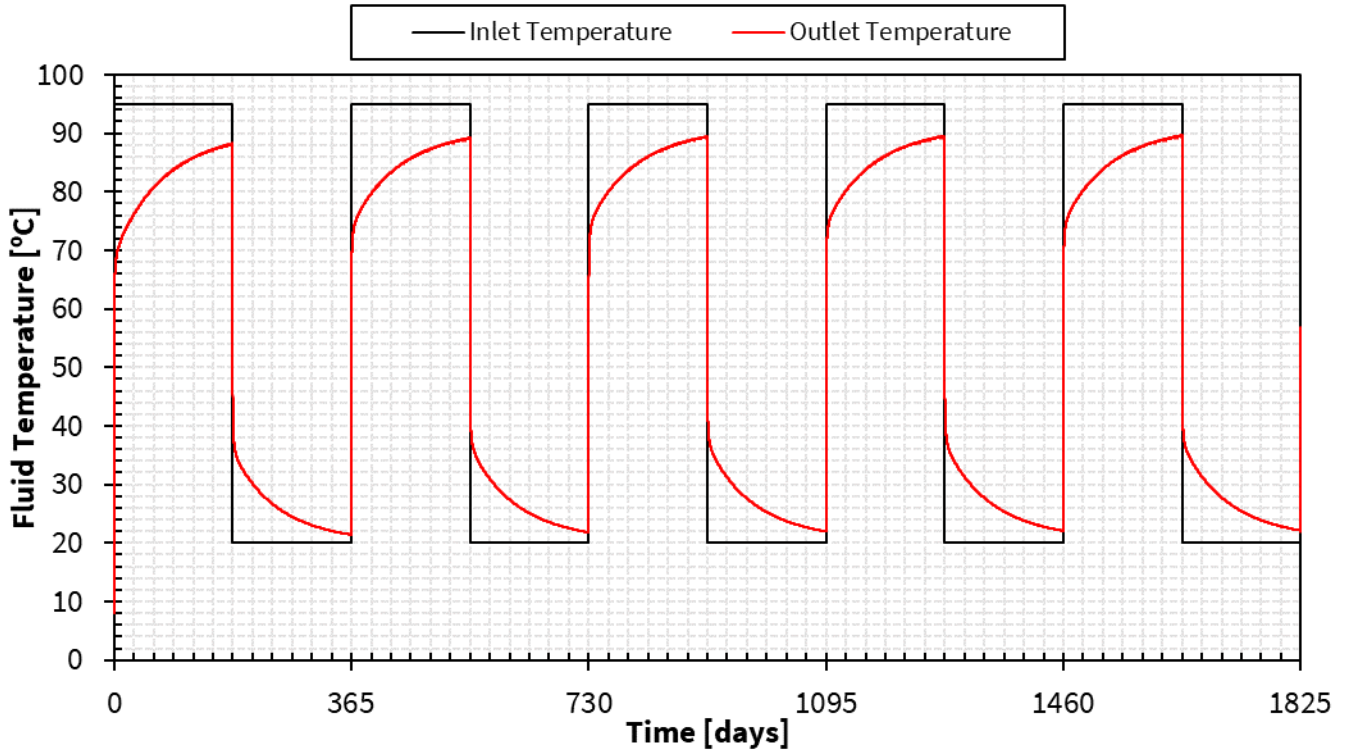
Figure 4.2: TRNSYS DST simulation input of fluid inlet temperature and simulation output of fluid outlet temperature. Fluid inlet temperature is held constant for 6 months which alternates between 95°C during BTES charging and 20°C during BTES discharging. The BTES is simulated for 5 years.
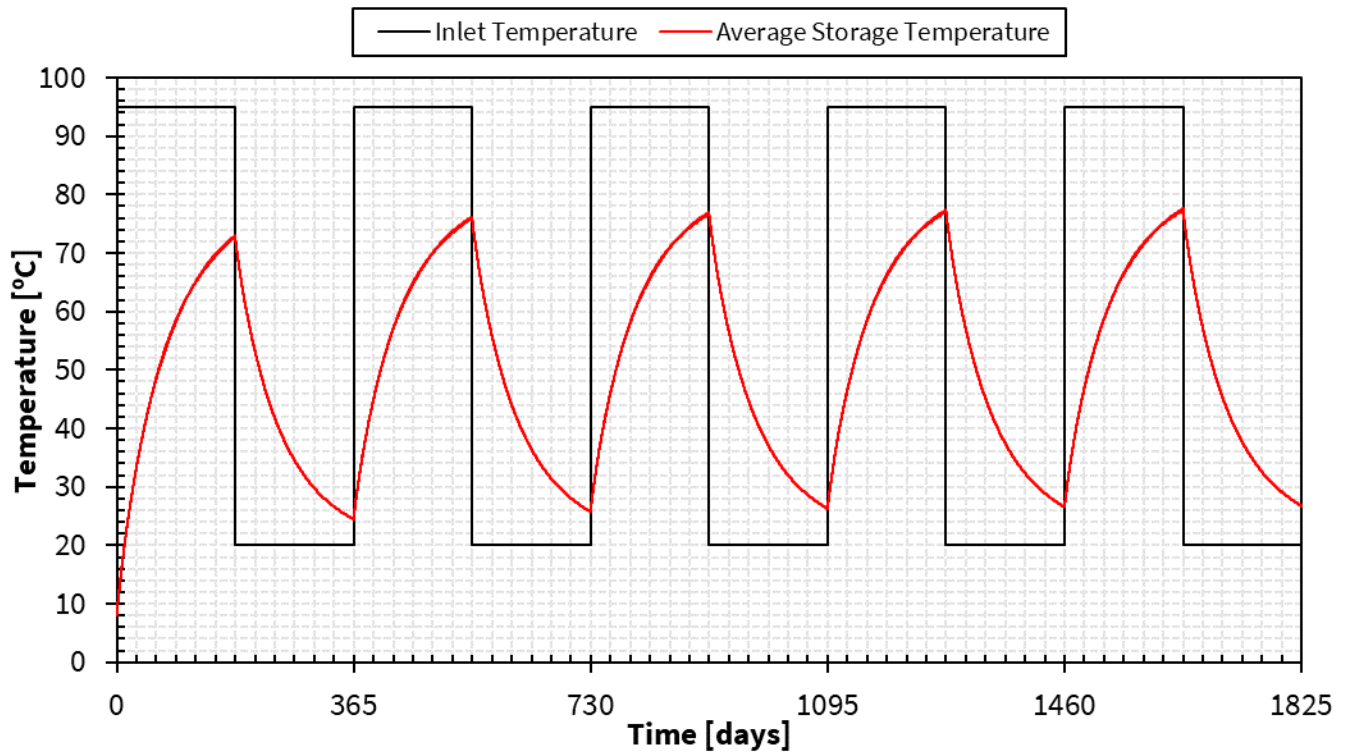
Figure 4.3: TRNSYS DST simulation input of fluid inlet temperature and simulation output of average storage volume temperature. The input and output are shown with respect to time for a 5-year simulation.
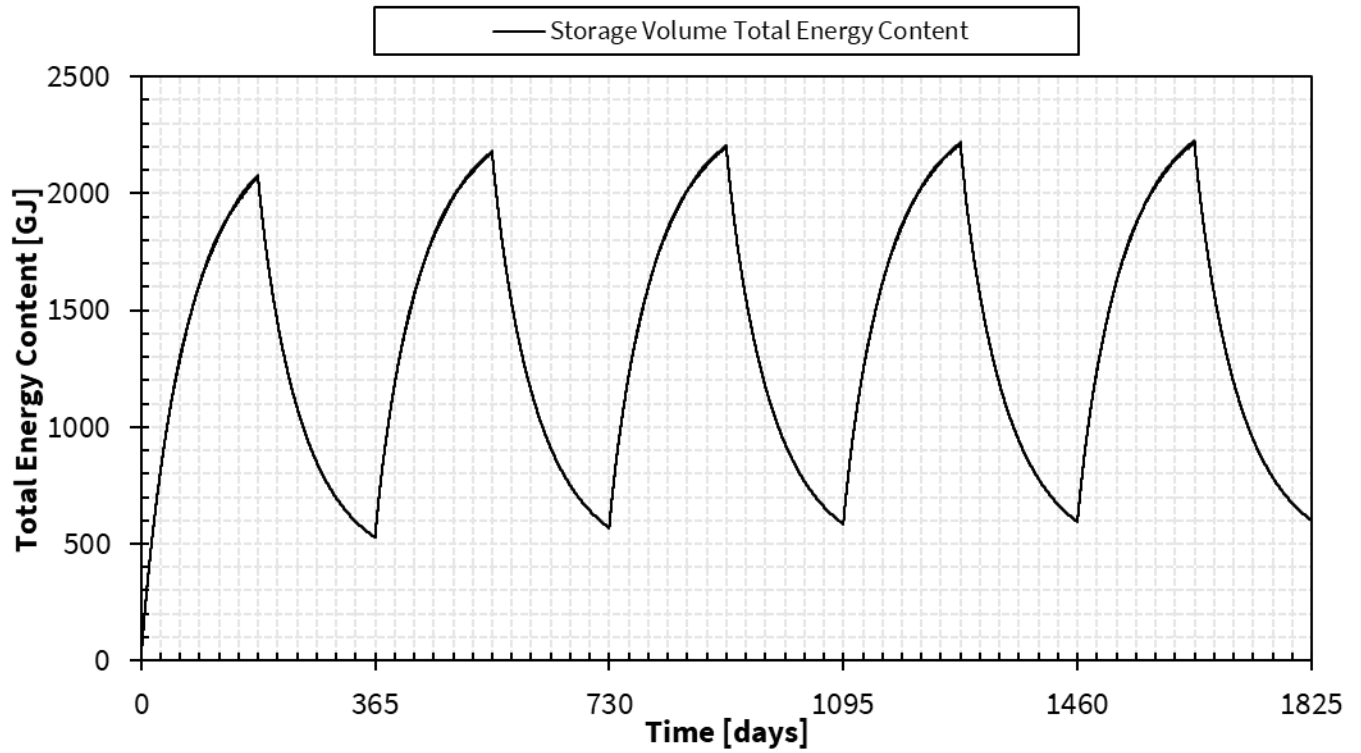
Figure 4.4: TRNSYS DST simulation output of total energy content of the BTES for 5 years. The output is calculated by inputting the average storage volume temperature output ($\tilde{T}_{SV}(t)$) into the energy equation $E(t) = V\rho c_p(\tilde{T}_{SV}(t) - T_\infty)$, where V, ρc_p, and T_∞ for the reference simulation are provided in the TRNSYS interpretation of the validation BTES presented in Chapter 3 (Table 3.1).
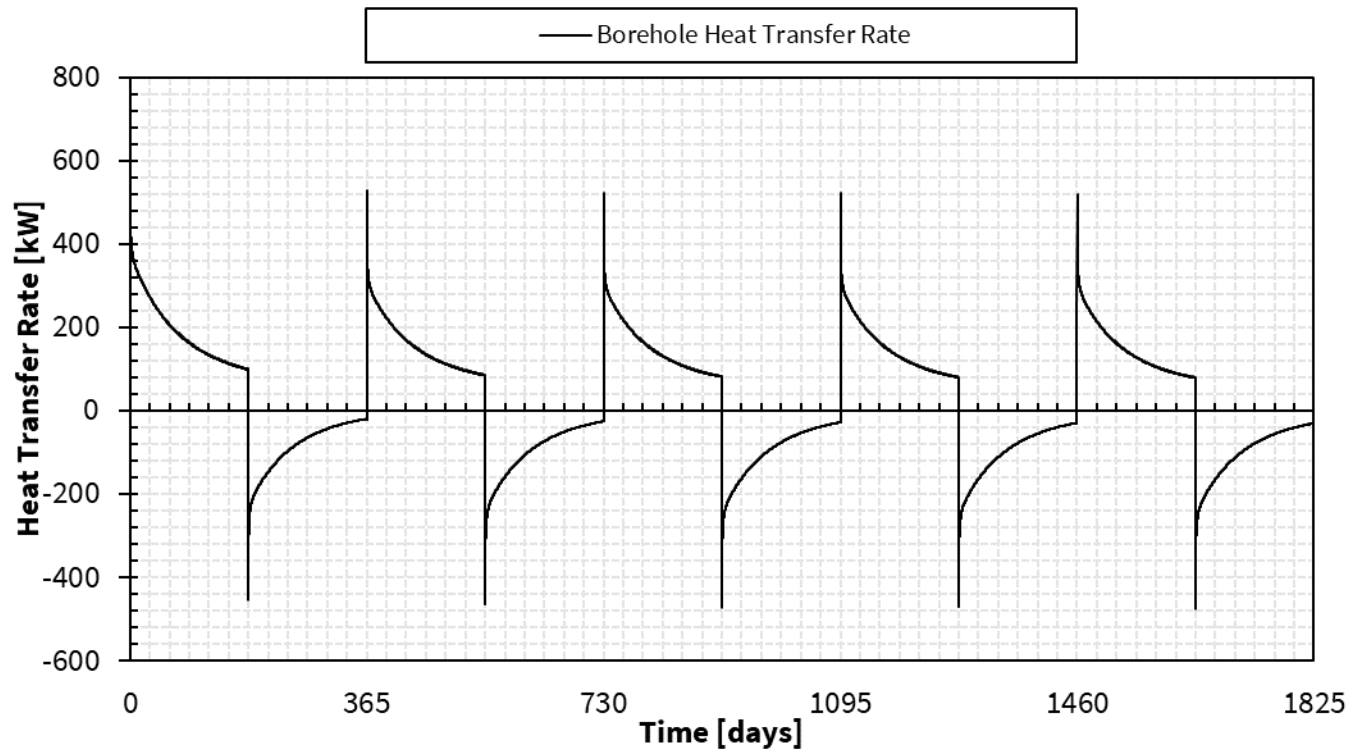
Figure 4.5: TRNSYS DST simulation output of borehole heat exchanger fluid to ground storage volume heat transfer rate with respect to time for a 5-year simulation. The heat transfer rate reacts to the 6-month constant fluid inlet temperature alternating between BTES charging and discharging (Figure 4.2). When the heat transfer rate is positive the direction of energy transfer is from the heat exchanger fluid to the storage volume and when the heat transfer rate is negative the direction of energy transfer is from the storage volume to the heat exchanger fluid.

4.4   Reference Simulation Heat Loss Transient Results

The 6-month exponential function shape for top loss heat transfer rate and side/bottom loss heat transfer rate are consistent with the shape of a first-order ordinary differential equation solution. Top loss heat transfer rate (Figure 4.6) and side/bottom loss heat transfer rate (Figure 4.7) approximately have the function shape of $f(t)=-e^{-t}$ during BTES charging and $f(t)=e^{-t}$ during BTES discharging.

44

The direction of BTES side/bottom loss heat transfer rate (Figure 4.7) changes during BTES discharging as the yearly charge and discharge cycle approaches periodic steady state operation. BTES heat loss increases the temperature of the ground surrounding the storage volume and the inlet fluid temperature during discharging reduces the BTES storage volume temperature. When the ground surrounding the BTES is a higher temperature than the periphery of the BTES storage volume, heat exchange direction is from the surrounding ground to the BTES.

The function shape of side/bottom heat loss (Figure 4.7) is not fully developed after 5 charge and discharge cycles. To ensure periodic steady state operation for the reduced model parameter sweep, simulation time is increased to 10 charge and discharge cycles. BTES fields with low ratios of borehole heat exchanger area to BTES storage volume area take more charge and discharge cycles to reach periodic steady state.

The outputs for top and side/bottom loss heat transfer rate approach periodic steady state when the operating conditions are a constant yearly cycle. This justifies the creation of a reduced model to classify the periodic steady state thermal response between a BTES storage volume and the surrounding air or ground. The constant operation and periodic steady state thermal response of the storage volume heat loss can be represented with thermal resistance values for BTES charging and discharging profiles, however, this model will be unable to replicate the change of direction for the BTES side/bottom loss heat transfer rate during discharging.
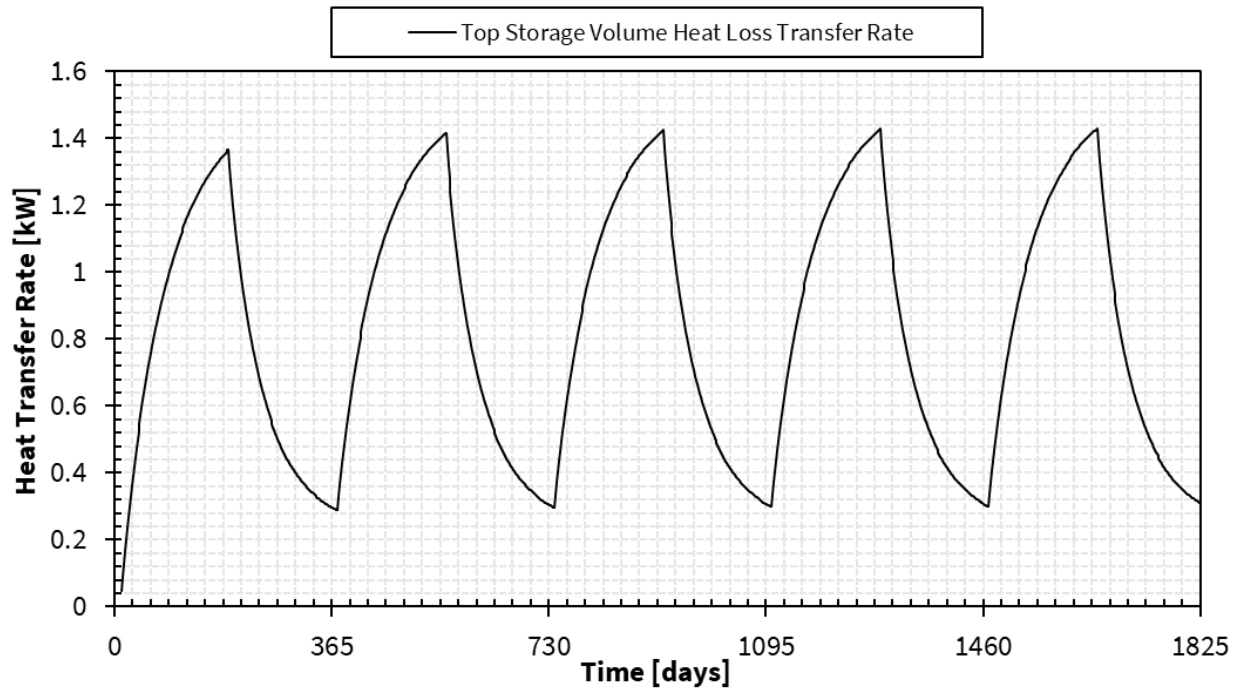
Figure 4.6: TRNSYS DST simulation output of BTES volume energy loss heat transfer rate through the top of the storage volume with respect to time for a 5-year simulation. A positive heat transfer rate represents energy exchange from the storage volume to the ambient air above the storage volume.
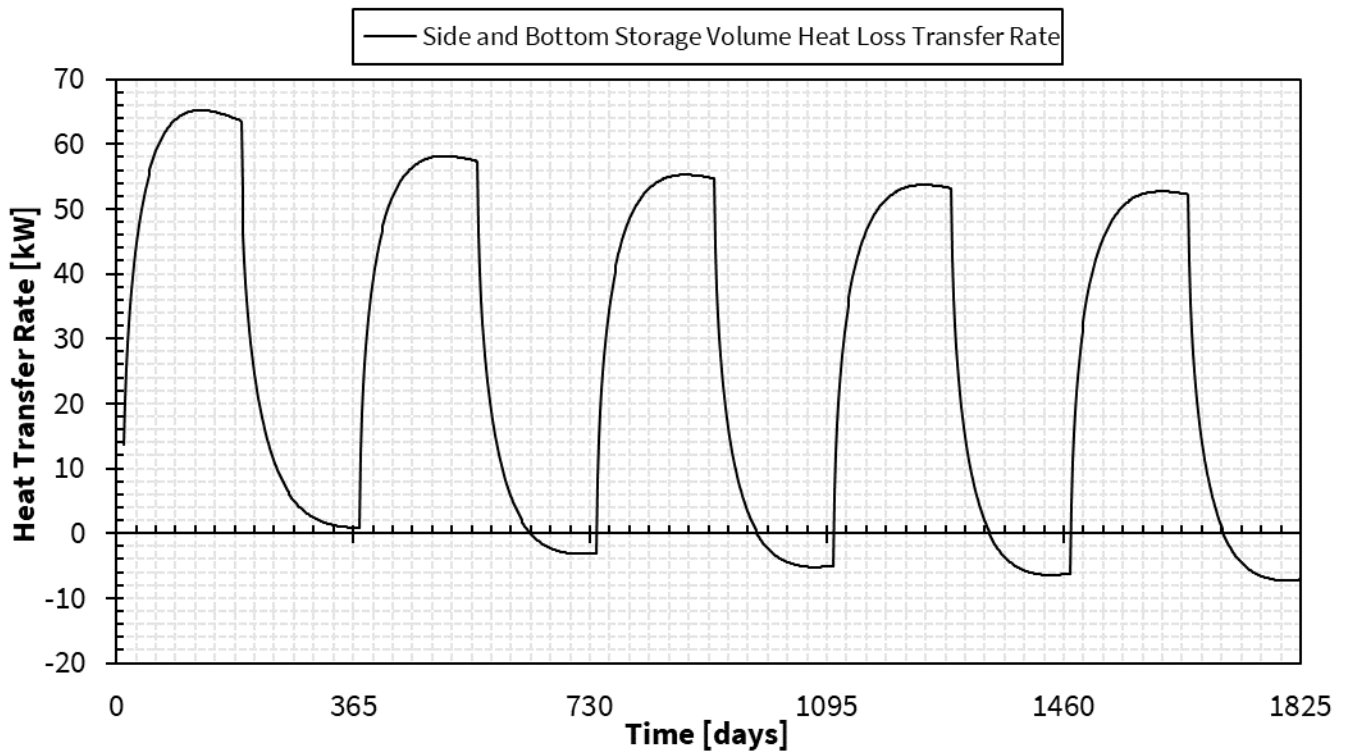
Figure 4.7: TRNSYS DST simulation output of BTES volume energy loss heat transfer rate through the sides and bottom of the storage volume with respect to time for a 5-year simulation. A positive heat transfer rate represents energy exchange from the storage volume to the ground volume surrounding the storage volume, and a negative heat transfer rate represents energy exchange from the surrounding ground volume to the storage volume.

4.5   Reference Simulation Integrated Results

The reference simulation reaches an approximate periodic steady state thermal response and thermal storage efficiency after 5 charge and discharge cycles (Figure 4.8). The difference between year 4 and year 5 thermal storage efficiency is 1% (Figure 4.9). To ensure all BTES fields of the reduced model parameter sweep reach periodic steady state operation, the simulation operation is increased to 10 charge and discharge cycles.

Total BTES energy loss through the storage volume's top during charging and discharging approach periodic steady state response by year 2 (Figure 4.10).

47

Total BTES energy loss through the storage volume's sides and bottom during discharging is significantly lower than during charging and decreases as the number of charge and discharge cycles increases (Figure 4.11). BTES discharging decreases the temperature of the BTES storage volume which will decrease the magnitude of total energy loss over the discharging timestep. As the number of charge and discharge cycles increases, the temperature of the ground surrounding the BTES storage volume increases and the magnitude of heat transfer from the surrounding ground to the BTES storage volume during discharging increases. Heat recovery from the ground surrounding the BTES during discharging counteracts heat loss and reduces the magnitude of periodic steady state total energy loss during discharging.

The magnitude of BTES heat exchanger total thermal energy exchange (Figure 4.8) is greater than the magnitudes of top (Figure 4.10) and side/bottom (Figure 4.11) total thermal energy loss over each 6-month timestep. The reduced model of BTES thermal response must prioritise accurately representing BTES heat exchanger thermal response over the heat loss thermal responses.
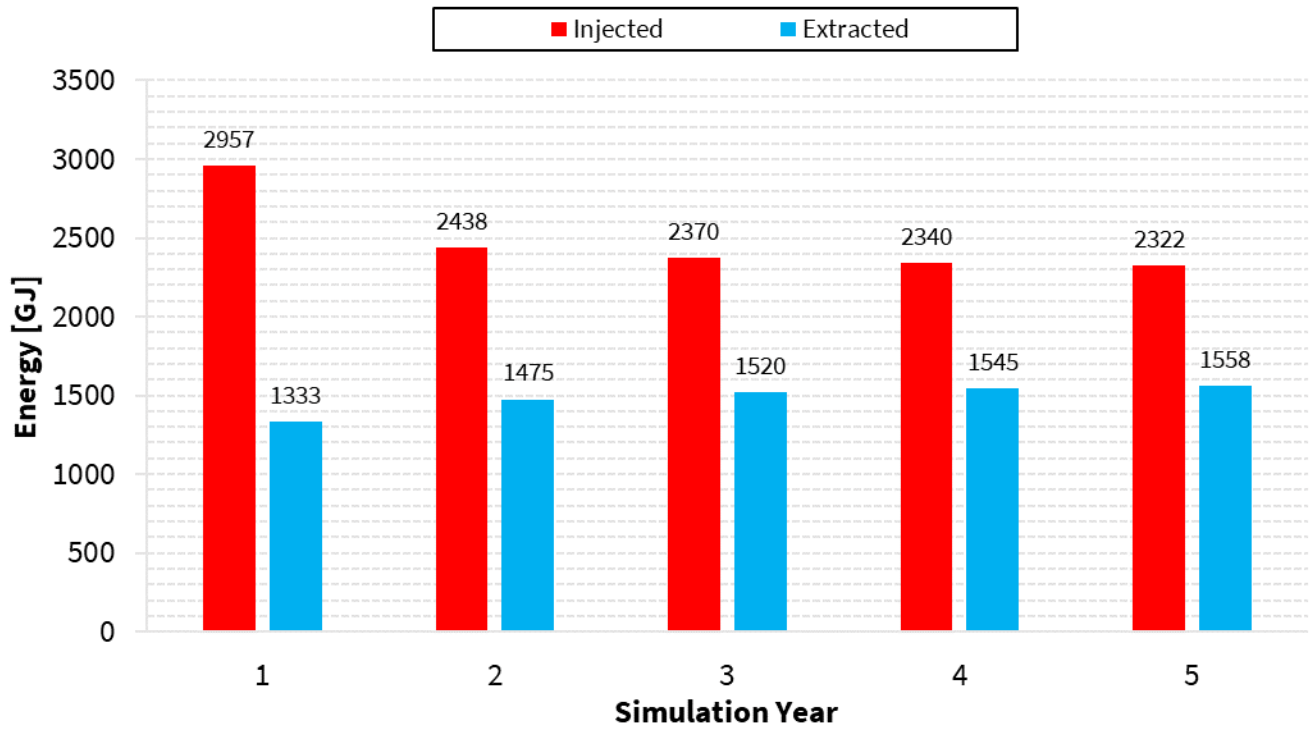
Figure 4.8: TRNSYS DST simulation integrated outputs for yearly total BTES energy injection and extraction for a 5-year simulation. Integrates borehole heat transfer rate from Figure 4.5 for yearly total energy injection, when the rate is positive, and yearly total extraction, when the rate is negative. Energy is injected into the BTES during charging and extracted from the BTES during discharging.
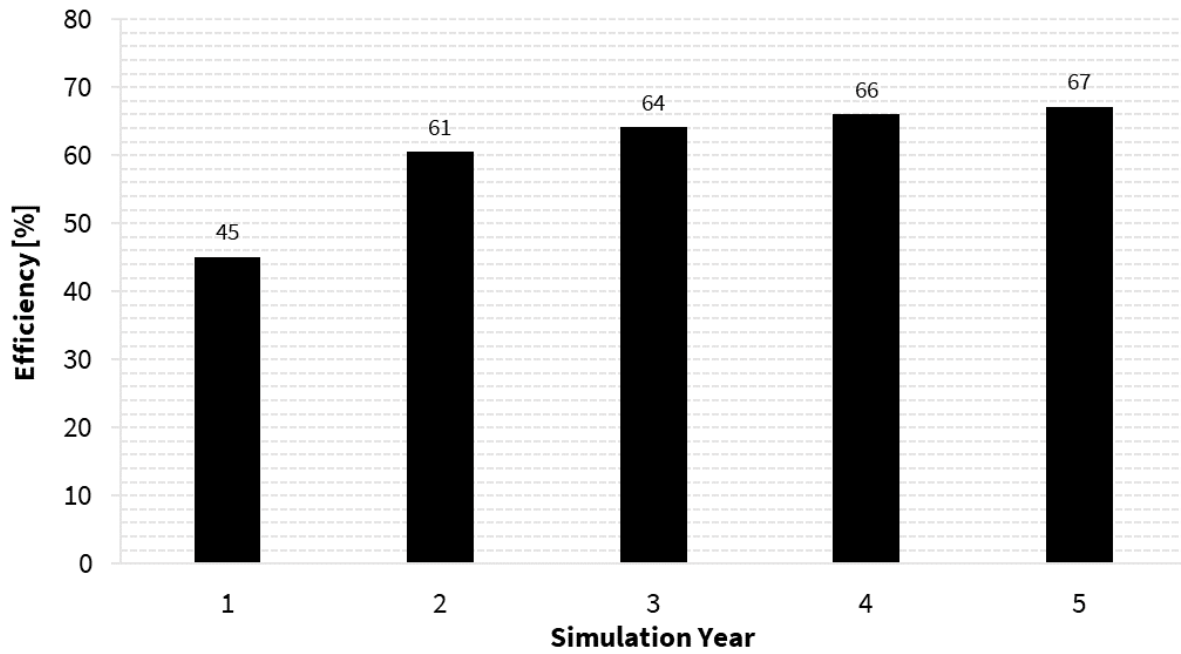
Figure 4.9: TRNSYS DST simulation integrated output of yearly thermal energy storage efficiency. Efficiency is calculated as the ratio of energy extracted to energy injected during a simulation year. The values of total energy injected and extracted in a year are displayed in Figure 4.8.
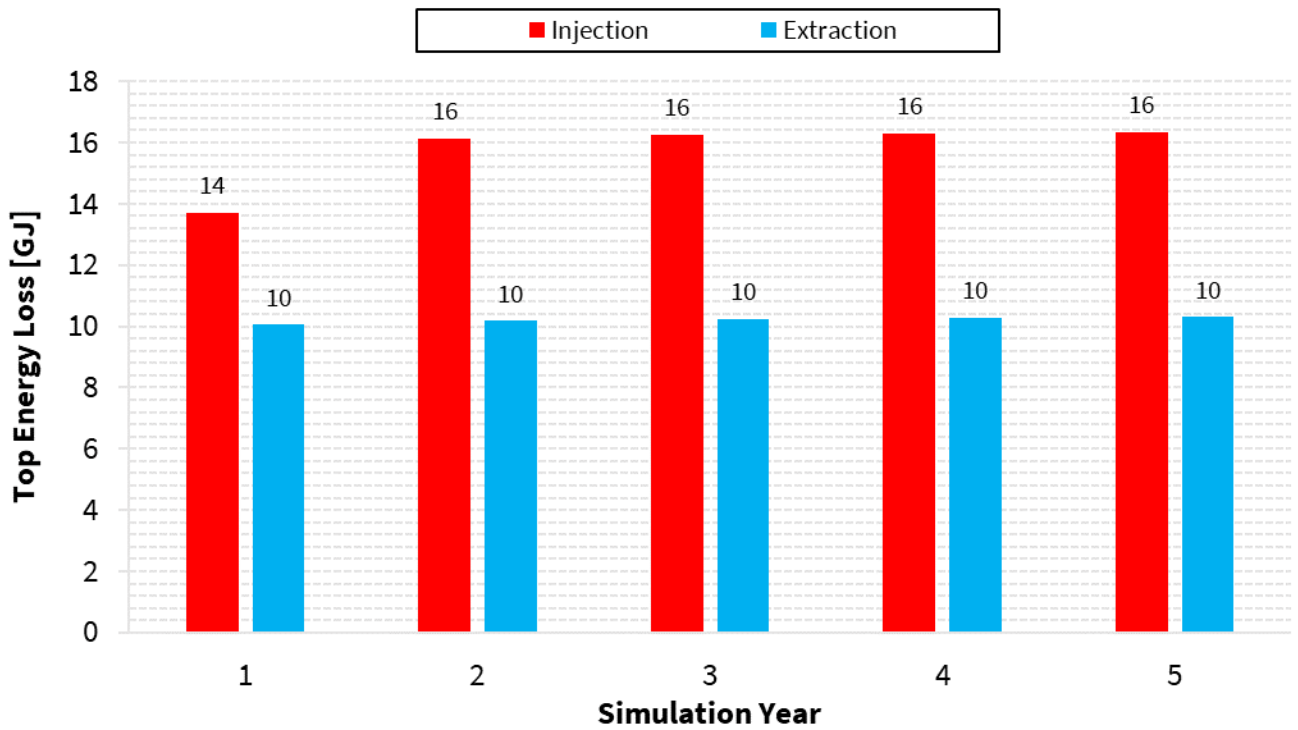
Figure 4.10: TRNSYS DST simulation integrated outputs for yearly total energy of BTES top heat loss during injection and extraction for a 5-year simulation. Integrates top loss heat transfer rate from Figure 4.6 depending on whether the heat carrier fluid is injecting or extracting heat at the time of the energy loss. Energy injection into the BTES happens during charging and extraction from the BTES happens during discharging.
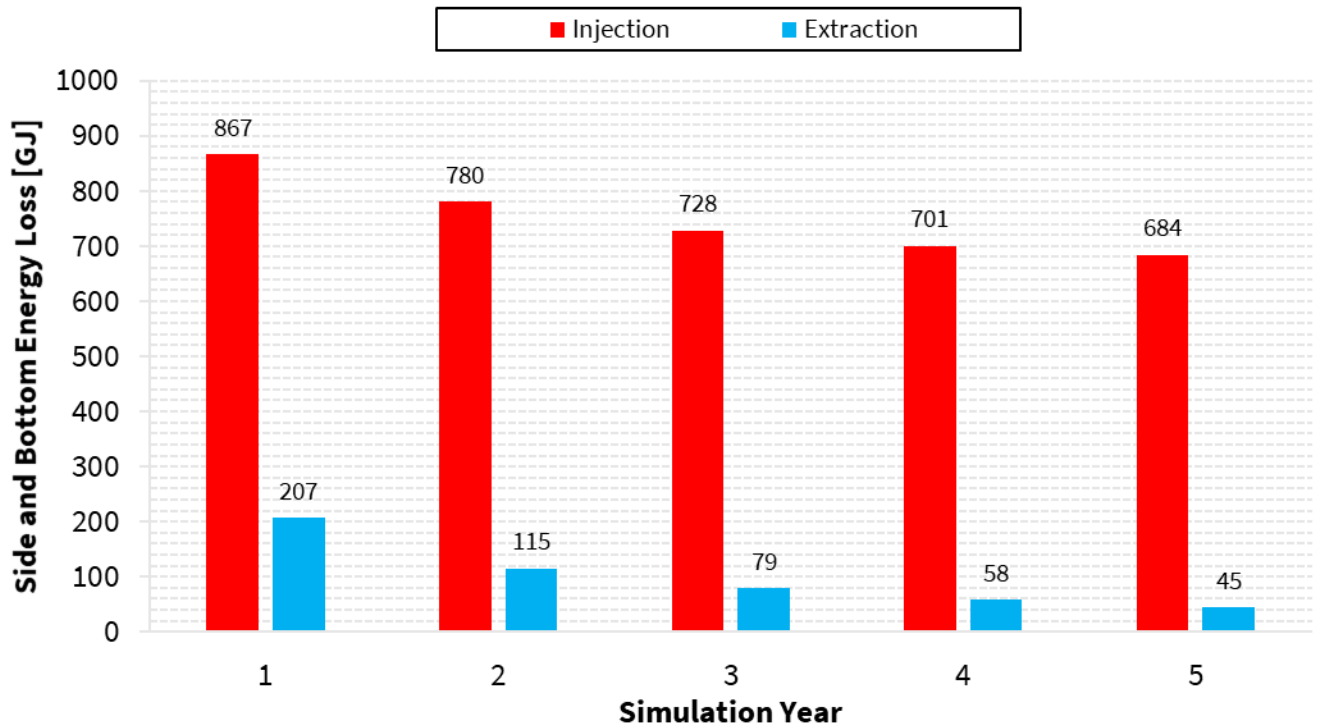
Figure 4.11: TRNSYS DST simulation integrated outputs for yearly total energy of BTES side and bottom heat loss during injection and extraction for a 5-year simulation. Integrates side and bottom loss heat transfer rates from Figure 4.7 depending on whether the heat carrier fluid is injecting or extracting heat at the time of the energy loss. Energy injection into the BTES happens during charging and extraction from the BTES happens during discharging.

4.6 Conclusion

The reference simulation provides an overview of the BTES thermal response to the simplified charging and discharging cycle which is the basis of the reduced model. All parameter sensitivity simulations follow the reference simulation's format to provide periodic steady state BTES data to be used by the reduced model. The parameter sensitivity simulations will be performed over 10 charge and discharge cycles to ensure periodic steady state operation is reached for all BTES fields. The periodic steady state constant charging and discharging cycle allows the reduced model to be represented by a series of thermal resistance values. The BTES

reduced model should accurately replicate heat exchanger thermal response over loss thermal responses due to heat exchanger thermal response having the greatest magnitude of total thermal energy exchange over each timestep.

5   Reduced Model and Parameter Sweep

5.1   Introduction

This chapter presents a simplified or "reduced" model to predict the performance of a borehole thermal energy storage (BTES) installation. The reduced model of BTES thermal response is formed from the solution of the BTES ground storage volume and heat exchanger fluid thermal energy equations. The energy equations are solved assuming constant charging and discharging operating conditions. The DST model implemented in TRNSYS simulates BTES thermal response and the TRNSYS solutions are used to generate thermal resistance values which are used in the reduced model. The effects of BTES design parameters on periodic steady state BTES thermal resistance is presented with respect to the reference simulation's design parameters. The reduced model and thermal resistance ranges provides engineers with a simplified tool for estimating BTES performance.

5.2   BTES Conservation of Thermal Energy Schematic
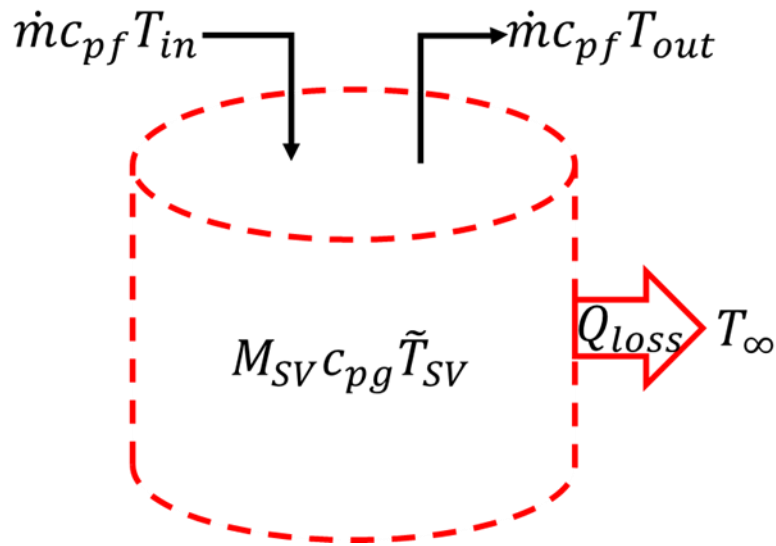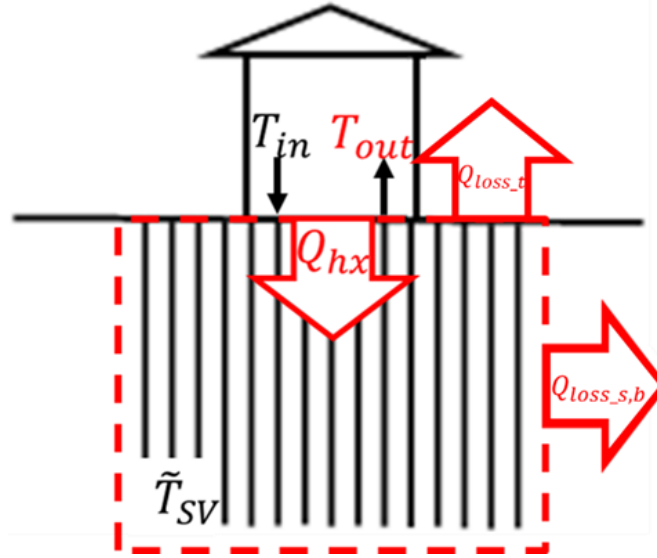
Figure 5.1: Schematics of the cylindrical BTES ground storage volume used for simplifying the thermal energy equations. The schematics show the average temperature of the storage volume is a function of the energy transfer imparted by the borehole heat exchanger and the energy lost to the storage volume's environment. Black arrows represent the direction of heat exchanger fluid, red arrows represent the direction of positive heat exchange.

$$\tilde{T}_f \xrightarrow{Q_{hx}} \tilde{T}_{SV} \begin{array}{c} \xrightarrow{Q_{loss\_t}} T_{\infty\_amb} \\ \xrightarrow[Q_{loss\_s,b}]{} T_{\infty\_ground} \end{array}$$

$$Q_{hx} = \frac{\tilde{T}_f - \tilde{T}_{SV}}{(R_{hx}/A_{TBA})}$$

$$Q_{loss\_t} = \frac{\tilde{T}_{SV} - T_{\infty\_amb}}{(R_{loss\_t}/A_{SV\_t})}$$

$$Q_{loss\_s,b} = \frac{\tilde{T}_{SV} - T_{\infty\_ground}}{(R_{loss\_s,b}/A_{SV\_s,b})}$$

Figure 5.2: The thermal resistance schematic of the reduced model which is the result of the thermal energy balance simplification.

5.3 BTES Thermal Energy Balance Solution Variable Definition

The energy balance for the BTES uses a lumped parameter approach with heat gains or losses of the storage volume calculated using thermal resistance modelling. The variables used in this model are defined in the table below.

Variable	Units	Definition
E_{SV}	J	Total energy content of the ground storage volume $M_{SV}c_{pg}\tilde{T}_{SV}$
E_f	J	Total energy content of the fluid mass circulating in the borehole heat exchangers

t	s	Time
Q_{hx}	J/s	Rate of heat exchange between the borehole heat exchanger area and the ground storage volume
Q_{loss}	J/s	Rate of heat exchange through the ground storage volume boundary a distance $r = \sqrt{(\#BH)} * (0.525 * Spacing)[m]$ from the central axis of the cylindrical ground storage volume and the top and bottom ground storage volume boundaries
$Q_{loss\_s,b}$	J/s	Rate of heat exchange through the ground storage volume boundary a distance $r = \sqrt{(\#BH)} * (0.525 * Spacing)[m]$ from the central axis of the cylindrical ground storage volume and the bottom ground storage volume boundary
Q_{loss_t}	J/s	Rate of heat exchange through the top boundary of the ground storage volume
$\dot{m}$	kg/s	Fluid mass flow rate through the BTES
M_{SV}	kg	Total ground storage volume mass
V	m^3	Volume of BTES ground storage $V=\pi*(\#BH)*H*(.525*Spacing)^2$
ρ_{SV}	kg/m^3	Density of the ground storage volume
c_{pf}	J/(kg*K)	Specific heat capacity of the heat exchanger fluid
c_{pg}	J/(kg*K)	Specific heat capacity of the ground storage volume
T_{in}	°C	Temperature of the heat exchanger fluid as it enters the BTES
T_{out}	°C	Temperature of the heat exchanger fluid as it exits the BTES
$\tilde{T}_f$	°C	Approximation of the average heat exchanger fluid temperature within the BTES $$\tilde{T}_f = \frac{1}{2}(T_{in} + T_{out})$$

$\tilde{T}_{SV}$	°C	Average temperature of the ground storage volume
$\tilde{T}_{SVi}$	°C	Initial average storage volume temperature when borehole charging or discharging begins
T_{∞_ground}	°C	Undisturbed average ground temperature at the location of the BTES installation
T_{∞_amb}	°C	Yearly average air temperature at the location of the BTES installation
A_{TBA}	m^2	Total borehole heat exchanger outer diameter circumferential area in contact with the ground storage volume $A_{TBA} = \pi*(\#BH)*H*D_{outer,BHE}$ (Reference simulation D$_{outer,BHE}$=0.15[m])
$A_{SV\_s,b}$	m^2	Total area of the side and bottom of the BTES storage volume. $$A_{SV\_s,b} = 2\pi H \left(\sqrt{(\#BH)} * 0.525 * Spacing \right) + \pi(\sqrt{(\#BH)} * 0.525 * Spacing)^2$$
A_{SV_t}	m^2	Top area of the BTES storage volume. $$A_{SV\_t} = \pi(\sqrt{(\#BH)} * 0.525 * Spacing)^2$$
R_{hx}	°C* m^2/W	Thermal resistance between the heat exchanger fluid and the ground storage volume with respect to the borehole heat exchangers' outer diameter circumferential area
$R_{loss\_s,b}$	°C* m^2/W	Thermal resistance between the ground storage volume and the ground surrounding the BTES with respect to the sum of the storage volume's side and bottom areas
R_{loss_t}	°C* m^2/W	Thermal resistance between the ground storage volume and the air above the BTES with respect to the storage volume's top area
A	-	Function constant
B	-	Function constant
α	-	Function constant

β	-	Function constant

Table 5.1: Variable definitions for the BTES reduced model thermal energy balance solution.

5.4 BTES Thermal Energy Balance Solution

The simplification of the thermal energy balance equation for BTES consists of the control volumes for the ground storage volume and the heat exchanger fluid. These are described below.

Ground:

The rate of change of the total energy content of the ground storage volume is the difference between the rate of heat flow imparted by the borehole heat exchangers and the rate of heat flow of the thermal losses for the ground storage volume.

$$\frac{dE_{SV}}{dt} = Q_{hx} - Q_{loss}$$

Fluid:

The rate of change for the total energy content of the BTES heat exchanger fluid is determined based on the rate of energy transfer by the fluid at the inlet and outlet and the rate of heat flow between the heat exchanger fluid and the ground storage volume. The heat exchanger fluid is incompressible so the mass flow of the BTES inlet is equal to the mass flow of the BTES outlet.

$$\frac{dE_f}{dt} = \dot{m}c_{pf}T_{in} - \dot{m}c_{pf}T_{out} - Q_{hx}$$

$$\frac{dE_f}{dt} = \dot{m}c_{pf}(T_{in} - T_{out}) - Q_{hx}$$

The rate of heat flow between the heat exchanger fluid and the ground storage volume is calculated using thermal resistance modelling. The rate of heat flow is represented as the ratio between the heat transfer driving temperature difference and the thermal resistance of the borehole heat exchangers with respect to the borehole heat exchangers' thermal contact area. The driving temperature difference is between the average temperature of the heat exchanger fluid ($\tilde{T}_f = \frac{1}{2}(T_{in} + T_{out})$) and the average temperature of the ground storage volume. The borehole heat exchangers' thermal contact area is approximated as the total borehole area (A_{TBA}).

$$Q_{hx} = \frac{A_{TBA}[\tilde{T}_f - \tilde{T}_{SV}(t)]}{R_{hx}} = \frac{A_{TBA}[\frac{1}{2}(T_{in} + T_{out}) - \tilde{T}_{SV}(t)]}{R_{hx}}$$

Ground:

The rate of heat flow for the thermal losses of the ground storage volume is represented by thermal resistance modelling. The rate of heat flow is represented as the ratio between the heat transfer driving temperature difference and the thermal resistance between the ground storage volume and the ground or air outside the storage volume with respect to the BTES storage volume's control surface area. The driving temperature difference is between the average temperature of the ground storage volume and the undisturbed ground or ambient air temperature. The rate of heat flow for the thermal losses is split into storage volume top surface and side/bottom surface components. The ground storage volume's top surface thermally interacts with the ambient air temperature above the storage volume through an insulation layer. The storage volume's side and bottom surfaces thermally interact with the undisturbed ground temperature of the ground surrounding the storage volume.

$$Q_{loss} = Q_{loss\_s,b} + Q_{loss\_t} = \frac{A_{SV\_s,b}[\tilde{T}_{SV}(t) - T_{\infty\_ground}]}{R_{loss\_s,b}} + \frac{A_{SV\_t}[\tilde{T}_{SV}(t) - T_{\infty\_amb}]}{R_{loss\_t}}$$

$$\frac{dE_{SV}}{dt} = Q_{hx} - Q_{loss\_s,b} - Q_{loss\_t}$$

The energy content of the ground storage volume is measured by the thermal capacity of the storage volume and the average storage volume temperature.

$$M_{SV}c_{pg}\frac{d\tilde{T}_{SV}(t)}{dt} = \frac{A_{TBA}[\frac{1}{2}(T_{in} + T_{out}) - \tilde{T}_{SV}(t)]}{R_{hx}} - \frac{A_{SV\_s,b}[\tilde{T}_{SV}(t) - T_{\infty\_ground}]}{R_{loss\_s,b}} - \frac{A_{SV\_t}[\tilde{T}_{SV}(t) - T_{\infty\_amb}]}{R_{loss\_t}}$$

$$M_{SV} = V\rho_{SV}$$

$$V\rho_{SV}c_{pg}\frac{d\tilde{T}_{SV}(t)}{dt} = \frac{A_{TBA}[\frac{1}{2}(T_{in} + T_{out}) - \tilde{T}_{SV}(t)]}{R_{hx}} - \frac{A_{SV\_s,b}[\tilde{T}_{SV}(t) - T_{\infty\_ground}]}{R_{loss\_s,b}} - \frac{A_{SV\_t}[\tilde{T}_{SV}(t) - T_{\infty\_amb}]}{R_{loss\_t}}$$

Fluid:

The reduced model assumes constant BTES fluid inlet temperature and mass flow rate. The total energy content rate for the heat exchanger fluid is neglected because the magnitude of the BTES ground storage volume's thermal mass is greater.

$$\frac{dE_f}{dt} \approx 0$$

$$\dot{m}c_{pf}(T_{in} - T_{out}) = Q_{hx}$$

$$\dot{m}c_{pf}(T_{in} - T_{out}) = \frac{A_{TBA}[\frac{1}{2}(T_{in} + T_{out}) - \tilde{T}_{SV}(t)]}{R_{hx}}$$

$$\left(\dot{m}c_{pf}R_{hx} + \frac{1}{2}A_{TBA}\right)T_{out} = \left(\dot{m}c_{pf}R_{hx} - \frac{1}{2}A_{TBA}\right)T_{in} + A_{TBA}\tilde{T}_{SV}(t)$$

$$T_{out} = \frac{\left(\dot{m}c_{pf}R_{hx} - \frac{1}{2}A_{TBA}\right)T_{in} + A_{TBA}\tilde{T}_{SV}(t)}{\left(\dot{m}c_{pf}R_{hx} + \frac{1}{2}A_{TBA}\right)}$$

$$A = \frac{\left(\dot{m}c_{pf}R_{hx} - \frac{1}{2}A_{TBA}\right)}{\left(\dot{m}c_{pf}R_{hx} + \frac{1}{2}A_{TBA}\right)}$$

$$B = \frac{A_{TBA}}{\left(\dot{m}c_{pf}R_{hx} + \frac{1}{2}A_{TBA}\right)}$$

$$T_{out} = AT_{in} + B\tilde{T}_{SV}(t)$$

Ground:

The fluid outlet temperature derivation from the heat exchanger fluid energy continuity simplification is substituted into the storage volume energy continuity simplification to create an ordinary differential equation with respect to the average temperature of the ground storage volume.

$$V\rho_{SV}c_{pg}\frac{d\tilde{T}_{SV}(t)}{dt} = \frac{A_{TBA}[\frac{1}{2}(T_{in} + AT_{in} + B\tilde{T}_{SV}(t)) - \tilde{T}_{SV}(t)]}{R_{hx}} - \frac{A_{SV\_s,b}[\tilde{T}_{SV}(t) - T_{\infty\_ground}]}{R_{loss\_s,b}} - \frac{A_{SV\_t}[\tilde{T}_{SV}(t) - T_{\infty\_amb}]}{R_{loss\_t}}$$

$$V\rho_{SV}c_{pg}\frac{d\tilde{T}_{SV}(t)}{dt} = \frac{\left(\frac{AA_{TBA}}{2} + \frac{A_{TBA}}{2}\right)T_{in} - (A_{TBA} - \frac{BA_{TBA}}{2})\tilde{T}_{SV}(t)}{R_{hx}} - \frac{A_{SV\_s,b}[\tilde{T}_{SV}(t) - T_{\infty\_ground}]}{R_{loss\_s,b}} - \frac{A_{SV\_t}[\tilde{T}_{SV}(t) - T_{\infty\_amb}]}{R_{loss\_t}}$$

$$V\rho_{SV}c_{pg}\frac{d\tilde{T}_{SV}(t)}{dt} = -\left\{\left(\frac{A_{TBA} - \frac{BA_{TBA}}{2}}{R_{hx}}\right) + \frac{A_{SV\_s,b}}{R_{loss\_s,b}} + \frac{A_{SV\_t}}{R_{loss\_t}}\right\}\tilde{T}_{SV}(t) + \left\{\left(\frac{\frac{AA_{TBA}}{2} + \frac{A_{TBA}}{2}}{R_{hx}}\right)T_{in} + \frac{A_{SV\_s,b}T_{\infty\_ground}}{R_{loss\_s,b}} + \frac{A_{SV\_t}T_{\infty\_amb}}{R_{loss\_t}}\right\}$$

$$\alpha = \frac{\left(\frac{A_{TBA} - \frac{BA_{TBA}}{2}}{R_{hx}}\right) + \frac{A_{SV\_s,b}}{R_{loss\_s,b}} + \frac{A_{SV\_t}}{R_{loss\_t}}}{V\rho_{SV}c_{pg}}$$

$$\beta = \frac{\left(\dfrac{\frac{AA_{TBA}}{2} + \frac{A_{TBA}}{2}}{R_{hx}}\right)T_{in} + \dfrac{A_{SV\_s,b}T_{\infty\_ground}}{R_{loss\_s,b}} + \dfrac{A_{SV\_t}T_{\infty\_amb}}{R_{loss\_t}}}{V\rho_{SV}c_{pg}}$$

$$\frac{d\tilde{T}_{SV}(t)}{dt} = -\alpha\tilde{T}_{SV}(t) + \beta$$

$$\frac{d\tilde{T}_{SV}(t)}{-\alpha\tilde{T}_{SV}(t) + \beta} = dt$$

$$\int_{\tilde{T}_{SVi}}^{\tilde{T}_{SV}(t)} \frac{1}{-\alpha\tilde{T}_{SV}(t) + \beta}\, d\tilde{T}_{SV}(t) = \int_0^t dt$$

$$-\frac{1}{\alpha}\ln\{-\alpha\tilde{T}_{SV}(t) + \beta\}\Big|_{\tilde{T}_{SVi}}^{\tilde{T}_{SV}(t)} = t$$

$$\ln\{-\alpha\tilde{T}_{SV}(t) + \beta\}\Big|_{\tilde{T}_{SVi}}^{\tilde{T}_{SV}(t)} = -\alpha t$$

$$\ln\{-\alpha\tilde{T}_{SV}(t) + \beta\} - \ln\{-\alpha\tilde{T}_{SVi} + \beta\} = -\alpha t$$

$$\ln\left\{\frac{-\alpha\tilde{T}_{SV}(t) + \beta}{-\alpha\tilde{T}_{SVi} + \beta}\right\} = -\alpha t$$

$$\frac{-\alpha\tilde{T}_{SV}(t) + \beta}{-\alpha\tilde{T}_{SVi} + \beta} = e^{-\alpha t}$$

$$\tilde{T}_{SV}(t) = -\frac{[-\alpha\tilde{T}_{SVi} + \beta]e^{-\alpha t} - \beta}{\alpha}$$

$$\tilde{T}_{SV}(t) = \frac{[\alpha\tilde{T}_{SVi} - \beta]e^{-\alpha t} + \beta}{\alpha}$$

5.5 Reduced Model Solution Summary

The solution for the average temperature of the storage volume with respect to time

depends on the values for the function constants: A, B, α, and β (Equation 1, 2, 3, and 4). The

components of the function constants are known for user specified BTES parameters and operation conditions except the thermal resistance values. The thermal resistance values for periodic steady state operation are calculated with the DST model for BTES installations with varying design parameters. The components of the reduced model of BTES thermal response include the simplified solution for the average temperature of the BTES storage volume and ranges of thermal resistance values required by the solution's function constants.

The ordinary differential equation solution predicts the average temperature of the storage volume with respect to time for constant BTES operation conditions (Equation 5). The average temperature of the storage volume with respect to time is used to predict the energy content of the storage volume (Equation 6), fluid outlet temperature (Equation 7), heat exchanger heat flow rate (Equation 8), and loss heat flow rates (Equation 9 and 10) with respect to time.

$$A = \frac{\left(\dot{m}c_{pf}R_{hx} - \frac{1}{2}A_{TBA}\right)}{\left(\dot{m}c_{pf}R_{hx} + \frac{1}{2}A_{TBA}\right)}$$

(1)

$$B = \frac{A_{TBA}}{\left(\dot{m}c_{pf}R_{hx} + \frac{1}{2}A_{TBA}\right)}$$

(2)

$$\alpha = \frac{\left(\dfrac{A_{TBA} - \dfrac{BA_{TBA}}{2}}{R_{hx}}\right) + \dfrac{A_{SV\_s,b}}{R_{loss\_s,b}} + \dfrac{A_{SV\_t}}{R_{loss\_t}}}{V\rho_{SV}c_{pg}}$$

(3)

$$\beta = \frac{\left(\dfrac{\frac{AA_{TBA}}{2} + \frac{A_{TBA}}{2}}{R_{hx}}\right) T_{in} + \dfrac{A_{SV\_s,b} T_{\infty\_ground}}{R_{loss\_s,b}} + \dfrac{A_{SV\_t} T_{\infty\_amb}}{R_{loss\_t}}}{V \rho_{SV} c_{pg}}$$

(4)

$$\tilde{T}_{SV}(t) = \frac{[\alpha \tilde{T}_{SVi} - \beta] e^{-\alpha t} + \beta}{\alpha}$$

(5)

$$E_{SV} = V \rho_{SV} c_{pg} \tilde{T}_{SV}(t)$$

(6)

$$T_{out} = A T_{in} + B \tilde{T}_{SV}(t)$$

(7)

$$Q_{hx} = \frac{A_{TBA}[\frac{1}{2}(T_{in} + T_{out}) - \tilde{T}_{SV}(t)]}{R_{hx}}$$

(8)

$$Q_{loss\_t} = \frac{A_{SV\_t}[\tilde{T}_{SV}(t) - T_{\infty\_amb}]}{R_{loss\_t}}$$

(9)

$$Q_{loss\_s,b} = \frac{A_{SV\_s,b}[\tilde{T}_{SV}(t) - T_{\infty\_ground}]}{R_{loss\_s,b}}$$

(10)

5.6   Reduced Model Operation Conditions, and Limitations

The reduced model of BTES thermal response is created from the simplification of the

BTES thermal energy balance equations and the thermal resistance values generated from the

DST model implemented in TRNSYS. The simplification of the thermal energy balance equations reduces the equations' complexity to a solvable form and sets the operation conditions and limitations for the reduced model's use. The reduced model's implementation of DST generated thermal resistance values imparts the limitations of the DST model to the reduced model.

The reduced model's operation assumes the temperature of the ground storage volume is represented by the average temperature of the storage volume. The temperature distribution of the ground storage volume is integrated into a single value to represent the total energy content of the storage volume and to reduce the complexity of the model. The reduced model's operation assumes the temperature distribution of the heat exchanger fluid from inlet to outlet is integrated into a single value. The heat transfer driving temperature difference of the reduced model's operation is between the average temperature of the heat exchanger fluid and the average temperature of the storage volume to reduce model complexity.

The reduced model's operation assumes the ground storage volume and the ground surrounding the BTES have constant density, specific thermal capacity, and thermal conductivity. The thermal properties of the BTES site's ground layers are integrated into a single value to reduce model complexity.

The ambient air temperature above the BTES is assumed to remain constant during BTES operation. Air temperature is represented by the BTES location's annual average air temperature. The undisturbed ground temperature for the BTES location provides an estimation of annual average air temperature above the BTES.

The undisturbed ground temperature for the BTES location is assumed to be constant and independent of depth below the ground's surface. This results in the reduced model's driving temperature difference for BTES thermal losses being the same for the side and bottom surfaces of the ground storage volume. BTES thermal losses through the side and bottom surfaces of the storage volume are between the same medium and with respect to the same temperature difference, therefore, the reduced model represents side and bottom heat transfer effects on the storage volume with a single thermal resistance value.

The reduced model considers the thermal mass of the borehole heat exchangers and heat exchanger fluid to be negligible relative to the thermal mass of the ground storage volume. The mass simplification results in the rate of change for the energy content of the BTES heat exchanger fluid to be neglected, therefore, the reduced model assumes all thermal energy exchange for the heat exchanger fluid is with the ground storage volume.

The reduced model assumes the heat exchanger fluid mass flow rate and inlet temperature are constant during BTES operation. The model approximates annual BTES thermal response with two 6-month states of BTES operation: charging and discharging.

The thermal resistance values used by the reduced model are generated by the DST model integrated into TRNSYS, therefore, the reduced model acquires the operation conditions and limitations of DST BTES simulations. The DST model does not account for the groundwater content of the BTES location, therefore, the reduced model does not simulate the convective heat transfer of the storage volume. The side and bottom loss thermal resistance only considering conductive heat transfer between the storage volume and the surrounding ground volume is a limitation of the reduced model, because convective heat transfer effects within the BTES storage volume can result in significant thermal losses and a reduction in storage efficiency.

The reduced model is limited to the simulation of axisymmetric BTES installations with constant borehole spacing within a hexagonal array, because of the limitations of the DST model. The reduced model's storage volume magnitude and dimensions are calculated by the same functions of number of boreholes, borehole depth, and borehole spacing as the DST model.

The thermal resistance values used by the reduced model are calculated for alternating constant charging and discharging BTES states from DST simulations at steady state operation. The reduced model simulates BTES thermal response assuming periodic steady state operation of the annual constant charging and discharging cycle.

The reduced model does not simulate the thermal mass of the ground surrounding the storage volume. The reduced model does not retain information of the ground temperature outside the storage volume boundary, therefore, it does not simulate the change in heat flow direction that occurs for periodic steady state discharging if the temperature of the storage volume decreases below the temperature of the ground outside the storage volume. The reduced model assumes the direction of BTES heat loss through the side and bottom boundaries to be from the storage volume to the surrounding ground.

5.7   Thermal Resistance Definitions

The thermal resistance values used by the reduced model are derived from TRNSYS DST simulations of BTES thermal response. The DST simulations are 10 years of alternating 6-month constant inlet fluid temperature and mass flow rate charging and discharging states. The inlet fluid temperature setpoints are 95°C for BTES charging and 20°C for BTES discharging. The charging inlet fluid temperature setpoint is 95°C because it is the maximum operation temperature of liquid water in BTES systems [25], and the discharging inlet fluid temperature

setpoint is 20°C as it is approximately room temperature. The fluid inlet temperature setpoints

for charging and discharging are chosen to maximize the temperature difference between the

heat exchanger fluid and the ground storage volume so the parameter sweep also presents

theoretical maximum periodic steady state thermal storage efficiencies of BTES with respect to

BTES design parameters. The impact of the inlet fluid temperature on the model performance is

assessed and results are presented in 5.9 Fluid Inlet Temperature Independence.

The thermal resistance values are derived from the periodic steady state DST

simulation's mean values for average fluid temperature ($\bar{\tilde{T}}_f$), average storage volume temperature

($\overline{\tilde{T}_{SV}}$), and heat flow rate ($Q_{hx}$, Q_{loss_t}, or $Q_{loss\_s,b}$) over the 6-month (4380 hour) charging or

discharging state. The values are normalized with respect to the thermal contact area of the heat

flow (A_{TBA}, A_{SV_t}, or $A_{SV\_s,b}$). The thermal resistance values of charging and discharging

presented in the parameter sweep are the average between the year 9 and 10 values, because

BTES thermal response is approximately at periodic steady state for year 9 and 10.

$$R_{hx} = \frac{\left(\bar{\tilde{T}}_f - \overline{\tilde{T}_{SV}}\right)A_{TBA}}{\left(\dfrac{\sum_{i=1}^{4380} Q_{hx_i}\, dt}{\Delta t}\right)}$$

$$R_{loss\_t} = \frac{\left(\overline{\tilde{T}_{SV}} - T_{\infty\_amb}\right)A_{SV\_t}}{\left(\dfrac{\sum_{i=1}^{4380} Q_{loss\_t_i}\, dt}{\Delta t}\right)}$$

$$R_{loss\_s,b} = \frac{(\overline{\tilde{T}}_{SV} - T_{\infty\_ground})A_{SV\_s,b}}{\left(\dfrac{\sum_{i=1}^{4380} Q_{loss\_s,b_i}\,\mathrm{d}t}{\Delta t}\right)}$$

The mean heat flow rate is calculated as the ratio of total energy imparted over the 6-month charging or discharging timestep to the timestep length, because thermal losses in TRNSYS DST operate on the simulation's global timestep which is greater than 1 hour.

If the periodic steady state thermal resistance of thermal losses through the sides and bottom is calculated to be a negative value, the thermal resistance can be approximated to approach infinity and the losses through the sides and bottom of the BTES storage volume over the timestep can be neglected.

5.8   Reduced Model Verification

The reduced model is compared to the TRNSYS DST simulation to prove its accurate representation of periodic steady state thermal response. The root mean square difference (RMSD) between the TRNSYS DST simulation and the reduced model is presented for the total 10 year simulation and each 6-month charging or discharging timestep for average storage volume temperature (Figure 5.3 and Figure 5.4), total energy of the storage volume (Figure 5.5), BTES fluid outlet temperature (Figure 5.6 and Figure 5.7), BTES heat exchanger heat flow rate (Figure 5.8 and Figure 5.9), BTES top loss heat flow rate (Figure 5.11 and Figure 5.12), and BTES side/bottom loss heat flow rate (Figure 5.14 and Figure 5.15). Percent difference of total energy application is presented for each 6-month charging or discharging timestep for BTES heat exchanger heat flow rate (Figure 5.10), BTES top loss heat flow rate (Figure 5.13), and BTES side/bottom loss heat flow rate (Figure 5.16).
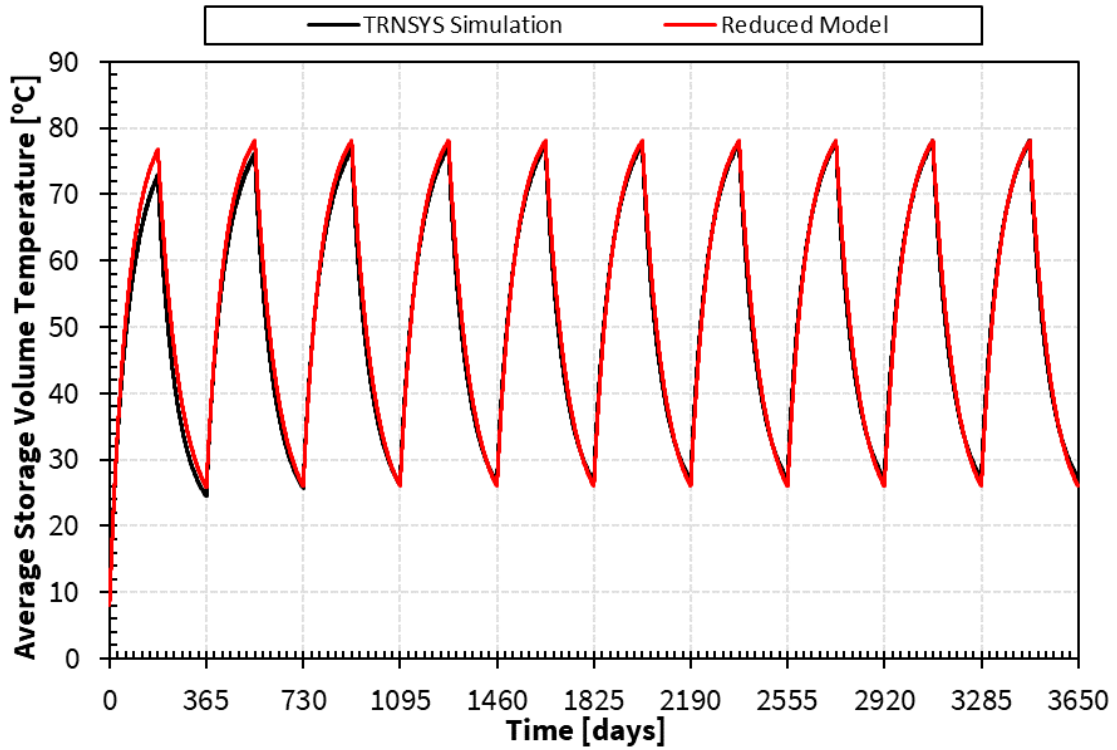
Figure 5.3: TRNSYS DST simulation output and reduced model approximation of average storage volume temperature with respect to time for a 10-year simulation (95 ℃ charging, 20 ℃ discharging). RMSD=1.74 ℃
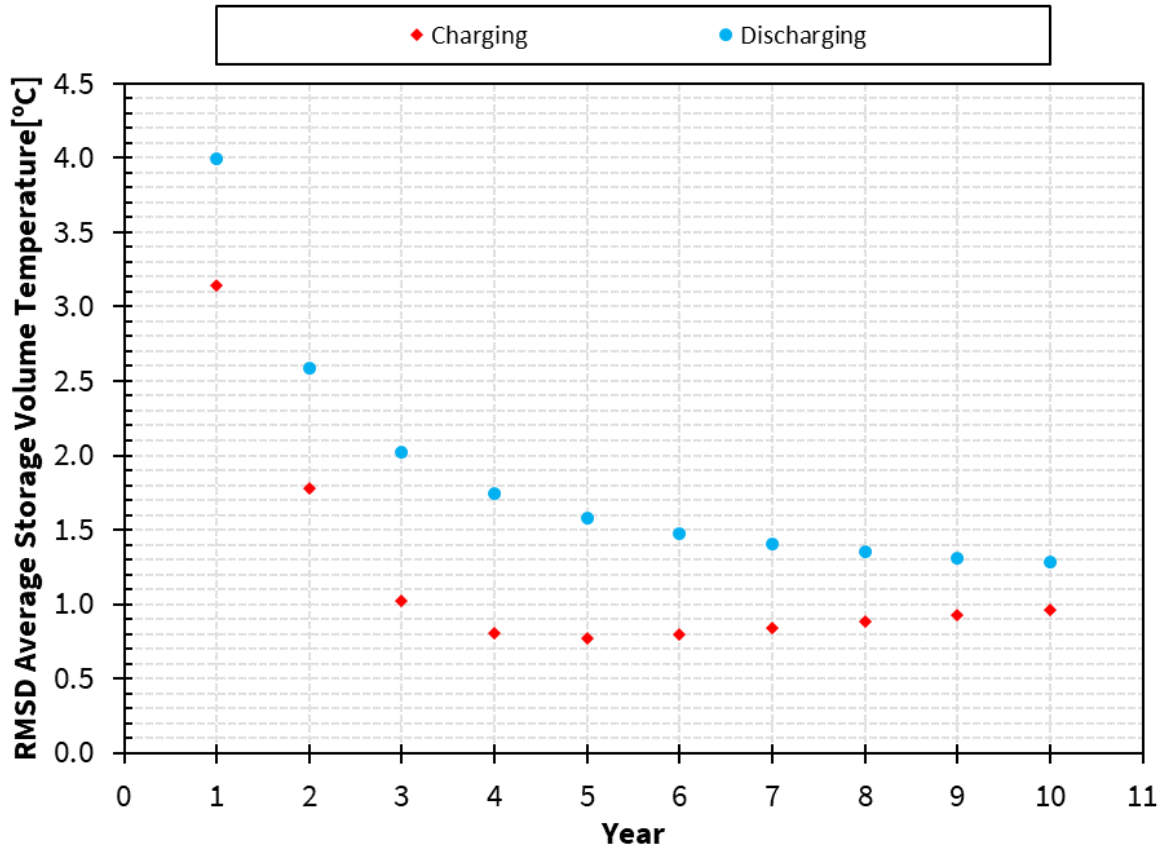
Figure 5.4: Yearly RMSD between the TRNSYS DST simulation output and the reduced model approximation of average storage volume temperature over each 6-month timestep for a 10-year simulation (95 ℃ charging, 20 ℃ discharging).
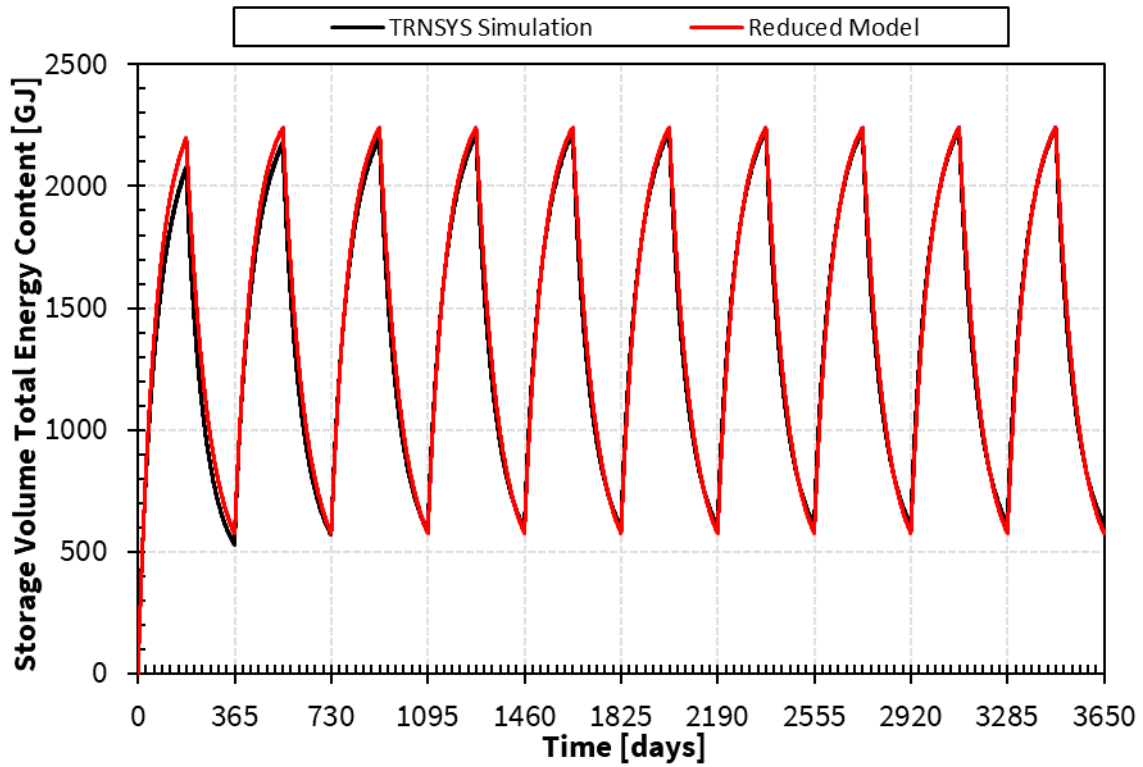
Figure 5.5: TRNSYS DST simulation output and reduced model approximation of BTES total energy content with respect to time for a 10-year simulation. BTES total energy content is calculated by applying the mass and thermal properties of the simulated BTES to $E(t)=V\rho c_p(\widetilde{T}_{SV}(t)-T_\infty)$ (95 °C charging, 20 °C discharging). RMSD=55 GJ
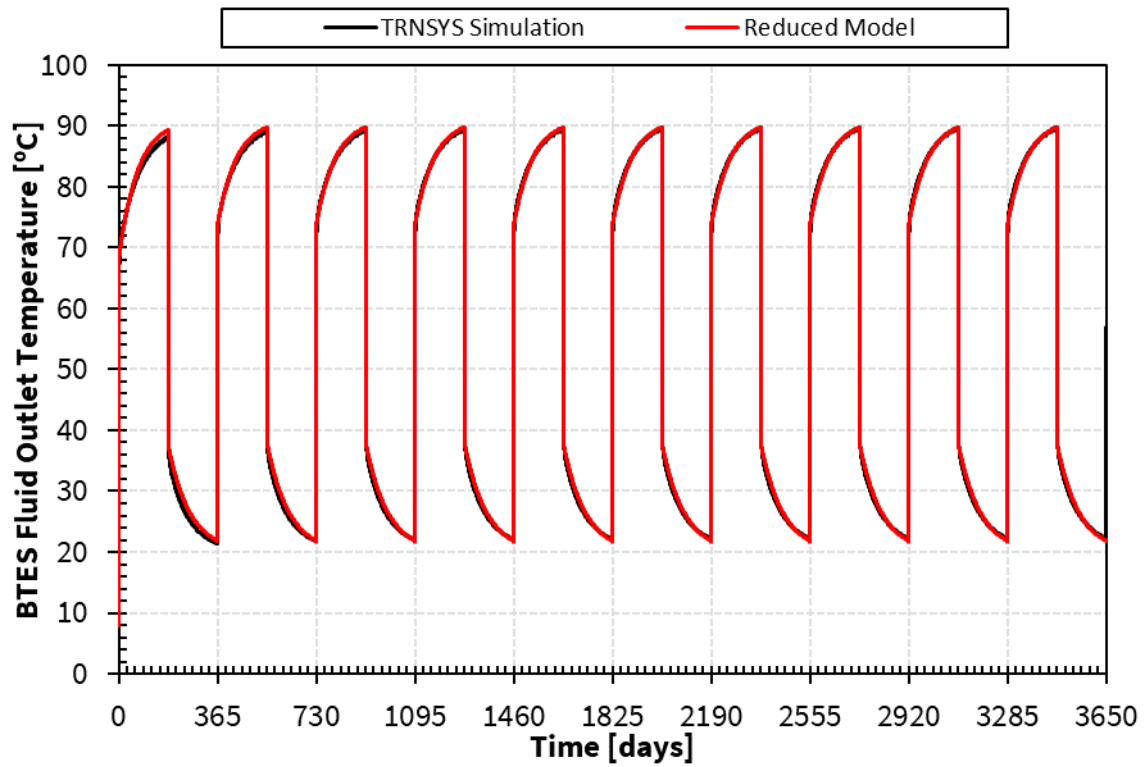
Figure 5.6: TRNSYS DST simulation output and reduced model approximation of fluid outlet temperature with respect to time for a 10-year simulation (95 ℃ charging, 20 ℃ discharging). RMSD=0.84 ℃
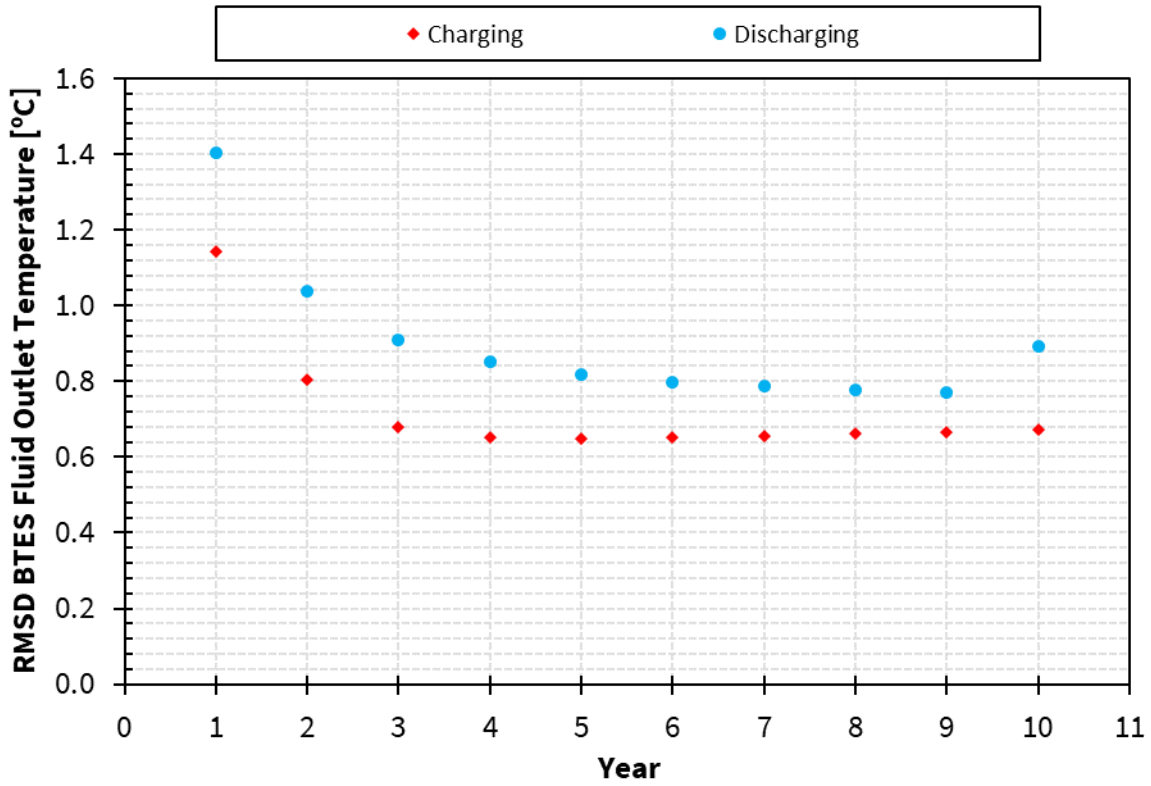
Figure 5.7: Yearly RMSD between the TRNSYS DST simulation output and the reduced model approximation of fluid outlet temperature over each 6-month timestep for a 10-year simulation (95 ℃ charging, 20 ℃ discharging).
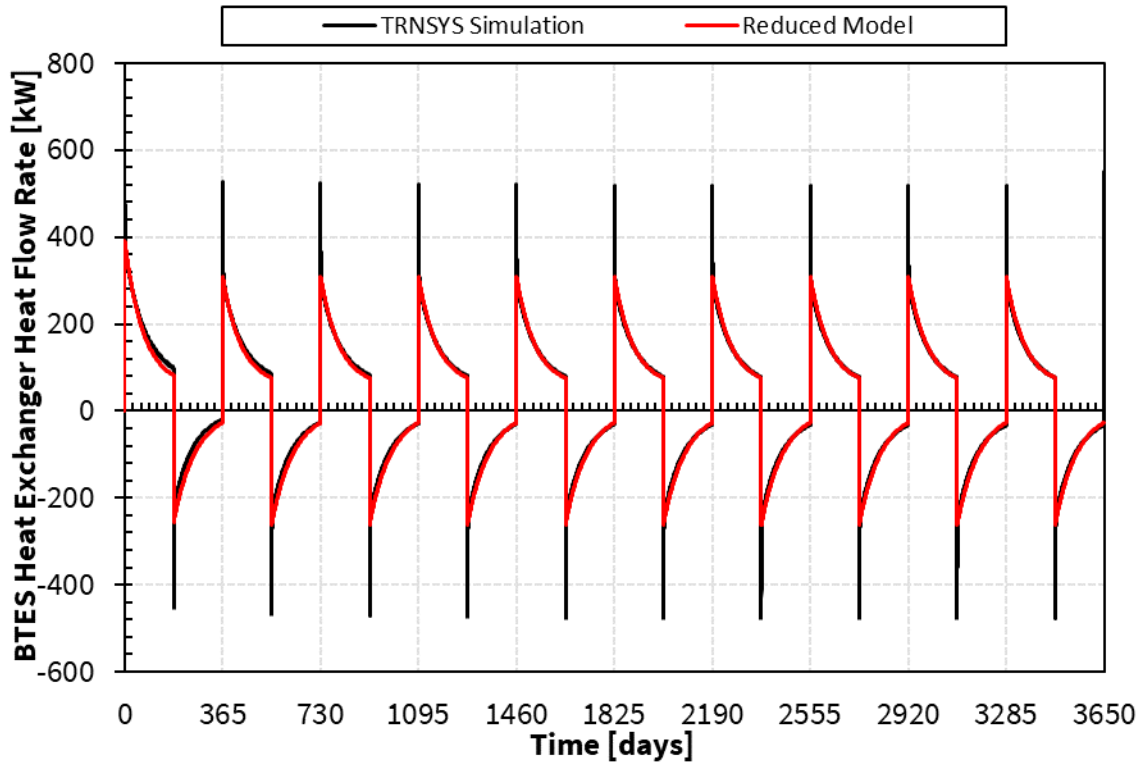
Figure 5.8: TRNSYS DST simulation output and reduced model approximation of BTES heat exchanger heat flow rate with respect to time for a 10-year simulation (95 ℃ charging, 20 ℃ discharging). RMSD=12.3 kW
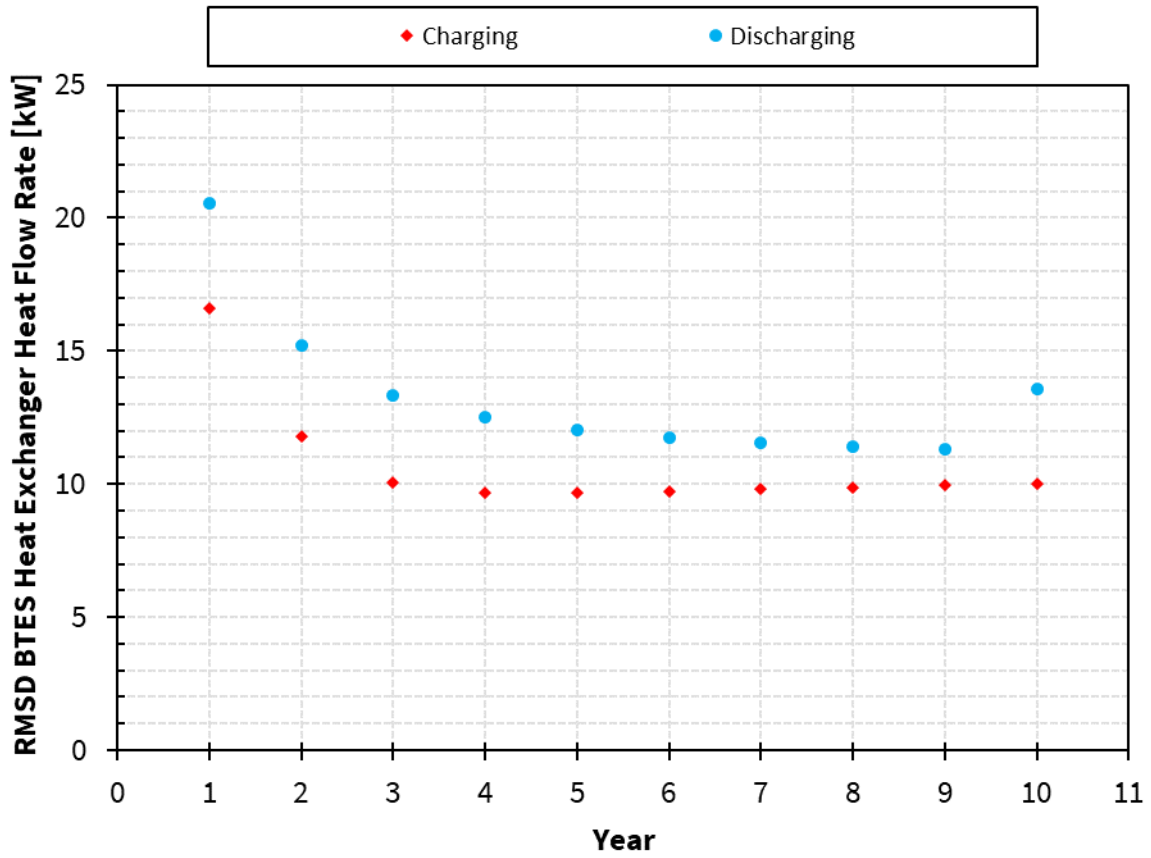
Figure 5.9: Yearly RMSD between the TRNSYS DST simulation output and the reduced model approximation of BTES heat exchanger heat flow rate over each 6-month timestep for a 10-year simulation (95 ℃ charging, 20 ℃ discharging).
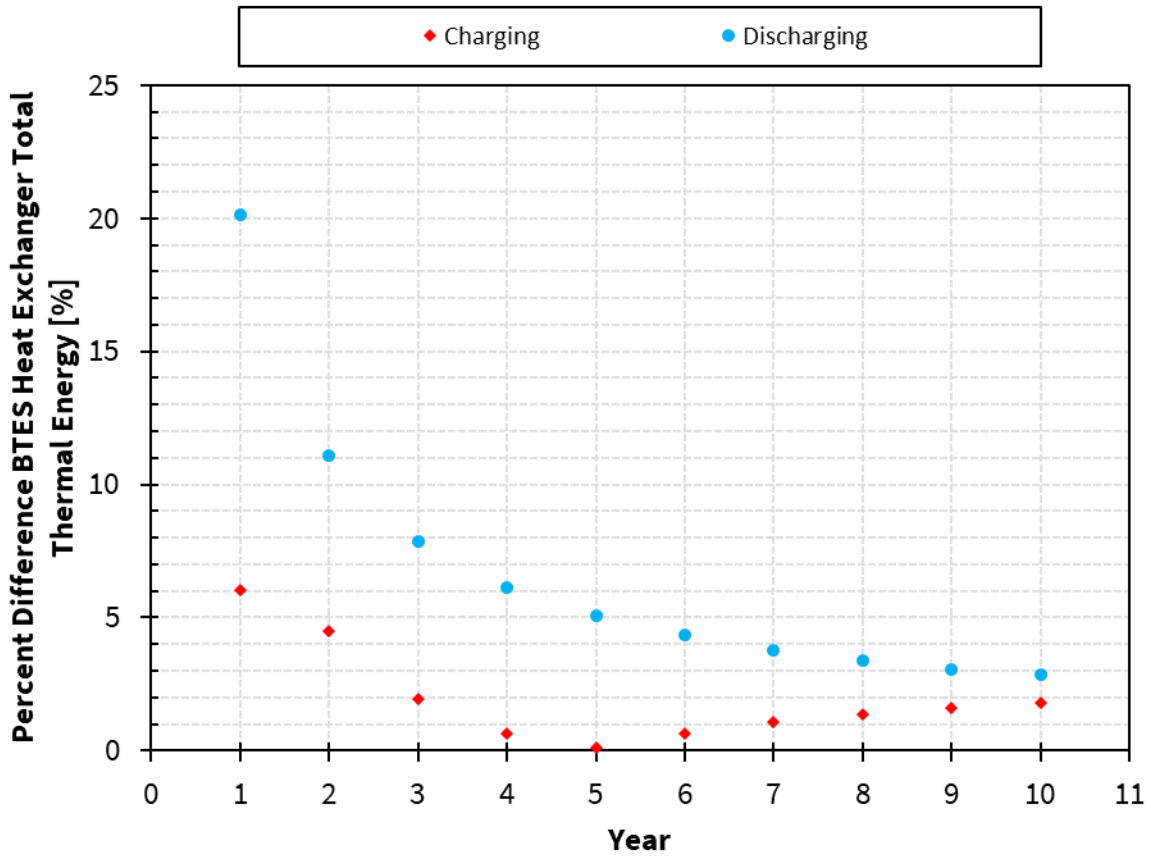
Figure 5.10: Yearly percent difference between the TRNSYS DST simulation output and the reduced model approximation of BTES heat exchanger total thermal energy application over each 6-month timestep for a 10-year simulation (95 ℃ charging, 20 ℃ discharging).
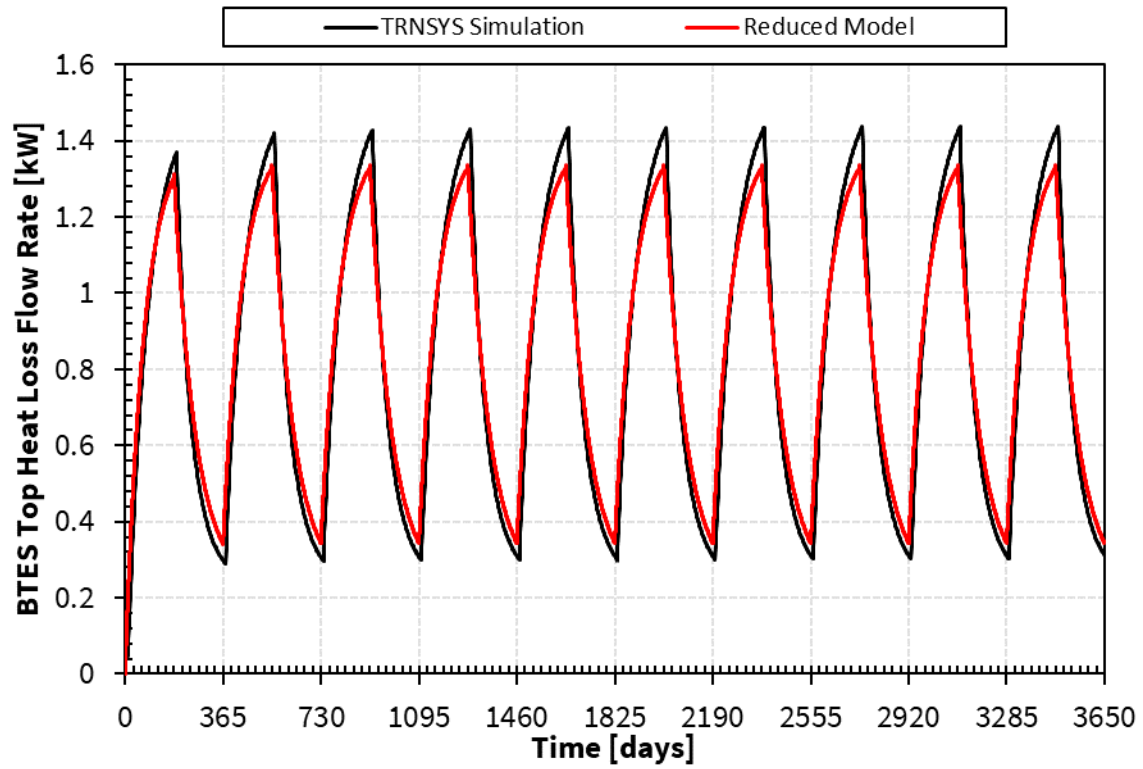
Figure 5.11: TRNSYS DST simulation output and reduced model approximation of BTES top loss heat flow rate with respect to time for a 10-year simulation (95 ℃ charging, 20 ℃ discharging). RMSD=7.01e-2 kW=70 W
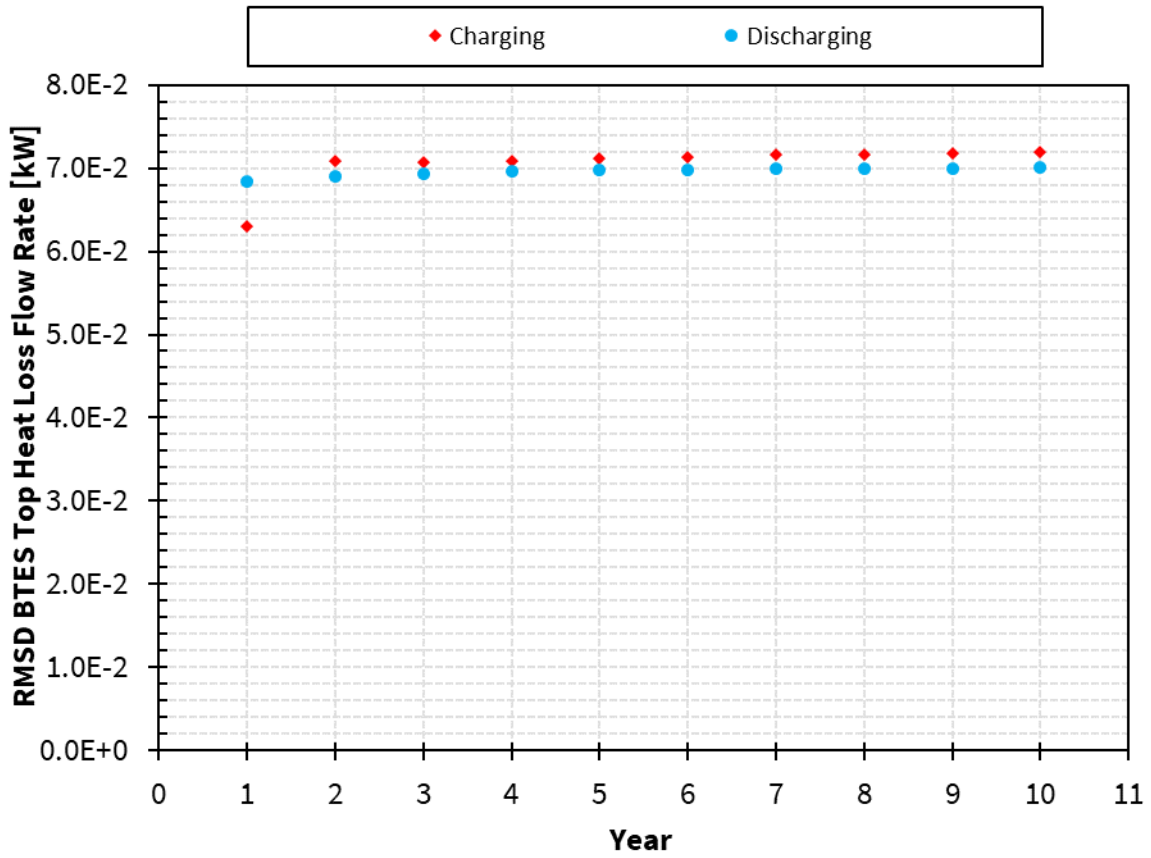
Figure 5.12: Yearly RMSD between the TRNSYS DST simulation output and the reduced model approximation of BTES top loss heat flow rate over each 6-month timestep for a 10-year simulation (95 ℃ charging, 20 ℃ discharging).
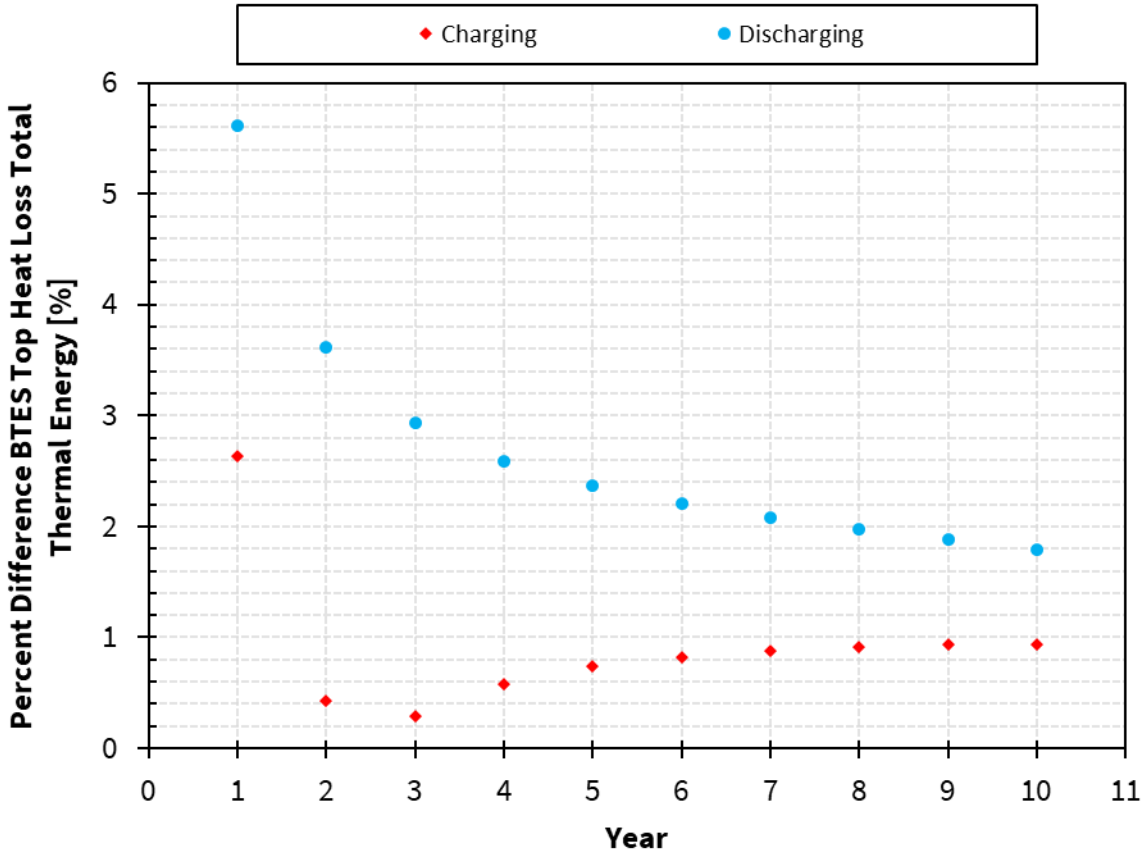
Figure 5.13: Yearly percent difference between the TRNSYS DST simulation output and the reduced model approximation of BTES total thermal energy loss through its top surface over each 6-month timestep for a 10-year simulation (95 ℃ charging, 20 ℃ discharging).
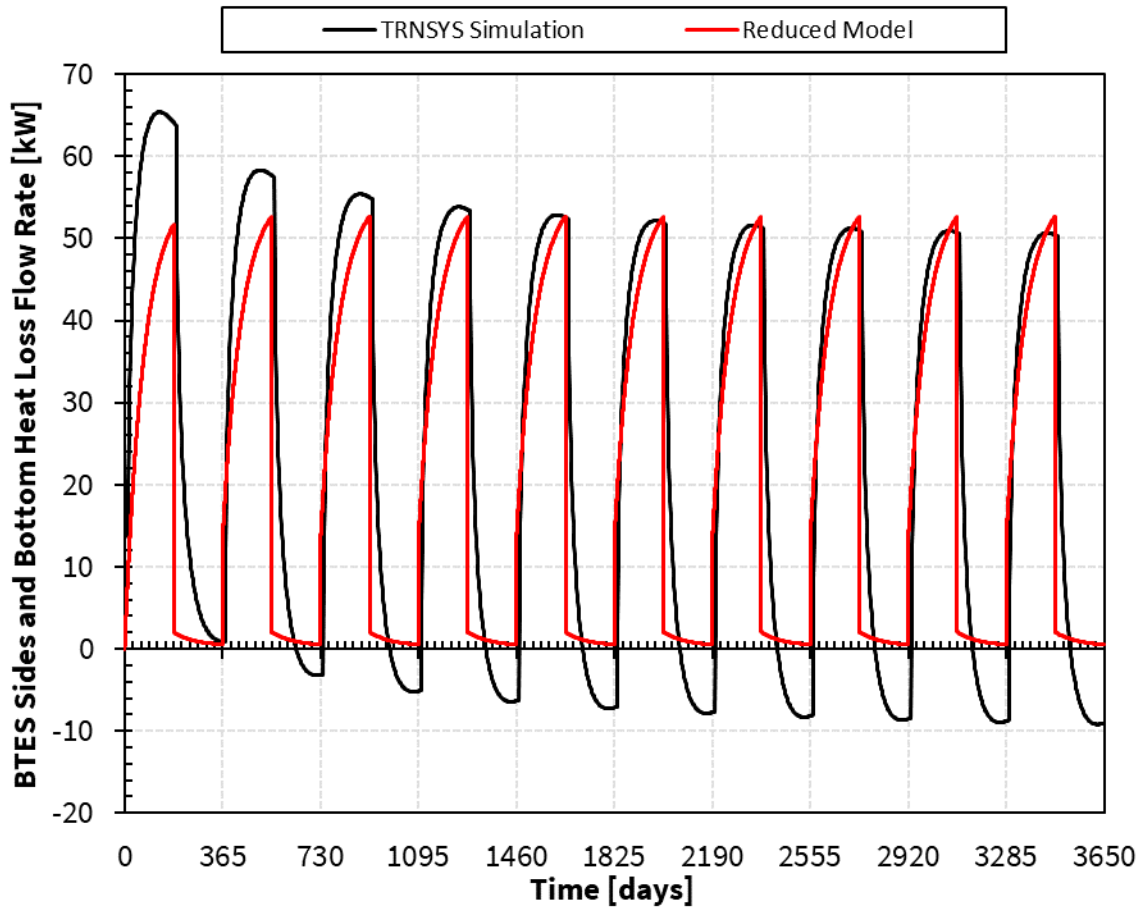
Figure 5.14: TRNSYS DST simulation output and reduced model approximation of BTES sides and bottom loss heat flow rate with respect to time for a 10-year simulation (95 ℃ charging, 20 ℃ discharging). RMSD=13.4 kW
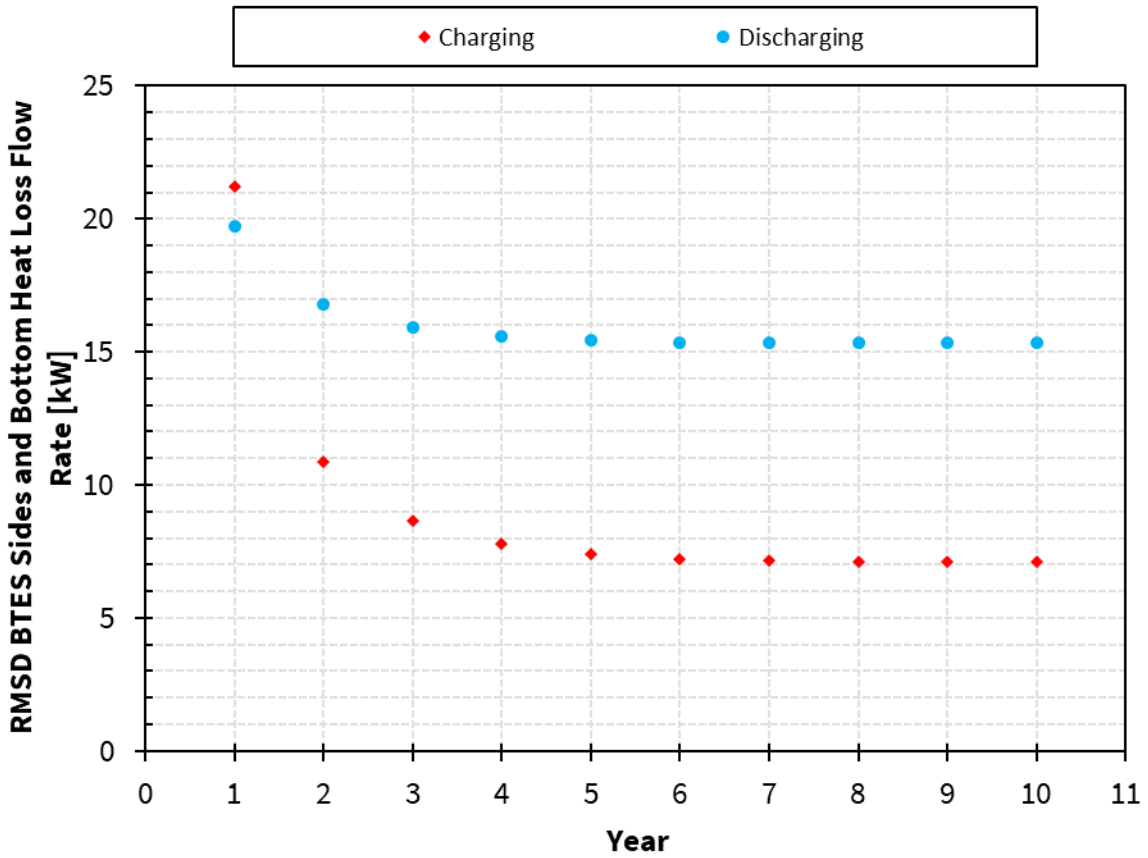
Figure 5.15: Yearly RMSD between the TRNSYS DST simulation output and the reduced model approximation of BTES sides and bottom loss heat flow rate over each 6-month timestep for a 10-year simulation (95 ℃ charging, 20 ℃ discharging).
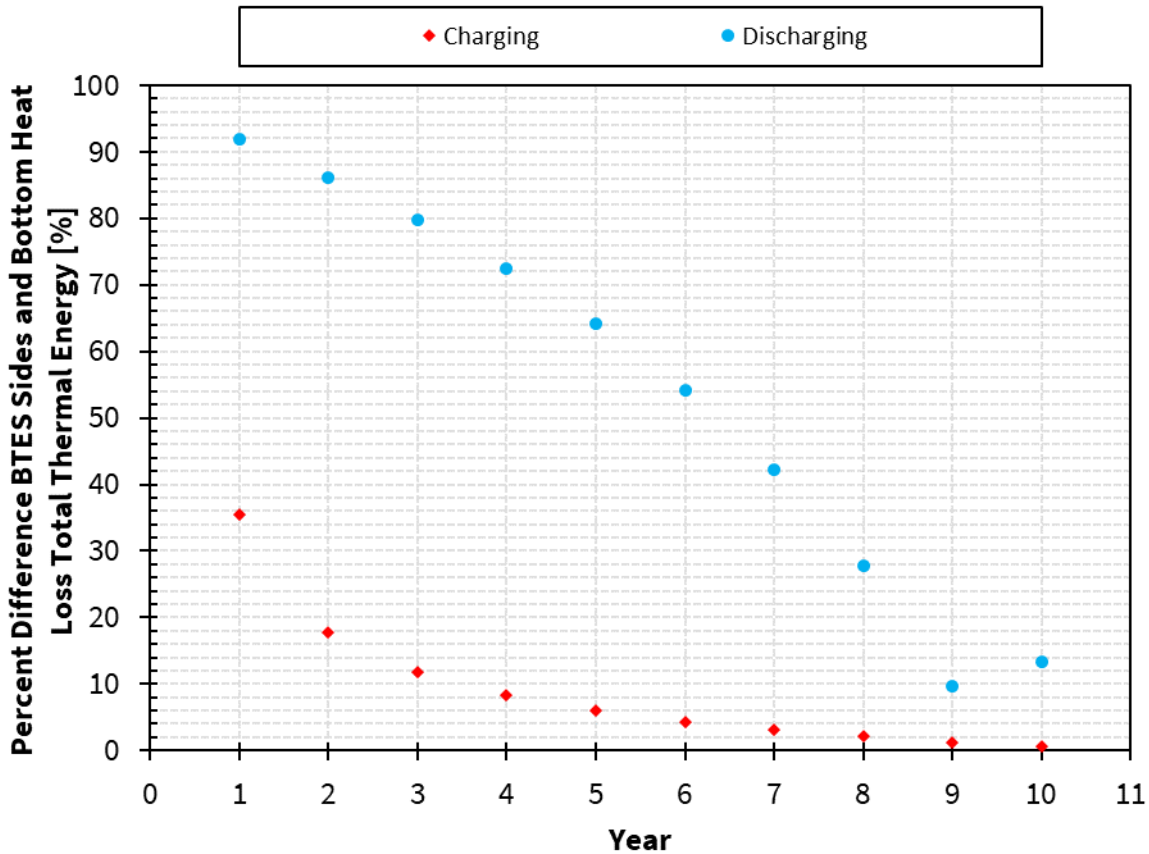
Figure 5.16: Yearly percent difference between the TRNSYS DST simulation output and the reduced model approximation of BTES total thermal energy loss through its side and bottom surfaces over each 6-month timestep for a 10-year simulation (95 ℃ charging, 20 ℃ discharging).

The reduced model demonstrates its ability to provide an accurate approximation of periodic steady state thermal response. The RMSD and percent total energy differences between the TRNSYS DST simulation and the reduced model's performance indicators decrease to acceptable levels as the TRNSYS DST simulation develops to a periodic steady state thermal response.

The reduced model does not retain information about the ground temperature outside the BTES storage volume boundary and it assumes the average storage volume temperature to be

interacting with the undisturbed ground temperature, therefore, the reduced model cannot represent the change in sides and bottom loss heat flow direction the TRNSYS DST simulation depicts (Figure 5.14). This occurs when the TRNSYS DST simulation switches from charging to discharging and the outer portion of the borehole field becomes cooler than the adjacent soil outside of the storage volume. The sides and bottom resistance value derivation includes the summation of total thermal energy losses through the sides and bottom surfaces, which includes a change in heat flow direction when the BTES reaches periodic steady state operation. This results in a lower magnitude of total thermal energy losses through the side and bottom surfaces over the 6-month timestep being incorporated into the side and bottom loss thermal resistance definition. The RMSD and percent difference of total energy application are greatest for side and bottom thermal losses during discharging, however, the effect of the discrepancy on the reduced model's accuracy is low due to the relative magnitude of total energy loss to the BTES heat exchanger total energy application. The relative magnitude of BTES storage volume side and bottom loss heat transfer rate is low compared to BTES heat exchanger heat transfer rate, therefore, negative derivations of side and bottom loss discharging timestep thermal resistances can be instead set to infinity which removes the side and bottom heat loss terms from the reduced model's function constants (Equation 3 and 4), removing side and bottom loss from the reduced model's approximation of average storage temperature (Equation 5).

5.9   Fluid Inlet Temperature Independence

Temperature independence of the reduced model is tested by changing the inlet fluid temperature setpoints of BTES charging and discharging for the reduced model and the TRNSYS DST simulation and verifying the agreement of their outputs. The BTES charging inlet temperature setpoint is changed from 95 ºC to 60 ºC, and the BTES discharging inlet temperature

setpoint is changed from 20 ℃ to 12 ℃. The thermal resistance values used by the reduced model, which are calculated from the TRNSYS DST simulation outputs operating with inlet temperature setpoints of 95 ℃ and 20 ℃, are unchanged when the reduced model is used to predict BTES thermal response for different inlet fluid temperature setpoints.

The root mean square difference (RMSD) between the TRNSYS DST simulation and the reduced model is presented for the total 10 year simulation and each 6-month charging or discharging timestep for average storage volume temperature (Figure 5.17 and Figure 5.18), total energy of the storage volume (Figure 5.19), BTES fluid outlet temperature (Figure 5.20 and Figure 5.21), BTES heat exchanger heat flow rate (Figure 5.22 and Figure 5.23), BTES top loss heat flow rate (Figure 5.25 and Figure 5.26), and BTES side/bottom loss heat flow rate (Figure 5.28 and Figure 5.29). Percent difference of total energy application is presented for each 6-month charging or discharging timestep for BTES heat exchanger heat flow rate (Figure 5.24), BTES top loss heat flow rate (Figure 5.27), and BTES side/bottom loss heat flow rate (Figure 5.30).
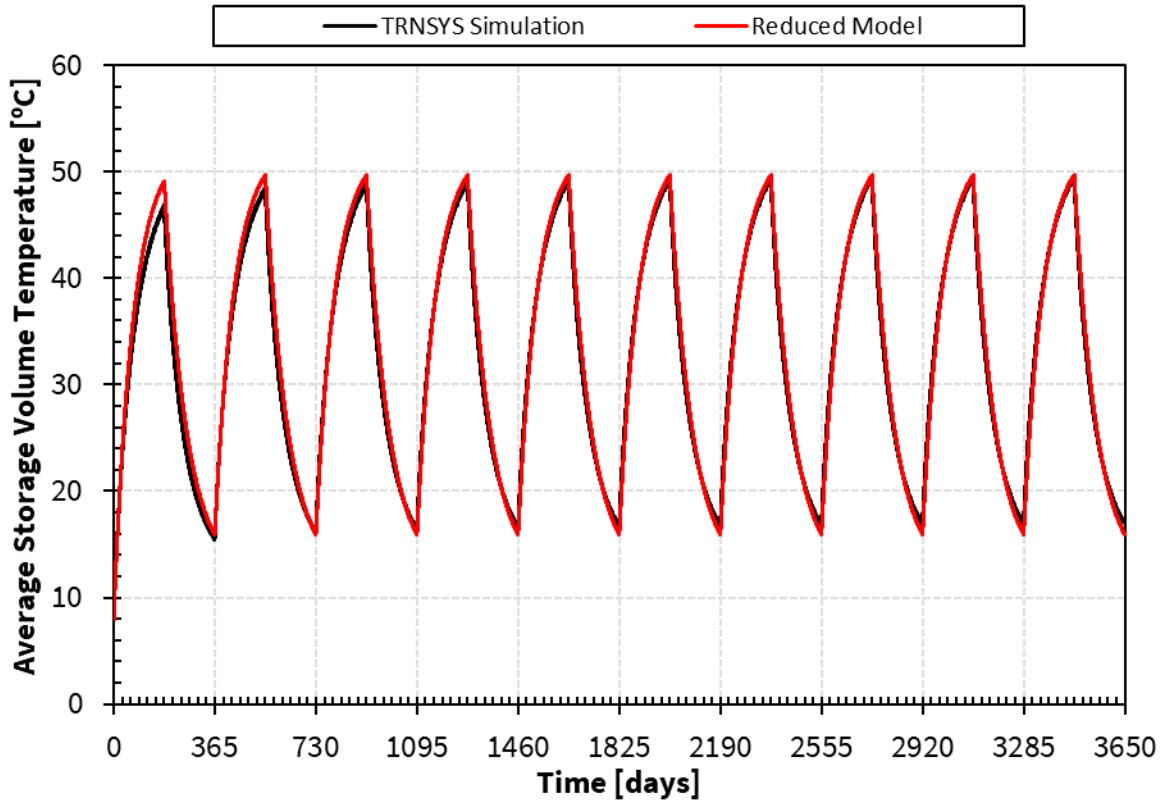
Figure 5.17: TRNSYS DST simulation output and reduced model approximation of average storage volume temperature with respect to time for a 10-year simulation (60 ℃ charging, 12 ℃ discharging). RMSD=1.06℃
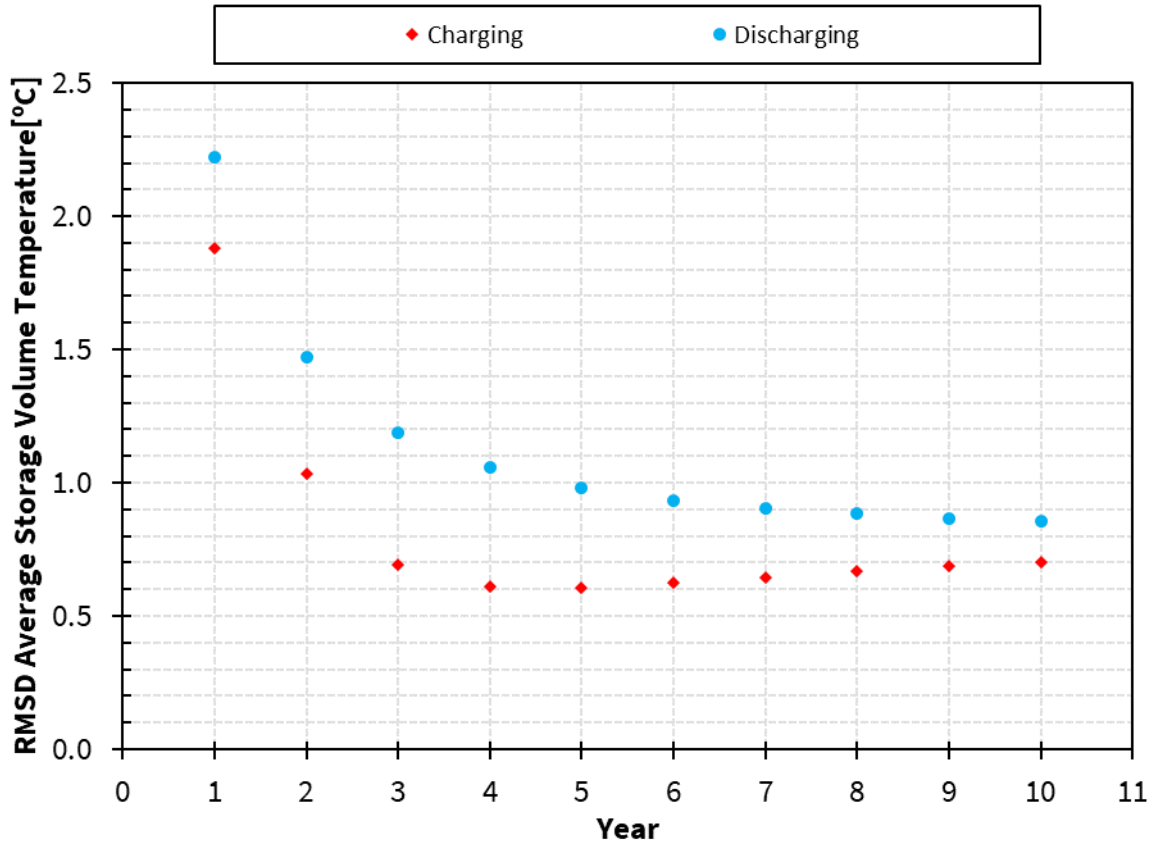
Figure 5.18: Yearly RMSD between the TRNSYS DST simulation output and the reduced model approximation of average storage volume temperature over each 6-month timestep for a 10-year simulation (60 ℃ charging, 12 ℃ discharging).
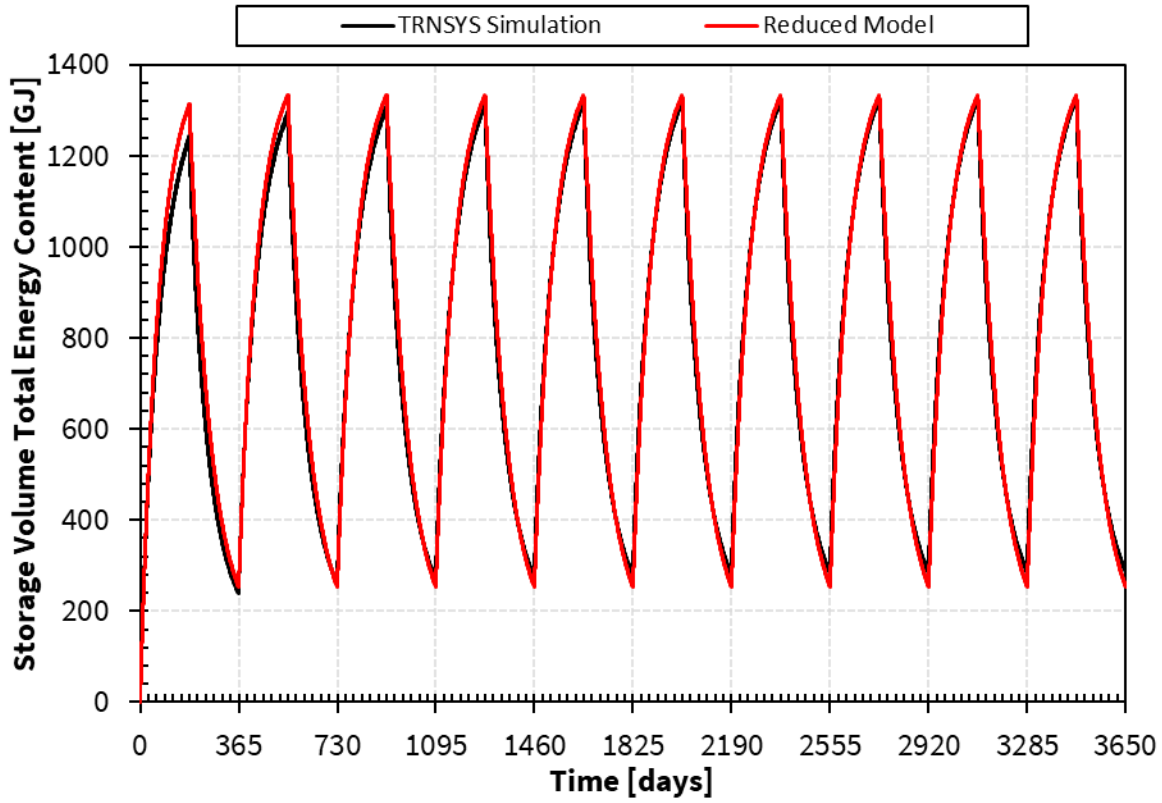
Figure 5.19: TRNSYS DST simulation output and reduced model approximation of BTES total energy content with respect to time for a 10-year simulation. BTES total energy content is calculated by applying the mass and thermal properties of the simulated BTES to $E(t)=V\rho c_p(\tilde{T}_{SV}(t)-T_\infty)$ (60 ℃ charging, 12 ℃ discharging). RMSD=34GJ
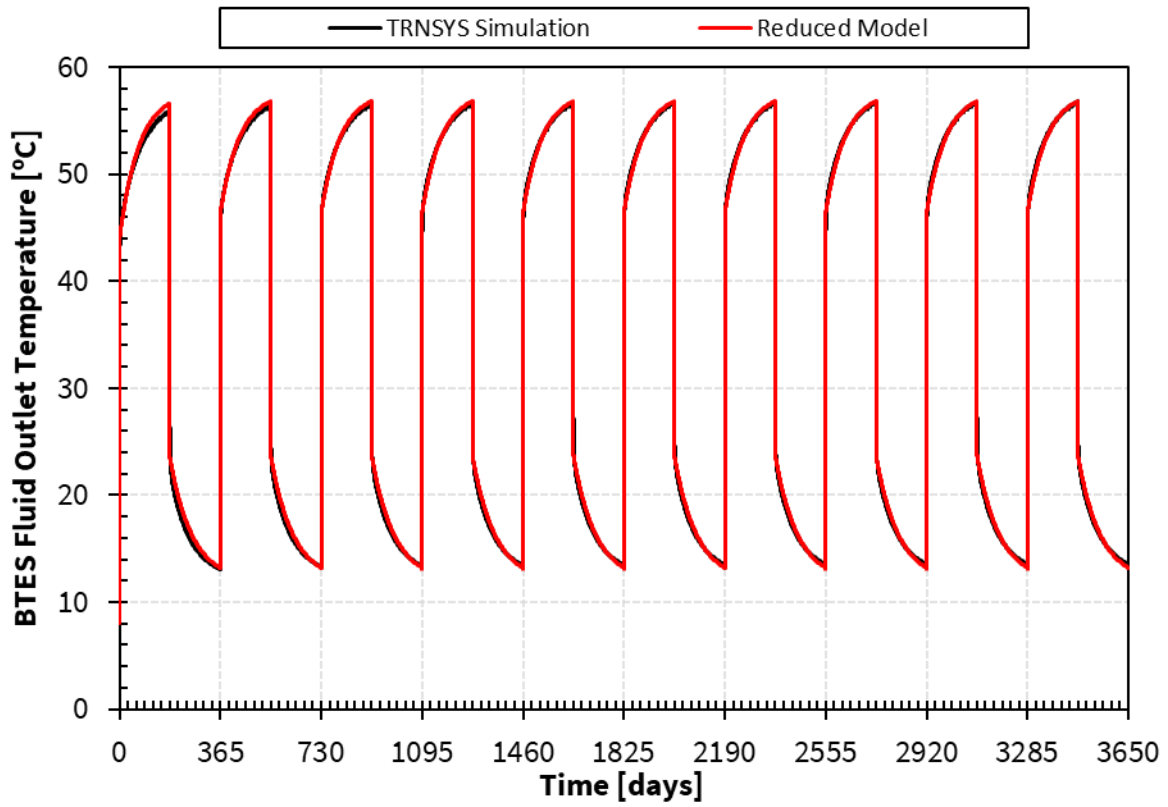
Figure 5.20: TRNSYS DST simulation output and reduced model approximation of fluid outlet temperature with respect to time for a 10-year simulation (60 ℃ charging, 12 ℃ discharging). RMSD=0.52 ℃
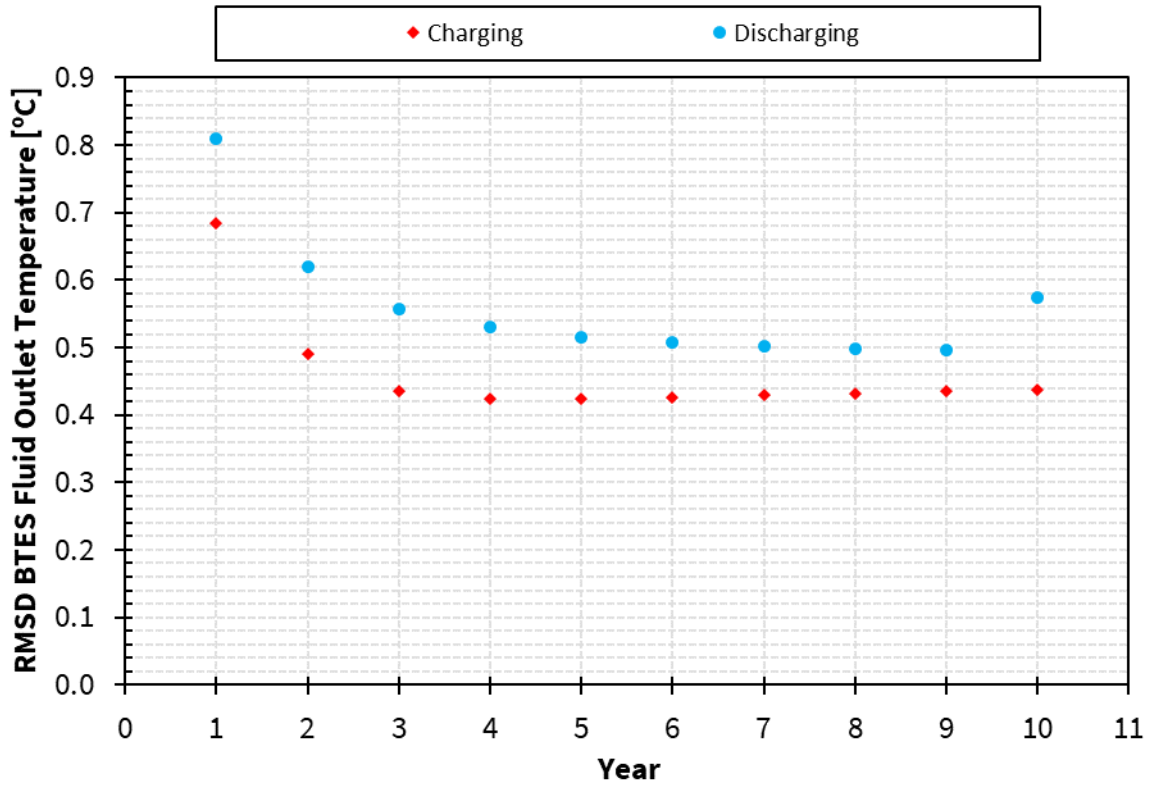
Figure 5.21: Yearly RMSD between the TRNSYS DST simulation output and the reduced model approximation of fluid outlet temperature over each 6-month timestep for a 10-year simulation (60 ℃ charging, 12 ℃ discharging).
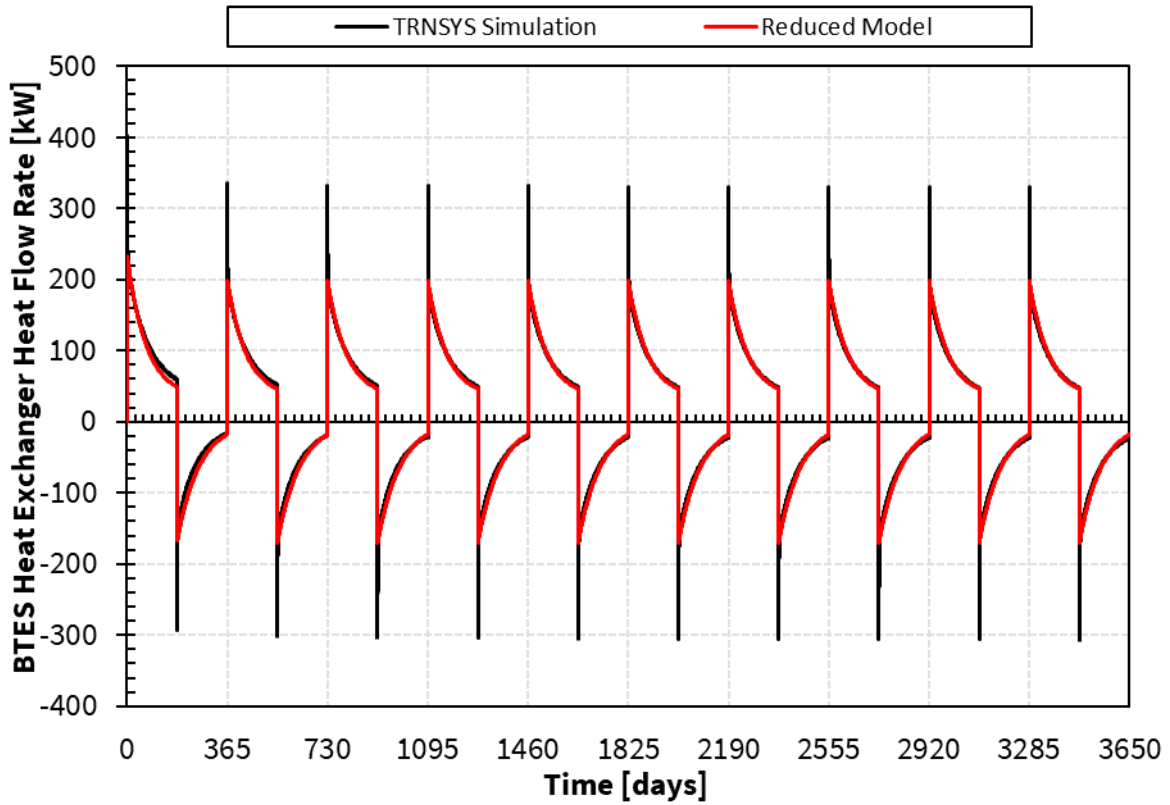
Figure 5.22: TRNSYS DST simulation output and reduced model approximation of BTES heat exchanger heat flow rate with respect to time for a 10-year simulation (60 ℃ charging, 12 ℃ discharging). RMSD=7.7 kW
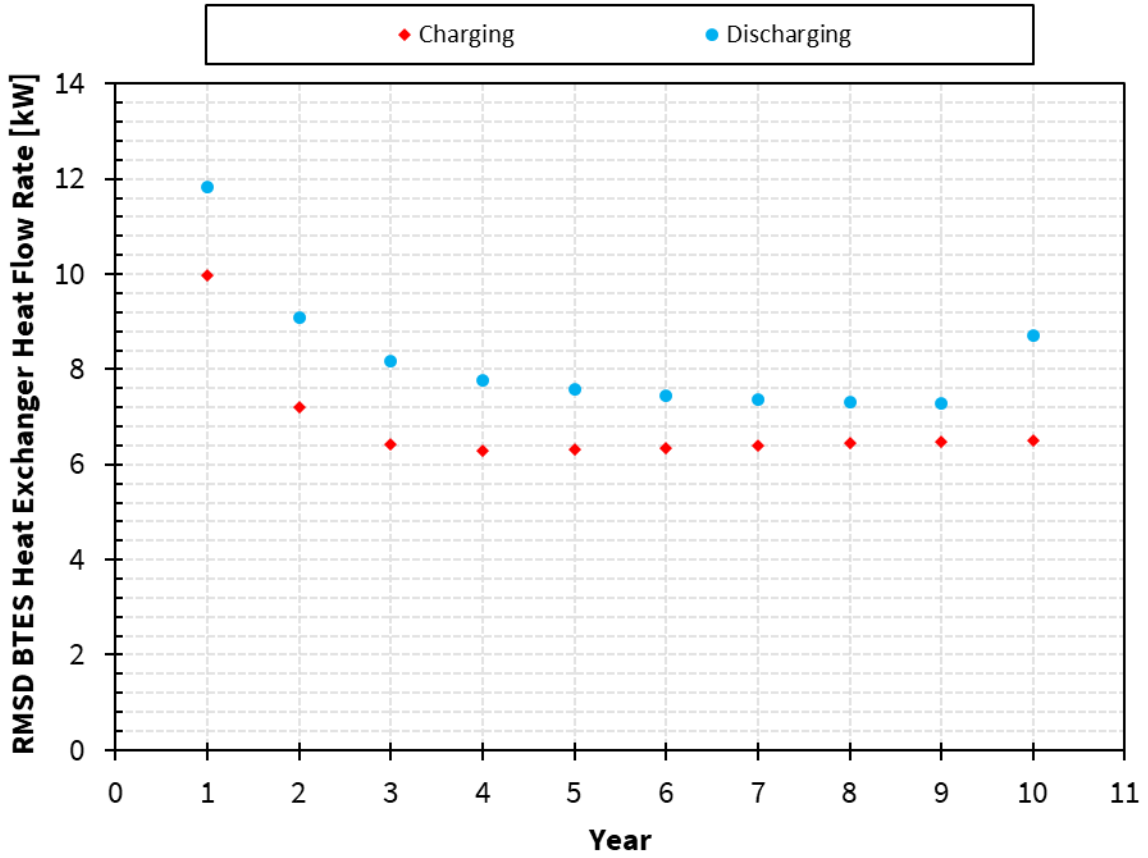
Figure 5.23: Yearly RMSD between the TRNSYS DST simulation output and the reduced model approximation of BTES heat exchanger heat flow rate over each 6-month timestep for a 10-year simulation (60 ℃ charging, 12 ℃ discharging).
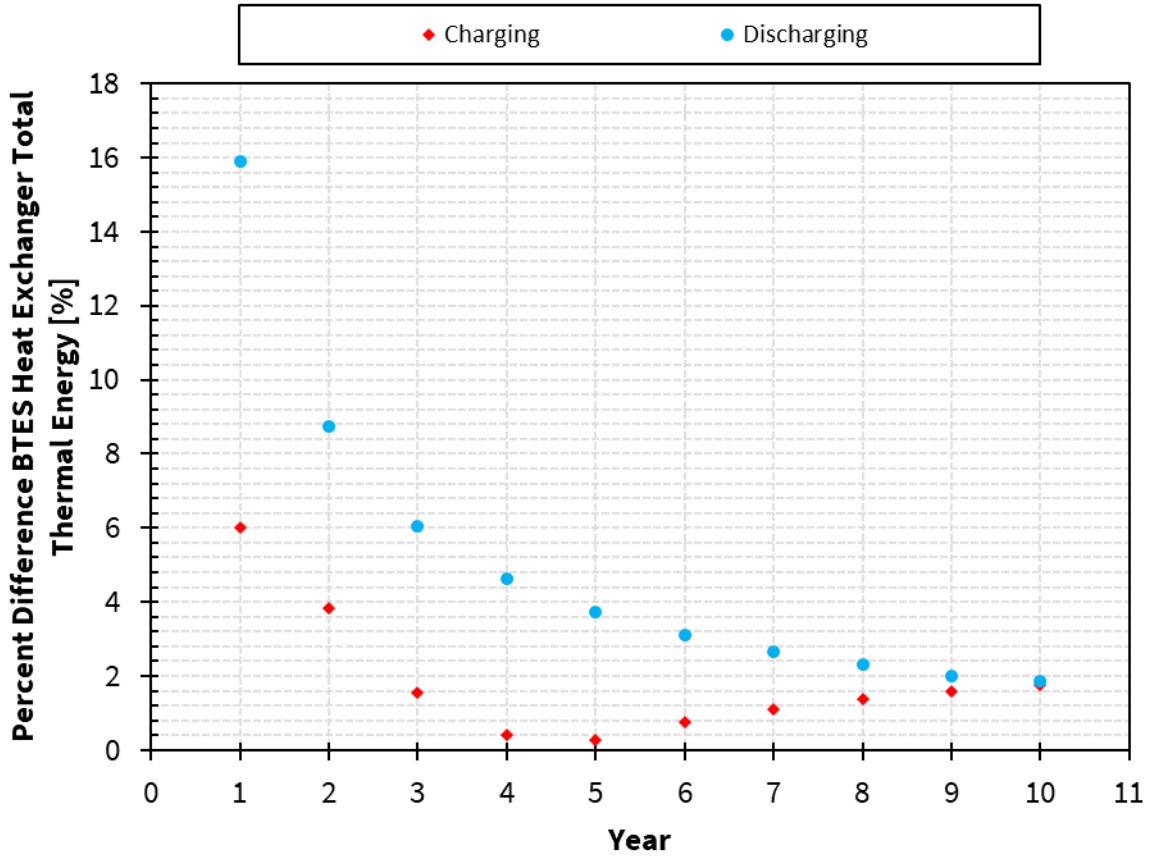
Figure 5.24: Yearly percent difference between the TRNSYS DST simulation output and the reduced model approximation of BTES heat exchanger total thermal energy application over each 6-month timestep for a 10-year simulation (60 ℃ charging, 12 ℃ discharging).
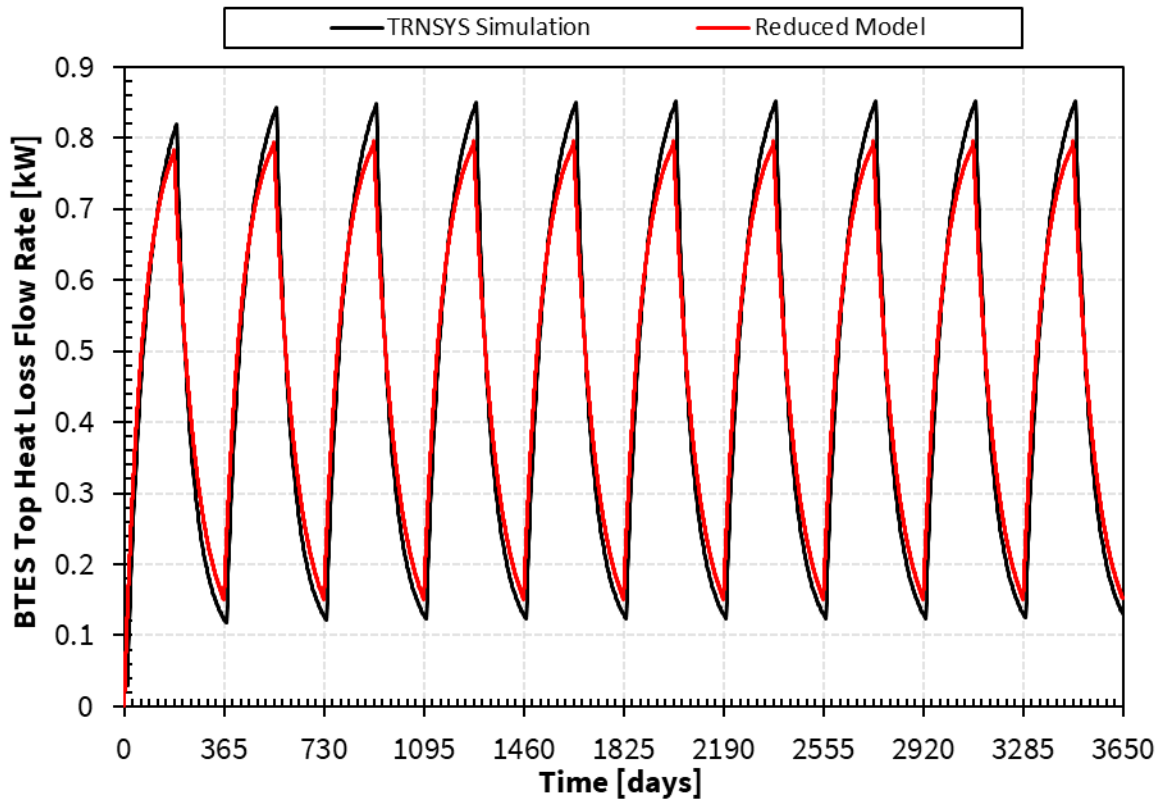
Figure 5.25: TRNSYS DST simulation output and reduced model approximation of BTES top loss heat flow rate with respect to time for a 10-year simulation (60 ℃ charging, 12 ℃ discharging). RMSD=4.4e-2 kW=44 W
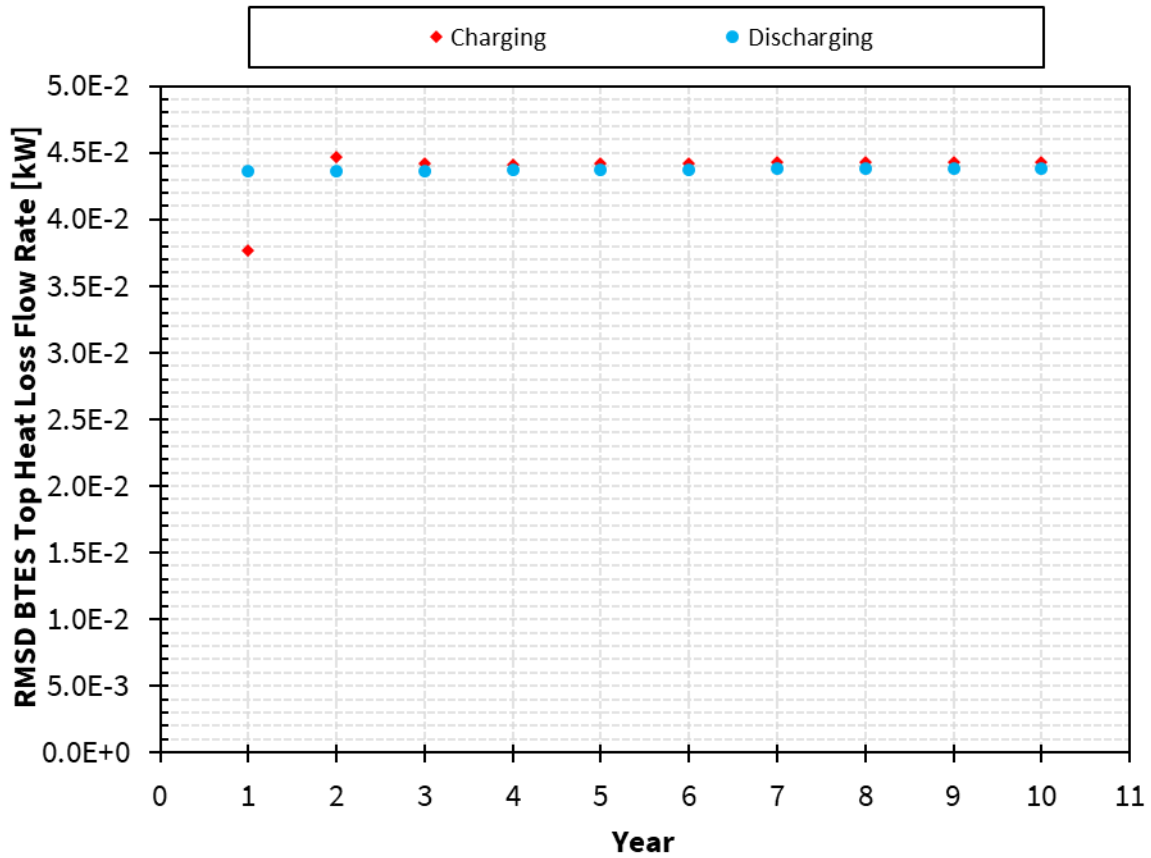
Figure 5.26: Yearly RMSD between the TRNSYS DST simulation output and the reduced model approximation of BTES top loss heat flow rate over each 6-month timestep for a 10-year simulation (60 ℃ charging, 12 ℃ discharging).
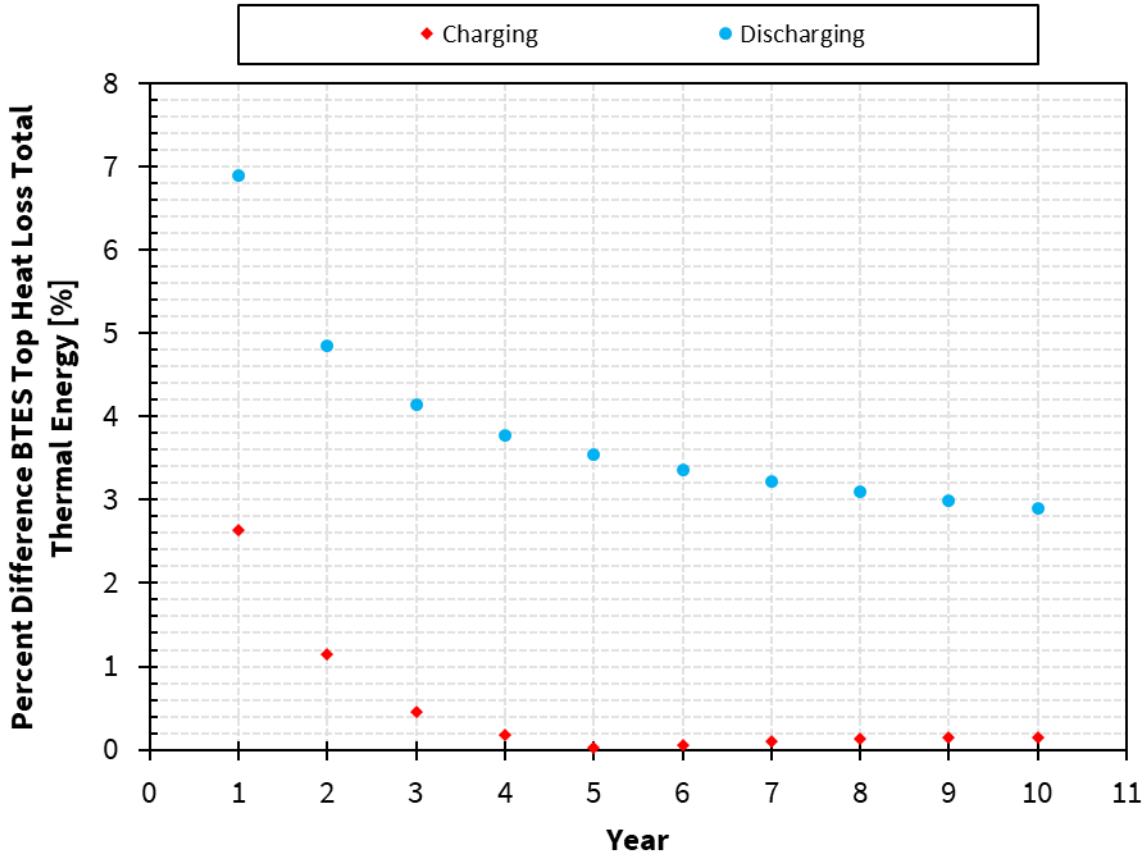
Figure 5.27: Yearly percent difference between the TRNSYS DST simulation output and the reduced model approximation of BTES total thermal energy loss through its top surface over each 6-month timestep for a 10-year simulation (60 ℃ charging, 12 ℃ discharging).
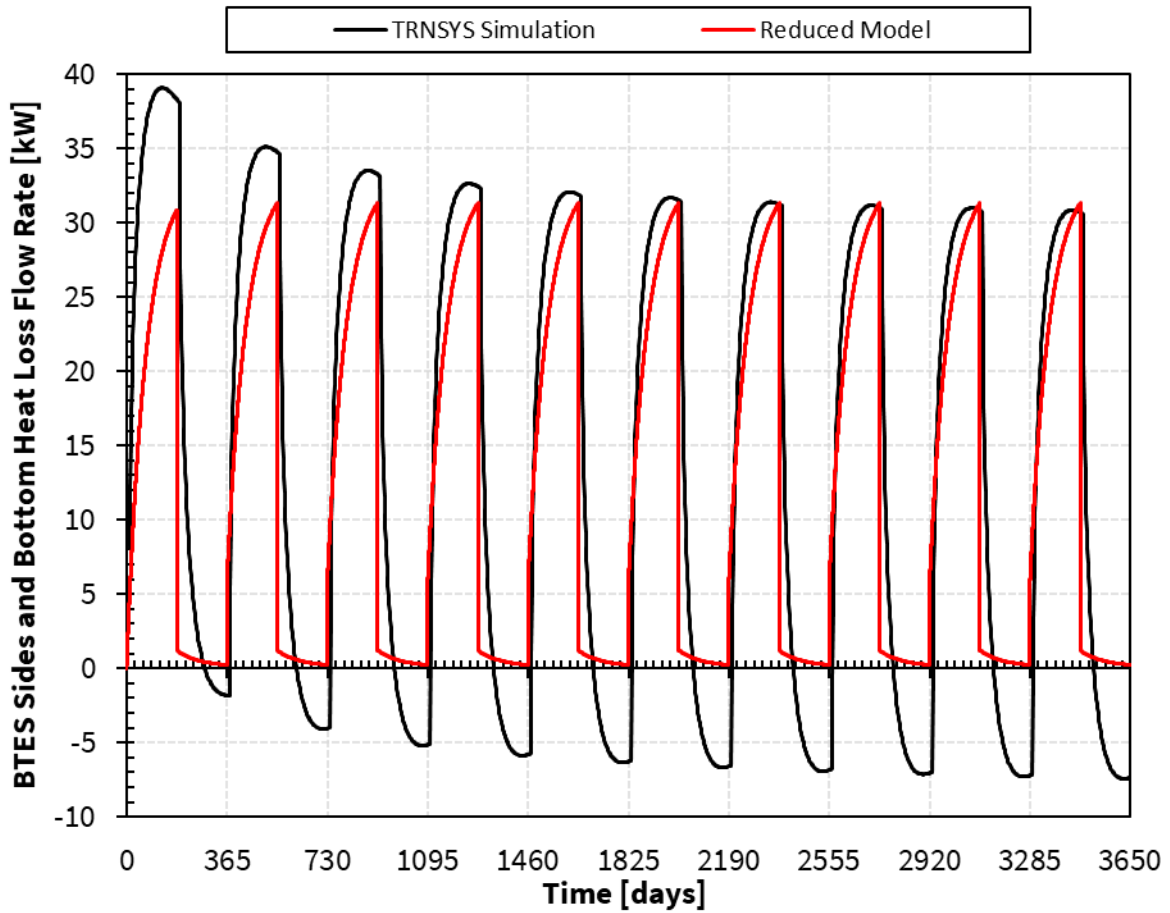
Figure 5.28: TRNSYS DST simulation output and reduced model approximation of BTES sides and bottom loss heat flow rate with respect to time for a 10-year simulation (60 ℃ charging, 12 ℃ discharging). RMSD=8.4 kW
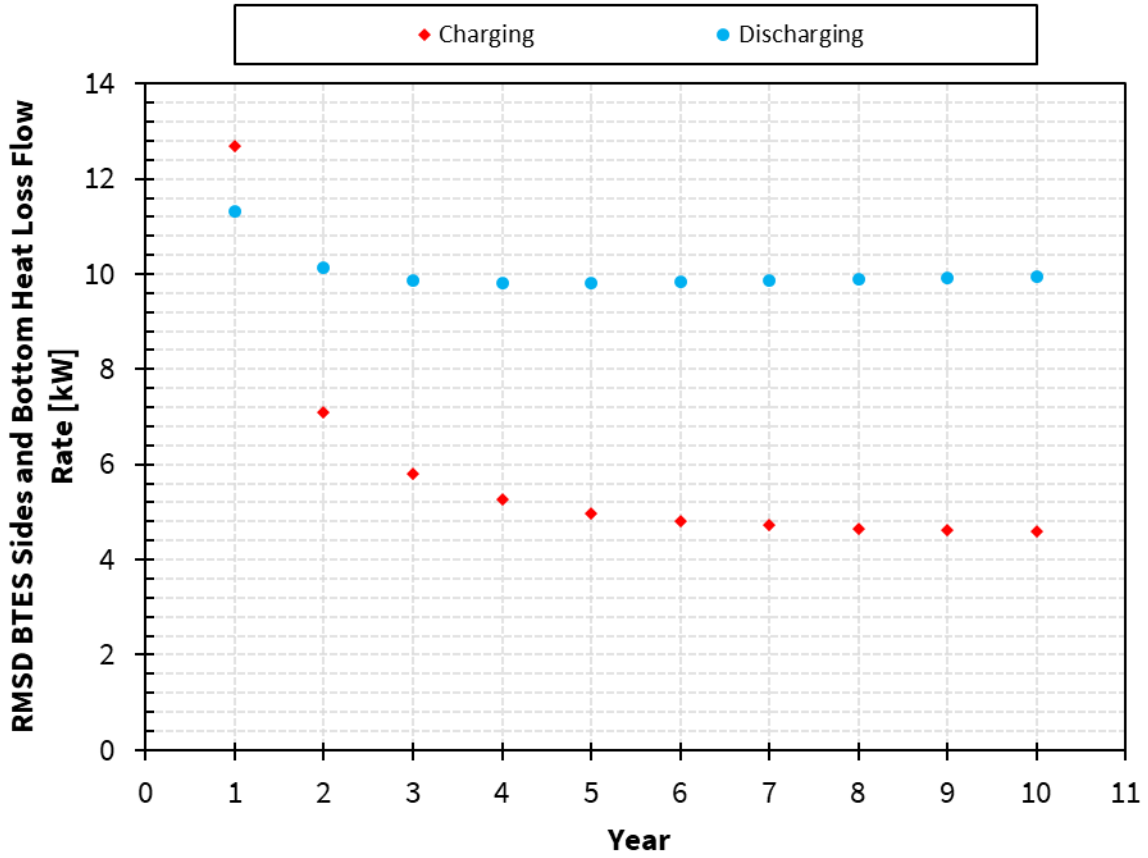
Figure 5.29: Yearly RMSD between the TRNSYS DST simulation output and the reduced model approximation of BTES sides and bottom loss heat flow rate over each 6-month timestep for a 10-year simulation (60 ℃ charging, 12 ℃ discharging).
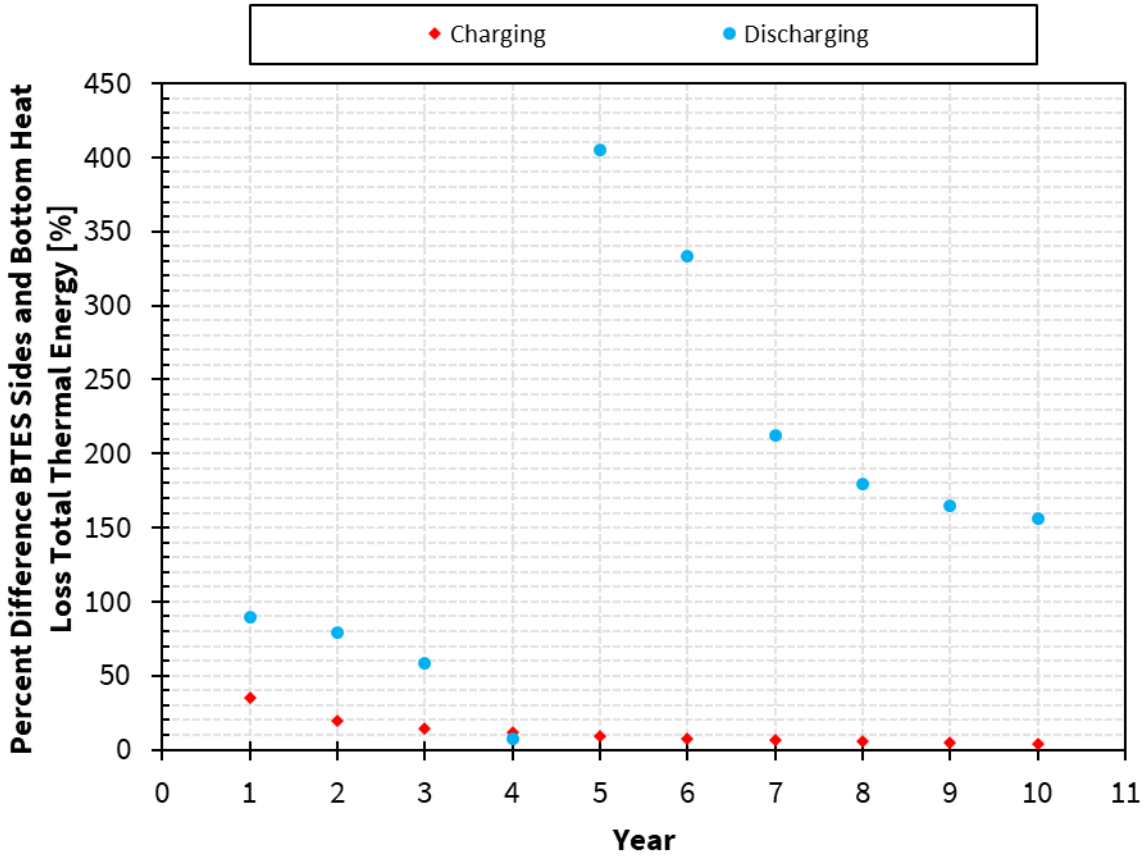
Figure 5.30: Yearly percent difference between the TRNSYS DST simulation output and the reduced model approximation of BTES total thermal energy loss through its side and bottom surfaces over each 6-month timestep for a 10-year simulation. The magnitude of the energy gained from the surrounding ground over the TRNSYS DST simulation's discharging timesteps increases as the simulation develops to a periodic steady state operation. At year 5 the magnitude of heat gained over the timestep is equal to the magnitude of heat loss which drives down the expected magnitude of thermal loss through the sides and bottom, which asymptoticly increases the percent difference value (60 ℃ charging, 12 ℃ discharging).
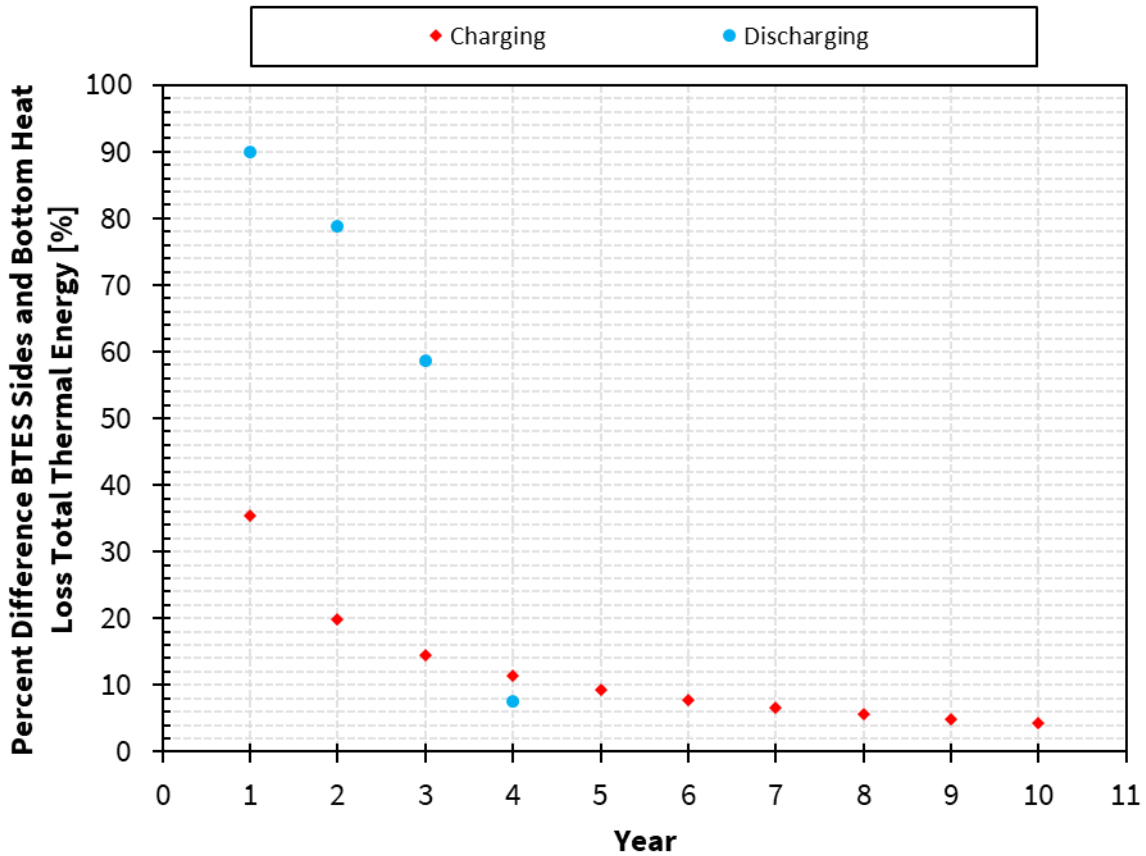
Figure 5.31: Yearly percent difference between the TRNSYS DST simulation output and the reduced model approximation of BTES total thermal energy loss through its side and bottom surfaces over each 6-month timestep for a 10-year simulation. The y-axis is restricted to a maximum of 100% to show the yearly development of the percent difference of charging (60 ℃ charging, 12 ℃ discharging).

The reduced model exhibits its fluid inlet temperature independence, and therefore, its ability to simulate periodic steady state BTES thermal response for user defined fluid inlet temperature setpoints. The thermal resistance values calculated from the TRNSYS DST reference simulation can be used to estimate BTES performance of varying charging and discharging temperature setpoints.

The heat transfer rate of thermal loss through the sides and bottom of the BTES storage volume at periodic steady state BTES discharging is dependent on the temperature of the ground outside the storage volume boundary, which is dependent on the simulation's inlet temperature setpoints. The reduced model can still predict periodic steady state thermal response because the total sides and bottom thermal energy loss over the discharging timestep has a low magnitude relative to the magnitude of the total energy application of the heat exchanger.

5.10 Thermal Resistance Parameter Sweep

The reduced model is a tool engineers can use to predict periodic steady state BTES thermal response and estimate steady state BTES performance, however, the thermal resistances used to solve the model must have their sensitivity to BTES design parameters investigated. The design parameters investigated are the geometric parameters that determine the BTES volume and the ground thermal properties of the BTES site. The geometric parameters that determine BTES volume are number of boreholes, borehole depth, and borehole spacing. The ground thermal properties investigated are volumetric heat capacity and thermal conductivity.

Each parametric sweep is performed with respect to the reference simulation's operation, geometric parameters, and ground thermal properties. For each sweep, two geometric design parameters (out of BTES volume, number of boreholes, borehole depth, and borehole spacing) are held constant and two geometric design parameters are varied. The change in periodic steady state thermal resistance values (heat exchanger, top loss, and side and bottom loss) calculated from the simulations are presented with respect to the changing geometric parameters. The change in BTES steady state storage efficiency (ratio of total energy extracted during discharging timestep to total energy injected during charging timestep for a simulation charging and discharging cycle) for the reference simulation's operation is also presented with respect to

the changing geometric parameters. Finally, the parametric sweep is repeated for two different

soil types. One soil has an increased volumetric thermal capacity relative to the reference

simulation, and the other has an increased thermal conductivity relative to the reference

simulation. The full set of parametric sweeps is available in the appendix.

Variable Parameters	Constant Parameters
Spacing, Volume	Number of Boreholes, Depth
Spacing, Depth	Number of Boreholes, Volume
Spacing, Number of Boreholes	Depth, Volume
Number of Boreholes, Volume	Spacing, Depth
Depth, Volume	Spacing, Number of Boreholes

Table 5.2: The variable parameters and constant parameters of each parameter sweep. The
constant parameters retain the same parameter values as the reference simulation while the
variable parameters are altered.

Soil	Volumetric Heat Capacity (ρc_{pg}) [kJ/(m^3*K)]	Thermal Conductivity (k) [W/(m*K)]
1	1900	1.42
2	4424	1.42
3	1900	2.22

Table 5.3: The thermal properties of the 3 soil types with parameter sweeps applied to them.
Each soil type has the full set of parameter sweep simulations applied to it. Soil 1 has the thermal
properties of the reference simulation. Soil 1 parameter sweeps are presented in Appendix A,
Soil 2 parameter sweeps are presented in Appendix B, and Soil 3 parameter sweeps are presented
in Appendix C.

s [m]	V [m³]	#BH	H [m]	A_{TBA} [m²]	$A_{SV\_s,b}$ [m²]	A_{SV_t} [m²]	R_{hx} (charge) [°Cm²/W]	R_{hx} (discharge) [°Cm²/W]	$R_{loss\_s,b}$ (charge) [°Cm²/W]	$R_{loss\_s,b}$ (discharge) [°Cm²/W]	R_{loss_t} (charge) [°Cm²/W]	R_{loss_t} (discharge) [°Cm²/W]	Efficiency [%]
1	1870	48	45	1018	1070	42	1.36E-01	1.35E-01	2.44E+00	-1.68E+00	1.65E+01	1.84E+01	51.3
2	7481	48	45	1018	2223	166	1.71E-01	1.70E-01	3.40E+00	-5.96E+00	1.81E+01	1.97E+01	65.4
3	16833	48	45	1018	3459	374	1.91E-01	1.91E-01	4.60E+00	1.19E+02	1.97E+01	1.96E+01	69.8
4	29926	48	45	1018	4779	665	2.06E-01	2.04E-01	6.16E+00	1.51E+01	2.12E+01	1.94E+01	68.5
5	46759	48	45	1018	6181	1039	2.16E-01	2.14E-01	7.76E+00	1.19E+01	2.21E+01	1.93E+01	65.2
6	67332	48	45	1018	7667	1496	2.25E-01	2.22E-01	9.22E+00	1.11E+01	2.24E+01	1.95E+01	61.3
7	91647	48	45	1018	9236	2037	2.31E-01	2.26E-01	1.05E+01	1.10E+01	2.24E+01	1.97E+01	57.3

Table 5.4: Design parameters, heat transfer areas, periodic steady state thermal resistances, and periodic steady state storage efficiencies for the soil 1 parameter sweep with variable parameters: spacing and volume and constant parameters: number of boreholes and depth. The periodic steady state thermal resistances of charging and discharging and the periodic steady state storage efficiency are presented in Figure 5.32 to Figure 5.41 with respect to the variable parameters.
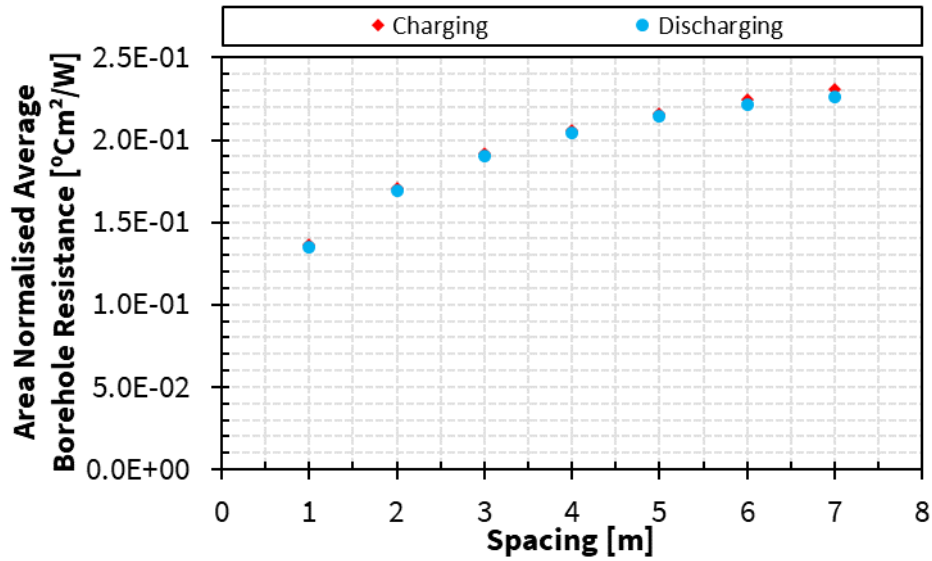
Figure 5.32: Borehole heat exchanger thermal resistance of periodic steady state BTES operation normalized against total borehole area with respect to borehole spacing. Spacing and volume are the variable parameters. Number of boreholes and depth are held constant. Soil 1.
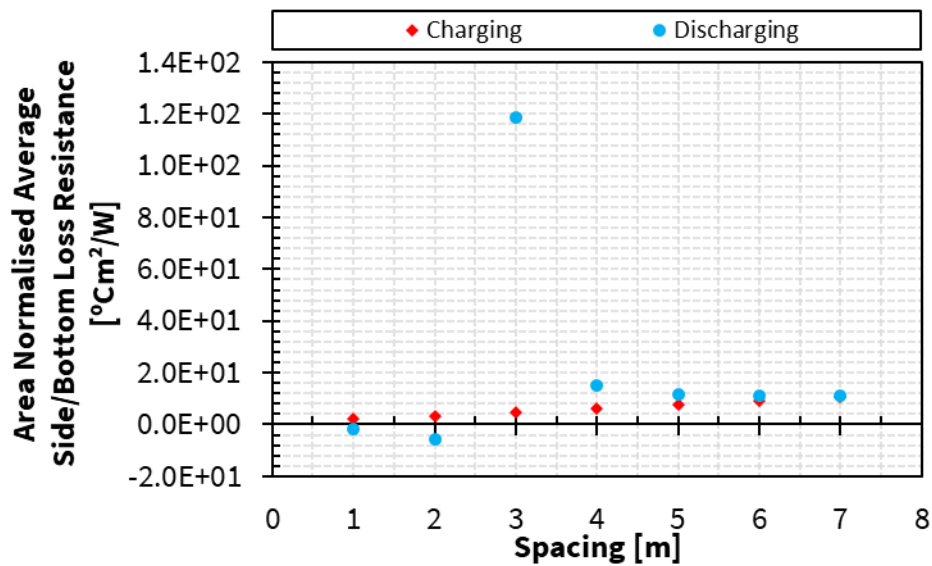
Figure 5.33: Sides and bottom loss resistance of periodic steady state BTES operation normalized against storage volume side and bottom area with respect to borehole spacing. The negative discharging resistance values and large magnitude of discharging resistance for 3 m spacing is a result of the change in heat transfer direction that occurs for periodic steady state

side/bottom loss heat transfer rate. Spacing and volume are the variable parameters. Number of boreholes and depth are held constant. Soil 1.
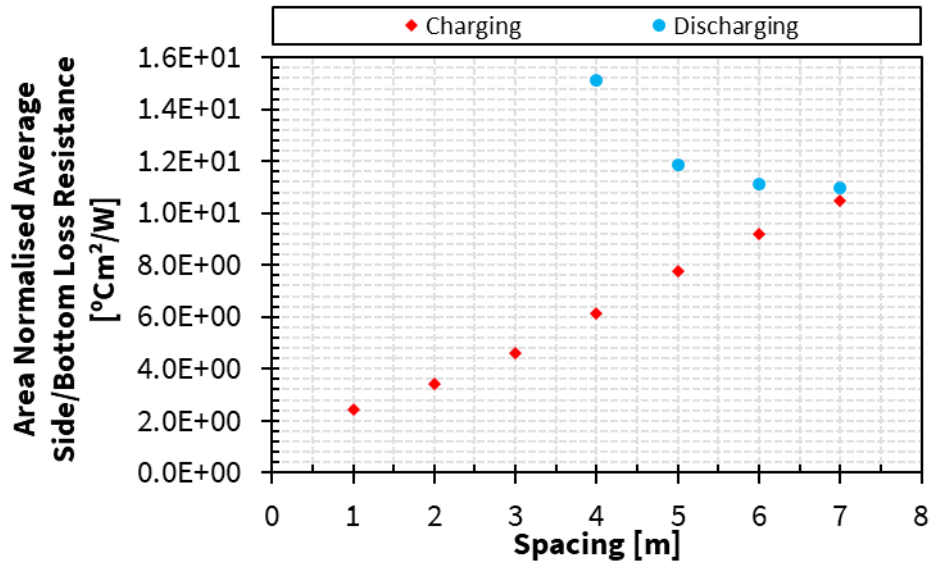
Figure 5.34: Sides and bottom loss resistance of periodic steady state BTES operation normalized against storage volume side and bottom area with respect to borehole spacing. The figure's y-axis is reduced to omit discharging resistance outliers and better display charging resistance values. Spacing and volume are the variable parameters. Number of boreholes and depth are held constant. Soil 1.
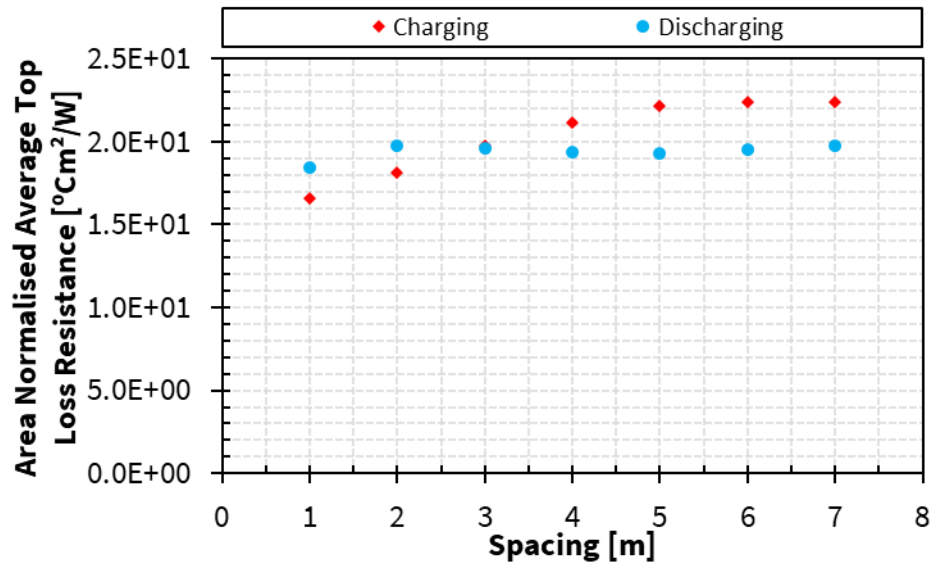
Figure 5.35: Top loss resistance of periodic steady state BTES operation normalized against storage volume top area with respect to borehole spacing. Spacing and volume are the variable parameters. Number of boreholes and depth are held constant. Soil 1.
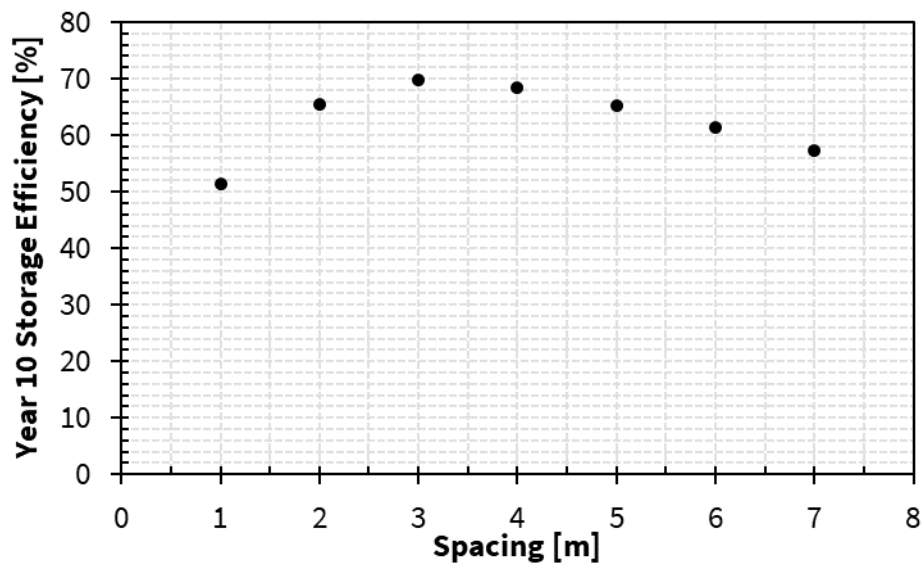
Figure 5.36: Periodic steady state BTES thermal storage efficiency with respect to borehole spacing. BTES thermal storage efficiency is defined as the ratio of the total energy extracted during discharging timestep to the total energy injected during charging timestep for a simulation charging and discharging cycle. Spacing and volume are the variable parameters. Number of

boreholes and depth are held constant. The inlet temperature setpoint of BTES charging is 95°C and BTES discharging is 20°C. Soil 1.
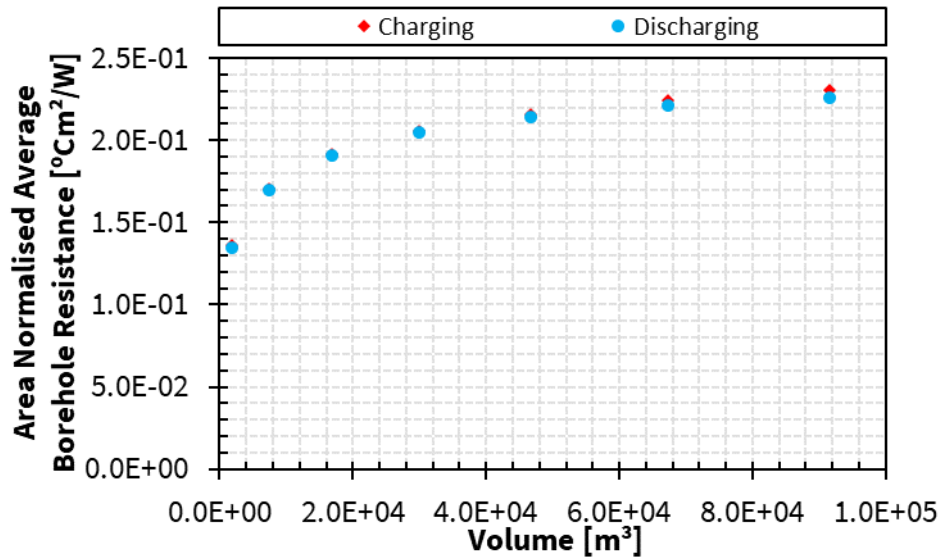
Figure 5.37: Borehole heat exchanger thermal resistance of periodic steady state BTES operation normalized against total borehole area with respect to storage volume. Spacing and volume are the variable parameters. Number of boreholes and depth are held constant. Soil 1.
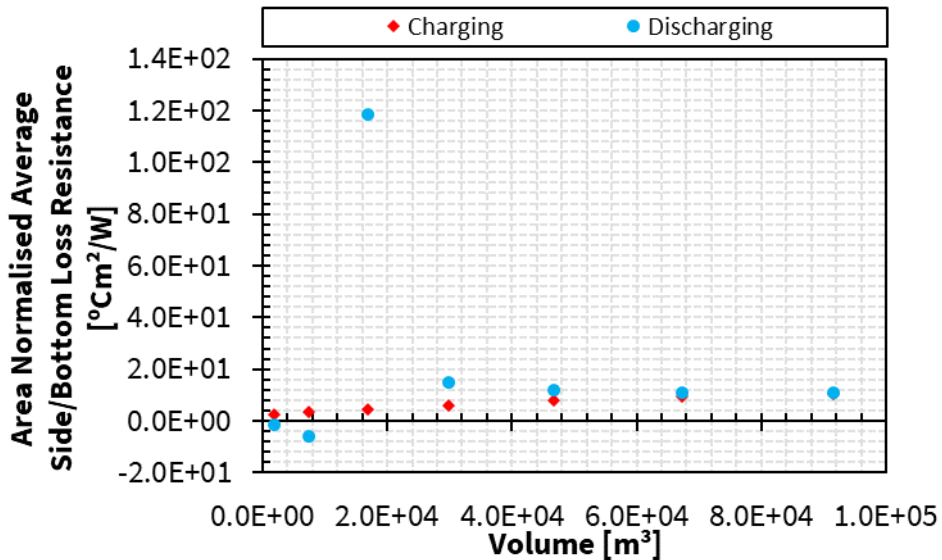
Figure 5.38: Sides and bottom loss resistance of periodic steady state BTES operation normalized against storage volume side and bottom area with respect to storage volume. The

negative discharging resistance values and large magnitude discharging resistance for 16 833m^3 volume is a result of the change in heat transfer direction that occurs for periodic steady state side/bottom loss heat transfer rate. Spacing and volume are the variable parameters. Number of boreholes and depth are held constant. Soil 1.
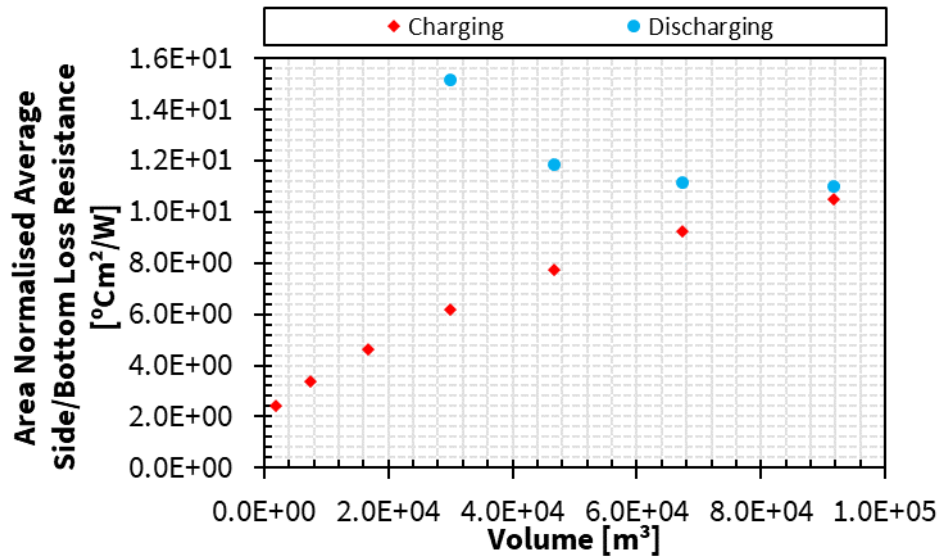
Figure 5.39: Sides and bottom loss resistance of periodic steady state BTES operation normalized against storage volume side and bottom area with respect to storage volume. The figure's y-axis is reduced to omit discharging resistance outliers and better display charging resistance values. Spacing and volume are the variable parameters. Number of boreholes and depth are held constant. Soil 1.
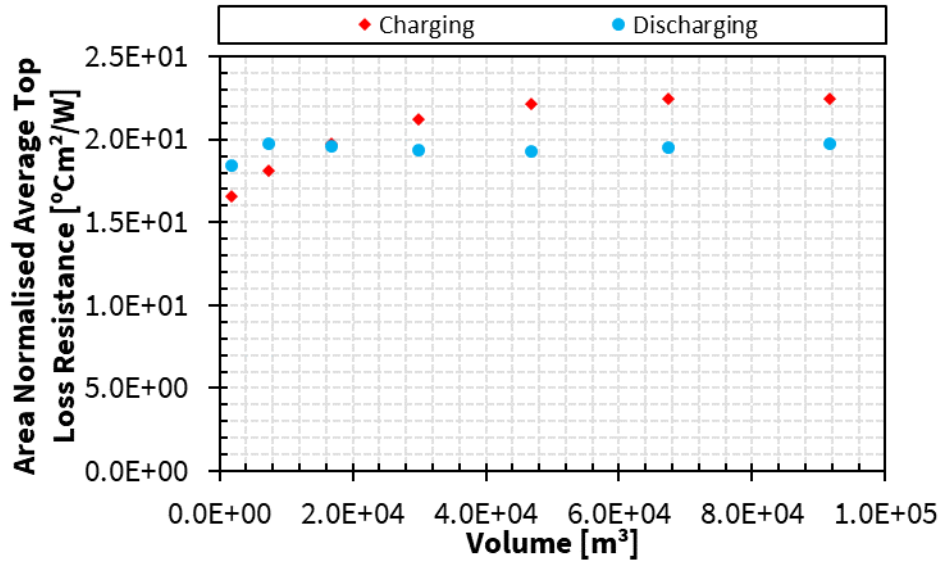
Figure 5.40: Top loss resistance of periodic steady state BTES operation normalized against storage volume top area with respect to storage volume. Spacing and volume are the variable parameters. Number of boreholes and depth are held constant. Soil 1.
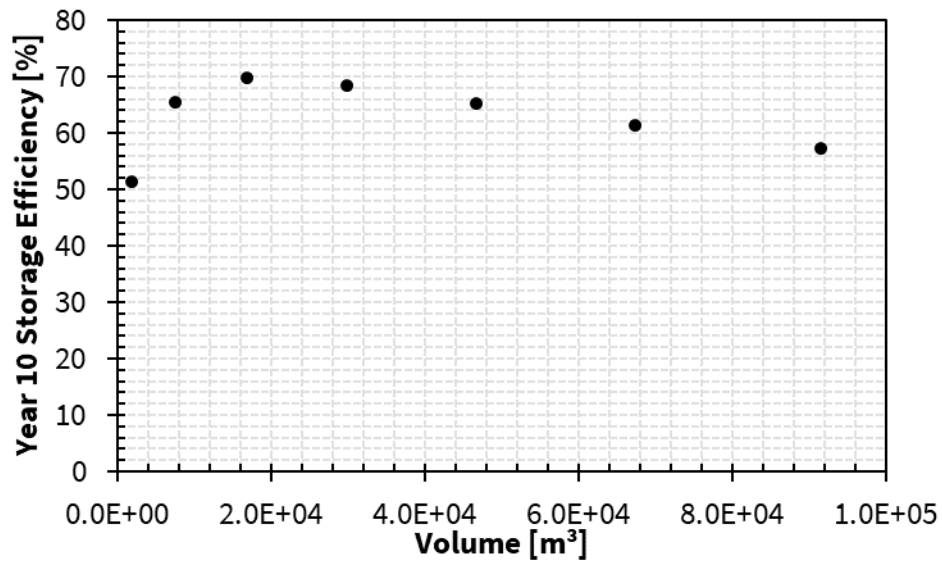
Figure 5.41: Periodic steady state BTES thermal storage efficiency with respect to storage volume. BTES thermal storage efficiency is defined as the ratio of the total energy extracted during discharging timestep to the total energy injected during charging timestep for a simulation charging and discharging cycle. Spacing and volume are the variable parameters. Number of

110

boreholes and depth are held constant. The inlet temperature setpoint of BTES charging is 95°C and BTES discharging is 20°C. Soil 1.

The remaining parameter sweep graphs are presented in Appendix A, B, and C.

5.11 Thermal Resistance Parameter Sweep Analysis

BTES heat exchanger thermal resistance is primarily a function of borehole spacing. The parameter sweeps with borehole spacing held constant display a more constant linear trend for heat exchanger thermal resistance compared to the parameter sweeps with variable borehole spacing. BTES side and bottom loss thermal resistance and BTES top thermal resistance are dependent on borehole spacing, number of boreholes, and borehole depth. Those 3 design parameters control BTES volume, BTES storage volume areas, and the temperatures the storage volume and its surroundings reach at periodic steady state operation which all greatly affect energy loss thermal resistance calculations. To design BTES with maximized steady state storage efficiency, heat exchanger thermal resistance should be minimized and loss thermal resistances should be maximized.

Increasing the storage volume's volumetric heat capacity for the BTES reference simulation from 1900 to 4424 [kJ/(m^3*K)] resulted in no significant change in the heat exchanger thermal resistances, however, loss thermal resistances of charging increased and of discharging decreased in such a way that there was an overall increase in the periodic steady state thermal storage efficiency from 69.8% to 72.3% (95°C charging, 20°C discharging). Increasing the volumetric heat capacity of the BTES storage volume reduces the value of optimal borehole spacing for maximizing periodic steady state storage efficiency.

Increasing the storage volume's thermal conductivity for the BTES reference simulation from 1.42 to 2.22 [W/(m*K)] reduced the heat exchanger thermal resistances from 1.91×10^{-1} to

111

1.48×10^{-1} [$°Cm^2/W$]. The loss thermal resistances during charging are decreased and during discharging are increased. The increase in thermal conductivity makes the thermal resistance of loss through the sides and bottom of the storage volume during discharging a negative value, which is interpreted by the reduced model as a thermal resistance value of infinity. The increase in thermal conductivity for the reference simulation results in a decrease in the periodic steady state thermal storage efficiency from 69.8% to 63.6% (95°C charging, 20°C discharging). Increasing the thermal conductivity of the BTES storage volume increases the value of optimal borehole spacing for maximizing periodic steady state storage efficiency.

5.12 Conclusion

The reduced model of BTES thermal response is formed from the simplified thermal energy balance solution with constant fluid inlet conditions and periodic steady state BTES operation. The reduced model's operation relies on the lumped representation of BTES storage volume temperature as average storage volume temperature, and thermal resistances derived from TRNSYS DST simulations of BTES operation. The derivation of the thermal resistance values is presented and the effect that changing BTES design parameters has on the thermal resistance values of the reference simulation is explored. The thermal response of the model is compared to a validated TRNSYS DST simulation and the temperature independence of the model is checked.

The reduced model compared to the TRNSYS DST reference simulation predicts the periodic steady state average storage temperature response of charging with a RMSD of 0.96°C and of discharging with a RMSD of 1.3°C. The reduced model compared to the TRNSYS DST reference simulation predicts periodic steady state BTES total heat exchanger energy application of charging within 1.8% and of discharging within 2.8%.

The reduced model can accurately simulate periodic steady state BTES thermal response, however, it cannot accurately represent periodic steady state side and bottom loss heat transfer rate during BTES discharging that has a change in heat transfer direction. The relative magnitude of BTES storage volume side and bottom loss heat transfer rate is low compared to BTES heat exchanger heat transfer rate, therefore, negative derivations of side and bottom loss discharging timestep thermal resistances can be instead set to infinity which removes the side and bottom heat loss terms from the reduced model's function constants (Equation 3 and 4), removing side and bottom loss from the reduced model's approximation of average storage temperature (Equation 5).

The reduced BTES thermal energy balance solution and thermal resistance ranges provides engineers with a simplified tool for estimating BTES performance for application in early siting, designing, optimizing, and control systems work in greater complexity community energy projects such as ICE-Harvest systems.

6   Conclusion

6.1   Introduction

Greenhouse gas (GHG) emissions are a major contributing factor to climate change. The residential building sector contributes 15% of Canadian GHG emissions with space heating comprising 63% of the average household's energy demand [1]. Canadian space heating demand is primarily met with natural gas combustion which produces GHG emissions [1]. The Integrated Community Energy Harvesting (ICE-Harvest) systems seek to integrate thermal and electrical energy production, storage, redistribution, and consumption in a way that significantly reduces the amount of GHG emissions required to meet space heating demand [3]. Borehole thermal energy storage (BTES) is utilized for seasonal energy storage in ICE-Harvest systems. Effective design and implementation of BTES in ICE-Harvest systems would benefit from the development of a simplified or "reduced" model of BTES operation which can be used to approximate periodic steady state BTES thermal response and storage efficiency. The reduced model aids in early siting, designing, optimizing, and control systems development work for ICE-Harvest systems.

6.2   Literature Review and Thesis Space Definition

The literature review determined TRNSYS DST provides robust and accurate simulations of BTES thermal response for BTES with varying design parameters and thermal properties which makes it an ideal basis for a reduced model of BTES thermal response. As part of the current work, TRNSYS was validated against data from a BTES installation and was found to provide and accurate prediction of BTES thermal response. This thesis presents a novel reduction of the thermal energy balance equations that govern BTES thermal response and the effects

114

varying BTES design parameters and thermal properties have on the reduced model. TRNSYS was used to generate thermal resistance constants required by the reduced model. The goal is to characterize simplified periodic steady state BTES thermal response and its dependency on design parameters and thermal properties.

6.3 Results of the Reduced Model of BTES Thermal Response

The BTES thermal energy balance equation is reduced and solved assuming simplified operation conditions which reach a periodic steady state operation. The reduction is applied with the definition of steady state thermal resistance values which dictate heat flow rates between the heat exchanger fluid and the storage volume and between the storage volume and its surroundings during BTES charging and discharging. The thermal resistances are defined from the mean of average temperature differences and area normalized mean heat transfer rates of simplified operation and periodic steady state TRNSYS simulations of BTES thermal response. The thermal resistances are presented with respect to changing BTES storage volume, spacing between boreholes, borehole depth, and number of boreholes as well as altering the thermal conductivity and thermal capacity of the BTES storage volume and surrounding ground. The model's outputs are compared to the TRNSYS simulations' outputs, and the resistance values are confirmed to be independent of inlet fluid temperature setpoints.

The reduced model uses an integrated thermal energy balance equation to define an ordinary differential equation that governs the temporal average storage volume temperature. The reduced model compared to the TRNSYS DST reference simulation predicts the periodic steady state average storage temperature response of charging with a RMSD of 0.96°C and the temperature response of discharging with a RMSD of 1.3°C. The reduced model compared to the reference simulation predicts steady state BTES total heat exchanger total energy application of

charging within 1.8% and the total heat exchanger energy application of discharging within 2.8%.

The reduced model is unable to account for the energy loss through the side and bottom boundaries of the storage volume during BTES discharging if the heat transfer direction changes to be from the surroundings to the storage volume. When this situation occurs, steady state energy loss through the side and bottom boundaries of the storage volume can be approximated to be negligible relative to the reduced model's total heat exchanger energy application to the storage volume.

6.4   Recommendations for Future Work

BTES storage volume is a function of spacing between boreholes, borehole depth, and number of boreholes, therefore, the individual effects each parameter has on the reduced model's steady state thermal resistance values cannot be isolated. Future work should focus on creating a design of experiments matrix which defines the reduced model's steady state thermal resistance values with respect to storage volume size, spacing between boreholes, borehole depth, and number of boreholes in the same equation. The thermal properties of thermal conductivity and capacity should be implemented into the design of experiments matrix and the periodic steady state resistance definition. The design of experiments relationship would allow the reduced model greater versatility in predicting the steady state efficiencies of different sized BTES with different BTES site locations.

Future work should consider a parameter sensitivity study of the reduced model's steady state thermal resistances for TRNSYS DST parameters that are held constant in the reference simulation and for the parameter sweep. A sensitivity study for parameters such as the number of

boreholes connected in series, the type of borehole heat exchanger used in the BTES (U-tube, double U-tube, coaxial), the design parameters and thermal properties of the borehole heat exchangers, and the thermal properties of the heat exchanger fluid should be performed. The effect that changing the magnitude of the constant inlet mass flow rate has on the reduced model's thermal resistances should be investigated. Finally, the effect of the charging and discharging inlet fluid temperatures on BTES with different ambient air and undisturbed ground temperatures should be explored.

Future work should investigate the definition of a steady state thermal resistance for heat loss through the side and bottom surfaces of the BTES storage volume that can represent the change in heat flow direction between the storage volume and the surrounding ground that occurs during BTES discharging. The reduced model presented defines thermal resistance in a way that the counteracting heat loss flow rate directions result in a negligible heat loss approximation during BTES discharging rather than a period of decreasing BTES heat loss followed by heat gain from the surrounding ground.

The ordinary differential equation reduction for the reduced model includes the assumptions of a constant mass flow rate, constant inlet temperatures for charging and discharging operation, neglecting the mass of the borehole heat exchangers, and neglecting the change of energy content within the heat exchanger fluid. Future work should investigate the error propagation of these assumptions and the viability of using the reduced model for operation conditions with more complexity. Complex operation conditions include the implementation of an energy storage "holding" operation (where the mass flow rate into the BTES is zero) between the charging and discharging timesteps, an annual sinusoidal inlet fluid temperature operation to represent both charging and discharging BTES inlet fluid temperatures in the same function, and

different inlet fluid temperature values than periodic steady state operation during the BTES warm-up period. Future work should investigate the viability of using a reduced model to predict the BTES thermal response of site measured BTES operation data that exhibits transient and on/off BTES inlet fluid temperature and mass flow rate.

A guide should be developed which details how long a BTES takes to reach periodic steady state thermal response and storage efficiency. The guide should provide the length of time as a function of inlet fluid temperature magnitudes, operation timestep lengths, and BTES thermal capacity. BTES thermal capacity is definable by BTES design parameters and storage volume thermal properties.

7 References

[1] N. R. Canada, "Energy Efficiency Trends in Canada, 1990 to 2009," 2012. https://oee.rncan.gc.ca/publications/statistics/trends11/chapter3.cfm?attr=0 (accessed June 1, 2022).

[2] F. G. H. Koene, "Basics of solar energy," 2014. http://www.e-hub.org/the-challenge.html (accessed June 1, 2022).

[3] McMaster Institute for Energy Studies, "ICE Harvest," 2017. https://energy.mcmaster.ca/icepick/ (accessed June 1, 2022).

[4] M. Lanahan and P. C. Tabares-Velasco, "Seasonal Thermal-Energy Storage: A Critical Review on BTES Systems, Modeling, and System Design for Higher System Efficiency," *Energies*, vol. 10, no. 6: 743, 2017, doi: 10.3390/en10060743.

[5] T. Schmidt, D. Mangold, and H. Müller-Steinhagen, "Seasonal Thermal Energy Storage in Germany," *Structural Engineering International*, vol. 14, no. 3, pp. 230-232, 2004, doi: 10.2749/101686604777963739.

[6] C. Millar, "Experimental Evaluation of Thermal Response Tests Performed on Borehole Strings," 2020.

[7] F. M. Rad and A. S. Fung, "Solar Community Heating and Cooling System with Borehole Thermal Energy Storage – Review of Systems," *Renewable & Sustainable Energy Reviews*, vol. 60, pp. 1550-1561, 2016, doi: 10.1016/j.rser.2016.03.025.

[8] B. Harris, "A CFD Study on the Extraction of Geothermal Energy from Abandoned Oil and Gas Wells," 2017.

[9] N. Catolico, S. Ge, and J. McCartney, "Numerical Modeling of a Soil-Borehole Thermal Energy Storage System," *Vadose Zone Journal,* vol. 15, no. 1, pp. 1-17, 2016, doi: 10.2136/vzj2015.05.0078.

[10] T. Baser, J. S. McCartney, A. Moradi, K. Smits, and N. Lu, "Impact of a Thermo-Hydraulic Insulation Layer on the Long-Term Response of Soil-Borehole Thermal Energy Storage Systems," *UC San Diego,* 2016, doi: 10.1061/9780784480137.013.

[11] P. Kandiah, "CFD Study of a Large Buried Tank Within a Borehole Field," 2014.

[12] Thermal Energy System Specialists LLC, "TRNSYS - Transient System Simulation Tool," 2019. https://www.trnsys.com (accessed June 1, 2022).

[13] G. Hellström, "Ground Heat Storage: Thermal Analyses of Duct Storage Systems," *Lund University,* 1991.

[14] G. Hellström, "Duct Ground Heat Storage Model, Manual for Computer Code," *Lund University,* 1989.

[15]   M. Ahmadfard and M. Bernier, "A Review of Vertical Ground Heat Exchanger Sizing Tools Including an Inter-Model Comparison," *Renewable and Sustainable Energy Reviews,* vol. 110, pp. 247-265, 2019, doi: 10.1016/j.rser.2019.04.045.

[16]   P. Eskilson, "Thermal Analysis of Heat Extraction Boreholes," *Lund University,* 1987.

[17]   M. Cimmino, "Semi-Analytical Method for g-Function Calculation of bore fields with series- and parallel-connected boreholes," *Science and Technology for the Built Environment,* vol. 25, no. 9, pp. 1007-1022, 2019, doi: 10.1080/23744731.2019.1622937.

[18]   D. E. Fisher, S. J. Rees, S. K. Padhmanabhan, and A. Murugappan, "Implementation and Validation of Ground-Source Heat Pump System Models in an Integrated Building and System Simulation Environment," *HVAC & R Research,* vol. 12, no. 3, pp. 693-710, 2006, doi: 10.1080/10789669.2006.10391201.

[19]   J. Ljunggren and T. Magnusson, "Thermal Performance Analysis of High Temperature Borehole Thermal Energy Storage Design from an Insulation Perspective," *Lund University,* 2019.

[20]   J. A. Shonder, V. D. Baxter, P. J. Hughes, and J. W. Thornton, "A Comparison of Vertical Ground Heat Exchanger Design Software for Commercial Applications," *ASHRAE Transactions,* vol. 106, no. 1, pp. 831-842, 2000.

[21]   S. Chapuis and M. Bernier, "Seasonal Storage of Solar Energy in Borehole Heat Exchangers," *Eleventh International IBPSA Conference,* pp. 599-606, 2009.

[22]   P. A. Sørensen et al. "Boreholes in Brædstrup, Final Report," *PlanEnergi,* 2013.

[23]   G. Gauthier, "HEATSTORE, Benchmarking, and Improving Models of Subsurface Heat Storage Dynamics," *Geothermica,* 2020.

[24]   G. Gauthier, Personal communication, *PlanEnergi,* 2021.

[25]   K. Nielson, "Thermal Energy Storage, A State-of-the-Art, A Report Within the Research Program Smart Energy-Efficient Buildings at NTNU and SINTEF 2002-2006," *Norwegian University of Science and Technology,* 2003

Appendix A

s [m]	H [m]	#BH	V [m³]	A_{TBA} [m²]	$A_{SV\_s,b}$ [m²]	A_{SV_t} [m²]	R_{hx} (charge) [°Cm²/W]	R_{hx} (discharge) [°Cm²/W]	$R_{loss\_s,b}$ (charge) [°Cm²/W]	$R_{loss\_s,b}$ (discharge) [°Cm²/W]	R_{loss_t} (charge) [°Cm²/W]	R_{loss_t} (discharge) [°Cm²/W]	Efficiency [%]
1	405	48	16833	9161	9297	42	1.59E-01	1.42E-01	2.80E+00	-2.68E+00	1.94E+01	2.58E+01	57.1
2	101.3	48	16833	2290	4794	166	1.72E-01	1.70E-01	3.71E+00	-6.29E+00	1.94E+01	2.23E+01	69.9
3	45	48	16833	1018	3459	374	1.91E-01	1.91E-01	4.60E+00	1.19E+02	1.97E+01	1.96E+01	69.8
4	25.3	48	16833	573	2979	665	2.05E-01	2.04E-01	5.43E+00	1.19E+01	1.97E+01	1.77E+01	62.5
5	16.2	48	16833	366	2890	1039	2.16E-01	2.14E-01	6.14E+00	8.67E+00	1.92E+01	1.62E+01	51.5
6	11.3	48	16833	254	3039	1496	2.25E-01	2.20E-01	6.93E+00	8.02E+00	1.85E+01	1.53E+01	39.6
7	8.3	48	16833	187	3359	2037	2.31E-01	2.20E-01	7.96E+00	7.92E+00	1.84E+01	1.49E+01	28.8

Table A.1: Design parameters, heat transfer areas, periodic steady state thermal resistances, and periodic steady state storage efficiencies for the soil 1 parameter sweep with variable parameters: spacing and depth and constant parameters: number of boreholes and volume. The periodic steady state thermal resistances of charging and discharging and the periodic steady state storage efficiency are presented in Figure A.1 to Figure A.10 with respect to the variable parameters.
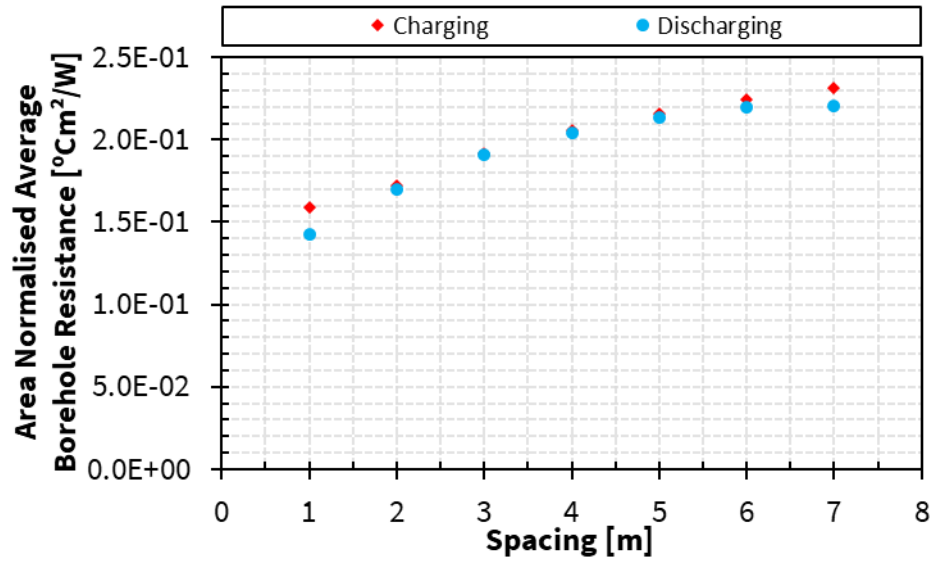
Figure A.1: Borehole heat exchanger thermal resistance of periodic steady state BTES operation normalized against total borehole area with respect to borehole spacing. Spacing and depth are the variable parameters. Number of boreholes and volume are held constant. Soil 1.
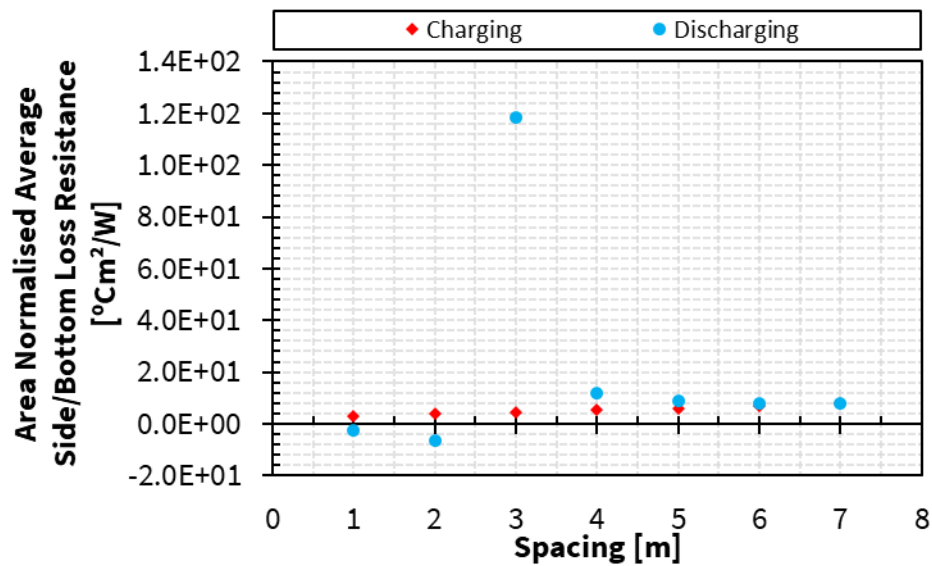
Figure A.2: Sides and bottom loss resistance of periodic steady state BTES operation normalized against storage volume side and bottom area with respect to borehole spacing. The negative discharging resistance values and large magnitude of discharging resistance for 3 m spacing is a result of the change in heat transfer direction that occurs for periodic steady state side/bottom

loss heat transfer rate. Spacing and depth are the variable parameters. Number of boreholes and volume are held constant. Soil 1.
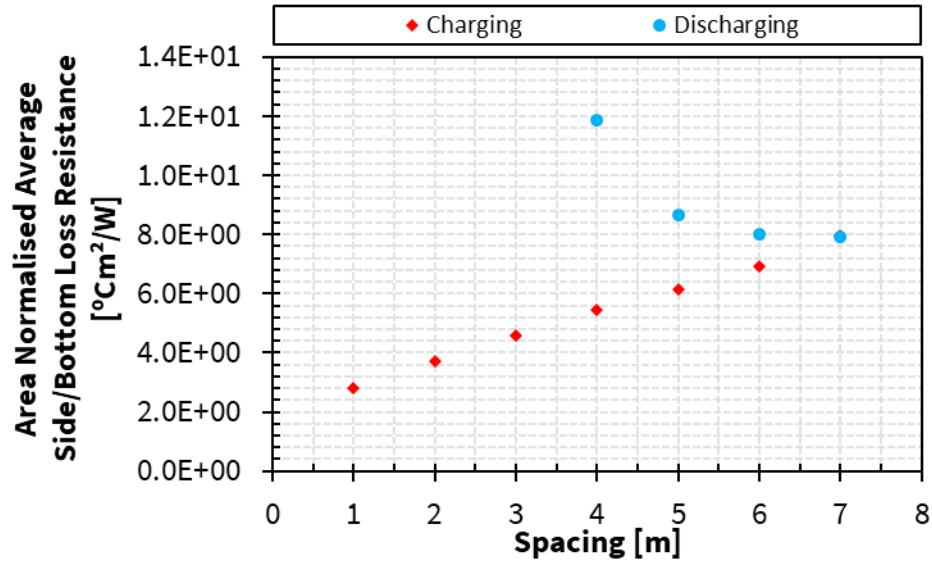
Figure A.3: Sides and bottom loss resistance of periodic steady state BTES operation normalized against storage volume side and bottom area with respect to borehole spacing. The figure's y-axis is reduced to omit discharging resistance outliers and better display charging resistance values. Spacing and depth are the variable parameters. Number of boreholes and volume are held constant. Soil 1.
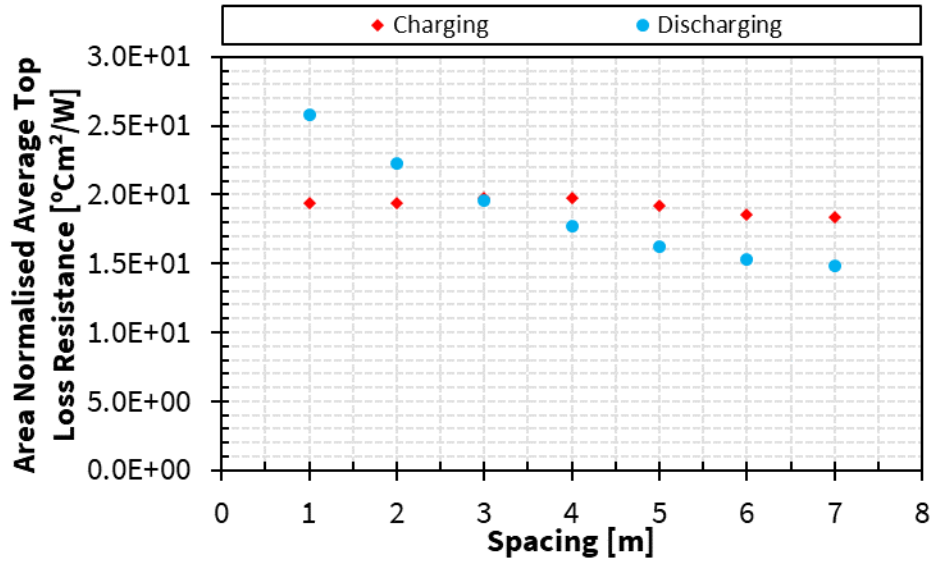
Figure A.4: Top loss resistance of periodic steady state BTES operation normalized against storage volume top area with respect to borehole spacing. Spacing and depth are the variable parameters. Number of boreholes and volume are held constant. Soil 1.
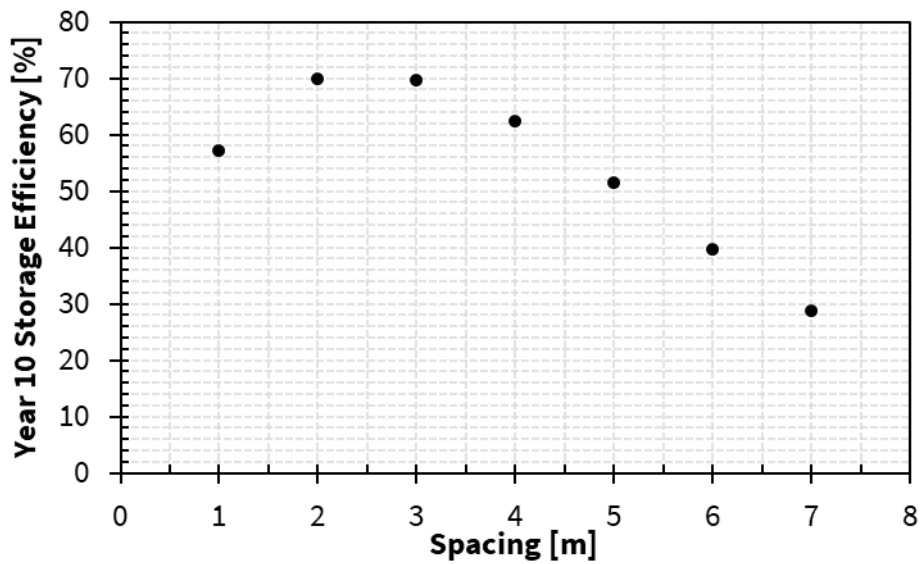
Figure A.5: Periodic steady state BTES thermal storage efficiency with respect to borehole spacing. BTES thermal storage efficiency is defined as the ratio of the total energy extracted during discharging timestep to the total energy injected during charging timestep for a simulation charging and discharging cycle. Spacing and depth are the variable parameters. Number of

124

boreholes and volume are held constant. The inlet temperature setpoint of BTES charging is 95°C and BTES discharging is 20°C. Soil 1.
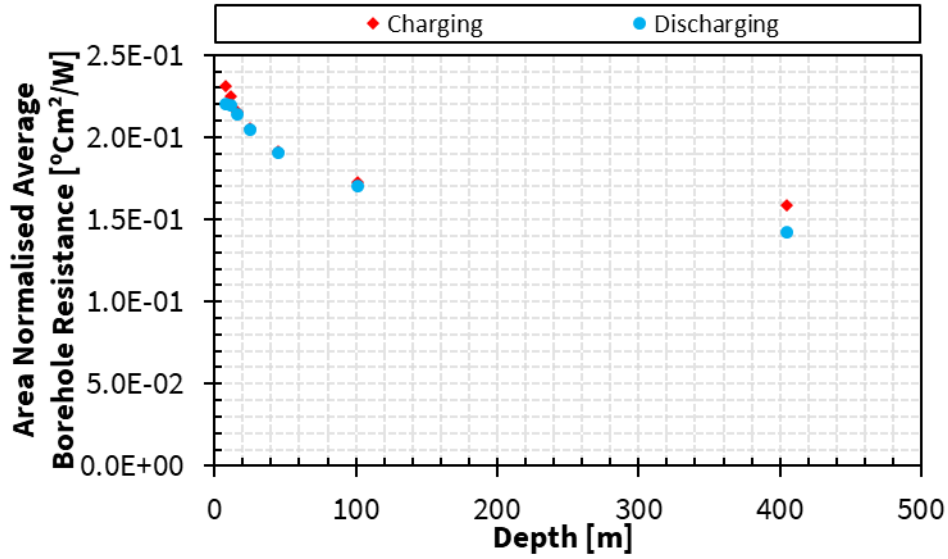
Figure A.6: Borehole heat exchanger thermal resistance of periodic steady state BTES operation normalized against total borehole area with respect to depth. Spacing and depth are the variable parameters. Number of boreholes and volume are held constant. Soil 1.
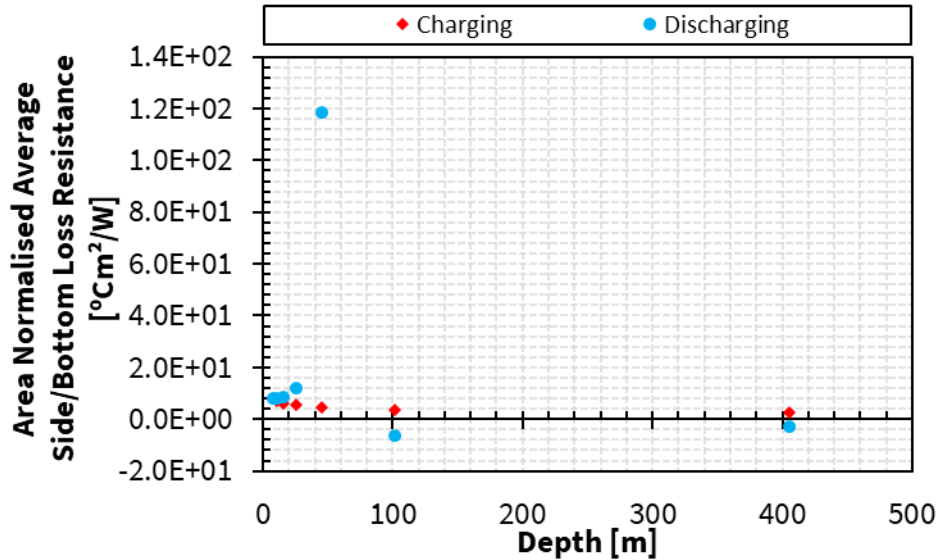
Figure A.7: Sides and bottom loss resistance of periodic steady state BTES operation normalized against storage volume side and bottom area with respect to depth. The negative discharging

resistance values and large magnitude discharging resistance for 45m depth is a result of the change in heat transfer direction that occurs for periodic steady state side/bottom loss heat transfer rate. Spacing and depth are the variable parameters. Number of boreholes and volume are held constant. Soil 1.
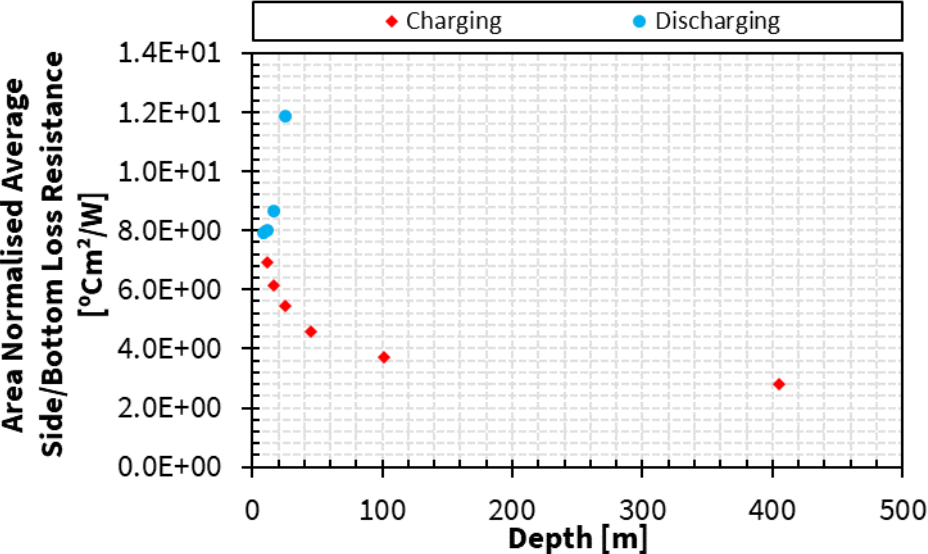
Figure A.8: Sides and bottom loss resistance of periodic steady state BTES operation normalized against storage volume side and bottom area with respect to depth. The figure's y-axis is reduced to omit discharging resistance outliers and better display charging resistance values. Spacing and depth are the variable parameters. Number of boreholes and volume are held constant. Soil 1.
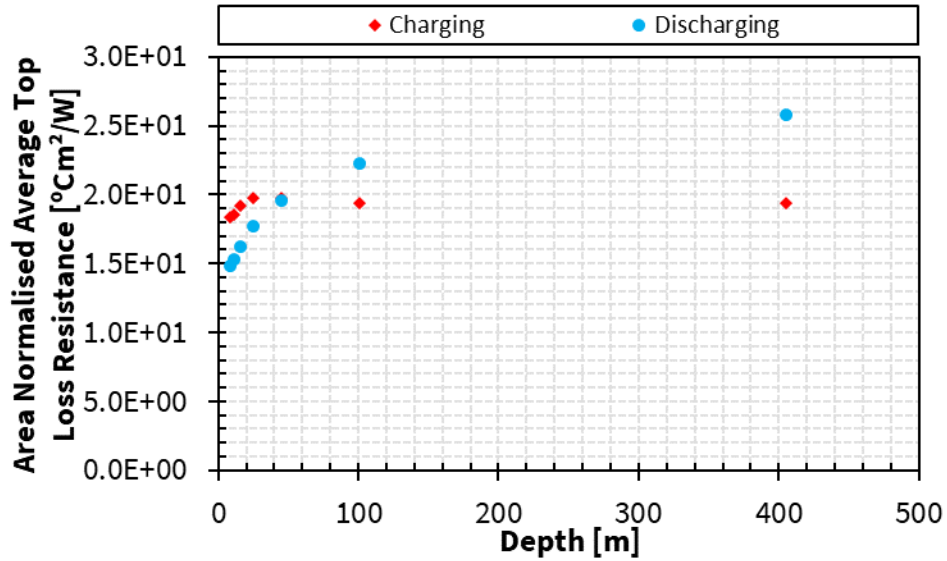
Figure A.9: Top loss resistance of periodic steady state BTES operation normalized against storage volume top area with respect to depth. Spacing and depth are the variable parameters. Number of boreholes and volume are held constant. Soil 1.
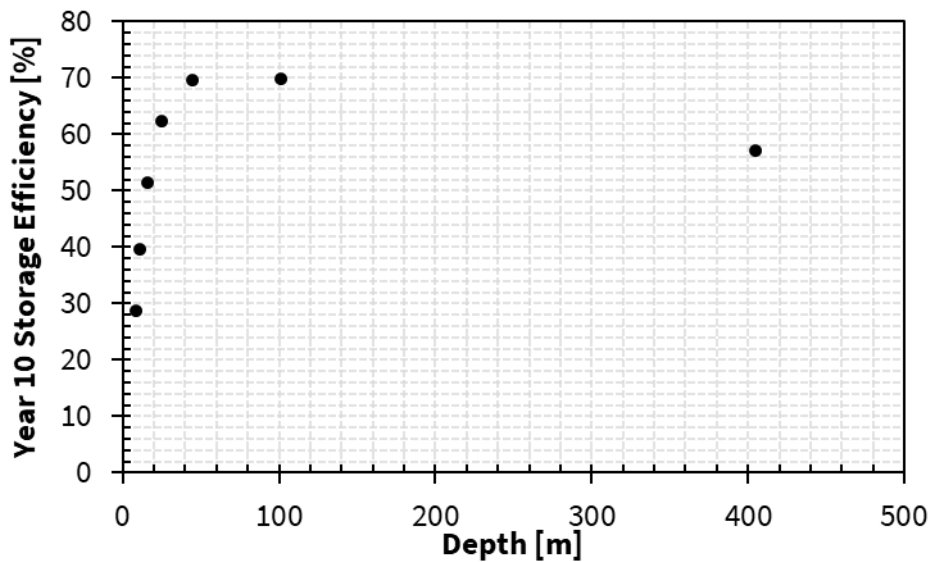
Figure A.10: Periodic steady state BTES thermal storage efficiency with respect to depth. BTES thermal storage efficiency is defined as the ratio of the total energy extracted during discharging timestep to the total energy injected during charging timestep for a simulation charging and discharging cycle. Spacing and depth are the variable parameters. Number of boreholes and

volume are held constant. The inlet temperature setpoint of BTES charging is 95°C and BTES discharging is 20°C. Soil 1.

s [m]	#BH	H [m]	V [m³]	A_{TBA} [m²]	$A_{SV\_s,b}$ [m²]	A_{SV_t} [m²]	R_{hx} (charge) [°Cm²/W]	R_{hx} (discharge) [°Cm²/W]	$R_{loss\_s,b}$ (charge) [°Cm²/W]	$R_{loss\_s,b}$ (discharge) [°Cm²/W]	R_{loss_t} (charge) [°Cm²/W]	R_{loss_t} (discharge) [°Cm²/W]	Efficiency [%]
1	432	45	16833	9161	3459	374	1.52E-01	1.32E-01	3.02E+00	-2.08E+00	1.69E+01	2.13E+01	76.3
1.5	192	45	16833	4072	3459	374	1.61E-01	1.53E-01	3.33E+00	-3.33E+00	1.76E+01	2.07E+01	75.9
2	108	45	16833	2290	3459	374	1.72E-01	1.69E-01	3.70E+00	-6.59E+00	1.83E+01	2.02E+01	74.8
3	48	45	16833	1018	3459	374	1.91E-01	1.91E-01	4.60E+00	1.19E+02	1.97E+01	1.96E+01	69.8
4	27	45	16833	573	3459	374	2.05E-01	2.04E-01	5.68E+00	1.38E+01	2.13E+01	1.95E+01	61.5
5	17	45	16833	360	3459	374	2.16E-01	2.14E-01	6.67E+00	1.01E+01	2.27E+01	1.99E+01	51.7
6	12	45	16833	254	3459	374	2.24E-01	2.20E-01	7.52E+00	8.95E+00	2.41E+01	2.04E+01	43.0
7	9	45	16833	191	3459	374	2.31E-01	2.22E-01	8.20E+00	8.39E+00	2.51E+01	2.09E+01	35.7

Table A.2: Design parameters, heat transfer areas, periodic steady state thermal resistances, and periodic steady state storage efficiencies for the soil 1 parameter sweep with variable parameters: spacing and number of boreholes and constant parameters: depth and volume. The periodic steady state thermal resistances of charging and discharging and the periodic steady state storage efficiency are presented in Figure A.11 to Figure A.20 with respect to the variable parameters.
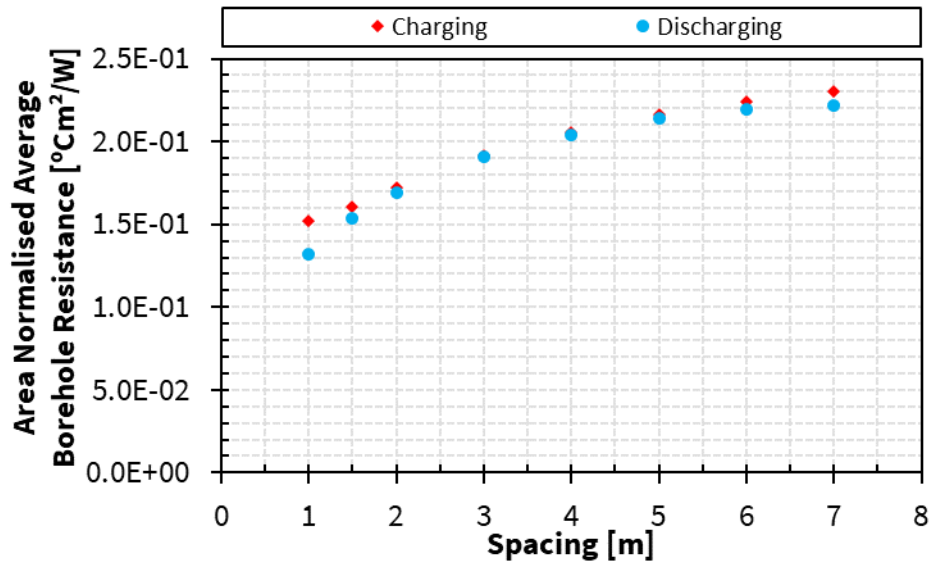
Figure A.11: Borehole heat exchanger thermal resistance of periodic steady state BTES operation normalized against total borehole area with respect to borehole spacing. Spacing and number of boreholes are the variable parameters. Depth and volume are held constant. Soil 1.
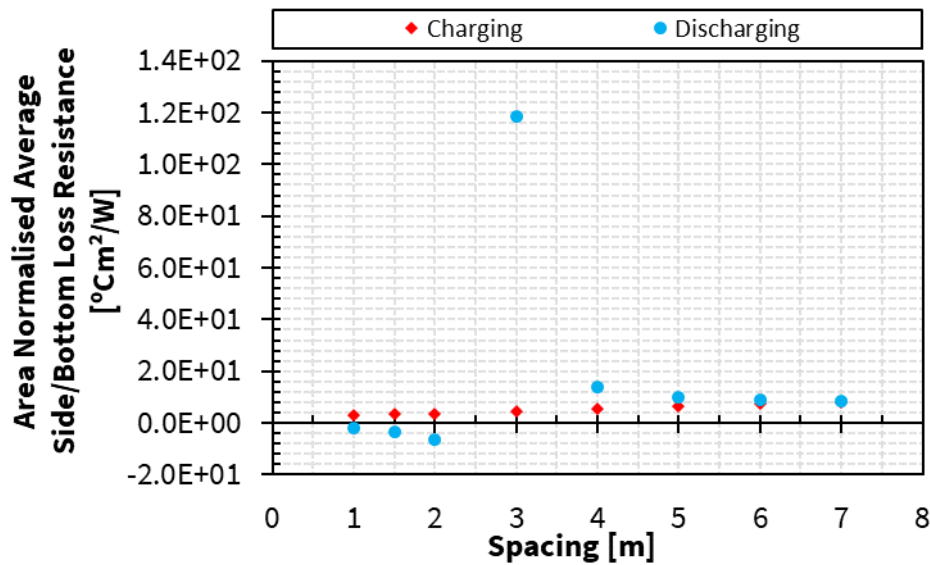
Figure A.12: Sides and bottom loss resistance of periodic steady state BTES operation normalized against storage volume side and bottom area with respect to borehole spacing. The negative discharging resistance values and large magnitude of discharging resistance for 3 m spacing is a result of the change in heat transfer direction that occurs for periodic steady state

side/bottom loss heat transfer rate. Spacing and number of boreholes are the variable parameters. Depth and volume are held constant. Soil 1.
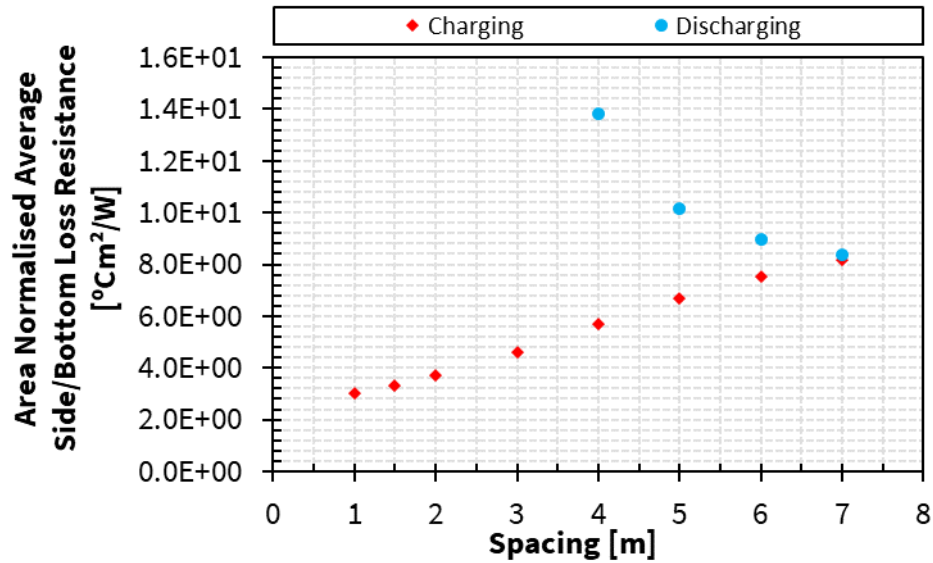
Figure A.13: Sides and bottom loss resistance of periodic steady state BTES operation normalized against storage volume side and bottom area with respect to borehole spacing. The figure's y-axis is reduced to omit discharging resistance outliers and better display charging resistance values. Spacing and number of boreholes are the variable parameters. Depth and volume are held constant. Soil 1.
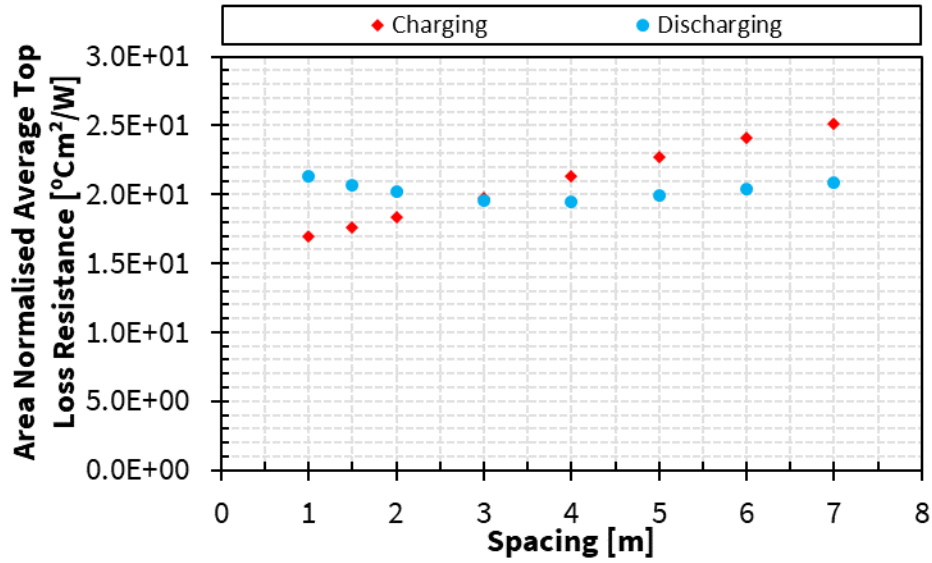
Figure A.14: Top loss resistance of periodic steady state BTES operation normalized against storage volume top area with respect to borehole spacing. Spacing and number of boreholes are the variable parameters. Depth and volume are held constant. Soil 1.
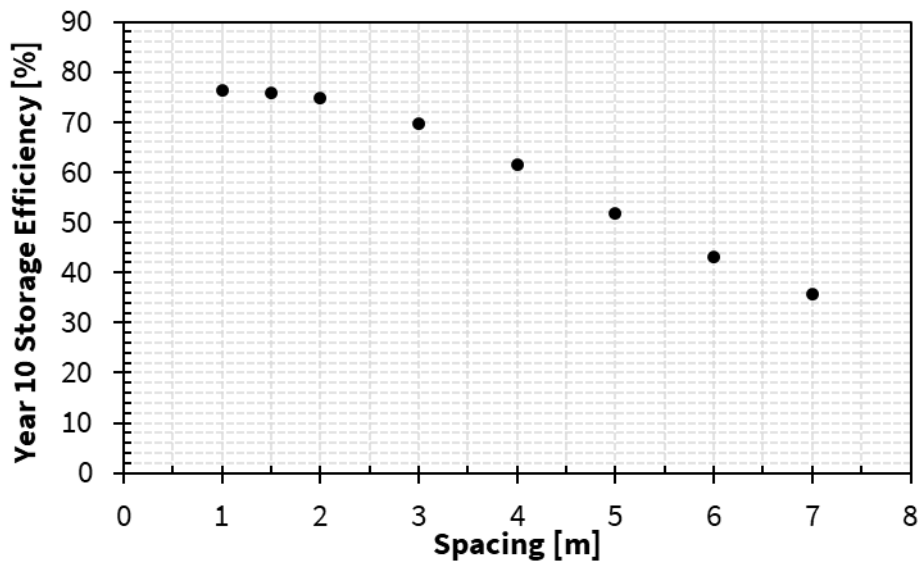
Figure A.15: Periodic steady state BTES thermal storage efficiency with respect to borehole spacing. BTES thermal storage efficiency is defined as the ratio of the total energy extracted during discharging timestep to the total energy injected during charging timestep for a simulation charging and discharging cycle. Spacing and number of boreholes are the variable parameters.

Depth and volume are held constant. The inlet temperature setpoint of BTES charging is 95°C and BTES discharging is 20°C. Soil 1.
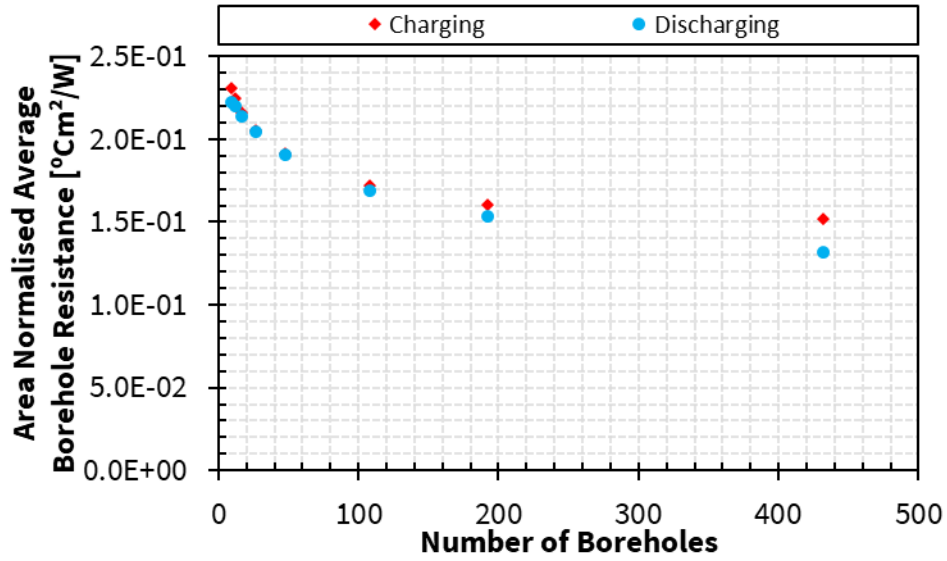
Figure A.16: Borehole heat exchanger thermal resistance of periodic steady state BTES operation normalized against total borehole area with respect to number of boreholes. Spacing and number of boreholes are the variable parameters. Depth and volume are held constant. Soil 1.
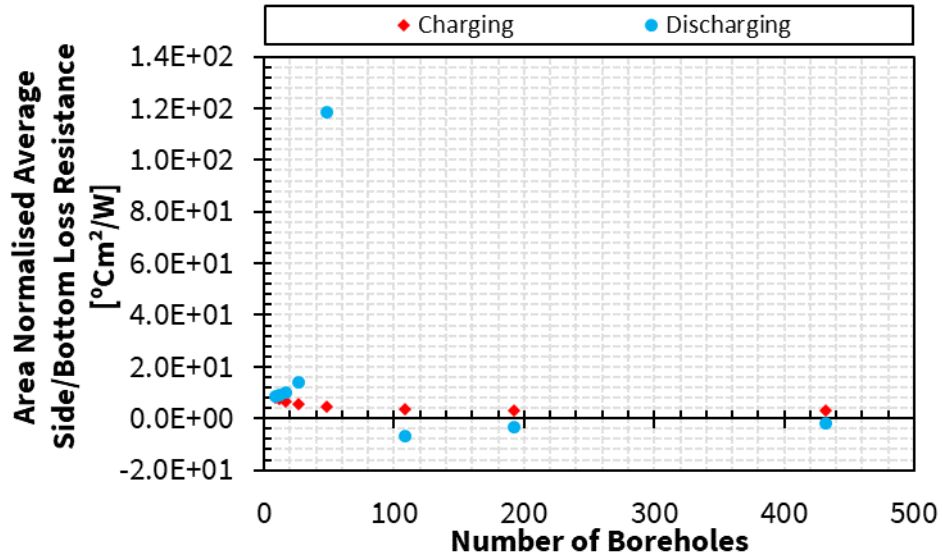
Figure A.17: Sides and bottom loss resistance of periodic steady state BTES operation normalized against storage volume side and bottom area with respect to number of boreholes. The negative discharging resistance values and large magnitude discharging resistance for 48 boreholes is a result of the change in heat transfer direction that occurs for periodic steady state side/bottom loss heat transfer rate. Spacing and number of boreholes are the variable parameters. Depth and volume are held constant. Soil 1.
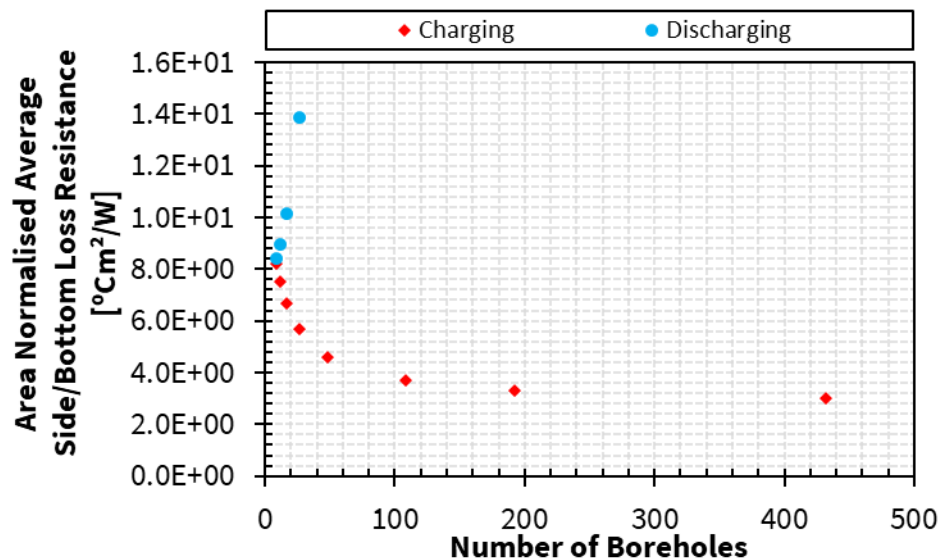
Figure A.18: Sides and bottom loss resistance of periodic steady state BTES operation normalized against storage volume side and bottom area with respect to number of boreholes.

The figure's y-axis is reduced to omit discharging resistance outliers and better display charging resistance values. Spacing and number of boreholes are the variable parameters. Depth and volume are held constant. Soil 1.
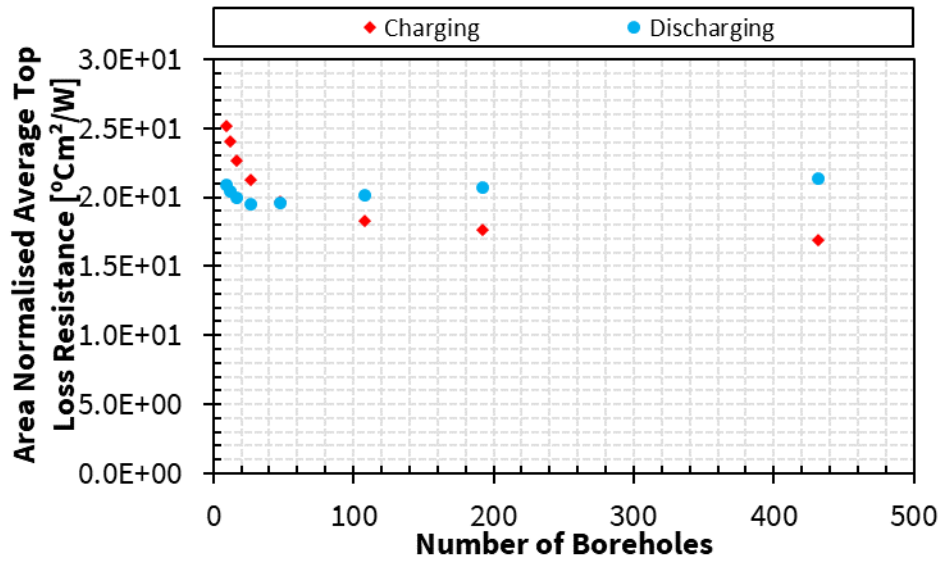
Figure A.19: Top loss resistance of periodic steady state BTES operation normalized against storage volume top area with respect to number of boreholes. Spacing and number of boreholes are the variable parameters. Depth and volume are held constant. Soil 1.
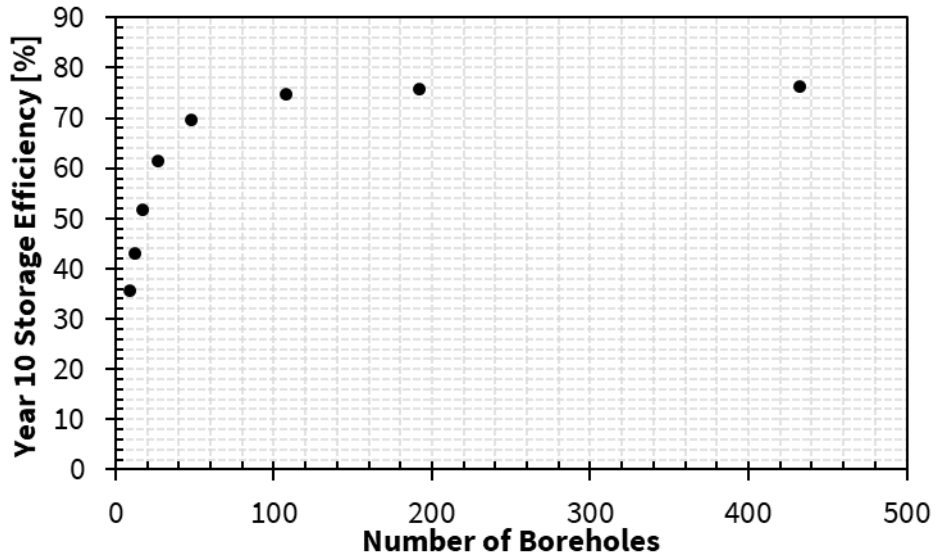
Figure A.20: Periodic steady state BTES thermal storage efficiency with respect to number of boreholes. BTES thermal storage efficiency is defined as the ratio of the total energy extracted during discharging timestep to the total energy injected during charging timestep for a simulation charging and discharging cycle. Spacing and number of boreholes are the variable parameters. Depth and volume are held constant. The inlet temperature setpoint of BTES charging is 95°C and BTES discharging is 20°C. Soil 1.

#BH	V [m^3]	s [m]	H [m]	A_{TBA} [m^2]	$A_{SV\_s,b}$ [m^2]	A_{SV_t} [m^2]	R_{hx} (charge) [°Cm^2/W]	R_{hx} (discharge) [°Cm^2/W]	$R_{loss\_s,b}$ (charge) [°Cm^2/W]	$R_{loss\_s,b}$ (discharge) [°Cm^2/W]	R_{loss_t} (charge) [°Cm^2/W]	R_{loss_t} (discharge) [°Cm^2/W]	Efficiency [%]
10	3507	3	45	212	1486	78	1.91E-01	1.90E-01	3.74E+00	3.10E+01	2.12E+01	2.25E+01	44.5
25	8767	3	45	530	2421	195	1.91E-01	1.91E-01	4.24E+00	7.34E+01	1.99E+01	2.01E+01	60.9
48	16833	3	45	1018	3459	374	1.91E-01	1.91E-01	4.60E+00	1.19E+02	1.97E+01	1.96E+01	69.8
75	26302	3	45	1590	4441	584	1.92E-01	1.91E-01	4.88E+00	9.53E+01	2.00E+01	1.99E+01	74.3
100	35069	3	45	2121	5233	779	1.93E-01	1.91E-01	5.09E+00	6.89E+01	2.05E+01	2.04E+01	76.6
150	52604	3	45	3181	6623	1169	1.94E-01	1.92E-01	5.43E+00	4.32E+01	2.15E+01	2.15E+01	79.1
200	70138	3	45	4241	7856	1559	1.97E-01	1.93E-01	5.73E+00	3.23E+01	2.26E+01	2.27E+01	80.2
500	175345	3	45	10603	13854	3897	2.26E-01	2.05E-01	6.90E+00	1.76E+01	2.80E+01	2.88E+01	80.3

Table A.3: Design parameters, heat transfer areas, periodic steady state thermal resistances, and periodic steady state storage efficiencies for the soil 1 parameter sweep with variable parameters: number of boreholes and volume and constant parameters: spacing and depth. The periodic steady state thermal resistances of charging and discharging and the periodic steady state storage efficiency are presented in Figure A.21 to Figure A.30 with respect to the variable parameters.
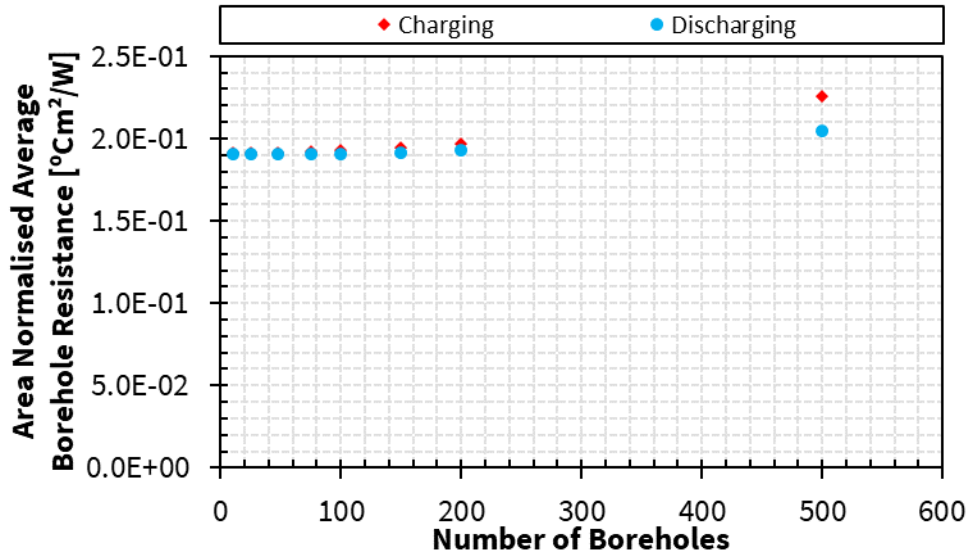
Figure A.21: Borehole heat exchanger thermal resistance of periodic steady state BTES operation normalized against total borehole area with respect to number of boreholes. Number of boreholes and volume are the variable parameters. Spacing and depth are held constant. Soil 1.
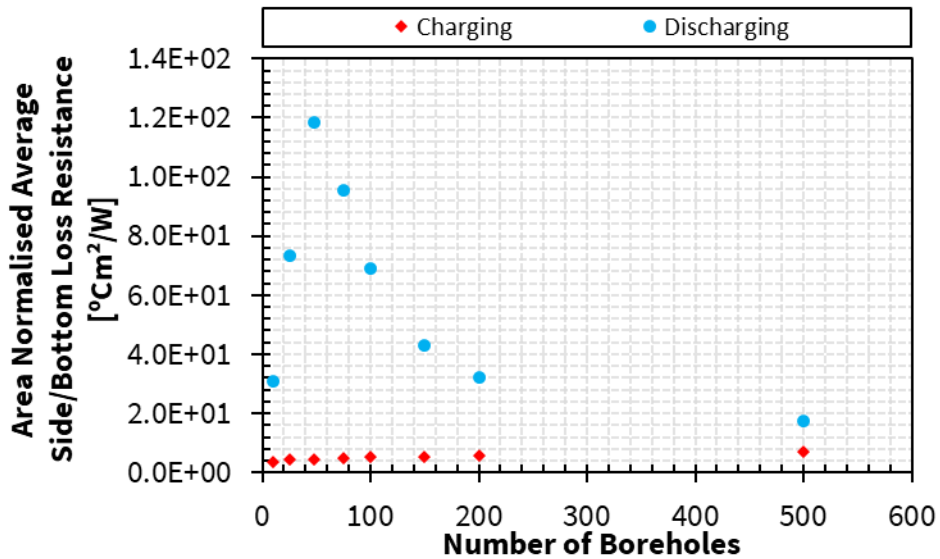
Figure A.22: Sides and bottom loss resistance of periodic steady state BTES operation normalized against storage volume side and bottom area with respect to number of boreholes. The larger magnitude of discharging resistances is a result of the change in heat transfer direction that occurs for periodic steady state side/bottom loss heat transfer rate. Number of boreholes and volume are the variable parameters. Spacing and depth are held constant. Soil 1.
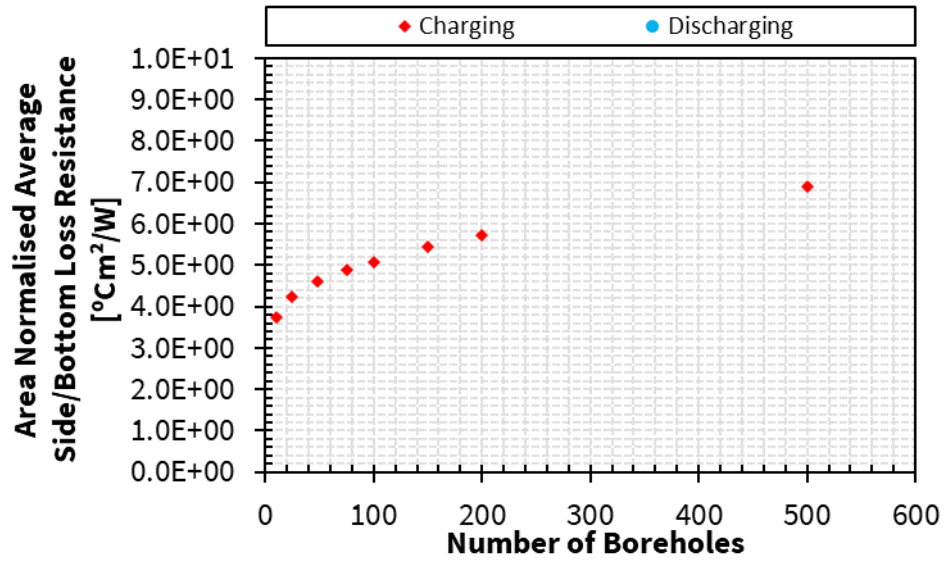
Figure A.23: Sides and bottom loss resistance of periodic steady state BTES operation normalized against storage volume side and bottom area with respect to number of boreholes. The figure's y-axis is reduced to omit discharging resistance outliers and better display charging resistance values. Number of boreholes and volume are the variable parameters. Spacing and depth are held constant. Soil 1.
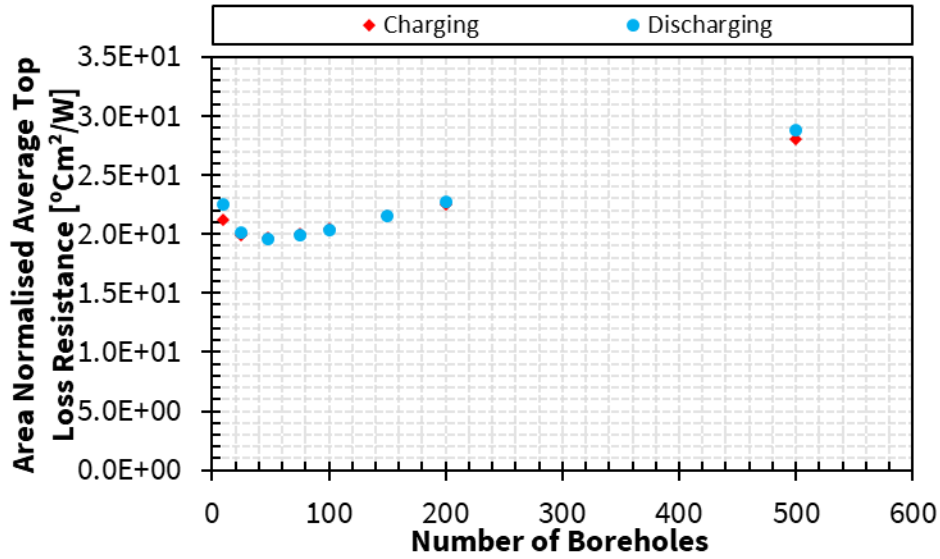
Figure A.24: Top loss resistance of periodic steady state BTES operation normalized against storage volume top area with respect to number of boreholes. Number of boreholes and volume are the variable parameters. Spacing and depth are held constant. Soil 1.
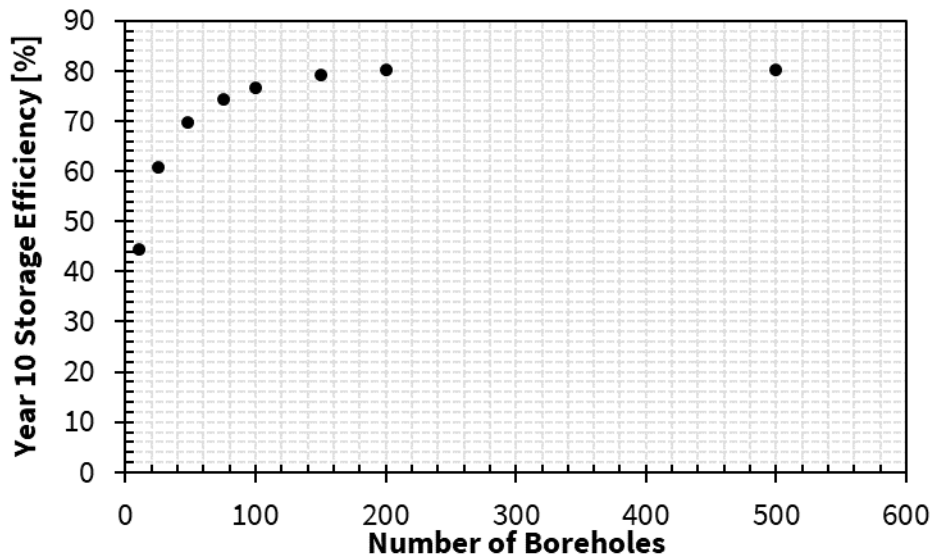
Figure A.25: Periodic steady state BTES thermal storage efficiency with respect to number of boreholes. BTES thermal storage efficiency is defined as the ratio of the total energy extracted during discharging timestep to the total energy injected during charging timestep for a simulation charging and discharging cycle. Number of boreholes and volume are the variable parameters.

Spacing and depth are held constant. The inlet temperature setpoint of BTES charging is 95°C and BTES discharging is 20°C. Soil 1.
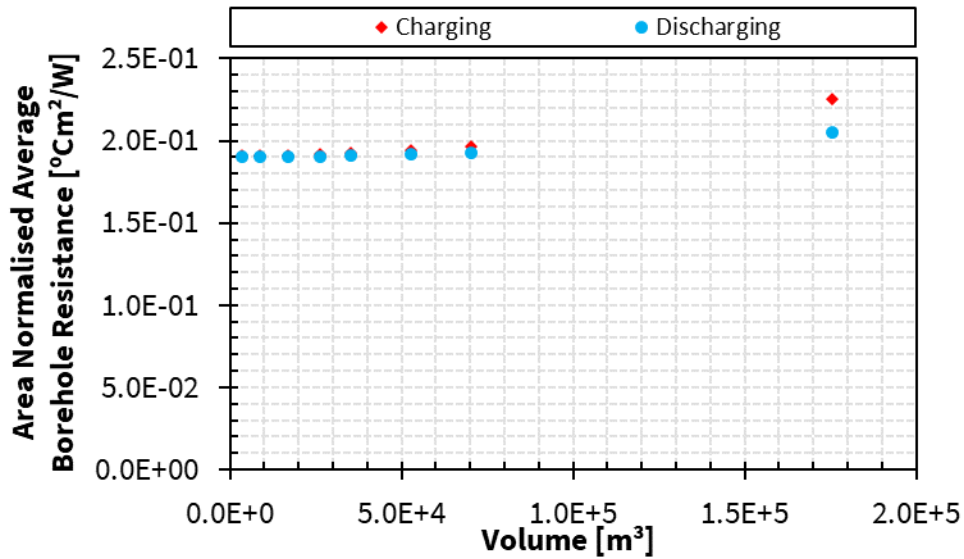
Figure A.26: Borehole heat exchanger thermal resistance of periodic steady state BTES operation normalized against total borehole area with respect to storage volume. Number of boreholes and volume are the variable parameters. Spacing and depth are held constant. Soil 1.
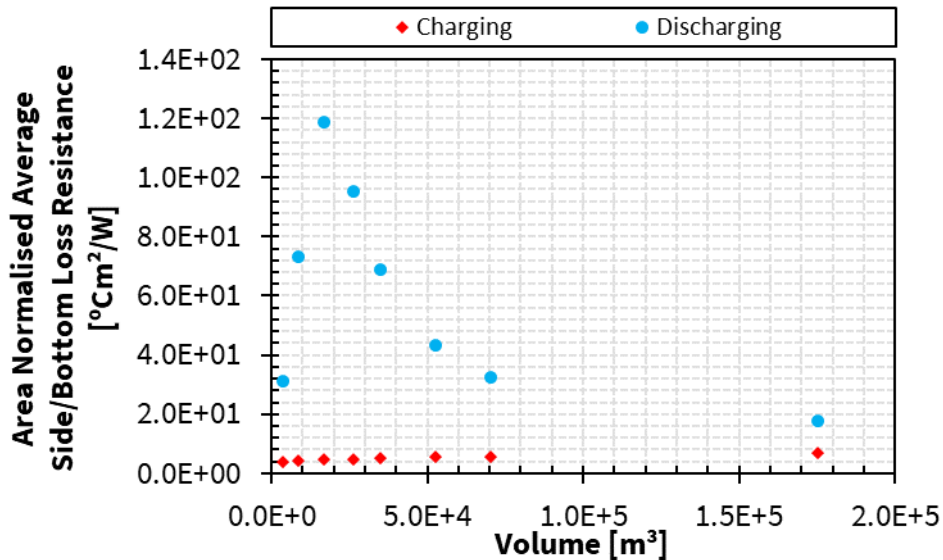
Figure A.27: Sides and bottom loss resistance of periodic steady state BTES operation normalized against storage volume side and bottom area with respect to storage volume. The

larger magnitude of discharging resistances is a result of the change in heat transfer direction that occurs for periodic steady state side/bottom loss heat transfer rate. Number of boreholes and volume are the variable parameters. Spacing and depth are held constant. Soil 1.
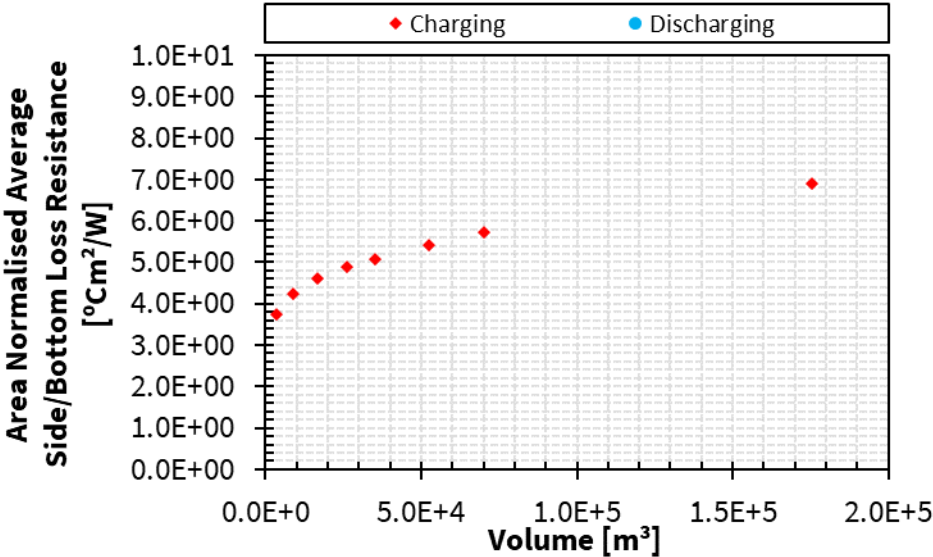
Figure A.28: Sides and bottom loss resistance of periodic steady state BTES operation normalized against storage volume side and bottom area with respect to storage volume. The figure's y-axis is reduced to omit discharging resistance outliers and better display charging resistance values. Number of boreholes and volume are the variable parameters. Spacing and depth are held constant. Soil 1.
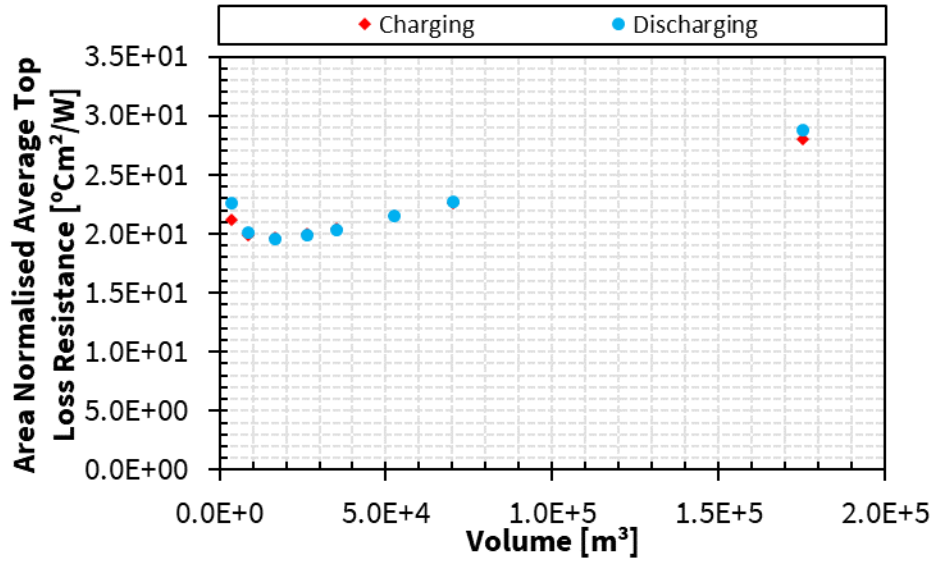
Figure A.29: Top loss resistance of periodic steady state BTES operation normalized against storage volume top area with respect to storage volume. Number of boreholes and volume are the variable parameters. Spacing and depth are held constant. Soil 1.
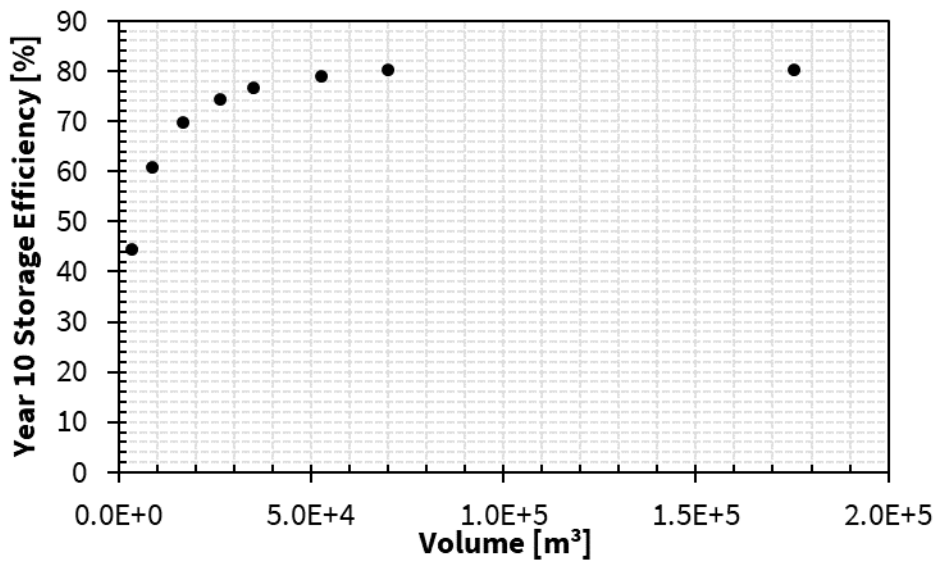
Figure A.30: Periodic steady state BTES thermal storage efficiency with respect to storage volume. BTES thermal storage efficiency is defined as the ratio of the total energy extracted during discharging timestep to the total energy injected during charging timestep for a simulation charging and discharging cycle. Number of boreholes and volume are the variable parameters.

Spacing and depth are held constant. The inlet temperature setpoint of BTES charging is 95°C and BTES discharging is 20°C. Soil 1.

H [m]	V [m^3]	s [m]	#BH	A$_{TBA}$ [m^2]	A$_{SV\_s,b}$ [m^2]	A$_{SV\_t}$ [m^2]	R$_{hx}$ (charge) [°Cm^2/W]	R$_{hx}$ (discharge) [°Cm^2/W]	R$_{loss\_s,b}$ (charge) [°Cm^2/W]	R$_{loss\_s,b}$ (discharge) [°Cm^2/W]	R$_{loss\_t}$ (charge) [°Cm^2/W]	R$_{loss\_t}$ (discharge) [°Cm^2/W]	Efficiency [%]
5	1870	3	48	113	717	374	1.91E-01	1.90E-01	3.13E+00	8.26E+00	1.62E+01	1.48E+01	33.4
10	3741	3	48	226	1060	374	1.91E-01	1.91E-01	3.47E+00	1.08E+01	1.71E+01	1.58E+01	48.1
25	9352	3	48	565	2088	374	1.91E-01	1.91E-01	4.13E+00	3.14E+01	1.86E+01	1.80E+01	63.7
45	16833	3	48	1018	3459	374	1.91E-01	1.91E-01	4.60E+00	1.19E+02	1.97E+01	1.96E+01	69.8
75	28055	3	48	1696	5516	374	1.92E-01	1.91E-01	5.00E+00	3.00E+02	2.10E+01	2.13E+01	72.5
100	37407	3	48	2262	7230	374	1.93E-01	1.91E-01	5.22E+00	1.58E+02	2.19E+01	2.25E+01	73.1
150	56110	3	48	3393	10658	374	1.96E-01	1.91E-01	5.57E+00	6.33E+01	2.37E+01	2.48E+01	72.9
250	93517	3	48	5655	17514	374	2.04E-01	1.90E-01	6.07E+00	3.05E+01	2.73E+01	2.88E+01	70.7
300	112221	3	48	6786	20943	374	2.12E-01	1.91E-01	6.28E+00	2.52E+01	2.88E+01	3.06E+01	69.3

Table A.4: Design parameters, heat transfer areas, periodic steady state thermal resistances, and periodic steady state storage efficiencies for the soil 1 parameter sweep with variable parameters: depth and volume and constant parameters: spacing and number of boreholes. The periodic steady state thermal resistances of charging and discharging and the periodic steady state storage efficiency are presented in Figure A.31 to Figure A.40 with respect to the variable parameters.
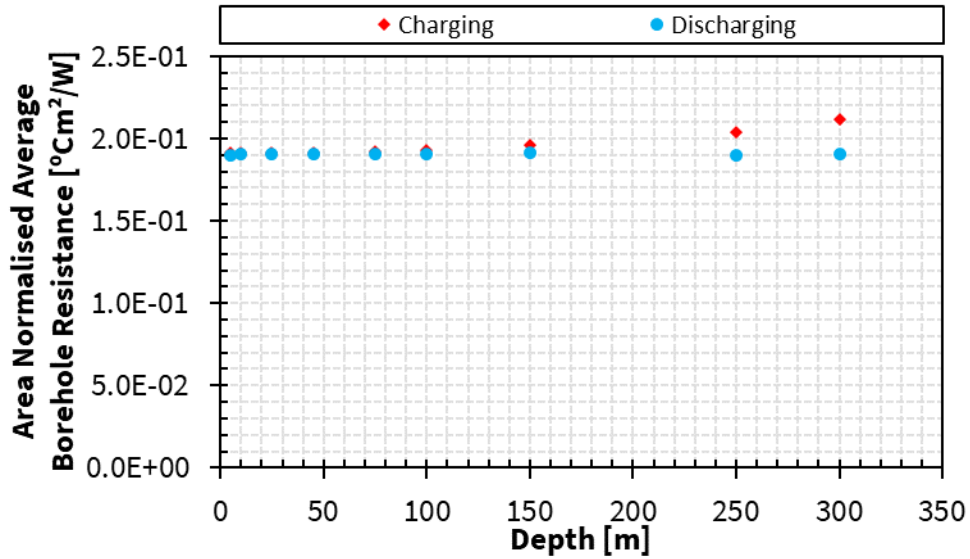
Figure A.31: Borehole heat exchanger thermal resistance of periodic steady state BTES operation normalized against total borehole area with respect to depth. Depth and volume are the variable parameters. Spacing and number of boreholes are held constant. Soil 1.
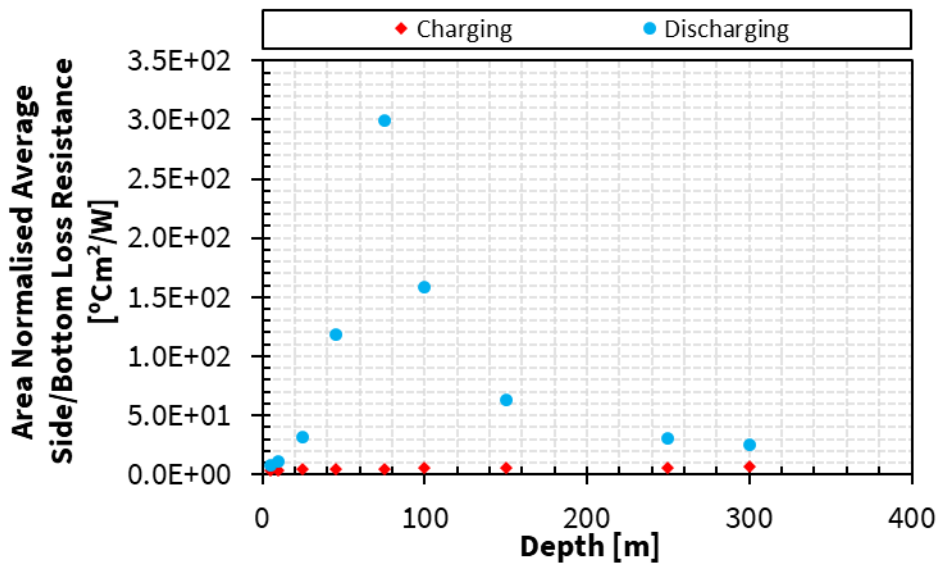
Figure A.32: Sides and bottom loss resistance of periodic steady state BTES operation normalized against storage volume side and bottom area with respect to depth. The larger magnitude of discharging resistances is a result of the change in heat transfer direction that occurs for periodic steady state side/bottom loss heat transfer rate. Depth and volume are the variable parameters. Spacing and number of boreholes are held constant. Soil 1.
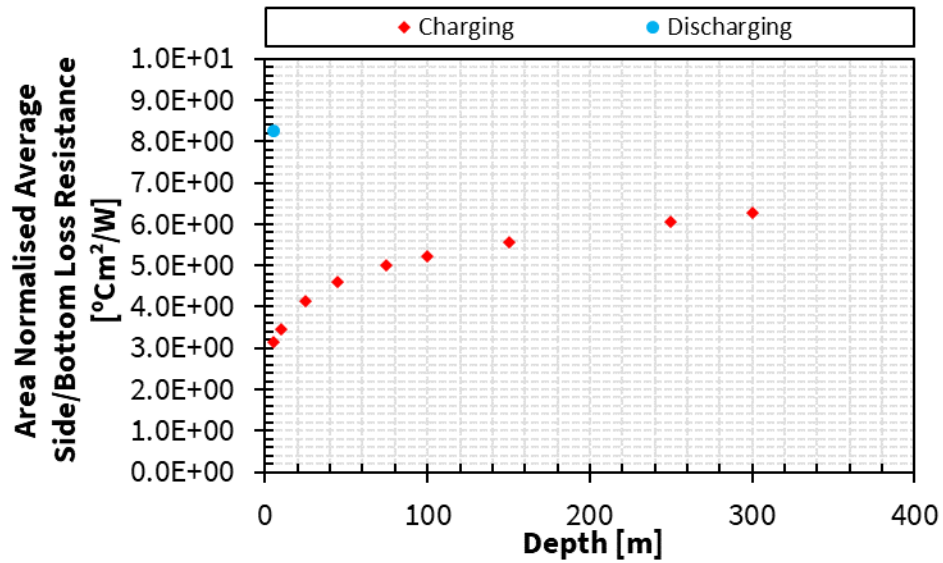
Figure A.33: Sides and bottom loss resistance of periodic steady state BTES operation normalized against storage volume side and bottom area with respect to depth. The figure's y-axis is reduced to omit discharging resistance outliers and better display charging resistance values. Depth and volume are the variable parameters. Spacing and number of boreholes are held constant. Soil 1.
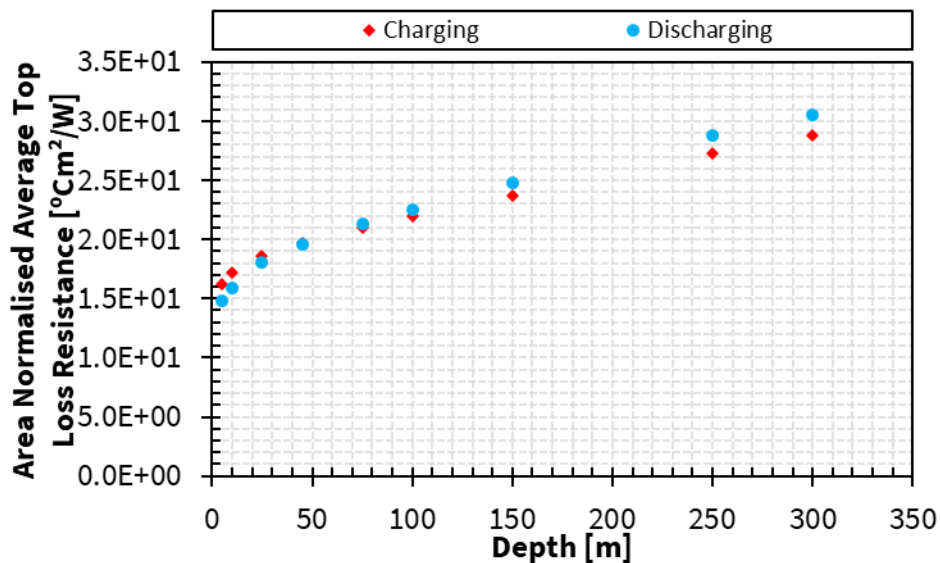
Figure A.34: Top loss resistance of periodic steady state BTES operation normalized against storage volume top area with respect to depth. Depth and volume are the variable parameters. Spacing and number of boreholes are held constant. Soil 1.
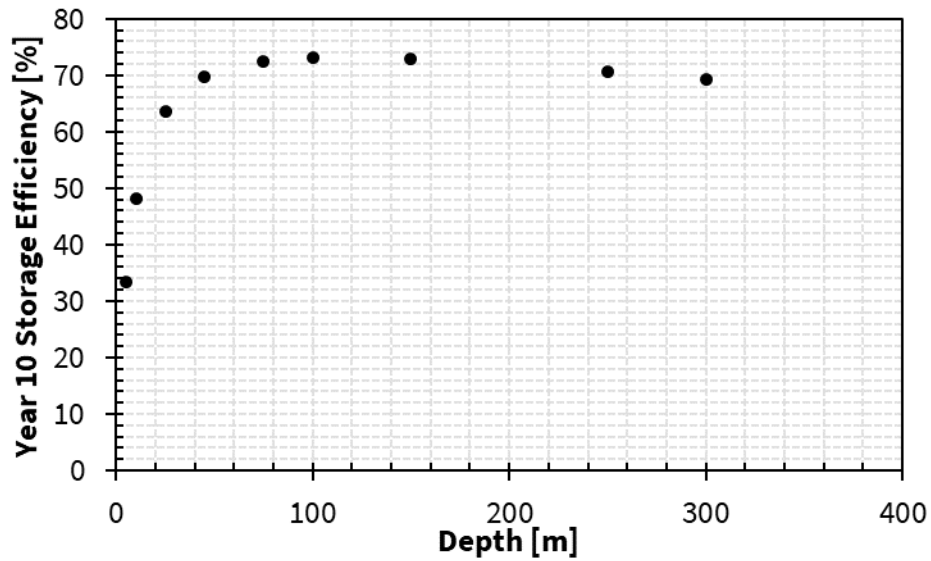
Figure A.35: Periodic steady state BTES thermal storage efficiency with respect to depth. BTES thermal storage efficiency is defined as the ratio of the total energy extracted during discharging timestep to the total energy injected during charging timestep for a simulation charging and discharging cycle. Depth and volume are the variable parameters. Spacing and number of boreholes are held constant. The inlet temperature setpoint of BTES charging is 95°C and BTES discharging is 20°C. Soil 1.
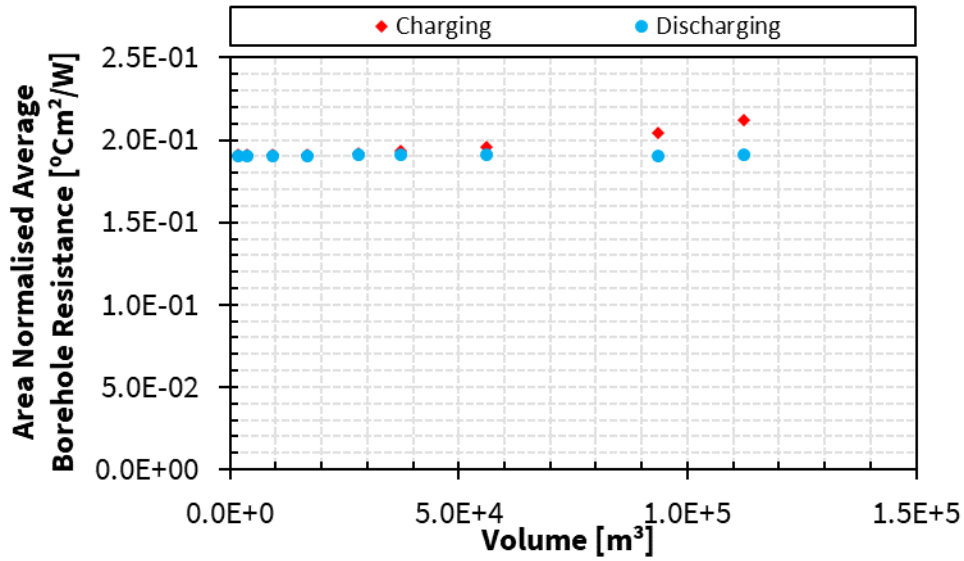
Figure A.36: Borehole heat exchanger thermal resistance of periodic steady state BTES operation normalized against total borehole area with respect to storage volume. Depth and volume are the variable parameters. Spacing and number of boreholes are held constant. Soil 1.
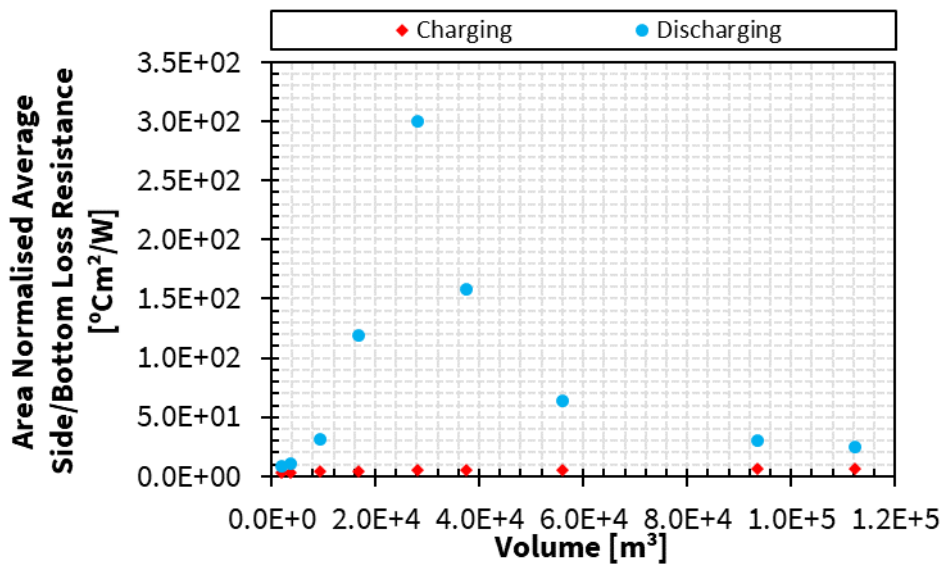
Figure A.37: Sides and bottom loss resistance of periodic steady state BTES operation normalized against storage volume side and bottom area with respect to storage volume. The larger magnitude of discharging resistances is a result of the change in heat transfer direction that occurs for periodic steady state side/bottom loss heat transfer rate. Depth and volume are the variable parameters. Spacing and number of boreholes are held constant. Soil 1.
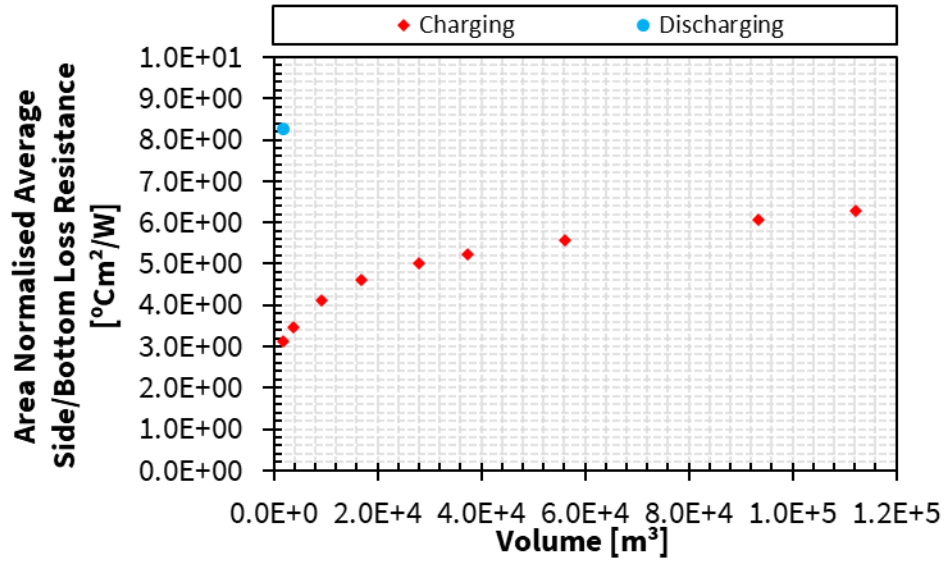
Figure A.38: Sides and bottom loss resistance of periodic steady state BTES operation normalized against storage volume side and bottom area with respect to storage volume. The figure's y-axis is reduced to omit discharging resistance outliers and better display charging resistance values. Depth and volume are the variable parameters. Spacing and number of boreholes are held constant. Soil 1.
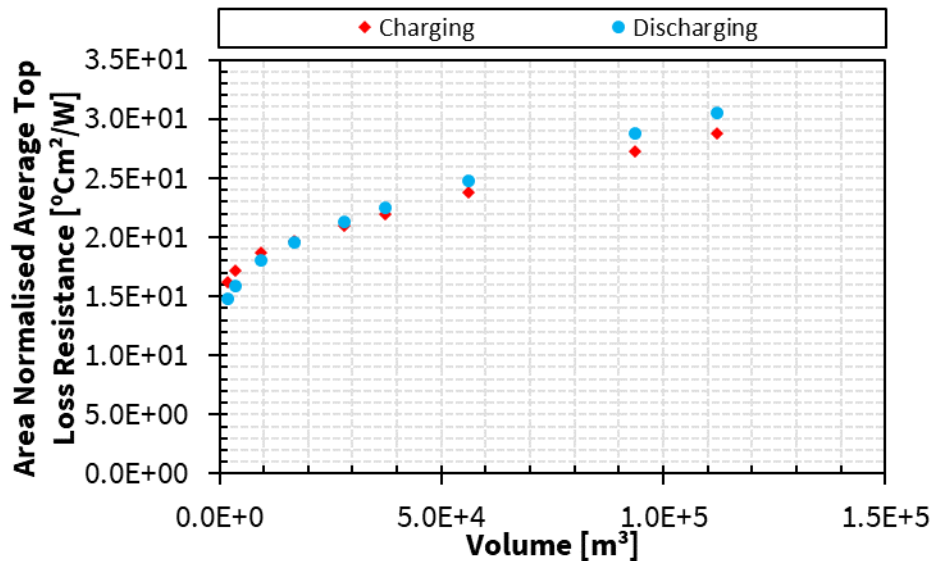
Figure A.39: Top loss resistance of periodic steady state BTES operation normalized against storage volume top area with respect to storage volume. Depth and volume are the variable parameters. Spacing and number of boreholes are held constant. Soil 1.
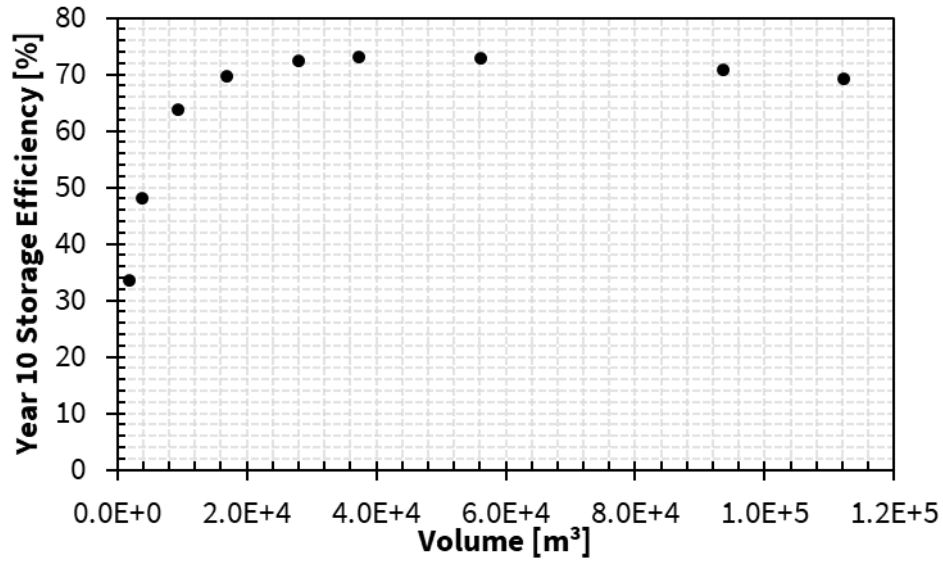
Figure A.40: Periodic steady state BTES thermal storage efficiency with respect to storage volume. BTES thermal storage efficiency is defined as the ratio of the total energy extracted during discharging timestep to the total energy injected during charging timestep for a simulation charging and discharging cycle. Depth and volume are the variable parameters. Spacing and number of boreholes are held constant. The inlet temperature setpoint of BTES charging is 95°C and BTES discharging is 20°C. Soil 1.

Appendix B

s [m]	V [m³]	#BH	H [m]	A_{TBA} [m²]	$A_{SV\_s,b}$ [m²]	A_{SV_t} [m²]	R_{hx} (charge) [°Cm²/W]	R_{hx} (discharge) [°Cm²/W]	$R_{loss\_s,b}$ (charge) [°Cm²/W]	$R_{loss\_s,b}$ (discharge) [°Cm²/W]	R_{loss_t} (charge) [°Cm²/W]	R_{loss_t} (discharge) [°Cm²/W]	Efficiency [%]
1	1870	48	45	1018	1070	42	1.37E-01	1.36E-01	1.96E+00	-1.58E+00	1.70E+01	1.90E+01	64.2
2	7481	48	45	1018	2223	166	1.71E-01	1.70E-01	3.16E+00	-4.97E+01	1.95E+01	1.90E+01	74.2
3	16833	48	45	1018	3459	374	1.90E-01	1.89E-01	4.84E+00	9.93E+00	2.13E+01	1.89E+01	72.3
4	29926	48	45	1018	4779	665	2.03E-01	2.01E-01	6.52E+00	7.93E+00	2.21E+01	1.89E+01	67.4
5	46759	48	45	1018	6181	1039	2.12E-01	2.08E-01	7.87E+00	7.62E+00	2.20E+01	1.92E+01	62.1
6	67332	48	45	1018	7667	1496	2.19E-01	2.11E-01	8.92E+00	7.57E+00	2.19E+01	1.93E+01	56.2
7	91647	48	45	1018	9236	2037	2.24E-01	2.10E-01	9.90E+00	7.66E+00	2.19E+01	1.95E+01	50.0

Table B.1: Design parameters, heat transfer areas, periodic steady state thermal resistances, and periodic steady state storage efficiencies for the soil 2 parameter sweep with variable parameters: spacing and volume and constant parameters: number of boreholes and depth. The periodic steady state thermal resistances of charging and discharging and the periodic steady state storage efficiency are presented in Figure B.1 to Figure B.10 with respect to the variable parameters.
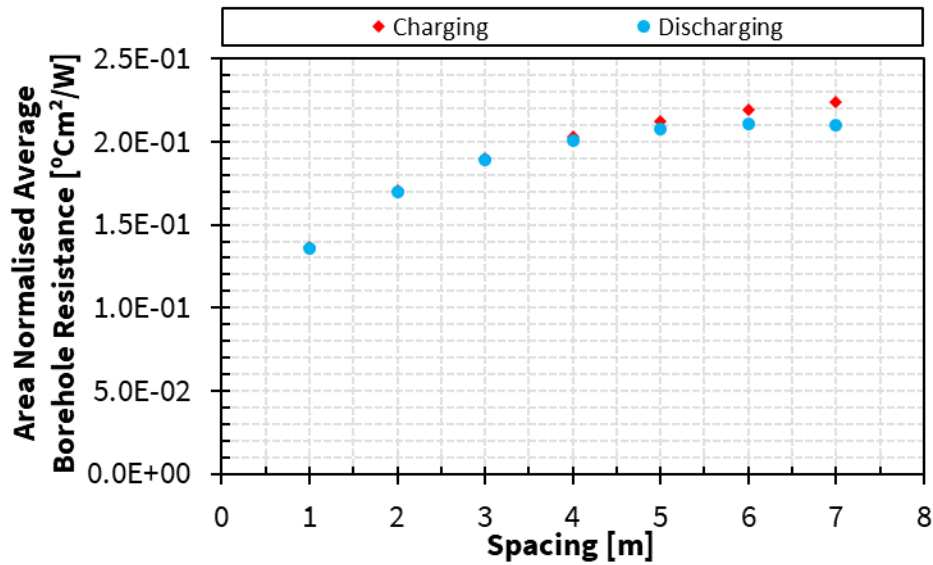
Figure B.1: Borehole heat exchanger thermal resistance of periodic steady state BTES operation normalized against total borehole area with respect to borehole spacing. Spacing and volume are the variable parameters. Number of boreholes and depth are held constant. Soil 2.
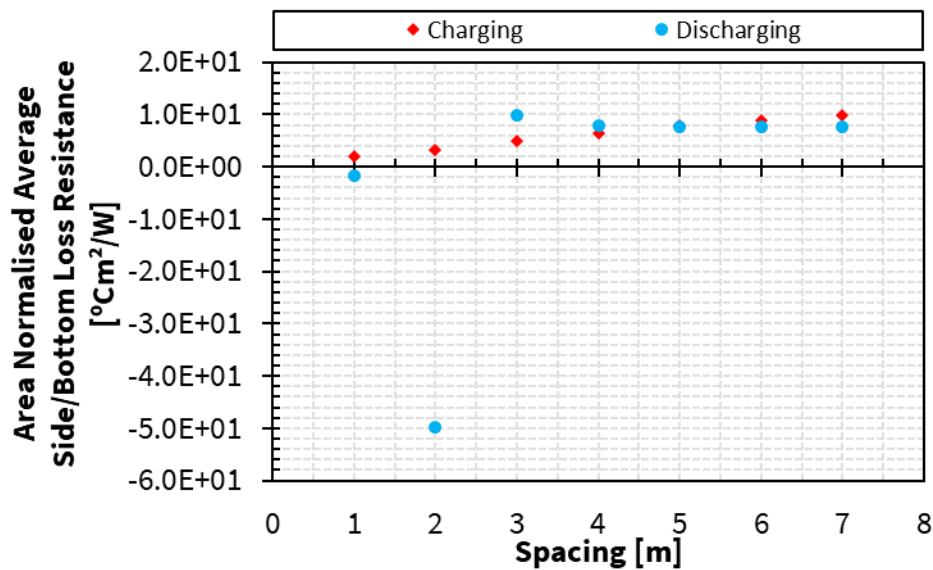
Figure B.2: Sides and bottom loss resistance of periodic steady state BTES operation normalized against storage volume side and bottom area with respect to borehole spacing. The negative discharging resistance values and are a result of the change in heat transfer direction that occurs for periodic steady state side/bottom loss heat transfer rate. Spacing and volume are the variable parameters. Number of boreholes and depth are held constant. Soil 2.
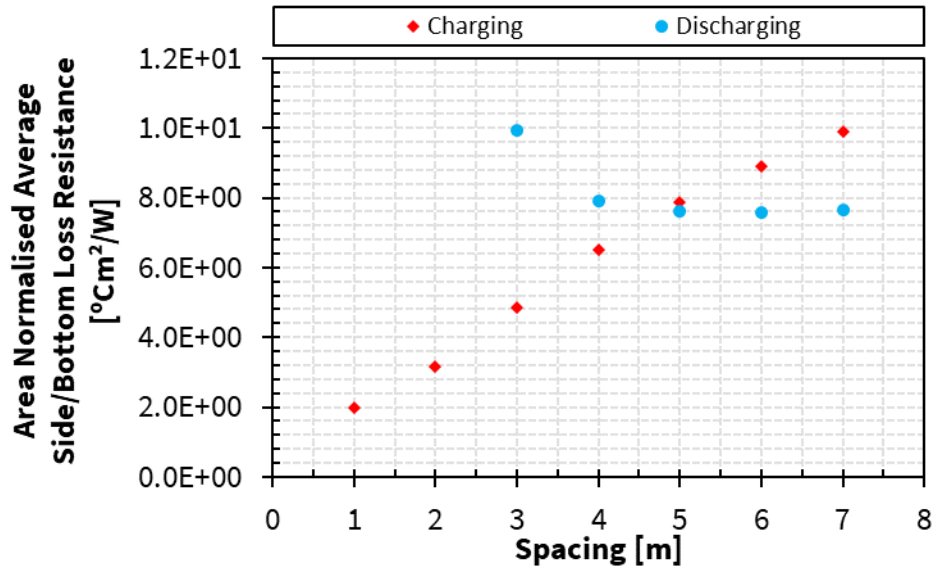
Figure B.3: Sides and bottom loss resistance of periodic steady state BTES operation normalized against storage volume side and bottom area with respect to borehole spacing. The figure's y-axis is reduced to omit discharging resistance outliers and better display charging resistance values. Spacing and volume are the variable parameters. Number of boreholes and depth are held constant. Soil 2.
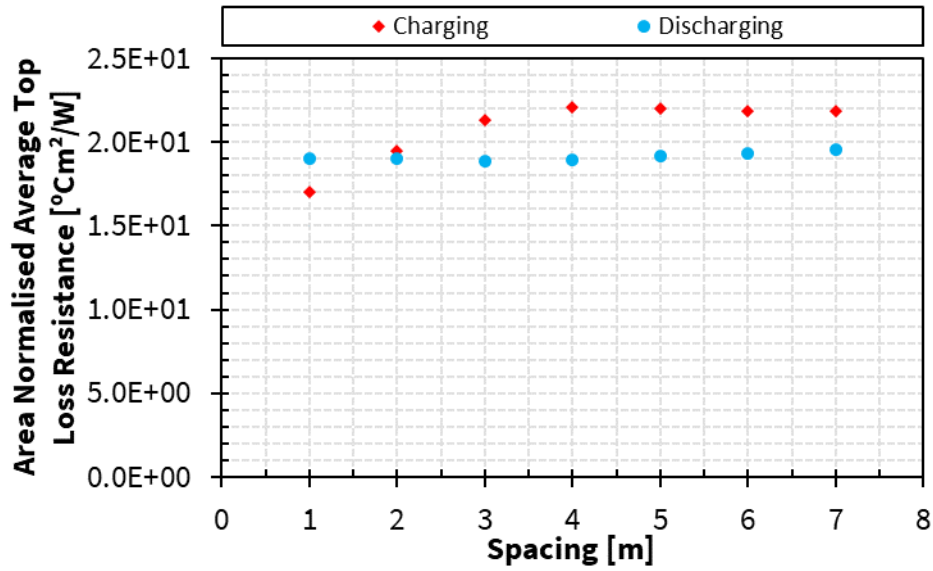
Figure B.4: Top loss resistance of periodic steady state BTES operation normalized against storage volume top area with respect to borehole spacing. Spacing and volume are the variable parameters. Number of boreholes and depth are held constant. Soil 2.
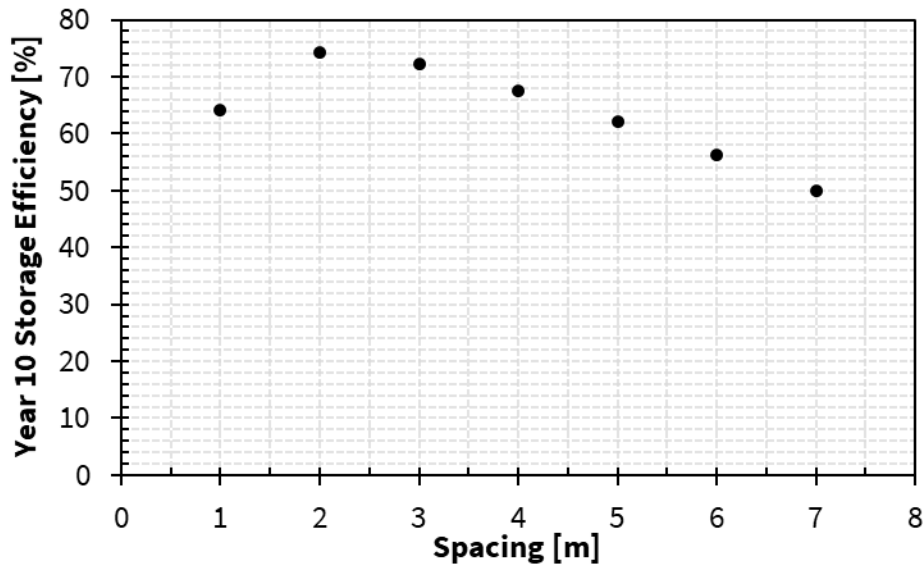
Figure B.5: Periodic steady state BTES thermal storage efficiency with respect to borehole spacing. BTES thermal storage efficiency is defined as the ratio of the total energy extracted during discharging timestep to the total energy injected during charging timestep for a simulation charging and discharging cycle. Spacing and volume are the variable parameters. Number of

boreholes and depth are held constant. The inlet temperature setpoint of BTES charging is 95°C and BTES discharging is 20°C. Soil 2.
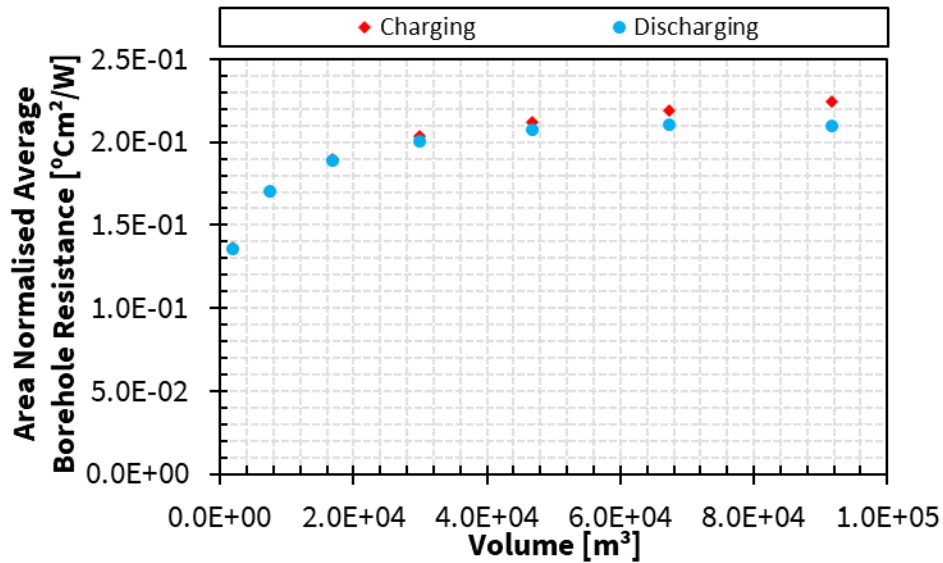
Figure B.6: Borehole heat exchanger thermal resistance of periodic steady state BTES operation normalized against total borehole area with respect to storage volume. Spacing and volume are the variable parameters. Number of boreholes and depth are held constant. Soil 2.
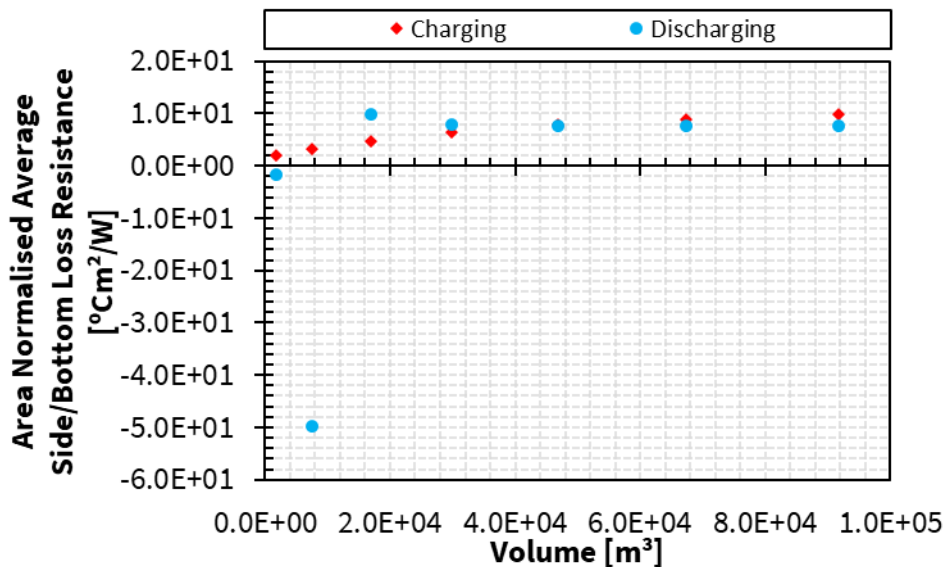
Figure B.7: Sides and bottom loss resistance of periodic steady state BTES operation normalized against storage volume side and bottom area with respect to storage volume. The negative

discharging resistance values are a result of the change in heat transfer direction that occurs for periodic steady state side/bottom loss heat transfer rate. Spacing and volume are the variable parameters. Number of boreholes and depth are held constant. Soil 2.
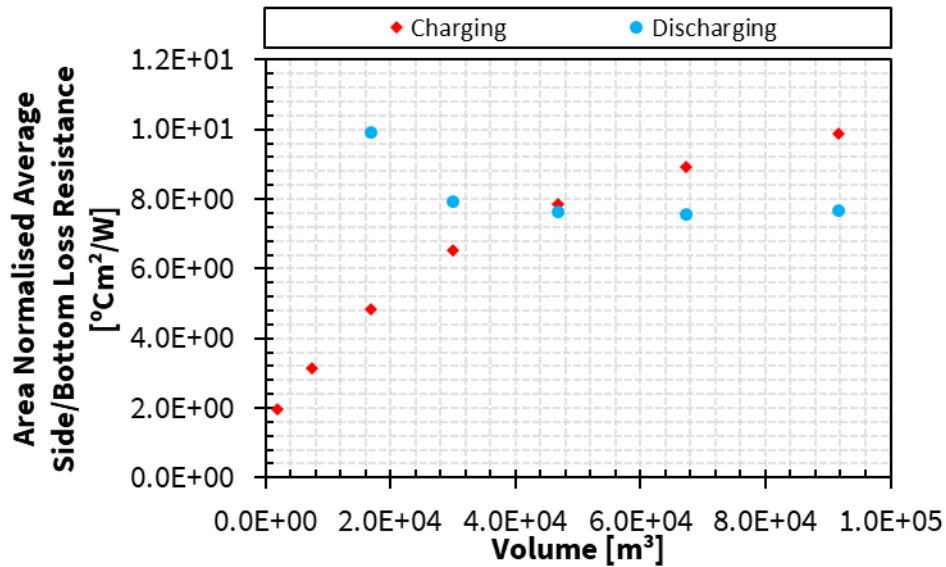
Figure B.8: Sides and bottom loss resistance of periodic steady state BTES operation normalized against storage volume side and bottom area with respect to storage volume. The figure's y-axis is reduced to omit discharging resistance outliers and better display charging resistance values. Spacing and volume are the variable parameters. Number of boreholes and depth are held constant. Soil 2.
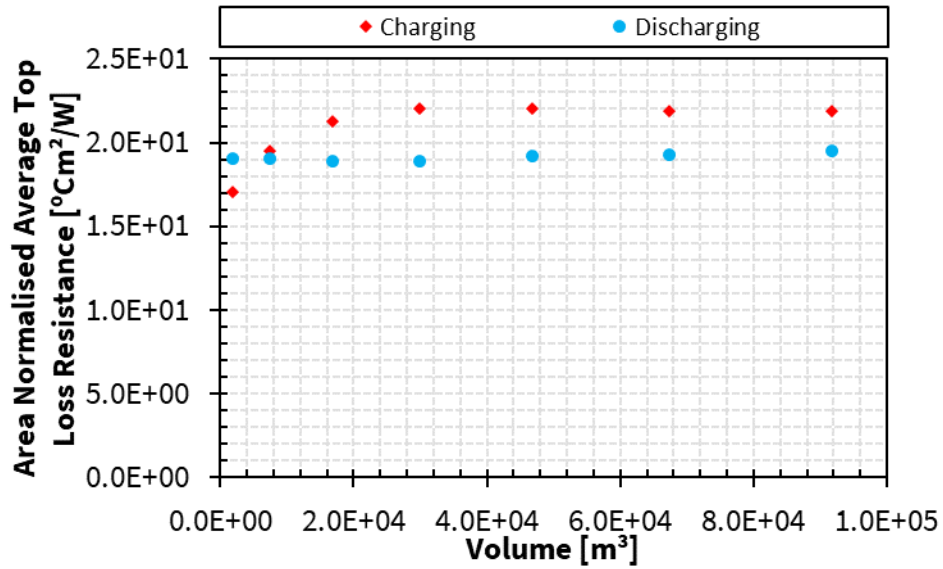
Figure B.9: Top loss resistance of periodic steady state BTES operation normalized against storage volume top area with respect to storage volume. Spacing and volume are the variable parameters. Number of boreholes and depth are held constant. Soil 2.
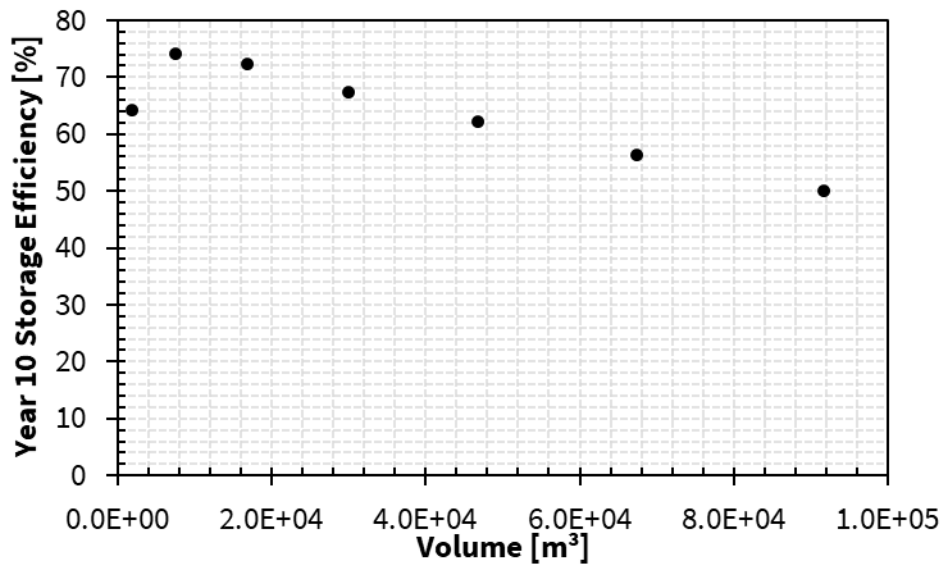
Figure B.10: Periodic steady state BTES thermal storage efficiency with respect to storage volume. BTES thermal storage efficiency is defined as the ratio of the total energy extracted during discharging timestep to the total energy injected during charging timestep for a simulation charging and discharging cycle. Spacing and volume are the variable parameters. Number of

boreholes and depth are held constant. The inlet temperature setpoint of BTES charging is 95°C and BTES discharging is 20°C. Soil 2.

s [m]	H [m]	#BH	V [m³]	A_{TBA} [m²]	$A_{SV\_s,b}$ [m²]	A_{SV_t} [m²]	R_{hx} (charge) [°Cm²/W]	R_{hx} (discharge) [°Cm²/W]	$R_{loss\_s,b}$ (charge) [°Cm²/W]	$R_{loss\_s,b}$ (discharge) [°Cm²/W]	R_{loss_t} (charge) [°Cm²/W]	R_{loss_t} (discharge) [°Cm²/W]	Efficiency [%]
1	405	48	16833	9161	9297	42	1.65E-01	1.44E-01	2.31E+00	-4.07E+00	2.21E+01	2.95E+01	65.1
2	101.3	48	16833	2290	4794	166	1.73E-01	1.71E-01	3.52E+00	-3.26E+02	2.17E+01	2.19E+01	75.7
3	45	48	16833	1018	3459	374	1.90E-01	1.89E-01	4.84E+00	9.93E+00	2.13E+01	1.89E+01	72.3
4	25.3	48	16833	573	2979	665	2.03E-01	2.01E-01	5.87E+00	7.06E+00	2.04E+01	1.74E+01	63.2
5	16.2	48	16833	366	2890	1039	2.12E-01	2.06E-01	6.55E+00	6.29E+00	1.90E+01	1.63E+01	51.4
6	11.3	48	16833	254	3039	1496	2.19E-01	2.06E-01	7.20E+00	6.02E+00	1.80E+01	1.55E+01	39.1
7	8.3	48	16833	187	3359	2037	2.25E-01	1.97E-01	8.13E+00	5.96E+00	1.78E+01	1.53E+01	28.2

Table B.2: Design parameters, heat transfer areas, periodic steady state thermal resistances, and periodic steady state storage efficiencies for the soil 2 parameter sweep with variable parameters: spacing and depth and constant parameters: number of boreholes and volume. The periodic steady state thermal resistances of charging and discharging and the periodic steady state storage efficiency are presented in Figure B.11 to Figure B.20 with respect to the variable parameters.
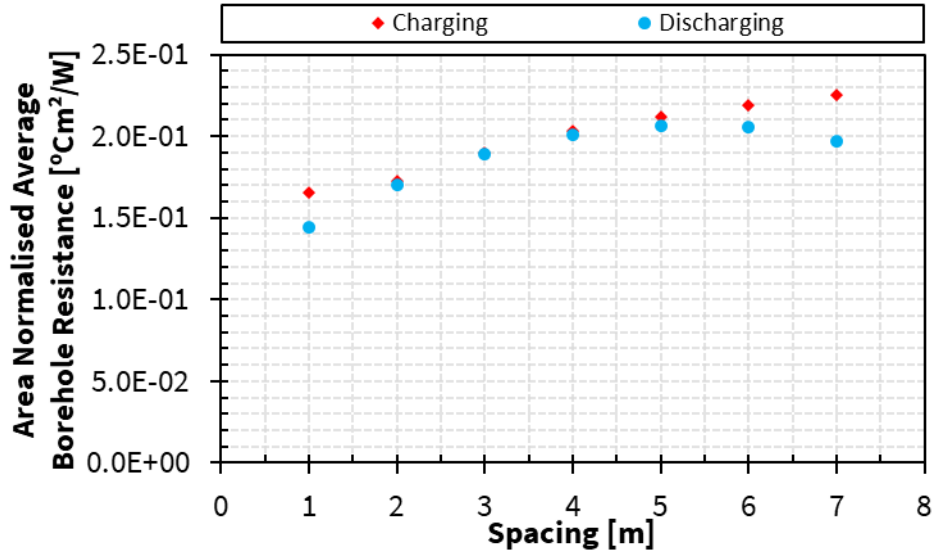
Figure B.11: Borehole heat exchanger thermal resistance of periodic steady state BTES operation normalized against total borehole area with respect to borehole spacing. Spacing and depth are the variable parameters. Number of boreholes and volume are held constant. Soil 2.
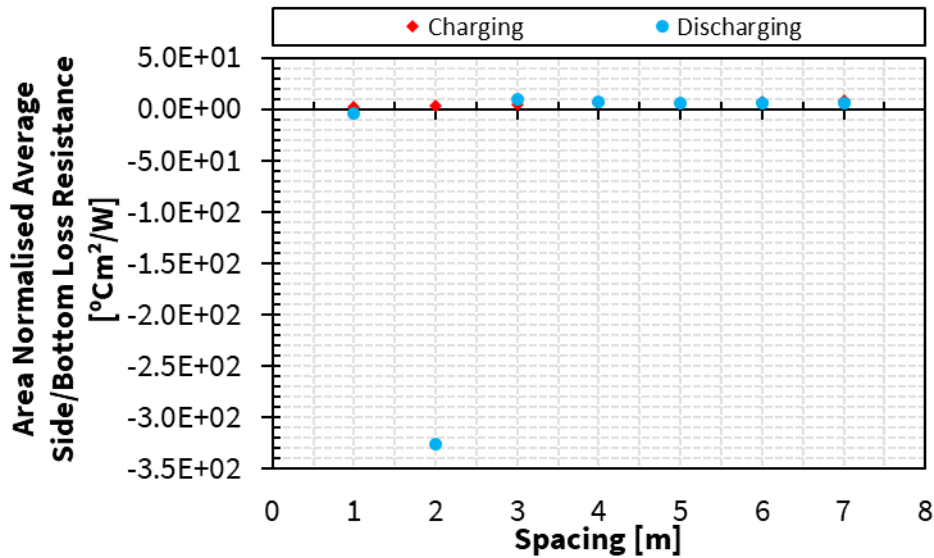
Figure B.12: Sides and bottom loss resistance of periodic steady state BTES operation normalized against storage volume side and bottom area with respect to borehole spacing. The negative discharging resistance values are a result of the change in heat transfer direction that occurs for periodic steady state side/bottom loss heat transfer rate. Spacing and depth are the variable parameters. Number of boreholes and volume are held constant. Soil 2.
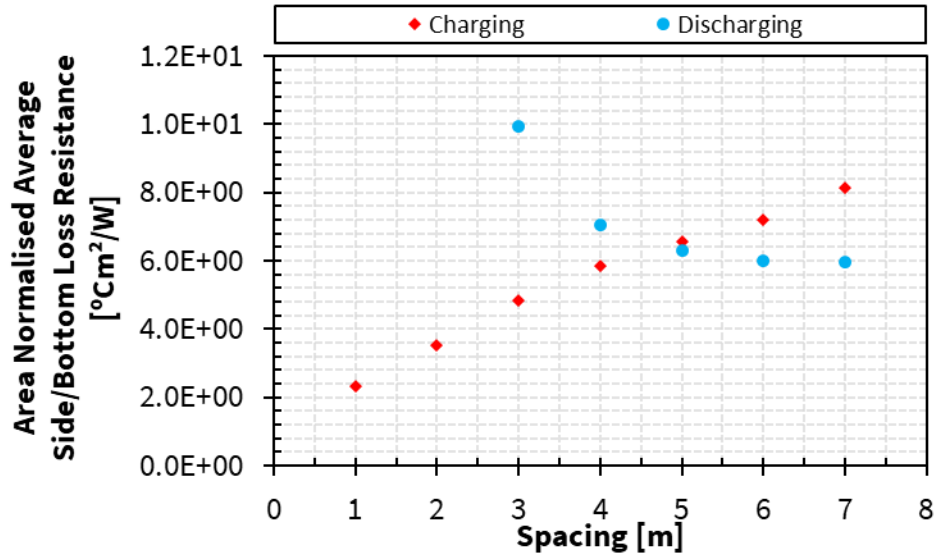
Figure B.13: Sides and bottom loss resistance of periodic steady state BTES operation normalized against storage volume side and bottom area with respect to borehole spacing. The figure's y-axis is reduced to omit discharging resistance outliers and better display charging resistance values. Spacing and depth are the variable parameters. Number of boreholes and volume are held constant. Soil 2.
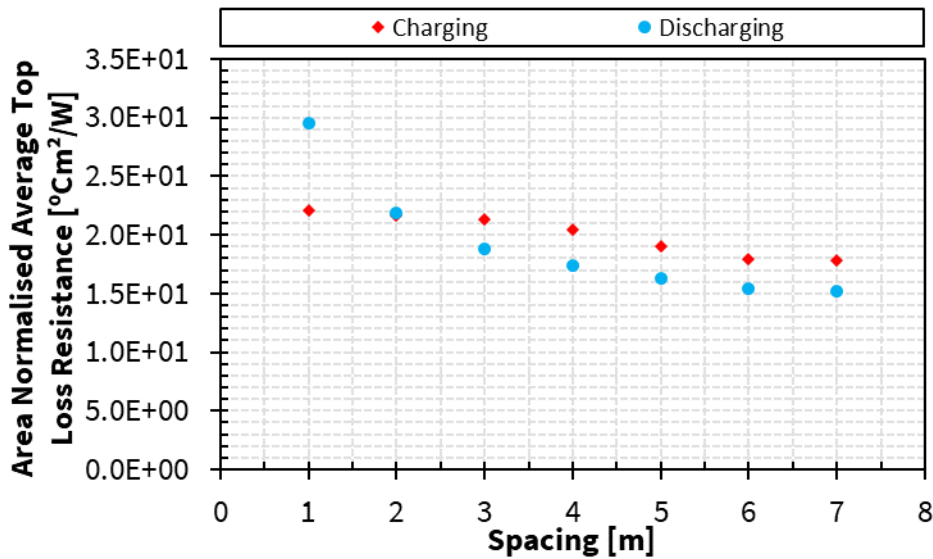
Figure B.14: Top loss resistance of periodic steady state BTES operation normalized against storage volume top area with respect to borehole spacing. Spacing and depth are the variable parameters. Number of boreholes and volume are held constant. Soil 2.
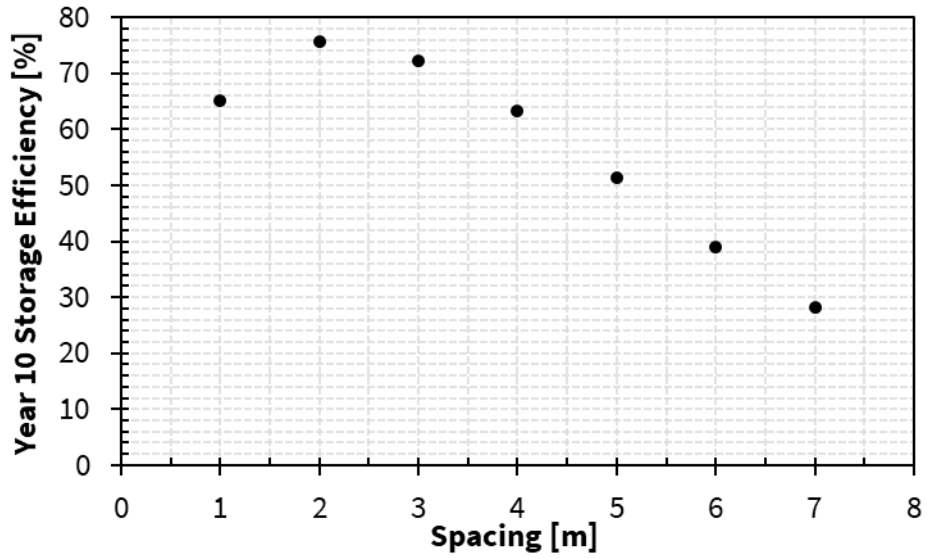
Figure B.15: Periodic steady state BTES thermal storage efficiency with respect to borehole spacing. BTES thermal storage efficiency is defined as the ratio of the total energy extracted during discharging timestep to the total energy injected during charging timestep for a simulation charging and discharging cycle. Spacing and depth are the variable parameters. Number of boreholes and volume are held constant. The inlet temperature setpoint of BTES charging is 95°C and BTES discharging is 20°C. Soil 2.
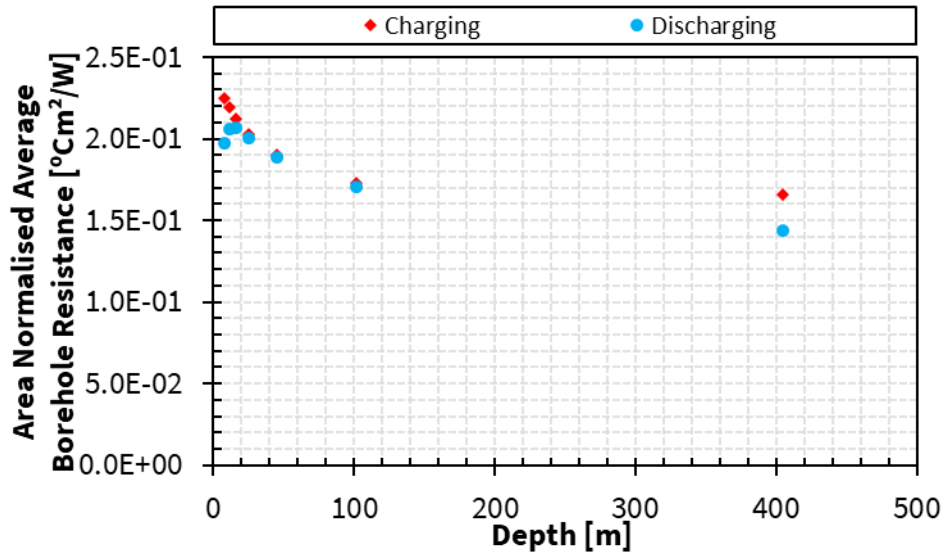
Figure B.16: Borehole heat exchanger thermal resistance of periodic steady state BTES operation normalized against total borehole area with respect to depth. Spacing and depth are the variable parameters. Number of boreholes and volume are held constant. Soil 2.
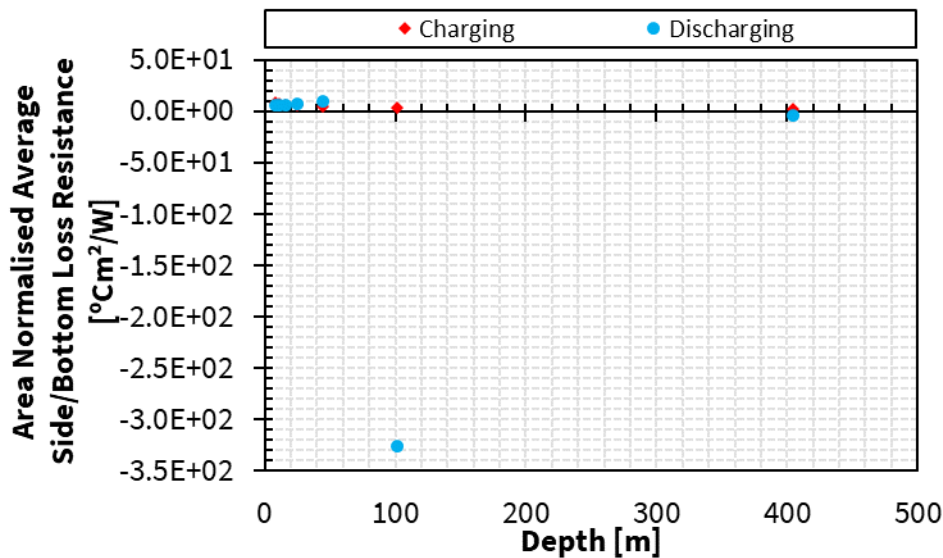
Figure B.17: Sides and bottom loss resistance of periodic steady state BTES operation normalized against storage volume side and bottom area with respect to depth. The negative discharging resistance values are a result of the change in heat transfer direction that occurs for periodic steady state side/bottom loss heat transfer rate. Spacing and depth are the variable parameters. Number of boreholes and volume are held constant. Soil 2.
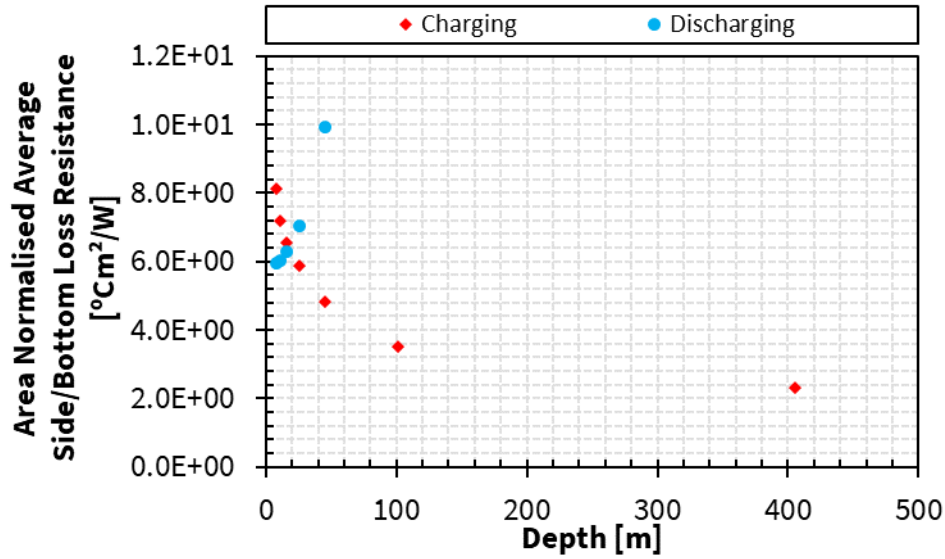
Figure B.18: Sides and bottom loss resistance of periodic steady state BTES operation normalized against storage volume side and bottom area with respect to depth. The figure's y-axis is reduced to omit discharging resistance outliers and better display charging resistance values. Spacing and depth are the variable parameters. Number of boreholes and volume are held constant. Soil 2.
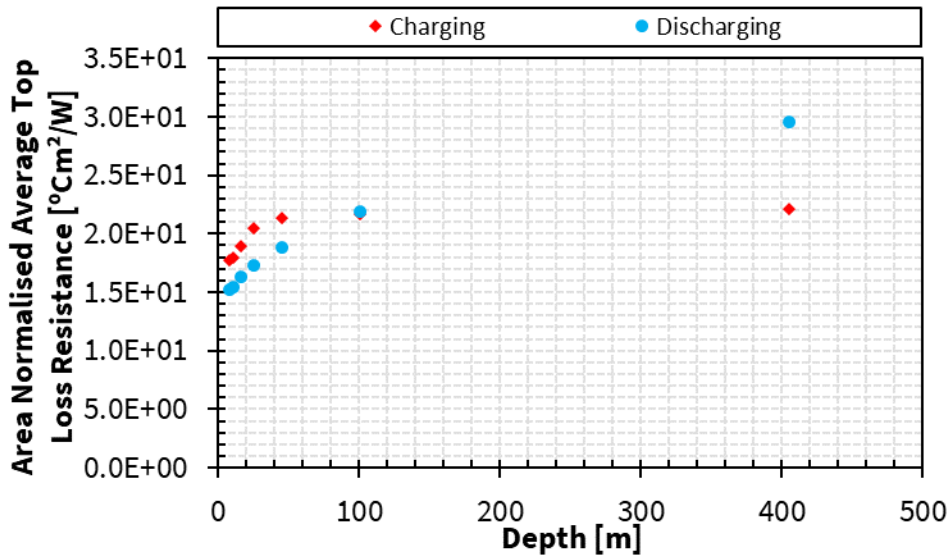
Figure B.19: Top loss resistance of periodic steady state BTES operation normalized against storage volume top area with respect to depth. Spacing and depth are the variable parameters. Number of boreholes and volume are held constant. Soil 2.
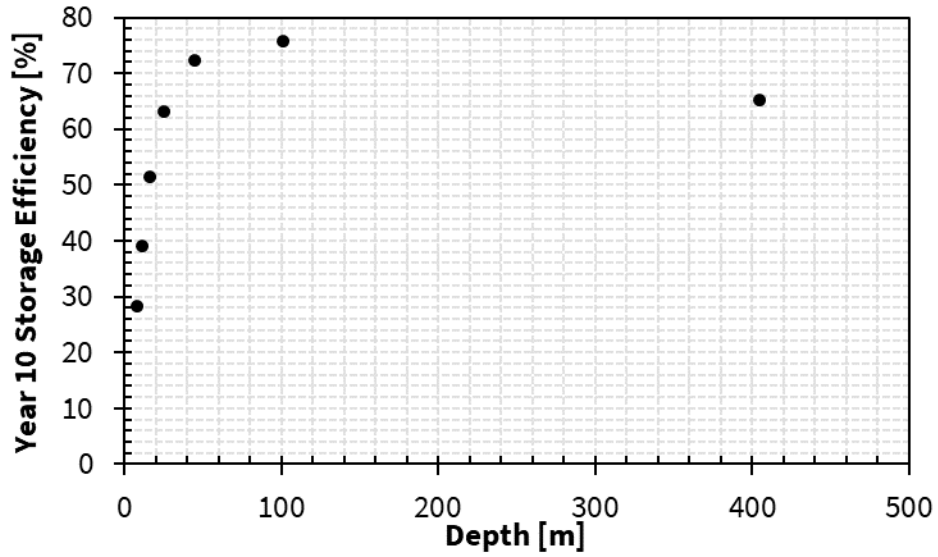
Figure B.20: Periodic steady state BTES thermal storage efficiency with respect to depth. BTES thermal storage efficiency is defined as the ratio of the total energy extracted during discharging timestep to the total energy injected during charging timestep for a simulation charging and discharging cycle. Spacing and depth are the variable parameters. Number of boreholes and volume are held constant. The inlet temperature setpoint of BTES charging is 95°C and BTES discharging is 20°C. Soil 2.

s [m]	#BH	H [m]	V [m³]	A_{TBA} [m²]	$A_{SV\_s,b}$ [m²]	A_{SV_t} [m²]	R_{hx} (charge) [°Cm²/W]	R_{hx} (discharge) [°Cm²/W]	$R_{loss\_s,b}$ (charge) [°Cm²/W]	$R_{loss\_s,b}$ (discharge) [°Cm²/W]	R_{loss_t} (charge) [°Cm²/W]	R_{loss_t} (discharge) [°Cm²/W]	Efficiency [%]
1	432	45	16833	9161	3459	374	1.55E-01	1.42E-01	2.47E+00	-3.06E+00	1.91E+01	2.52E+01	85.0
1.5	192	45	16833	4072	3459	374	1.61E-01	1.57E-01	2.94E+00	-8.03E+00	1.99E+01	2.23E+01	83.8
2	108	45	16833	2290	3459	374	1.72E-01	1.71E-01	3.55E+00	9.21E+01	2.05E+01	2.02E+01	81.1
3	48	45	16833	1018	3459	374	1.90E-01	1.89E-01	4.84E+00	9.93E+00	2.13E+01	1.89E+01	72.3
4	27	45	16833	573	3459	374	2.03E-01	2.00E-01	6.03E+00	7.34E+00	2.23E+01	1.89E+01	61.2
5	17	45	16833	360	3459	374	2.12E-01	2.06E-01	6.92E+00	6.63E+00	2.29E+01	1.95E+01	49.8
6	12	45	16833	254	3459	374	2.19E-01	2.06E-01	7.58E+00	6.29E+00	2.36E+01	1.99E+01	40.5
7	9	45	16833	191	3459	374	2.24E-01	2.01E-01	8.10E+00	6.15E+00	2.42E+01	2.06E+01	33.1

Table B.3: Design parameters, heat transfer areas, periodic steady state thermal resistances, and periodic steady state storage efficiencies for the soil 2 parameter sweep with variable parameters: spacing and number of boreholes and constant parameters: depth and volume. The periodic steady state thermal resistances of charging and discharging and the periodic steady state storage efficiency are presented in Figure B.21 to Figure B.30 with respect to the variable parameters.
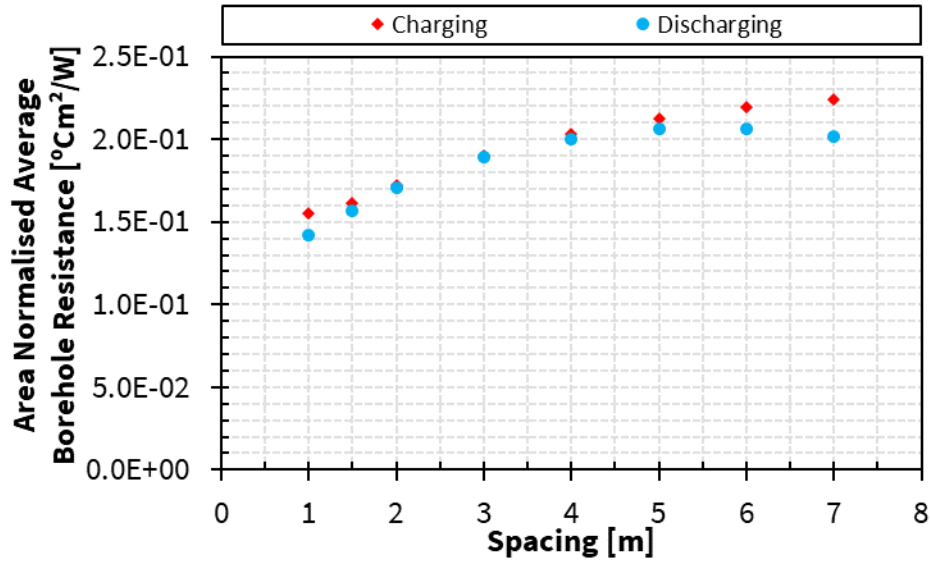
Figure B.21: Borehole heat exchanger thermal resistance of periodic steady state BTES operation normalized against total borehole area with respect to borehole spacing. Spacing and number of boreholes are the variable parameters. Depth and volume are held constant. Soil 2.
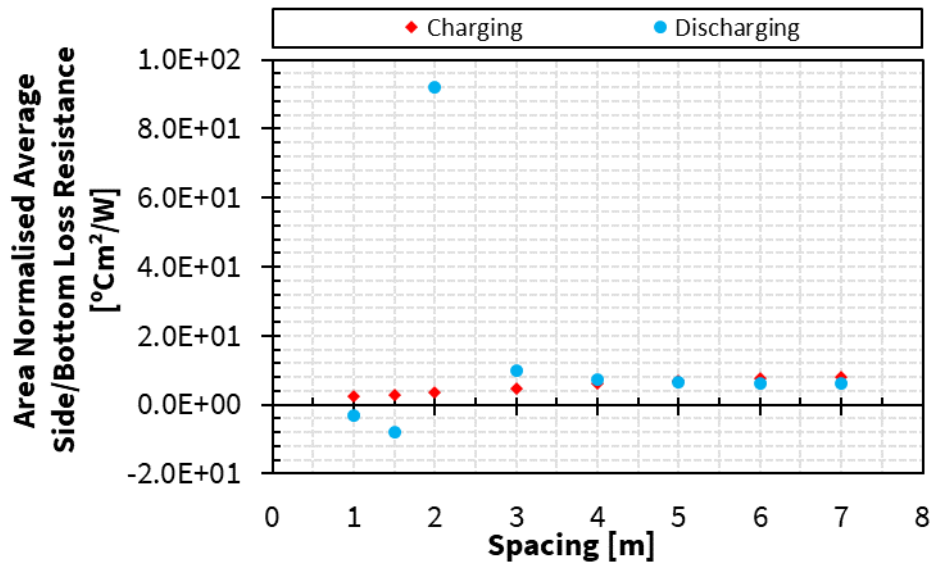
Figure B.22: Sides and bottom loss resistance of periodic steady state BTES operation normalized against storage volume side and bottom area with respect to borehole spacing. The negative discharging resistance values and large magnitude of discharging resistance for 2 m spacing is a result of the change in heat transfer direction that occurs for periodic steady state

side/bottom loss heat transfer rate. Spacing and number of boreholes are the variable parameters. Depth and volume are held constant. Soil 2.
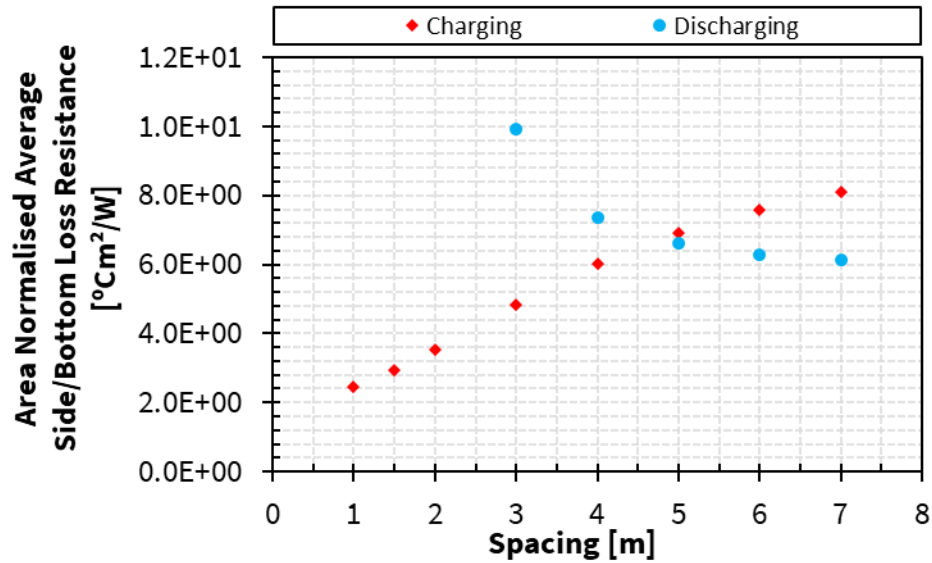
Figure B.23: Sides and bottom loss resistance of periodic steady state BTES operation normalized against storage volume side and bottom area with respect to borehole spacing. The figure's y-axis is reduced to omit discharging resistance outliers and better display charging resistance values. Spacing and number of boreholes are the variable parameters. Depth and volume are held constant. Soil 2.
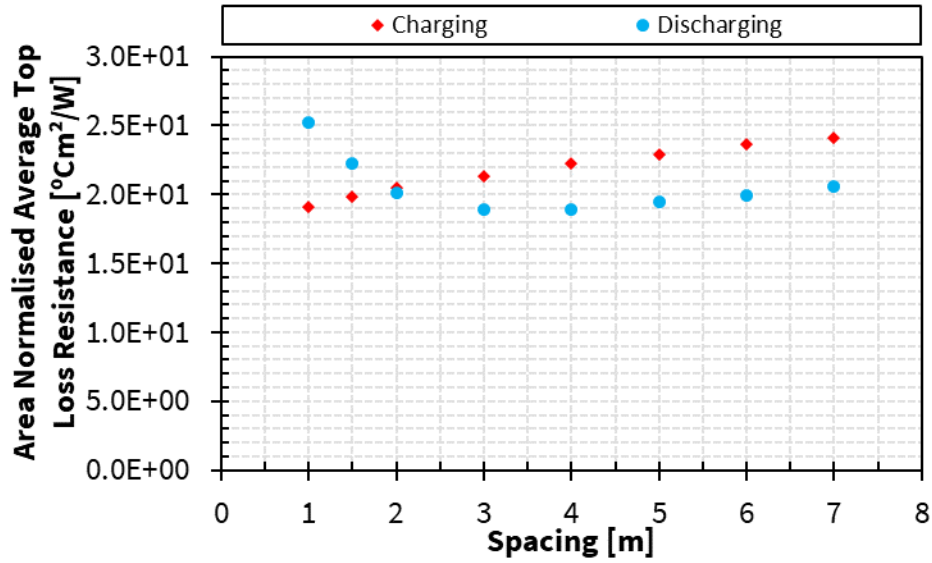
Figure B.24: Top loss resistance of periodic steady state BTES operation normalized against storage volume top area with respect to borehole spacing. Spacing and number of boreholes are the variable parameters. Depth and volume are held constant. Soil 2.
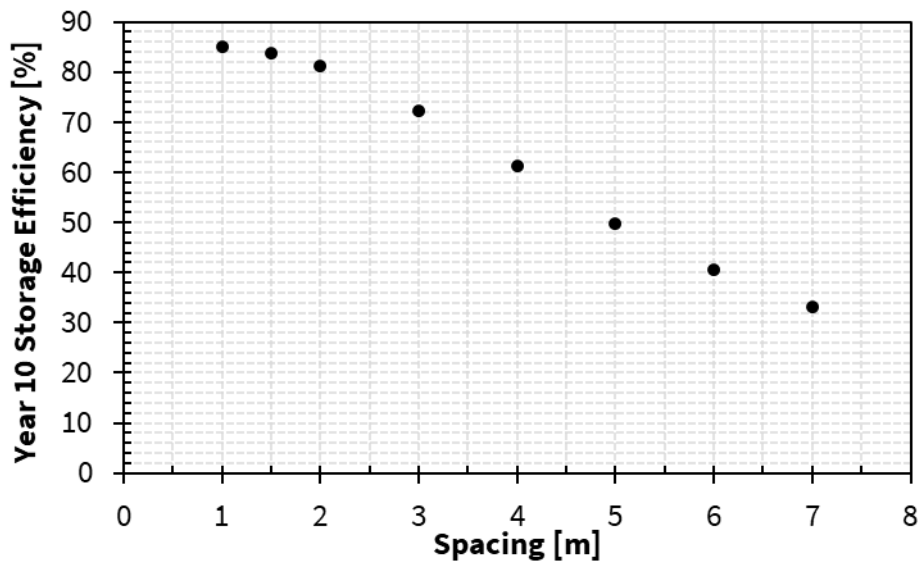
Figure B.25: Periodic steady state BTES thermal storage efficiency with respect to borehole spacing. BTES thermal storage efficiency is defined as the ratio of the total energy extracted during discharging timestep to the total energy injected during charging timestep for a simulation charging and discharging cycle. Spacing and number of boreholes are the variable parameters.

Depth and volume are held constant. The inlet temperature setpoint of BTES charging is 95°C and BTES discharging is 20°C. Soil 2.
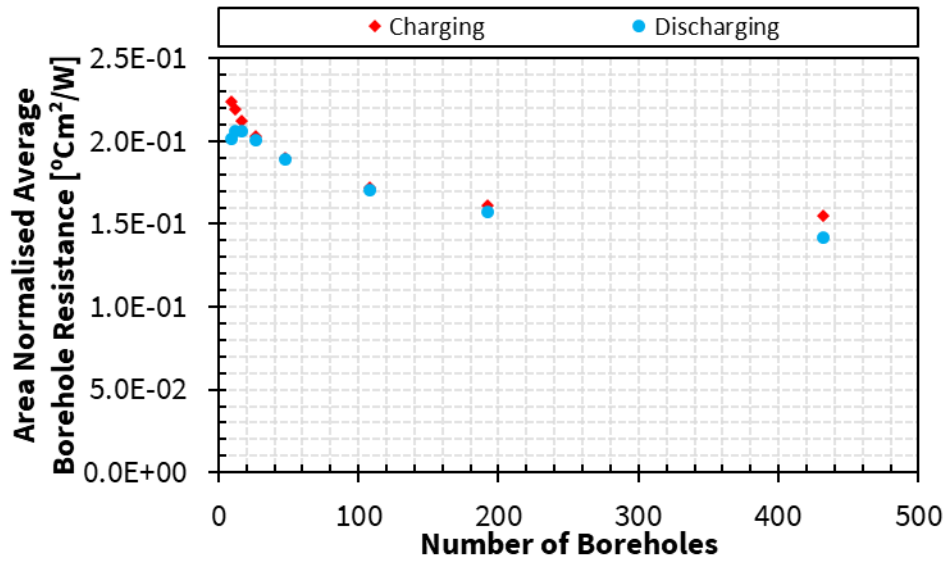
Figure B.26: Borehole heat exchanger thermal resistance of periodic steady state BTES operation normalized against total borehole area with respect to number of boreholes. Spacing and number of boreholes are the variable parameters. Depth and volume are held constant. Soil 2.
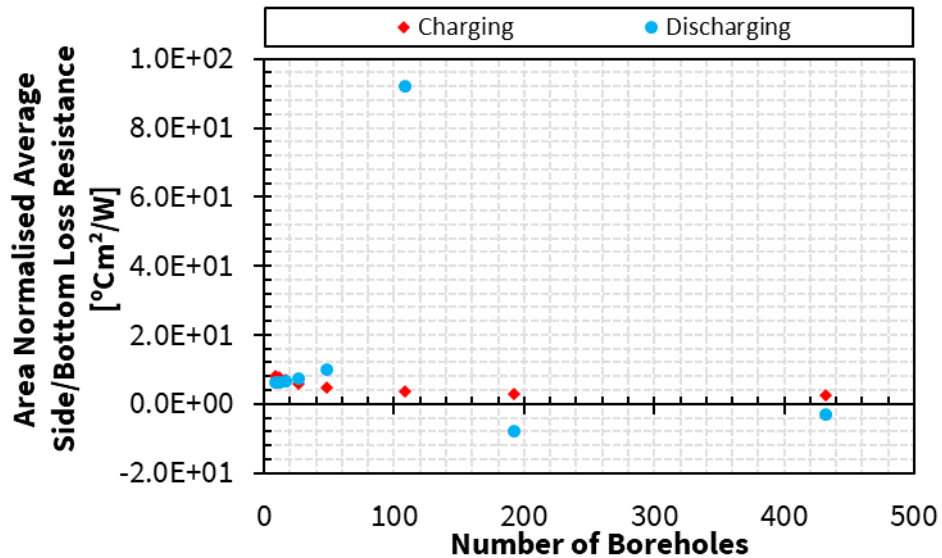
Figure B.27: Sides and bottom loss resistance of periodic steady state BTES operation normalized against storage volume side and bottom area with respect to number of boreholes.

The negative discharging resistance values and large magnitude discharging resistance for 108 boreholes is a result of the change in heat transfer direction that occurs for periodic steady state side/bottom loss heat transfer rate. Spacing and number of boreholes are the variable parameters. Depth and volume are held constant. Soil 2.
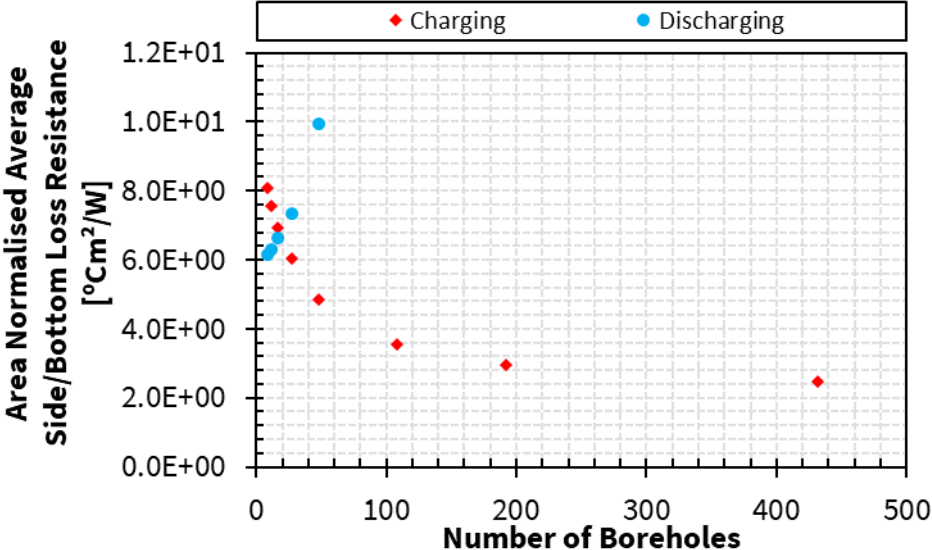
Figure B.28: Sides and bottom loss resistance of periodic steady state BTES operation normalized against storage volume side and bottom area with respect to number of boreholes. The figure's y-axis is reduced to omit discharging resistance outliers and better display charging resistance values. Spacing and number of boreholes are the variable parameters. Depth and volume are held constant. Soil 2.
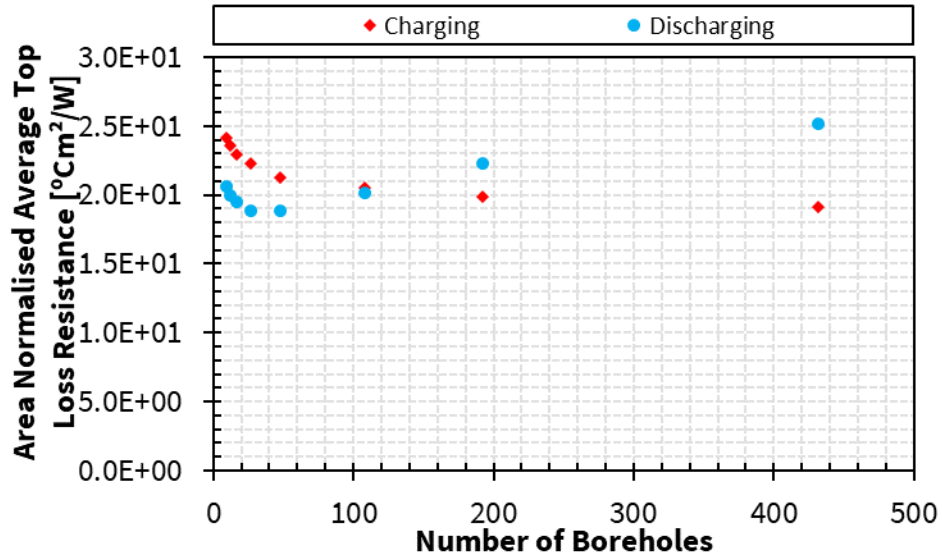
Figure B.29: Top loss resistance of periodic steady state BTES operation normalized against storage volume top area with respect to number of boreholes. Spacing and number of boreholes are the variable parameters. Depth and volume are held constant. Soil 2.
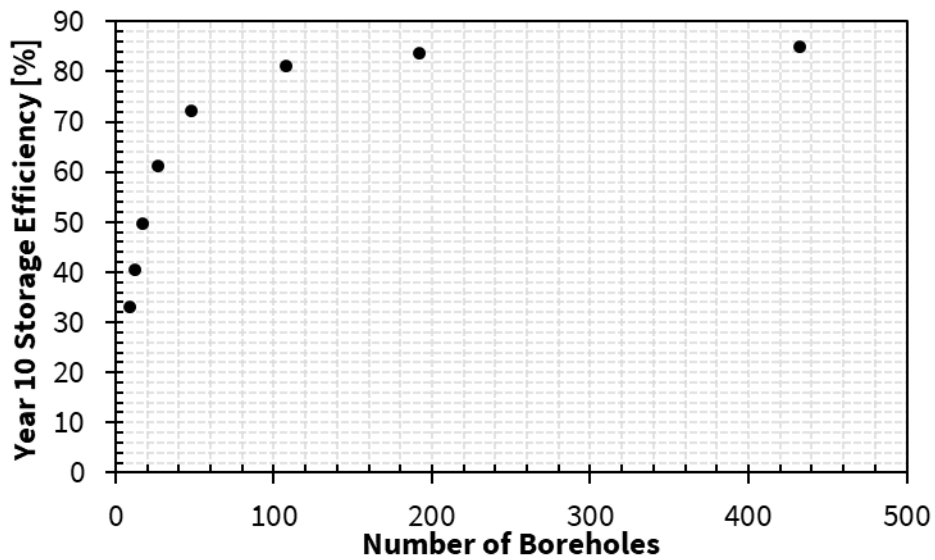
Figure B.30: Periodic steady state BTES thermal storage efficiency with respect to number of boreholes. BTES thermal storage efficiency is defined as the ratio of the total energy extracted during discharging timestep to the total energy injected during charging timestep for a simulation charging and discharging cycle. Spacing and number of boreholes are the variable parameters.

Depth and volume are held constant. The inlet temperature setpoint of BTES charging is 95°C and BTES discharging is 20°C. Soil 2.

#BH	V [m^3]	s [m]	H [m]	A_{TBA} [m^2]	$A_{SV\_s,b}$ [m^2]	A_{SV_t} [m^2]	R_{hx} (charge) [°Cm^2/W]	R_{hx} (discharge) [°Cm^2/W]	$R_{loss\_s,b}$ (charge) [°Cm^2/W]	$R_{loss\_s,b}$ (discharge) [°Cm^2/W]	R_{loss_t} (charge) [°Cm^2/W]	R_{loss_t} (discharge) [°Cm^2/W]	Efficiency [%]
10	3507	3	45	212	1486	78	1.90E-01	1.88E-01	3.83E+00	7.37E+00	2.31E+01	2.07E+01	49.6
25	8767	3	45	530	2421	195	1.90E-01	1.89E-01	4.41E+00	9.06E+00	2.14E+01	1.90E+01	64.8
48	16833	3	45	1018	3459	374	1.90E-01	1.89E-01	4.84E+00	9.93E+00	2.13E+01	1.89E+01	72.3
75	26302	3	45	1590	4441	584	1.91E-01	1.89E-01	5.16E+00	1.02E+01	2.17E+01	1.94E+01	75.9
100	35069	3	45	2121	5233	779	1.91E-01	1.90E-01	5.38E+00	1.03E+01	2.23E+01	2.00E+01	77.5
150	52604	3	45	3181	6623	1169	1.94E-01	1.91E-01	5.71E+00	1.01E+01	2.36E+01	2.13E+01	79.0
200	70138	3	45	4241	7856	1559	1.97E-01	1.92E-01	5.94E+00	9.88E+00	2.48E+01	2.26E+01	79.3
500	175345	3	45	10603	13854	3897	2.36E-01	2.02E-01	6.41E+00	8.90E+00	3.00E+01	2.83E+01	75.8

Table B.4: Design parameters, heat transfer areas, periodic steady state thermal resistances, and periodic steady state storage efficiencies for the soil 2 parameter sweep with variable parameters: number of boreholes and volume and constant parameters: spacing and depth. The periodic steady state thermal resistances of charging and discharging and the periodic steady state storage efficiency are presented in Figure B.31 to Figure B.40 with respect to the variable parameters.
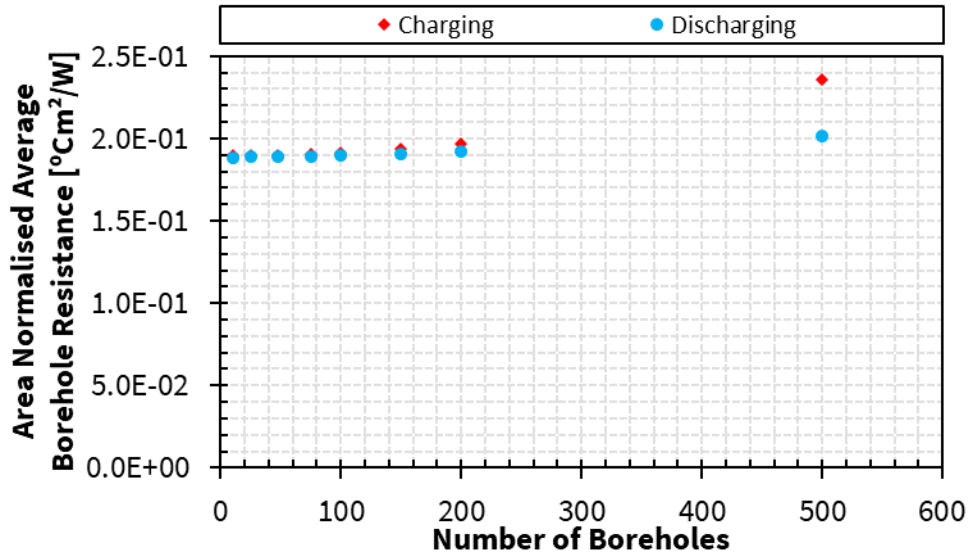
Figure B.31: Borehole heat exchanger thermal resistance of periodic steady state BTES operation normalized against total borehole area with respect to number of boreholes. Number of boreholes and volume are the variable parameters. Spacing and depth are held constant. Soil 2.
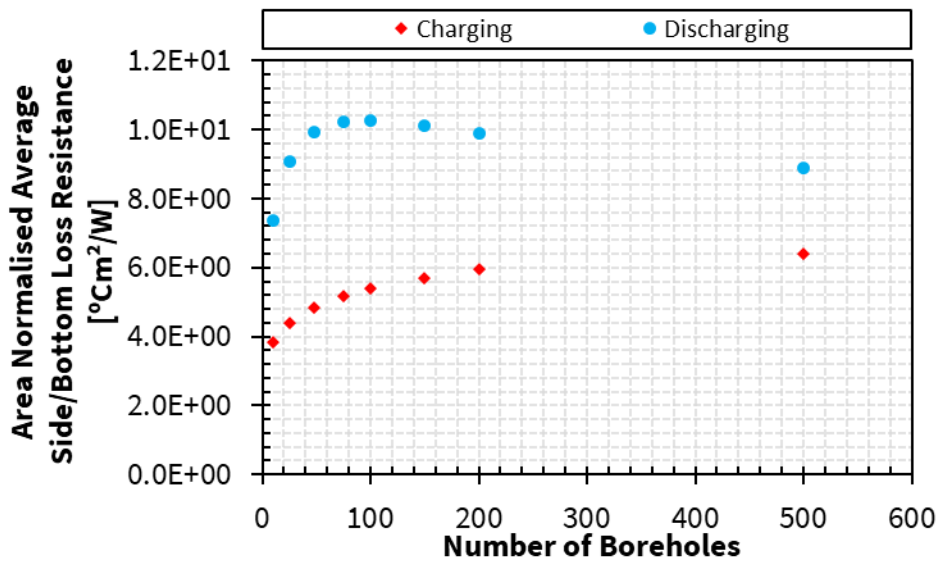
Figure B.32: Sides and bottom loss resistance of periodic steady state BTES operation normalized against storage volume side and bottom area with respect to number of boreholes. The larger magnitude of discharging resistances is a result of the change in heat transfer direction that occurs for periodic steady state side/bottom loss heat transfer rate. Number of boreholes and volume are the variable parameters. Spacing and depth are held constant. Soil 2.
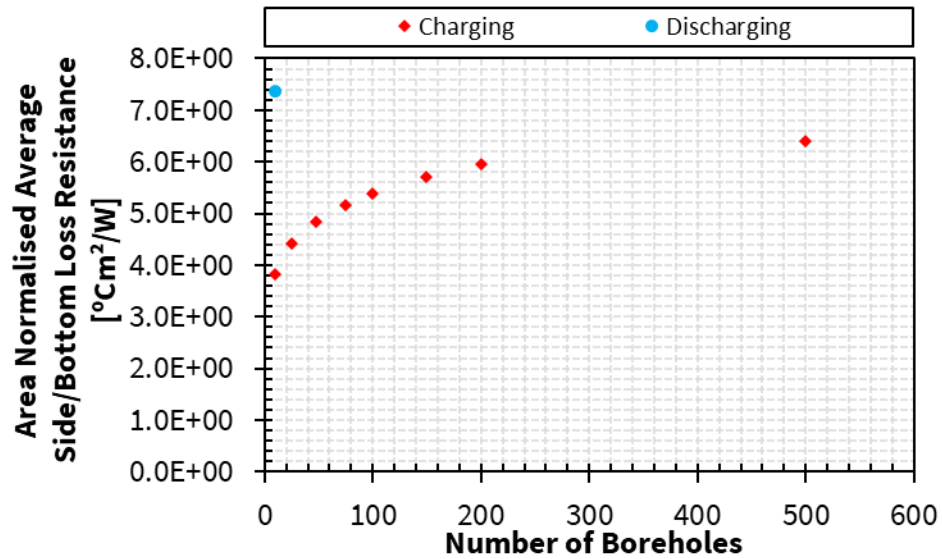
Figure B.33: Sides and bottom loss resistance of periodic steady state BTES operation normalized against storage volume side and bottom area with respect to number of boreholes. The figure's y-axis is reduced to omit most discharging resistances and better display charging resistance values. Number of boreholes and volume are the variable parameters. Spacing and depth are held constant. Soil 2.
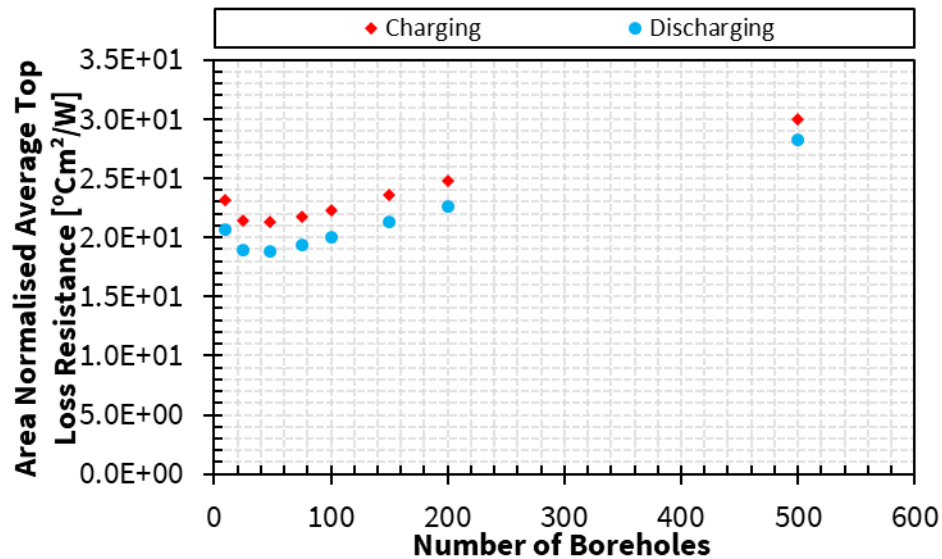
Figure B.34: Top loss resistance of periodic steady state BTES operation normalized against storage volume top area with respect to number of boreholes. Number of boreholes and volume are the variable parameters. Spacing and depth are held constant. Soil 2.
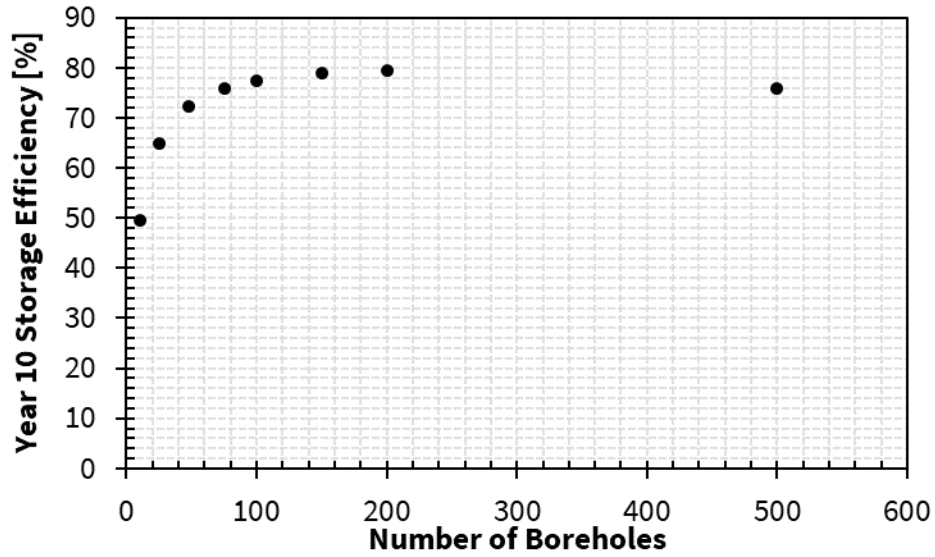
Figure B.35: Periodic steady state BTES thermal storage efficiency with respect to number of boreholes. BTES thermal storage efficiency is defined as the ratio of the total energy extracted during discharging timestep to the total energy injected during charging timestep for a simulation charging and discharging cycle. Number of boreholes and volume are the variable parameters. Spacing and depth are held constant. The inlet temperature setpoint of BTES charging is 95°C and BTES discharging is 20°C. Soil 2.
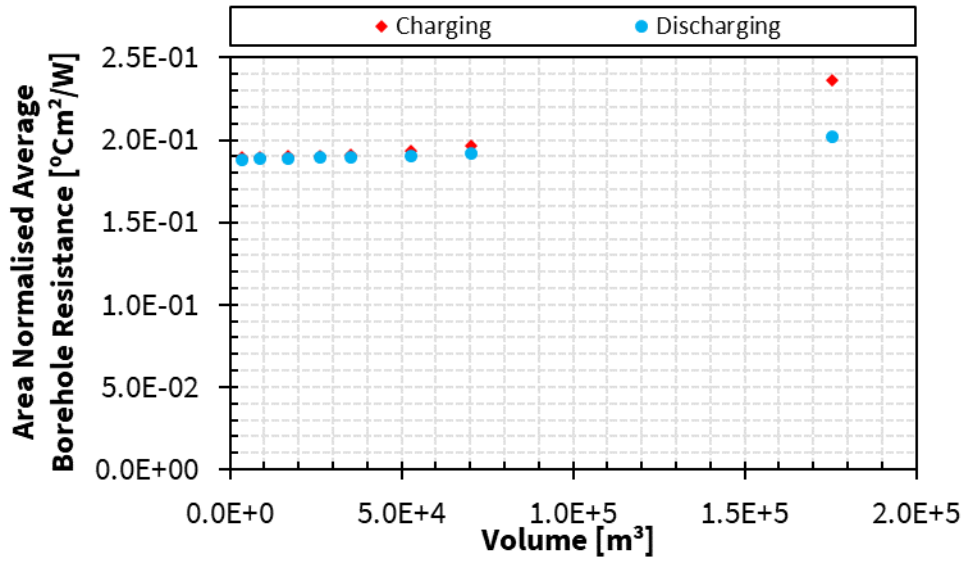
Figure B.36: Borehole heat exchanger thermal resistance of periodic steady state BTES operation normalized against total borehole area with respect to storage volume. Number of boreholes and volume are the variable parameters. Spacing and depth are held constant. Soil 2.
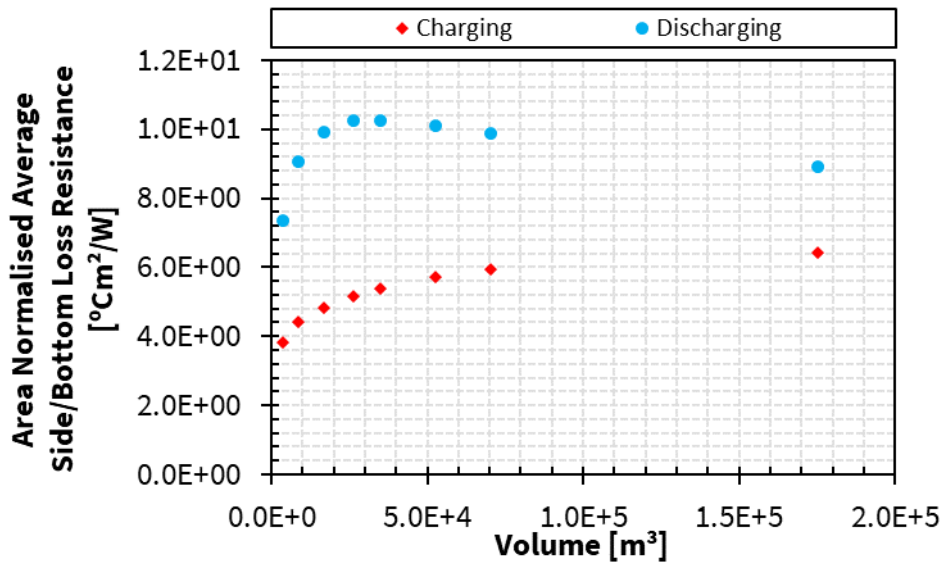
Figure B.37: Sides and bottom loss resistance of periodic steady state BTES operation normalized against storage volume side and bottom area with respect to storage volume. The larger magnitude of discharging resistances is a result of the change in heat transfer direction that occurs for periodic steady state side/bottom loss heat transfer rate. Number of boreholes and volume are the variable parameters. Spacing and depth are held constant. Soil 2.
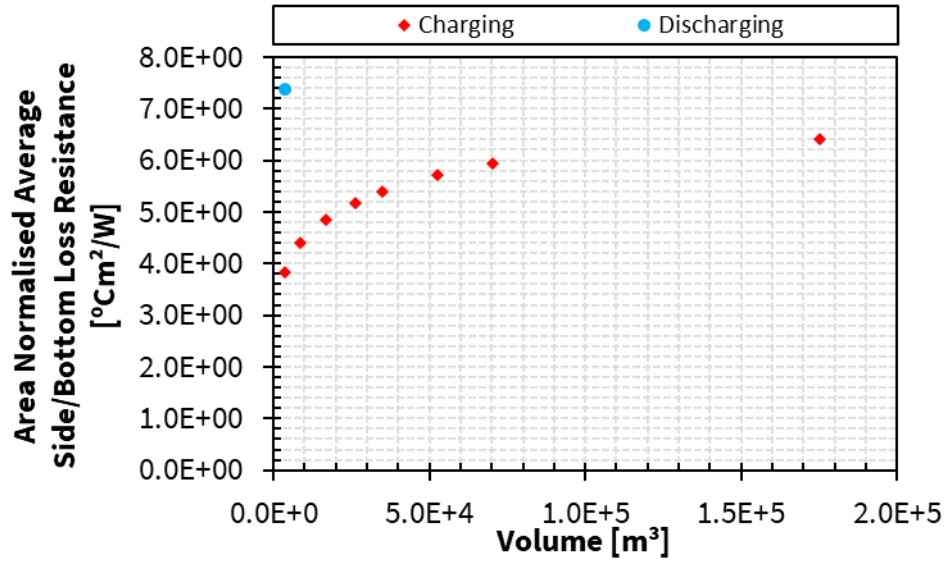
Figure B.38: Sides and bottom loss resistance of periodic steady state BTES operation normalized against storage volume side and bottom area with respect to storage volume. The figure's y-axis is reduced to omit most discharging resistances and better display charging resistance values. Number of boreholes and volume are the variable parameters. Spacing and depth are held constant. Soil 2.
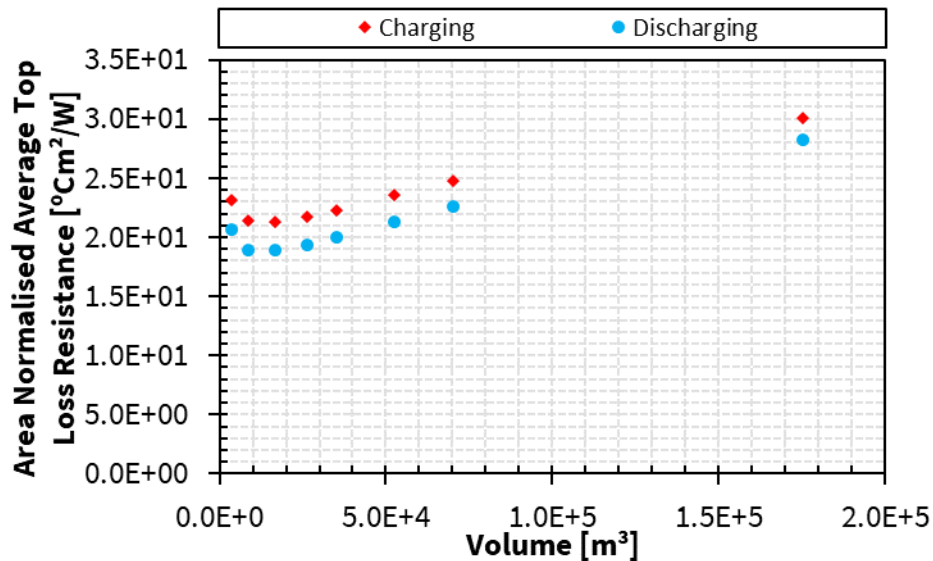
Figure B.39: Top loss resistance of periodic steady state BTES operation normalized against storage volume top area with respect to storage volume. Number of boreholes and volume are the variable parameters. Spacing and depth are held constant. Soil 2.
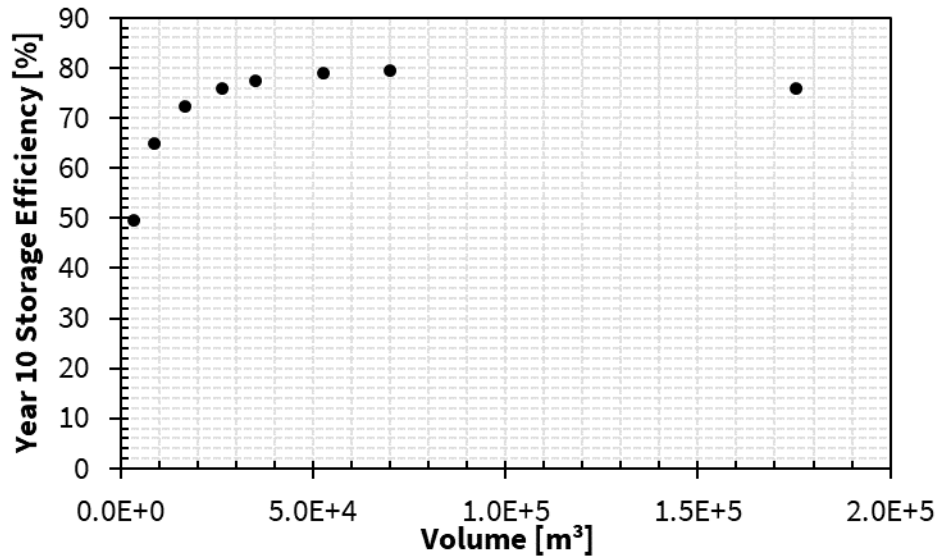
Figure B.40: Periodic steady state BTES thermal storage efficiency with respect to storage volume. BTES thermal storage efficiency is defined as the ratio of the total energy extracted during discharging timestep to the total energy injected during charging timestep for a simulation charging and discharging cycle. Number of boreholes and volume are the variable parameters. Spacing and depth are held constant. The inlet temperature setpoint of BTES charging is 95°C and BTES discharging is 20°C. Soil 2.

H [m]	V [m³]	s [m]	#BH	A_{TBA} [m²]	$A_{SV\_s,b}$ [m²]	A_{SV_t} [m²]	R_{hx} (charge) [°Cm²/W]	R_{hx} (discharge) [°Cm²/W]	$R_{loss\_s,b}$ (charge) [°Cm²/W]	$R_{loss\_s,b}$ (discharge) [°Cm²/W]	R_{loss_t} (charge) [°Cm²/W]	R_{loss_t} (discharge) [°Cm²/W]	Efficiency [%]
5	1870	3	48	113	717	374	1.90E-01	1.88E-01	3.18E+00	4.96E+00	1.71E+01	1.41E+01	42.2
10	3741	3	48	226	1060	374	1.90E-01	1.89E-01	3.54E+00	5.89E+00	1.81E+01	1.53E+01	55.8
25	9352	3	48	565	2088	374	1.90E-01	1.89E-01	4.33E+00	8.41E+00	1.99E+01	1.74E+01	68.4
45	16833	3	48	1018	3459	374	1.90E-01	1.89E-01	4.84E+00	9.93E+00	2.13E+01	1.89E+01	72.3
75	28055	3	48	1696	5516	374	1.91E-01	1.89E-01	5.24E+00	1.05E+01	2.30E+01	2.06E+01	73.3
100	37407	3	48	2262	7230	374	1.92E-01	1.89E-01	5.45E+00	1.05E+01	2.42E+01	2.18E+01	73.0
150	56110	3	48	3393	10658	374	1.95E-01	1.88E-01	5.73E+00	1.02E+01	2.65E+01	2.42E+01	71.5
250	93517	3	48	5655	17514	374	2.07E-01	1.85E-01	6.05E+00	9.54E+00	3.06E+01	2.83E+01	67.5
300	112221	3	48	6786	20943	374	2.14E-01	1.80E-01	6.14E+00	9.27E+00	3.24E+01	3.02E+01	65.5

Table B.5: Design parameters, heat transfer areas, periodic steady state thermal resistances, and periodic steady state storage efficiencies for the soil 2 parameter sweep with variable parameters: depth and volume and constant parameters: spacing and number of boreholes. The periodic steady state thermal resistances of charging and discharging and the periodic steady state storage efficiency are presented in Figure B.41 to Figure B.50 with respect to the variable parameters.
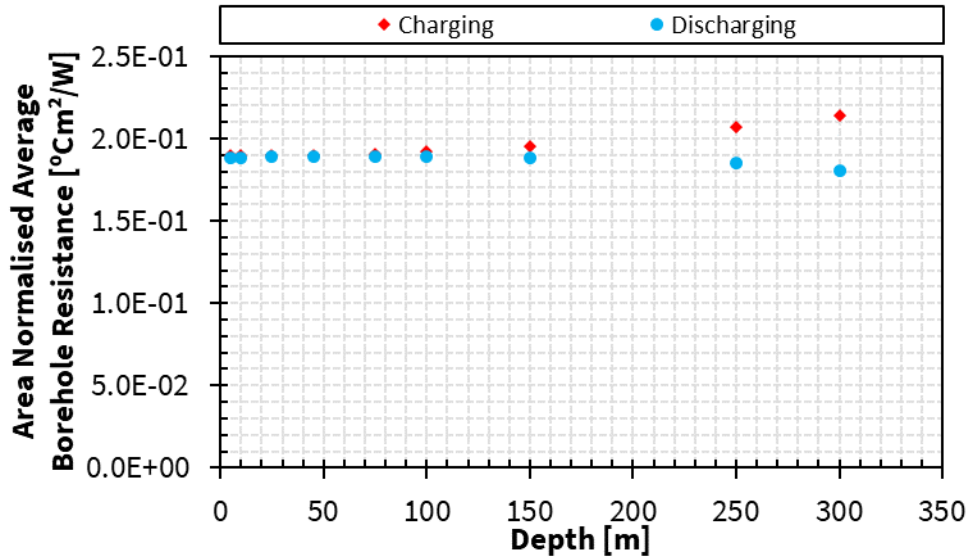
Figure B.41: Borehole heat exchanger thermal resistance of periodic steady state BTES operation normalized against total borehole area with respect to depth. Depth and volume are the variable parameters. Spacing and number of boreholes are held constant. Soil 2.
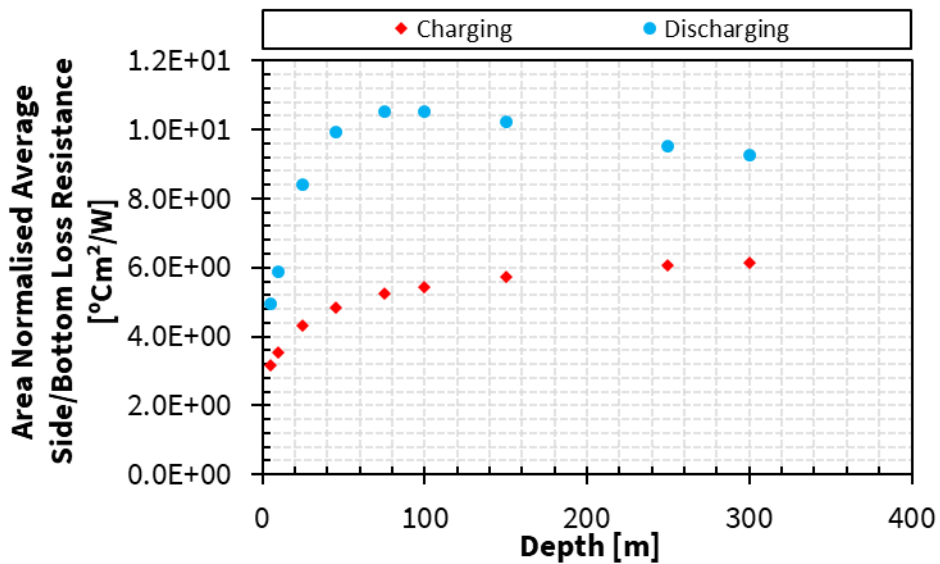
Figure B.42: Sides and bottom loss resistance of periodic steady state BTES operation normalized against storage volume side and bottom area with respect to depth. The larger magnitude of discharging resistances is a result of the change in heat transfer direction that occurs for periodic steady state side/bottom loss heat transfer rate. Depth and volume are the variable parameters. Spacing and number of boreholes are held constant. Soil 2.
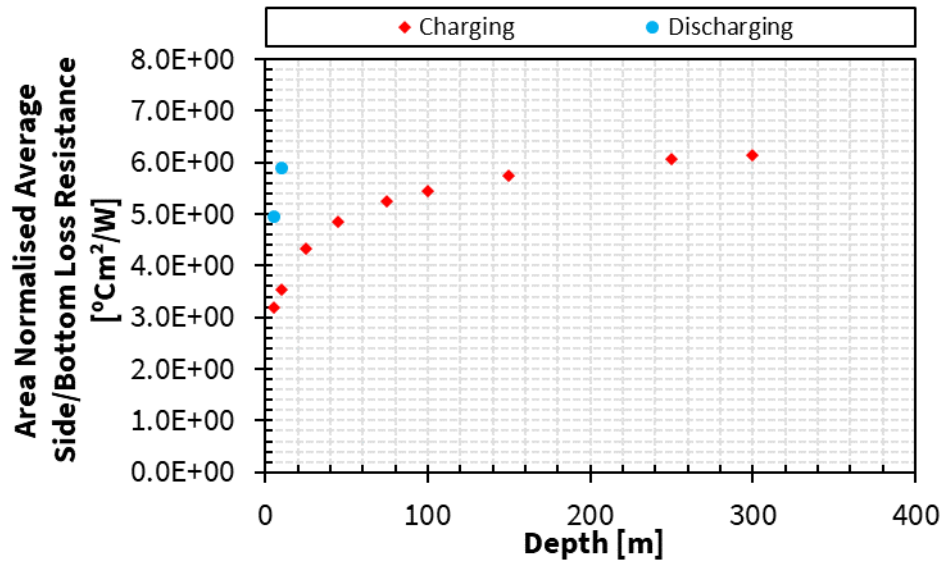
Figure B.43: Sides and bottom loss resistance of periodic steady state BTES operation normalized against storage volume side and bottom area with respect to depth. The figure's y-axis is reduced to omit most discharging resistances and better display charging resistance values. Depth and volume are the variable parameters. Spacing and number of boreholes are held constant. Soil 2.
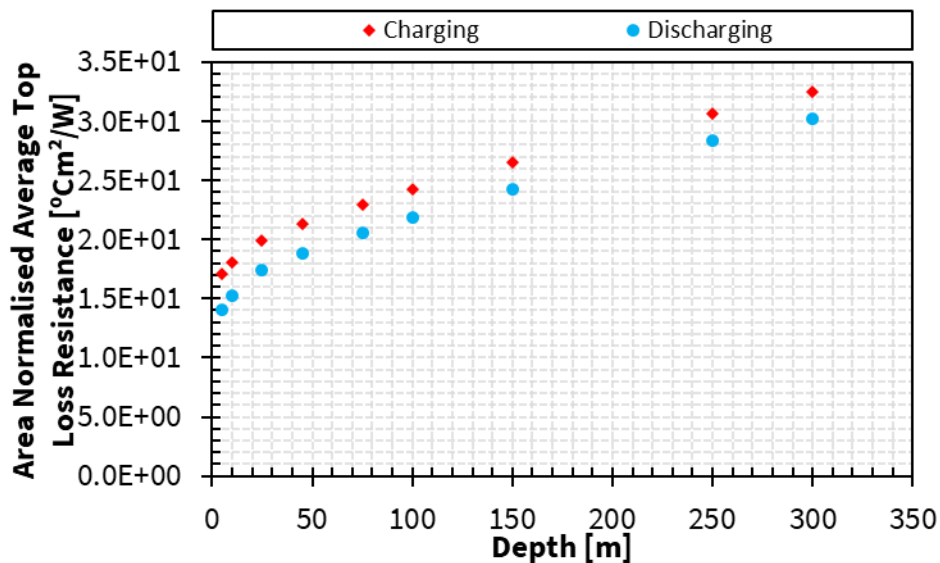
Figure B.44: Top loss resistance of periodic steady state BTES operation normalized against storage volume top area with respect to depth. Depth and volume are the variable parameters. Spacing and number of boreholes are held constant. Soil 2.
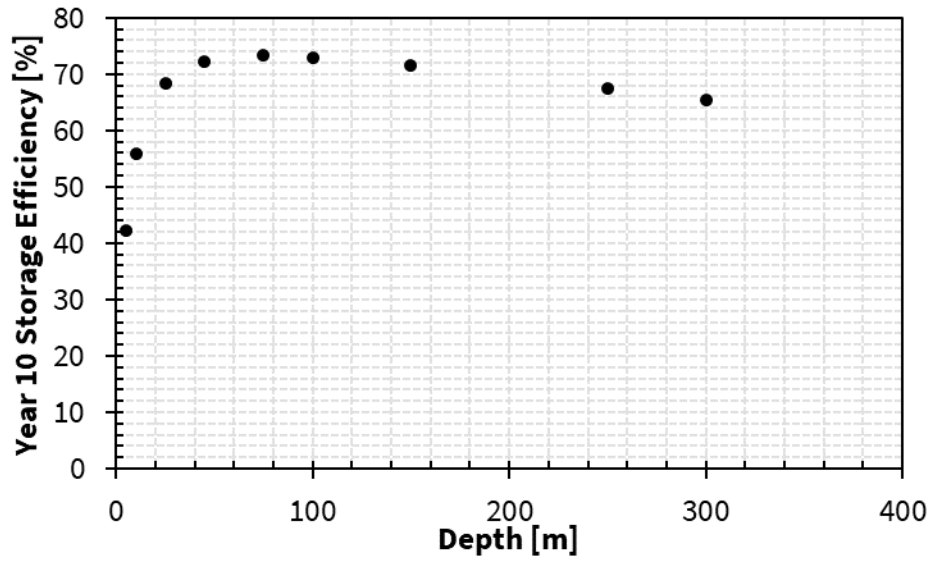
Figure B.45: Periodic steady state BTES thermal storage efficiency with respect to depth. BTES thermal storage efficiency is defined as the ratio of the total energy extracted during discharging timestep to the total energy injected during charging timestep for a simulation charging and discharging cycle. Depth and volume are the variable parameters. Spacing and number of boreholes are held constant. The inlet temperature setpoint of BTES charging is 95°C and BTES discharging is 20°C. Soil 2.
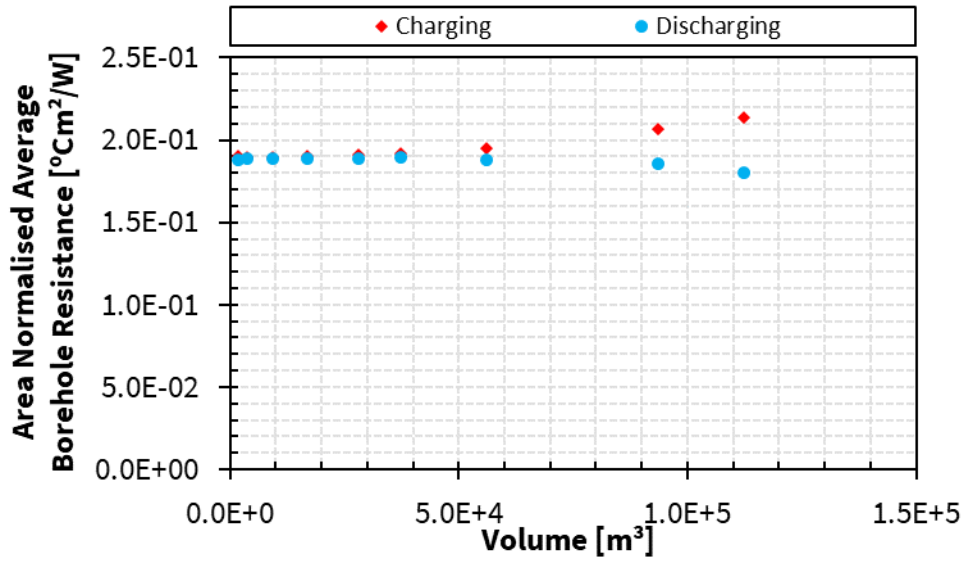
Figure B.46: Borehole heat exchanger thermal resistance of periodic steady state BTES operation normalized against total borehole area with respect to storage volume. Depth and volume are the variable parameters. Spacing and number of boreholes are held constant. Soil 2.
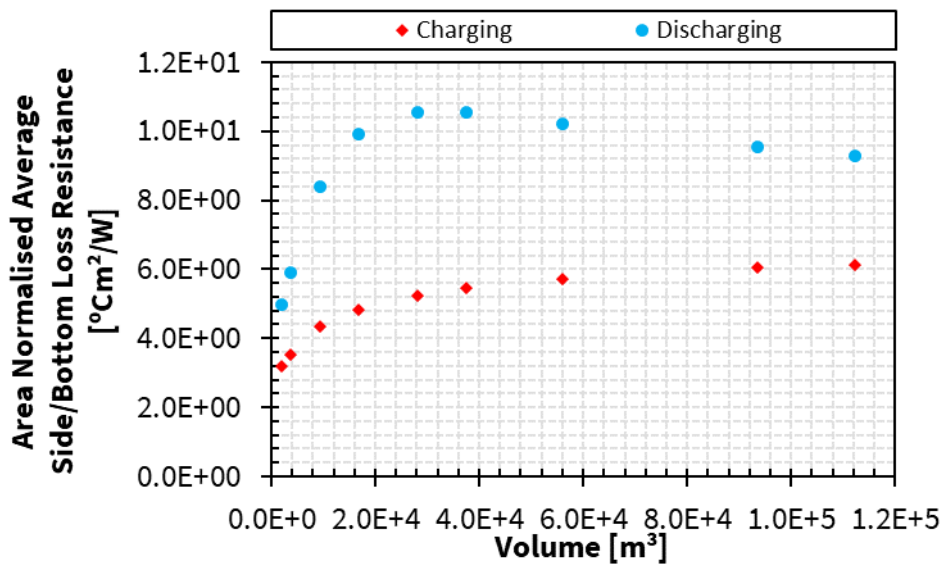
Figure B.47: Sides and bottom loss resistance of periodic steady state BTES operation normalized against storage volume side and bottom area with respect to storage volume. The larger magnitude of discharging resistances is a result of the change in heat transfer direction that occurs for periodic steady state side/bottom loss heat transfer rate. Depth and volume are the variable parameters. Spacing and number of boreholes are held constant. Soil 2.
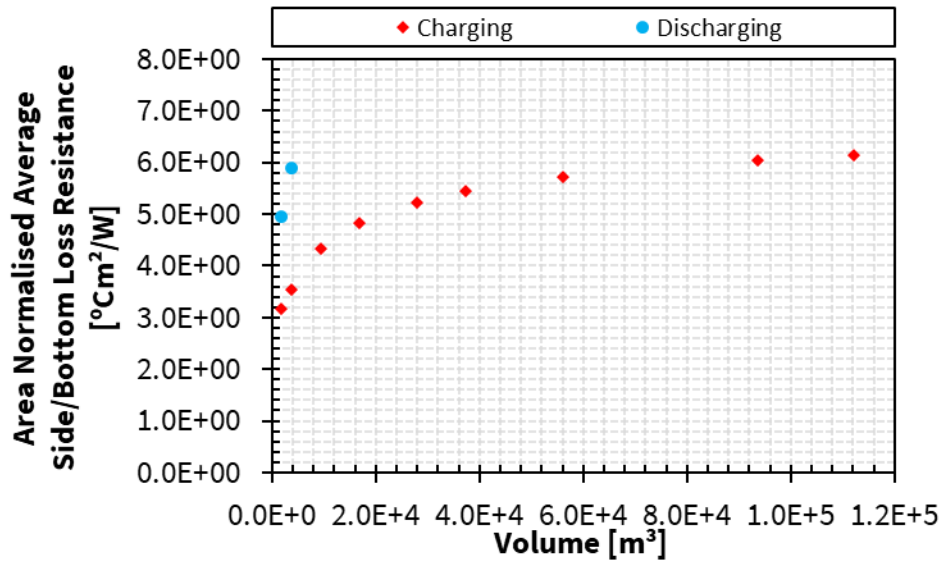
Figure B.48: Sides and bottom loss resistance of periodic steady state BTES operation normalized against storage volume side and bottom area with respect to storage volume. The figure's y-axis is reduced to omit most discharging resistances and better display charging resistance values. Depth and volume are the variable parameters. Spacing and number of boreholes are held constant. Soil 2.
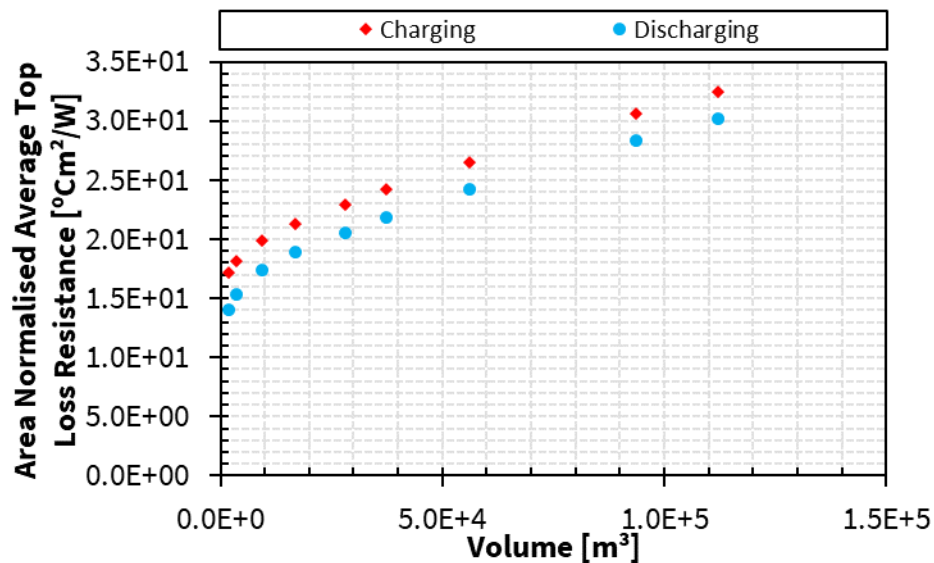
Figure B.49: Top loss resistance of periodic steady state BTES operation normalized against storage volume top area with respect to storage volume. Depth and volume are the variable parameters. Spacing and number of boreholes are held constant. Soil 2.
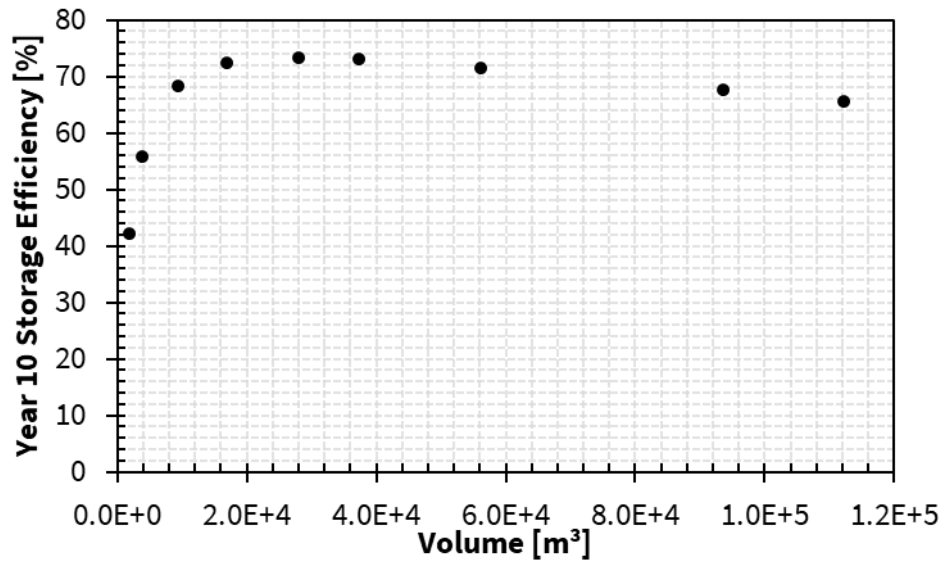
Figure B.50: Periodic steady state BTES thermal storage efficiency with respect to storage volume. BTES thermal storage efficiency is defined as the ratio of the total energy extracted during discharging timestep to the total energy injected during charging timestep for a simulation charging and discharging cycle. Depth and volume are the variable parameters. Spacing and number of boreholes are held constant. The inlet temperature setpoint of BTES charging is 95°C and BTES discharging is 20°C. Soil 2.

Appendix C

s [m]	V [m^3]	#BH	H [m]	A_{TBA} [m^2]	$A_{SV\_s,b}$ [m^2]	A_{SV_t} [m^2]	R_{hx} (charge) [°Cm^2/W]	R_{hx} (discharge) [°Cm^2/W]	$R_{loss\_s,b}$ (charge) [°Cm^2/W]	$R_{loss\_s,b}$ (discharge) [°Cm^2/W]	R_{loss_t} (charge) [°Cm^2/W]	R_{loss_t} (discharge) [°Cm^2/W]	Efficiency [%]
1	1870	48	45	1018	1070	42	1.12E-01	1.10E-01	1.78E+00	-1.42E+00	1.64E+01	1.86E+01	43.3
2	7481	48	45	1018	2223	166	1.35E-01	1.33E-01	2.41E+00	-4.17E+00	1.77E+01	2.03E+01	57.8
3	16833	48	45	1018	3459	374	1.48E-01	1.46E-01	3.16E+00	-1.25E+02	1.92E+01	1.99E+01	63.6
4	29926	48	45	1018	4779	665	1.57E-01	1.56E-01	4.05E+00	1.33E+01	2.04E+01	1.96E+01	63.9
5	46759	48	45	1018	6181	1039	1.64E-01	1.63E-01	4.99E+00	9.56E+00	2.11E+01	1.94E+01	61.5
6	67332	48	45	1018	7667	1496	1.70E-01	1.68E-01	5.93E+00	8.63E+00	2.14E+01	1.92E+01	58.2
7	91647	48	45	1018	9236	2037	1.75E-01	1.72E-01	6.79E+00	8.40E+00	2.15E+01	1.92E+01	54.6

Table C.1: Design parameters, heat transfer areas, periodic steady state thermal resistances, and periodic steady state storage efficiencies for the soil 3 parameter sweep with variable parameters: spacing and volume and constant parameters: number of boreholes and depth. The periodic steady state thermal resistances of charging and discharging and the periodic steady state storage efficiency are presented in Figure C.1 to Figure C.10 with respect to the variable parameters.
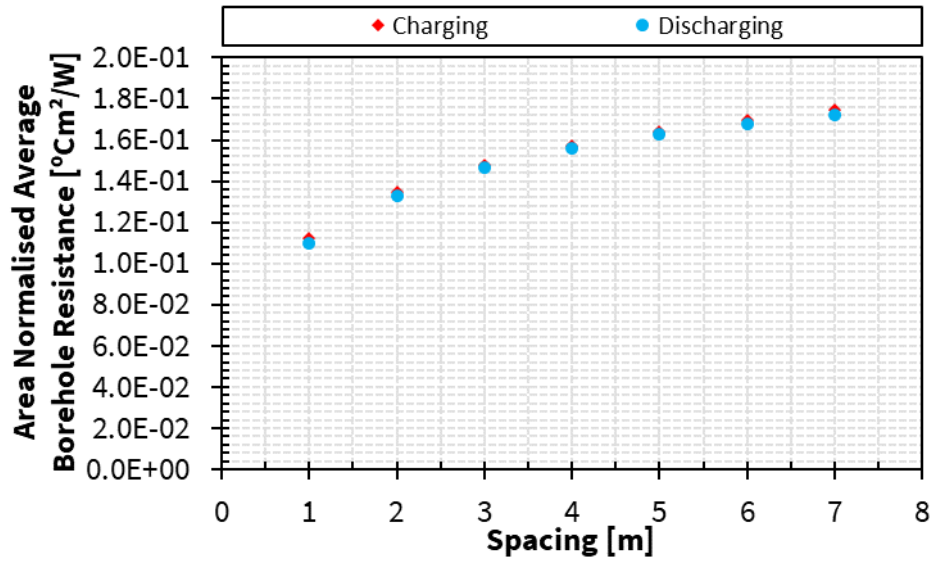
Figure C.1: Borehole heat exchanger thermal resistance of periodic steady state BTES operation normalized against total borehole area with respect to borehole spacing. Spacing and volume are the variable parameters. Number of boreholes and depth are held constant. Soil 3.
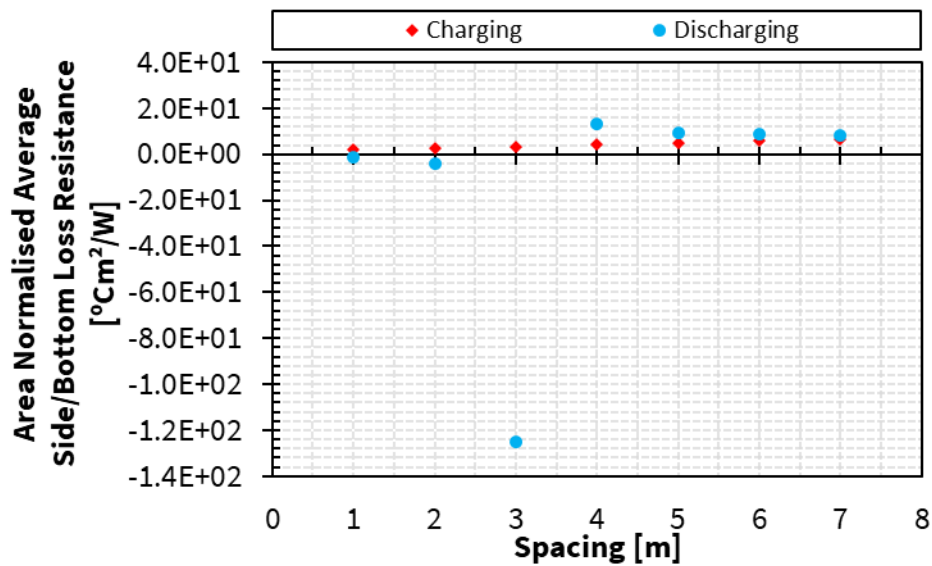
Figure C.2: Sides and bottom loss resistance of periodic steady state BTES operation normalized against storage volume side and bottom area with respect to borehole spacing. The negative discharging resistance values are a result of the change in heat transfer direction that occurs for periodic steady state side/bottom loss heat transfer rate. Spacing and volume are the variable parameters. Number of boreholes and depth are held constant. Soil 3.
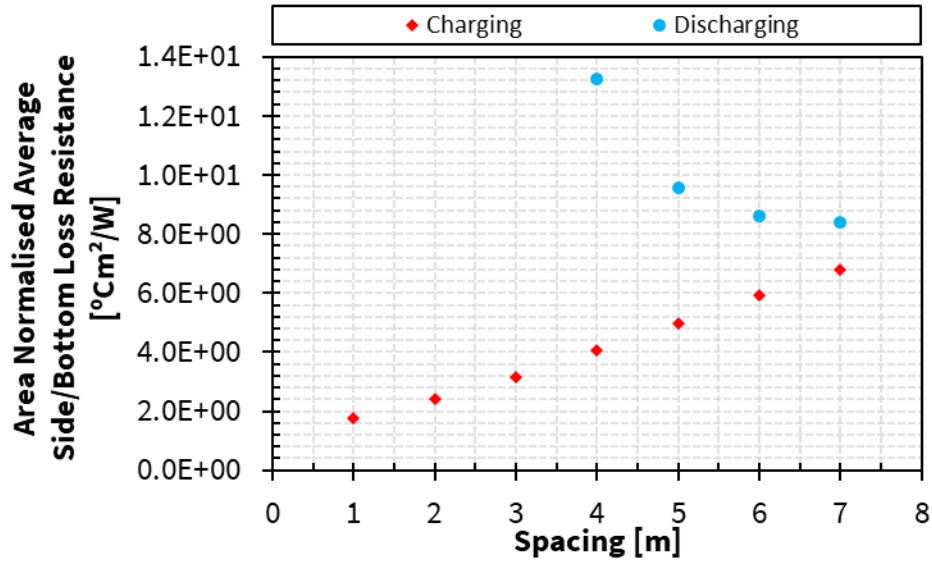
Figure C.3: Sides and bottom loss resistance of periodic steady state BTES operation normalized against storage volume side and bottom area with respect to borehole spacing. The figure's y-axis is reduced to omit discharging resistance outliers and better display charging resistance values. Spacing and volume are the variable parameters. Number of boreholes and depth are held constant. Soil 3.
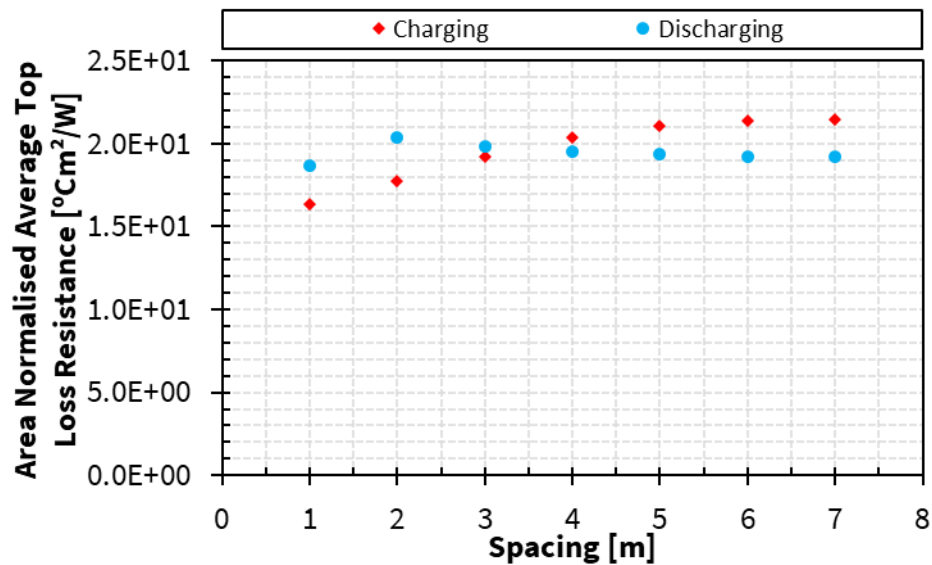
Figure C.4: Top loss resistance of periodic steady state BTES operation normalized against storage volume top area with respect to borehole spacing. Spacing and volume are the variable parameters. Number of boreholes and depth are held constant. Soil 3.
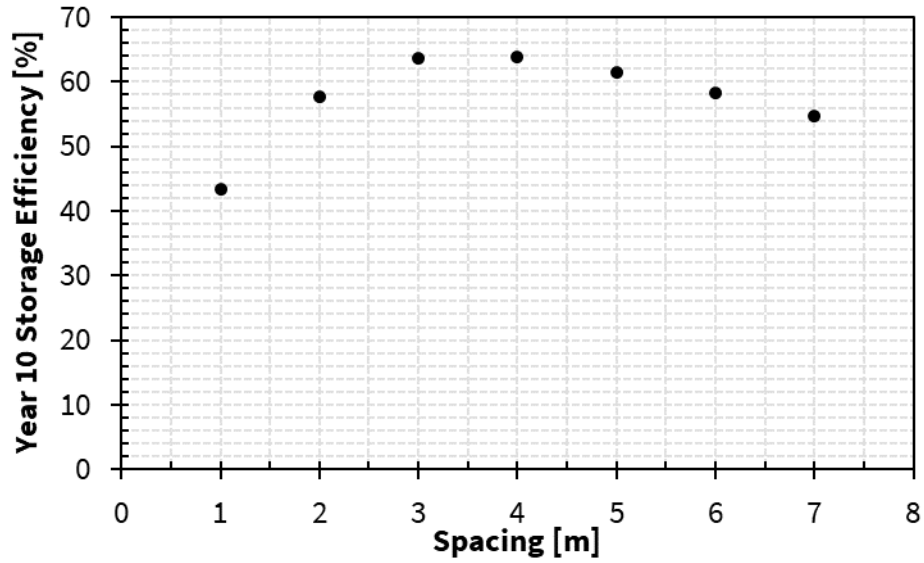
Figure C.5: Periodic steady state BTES thermal storage efficiency with respect to borehole spacing. BTES thermal storage efficiency is defined as the ratio of the total energy extracted during discharging timestep to the total energy injected during charging timestep for a simulation charging and discharging cycle. Spacing and volume are the variable parameters. Number of boreholes and depth are held constant. The inlet temperature setpoint of BTES charging is 95°C and BTES discharging is 20°C. Soil 3.
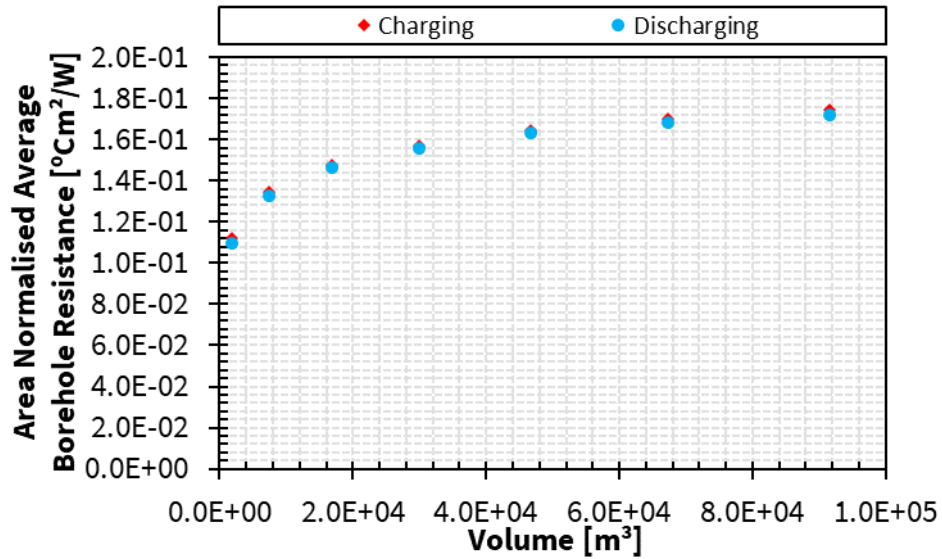
Figure C.6: Borehole heat exchanger thermal resistance of periodic steady state BTES operation normalized against total borehole area with respect to storage volume. Spacing and volume are the variable parameters. Number of boreholes and depth are held constant. Soil 3.
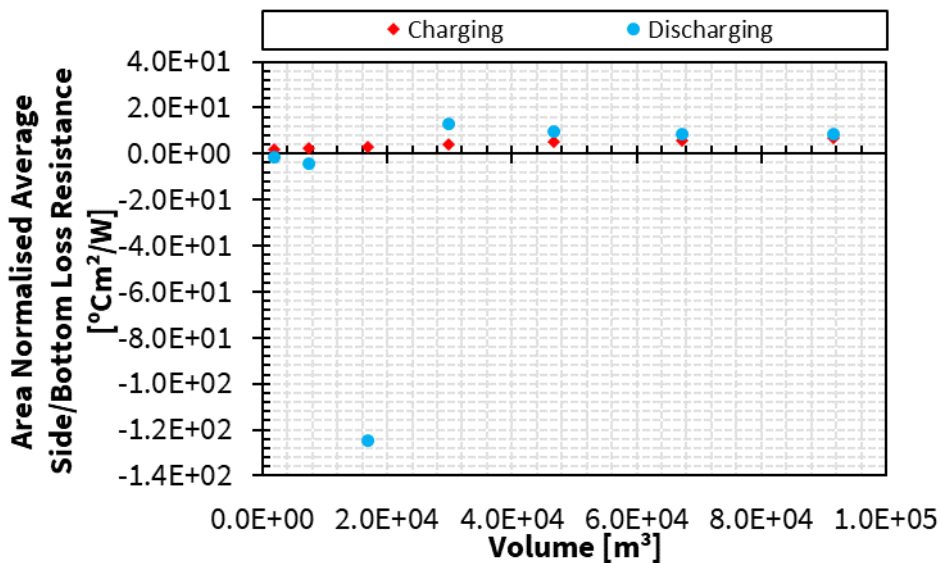
Figure C.7: Sides and bottom loss resistance of periodic steady state BTES operation normalized against storage volume side and bottom area with respect to storage volume. The negative discharging resistance values are a result of the change in heat transfer direction that occurs for periodic steady state side/bottom loss heat transfer rate. Spacing and volume are the variable parameters. Number of boreholes and depth are held constant. Soil 3.
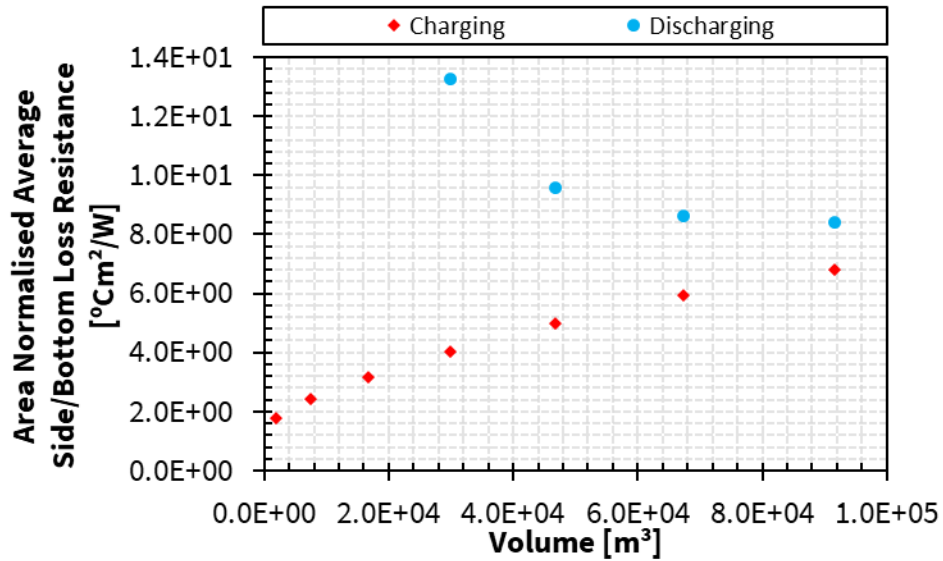
Figure C.8: Sides and bottom loss resistance of periodic steady state BTES operation normalized against storage volume side and bottom area with respect to storage volume. The figure's y-axis is reduced to omit discharging resistance outliers and better display charging resistance values. Spacing and volume are the variable parameters. Number of boreholes and depth are held constant. Soil 3.
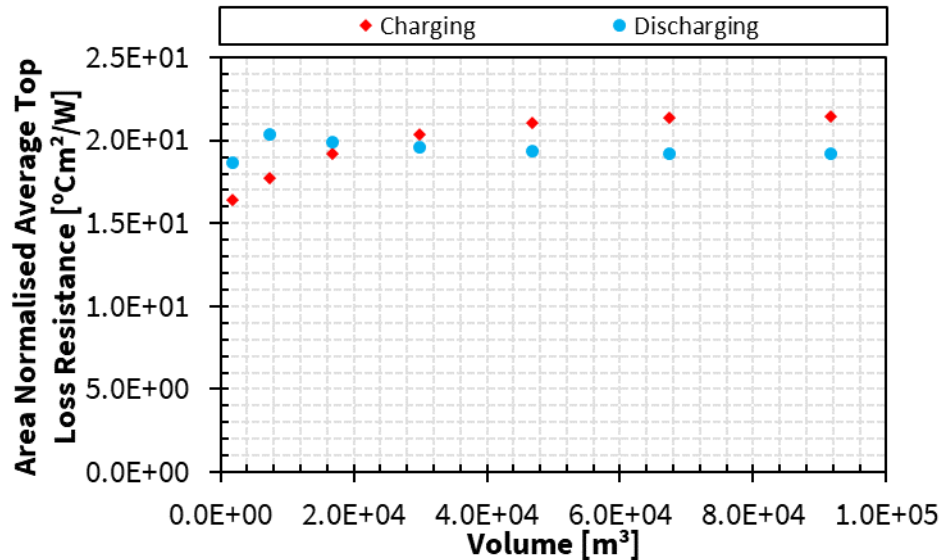
Figure C.9: Top loss resistance of periodic steady state BTES operation normalized against storage volume top area with respect to storage volume. Spacing and volume are the variable parameters. Number of boreholes and depth are held constant. Soil 3.
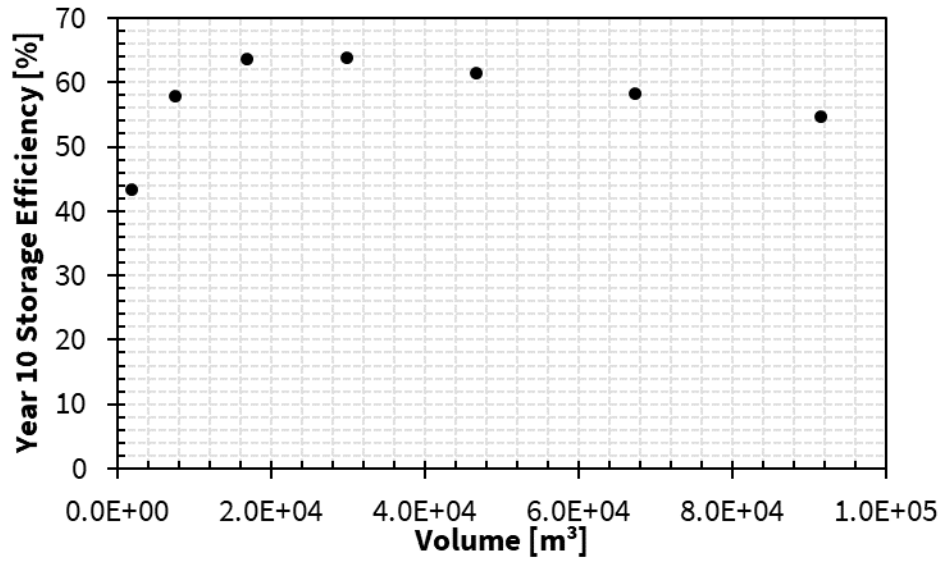
Figure C.10: Periodic steady state BTES thermal storage efficiency with respect to storage volume. BTES thermal storage efficiency is defined as the ratio of the total energy extracted during discharging timestep to the total energy injected during charging timestep for a simulation charging and discharging cycle. Spacing and volume are the variable parameters. Number of boreholes and depth are held constant. The inlet temperature setpoint of BTES charging is 95°C and BTES discharging is 20°C. Soil 3.

s [m]	H [m]	#BH	V [m³]	A_{TBA} [m²]	$A_{SV\_s,b}$ [m²]	A_{SV_t} [m²]	R_{hx} (charge) [°Cm²/W]	R_{hx} (discharge) [°Cm²/W]	$R_{loss\_s,b}$ (charge) [°Cm²/W]	$R_{loss\_s,b}$ (discharge) [°Cm²/W]	R_{loss_t} (charge) [°Cm²/W]	R_{loss_t} (discharge) [°Cm²/W]	Efficiency [%]
1	405	48	16833	9161	9297	42	1.43E-01	1.20E-01	2.08E+00	-2.35E+00	1.97E+01	2.65E+01	49.5
2	101.3	48	16833	2290	4794	166	1.37E-01	1.33E-01	2.66E+00	-4.34E+00	1.91E+01	2.34E+01	63.3
3	45	48	16833	1018	3459	374	1.48E-01	1.46E-01	3.16E+00	-1.25E+02	1.92E+01	1.99E+01	63.6
4	25.3	48	16833	573	2979	665	1.57E-01	1.56E-01	3.55E+00	9.60E+00	1.88E+01	1.76E+01	57.2
5	16.2	48	16833	366	2890	1039	1.64E-01	1.63E-01	3.90E+00	6.58E+00	1.80E+01	1.59E+01	47.2
6	11.3	48	16833	254	3039	1496	1.69E-01	1.67E-01	4.38E+00	5.96E+00	1.75E+01	1.48E+01	36.5
7	8.3	48	16833	187	3359	2037	1.74E-01	1.69E-01	4.98E+00	6.01E+00	1.73E+01	1.45E+01	26.6

Table C.2: Design parameters, heat transfer areas, periodic steady state thermal resistances, and periodic steady state storage efficiencies for the soil 3 parameter sweep with variable parameters: spacing and depth and constant parameters: number of boreholes and volume. The periodic steady state thermal resistances of charging and discharging and the periodic steady state storage efficiency are presented in Figure C.11 to Figure C.20 with respect to the variable parameters.
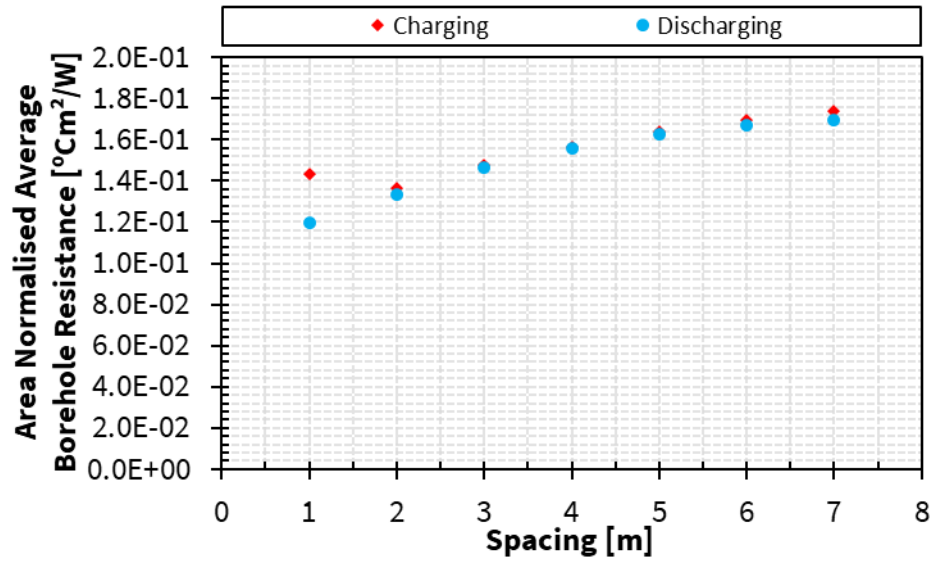
Figure C.11: Borehole heat exchanger thermal resistance of periodic steady state BTES operation normalized against total borehole area with respect to borehole spacing. Spacing and depth are the variable parameters. Number of boreholes and volume are held constant. Soil 3.
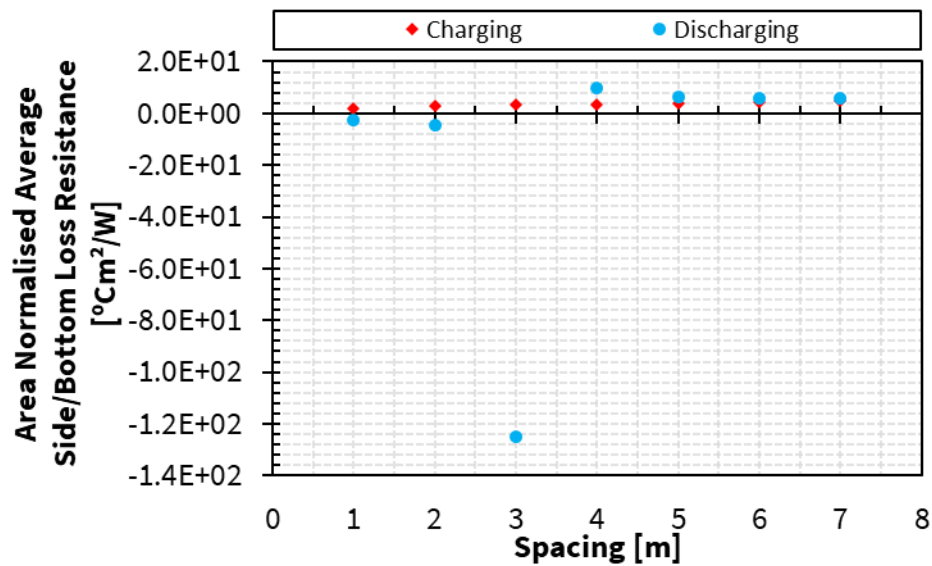
Figure C.12: Sides and bottom loss resistance of periodic steady state BTES operation normalized against storage volume side and bottom area with respect to borehole spacing. The negative discharging resistance values are a result of the change in heat transfer direction that occurs for periodic steady state side/bottom loss heat transfer rate. Spacing and depth are the variable parameters. Number of boreholes and volume are held constant. Soil 3.
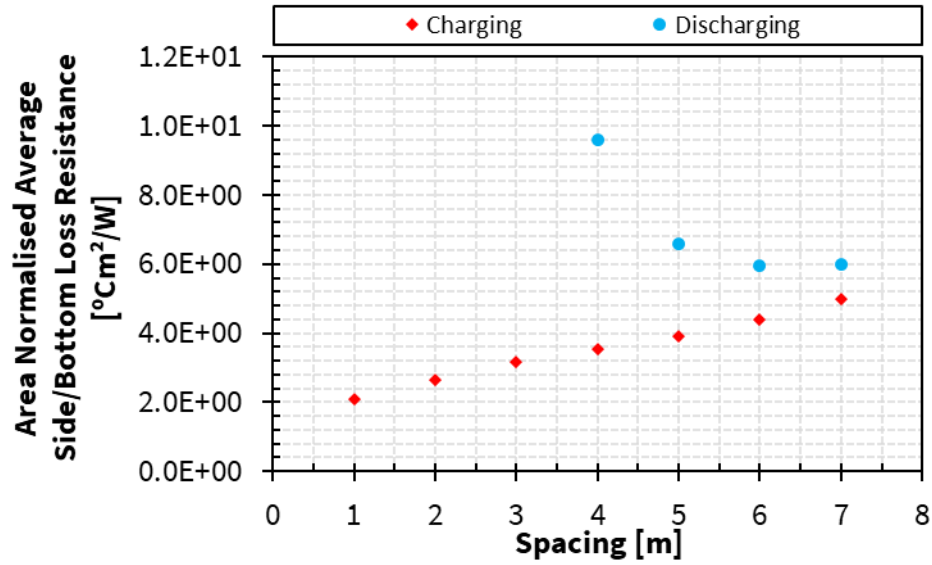
Figure C.13: Sides and bottom loss resistance of periodic steady state BTES operation normalized against storage volume side and bottom area with respect to borehole spacing. The figure's y-axis is reduced to omit discharging resistance outliers and better display charging resistance values. Spacing and depth are the variable parameters. Number of boreholes and volume are held constant. Soil 3.
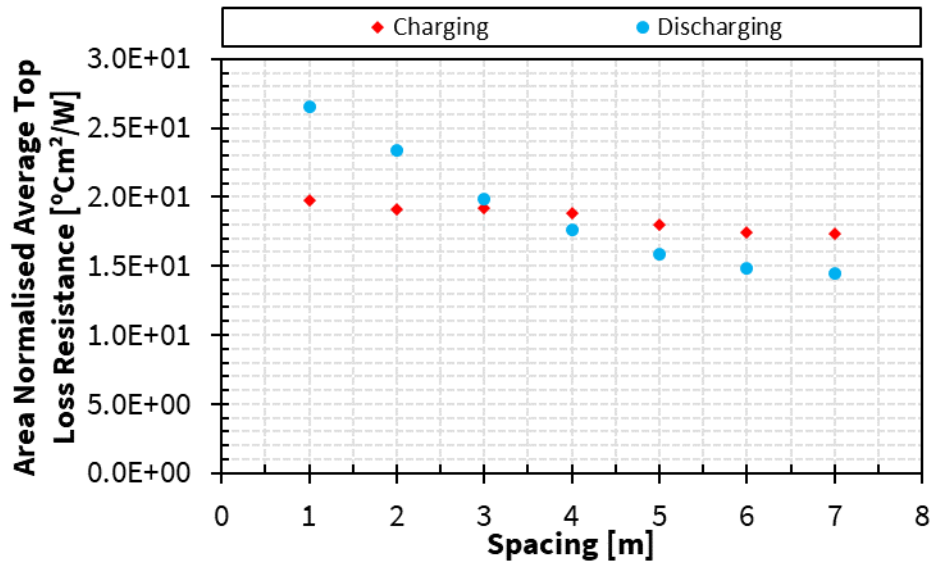
Figure C.14: Top loss resistance of periodic steady state BTES operation normalized against storage volume top area with respect to borehole spacing. Spacing and depth are the variable parameters. Number of boreholes and volume are held constant. Soil 3.
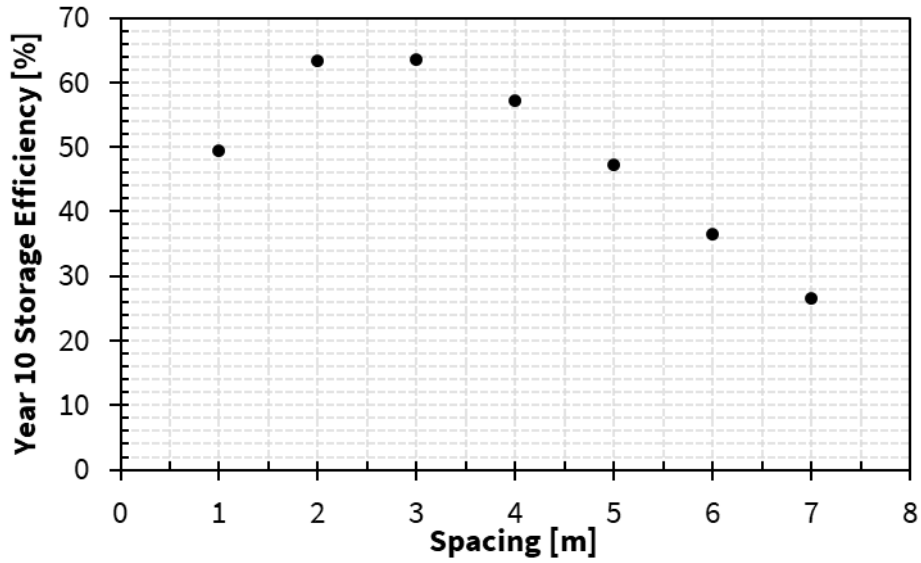
Figure C.15: Periodic steady state BTES thermal storage efficiency with respect to borehole spacing. BTES thermal storage efficiency is defined as the ratio of the total energy extracted during discharging timestep to the total energy injected during charging timestep for a simulation charging and discharging cycle. Spacing and depth are the variable parameters. Number of boreholes and volume are held constant. The inlet temperature setpoint of BTES charging is 95°C and BTES discharging is 20°C. Soil 3.
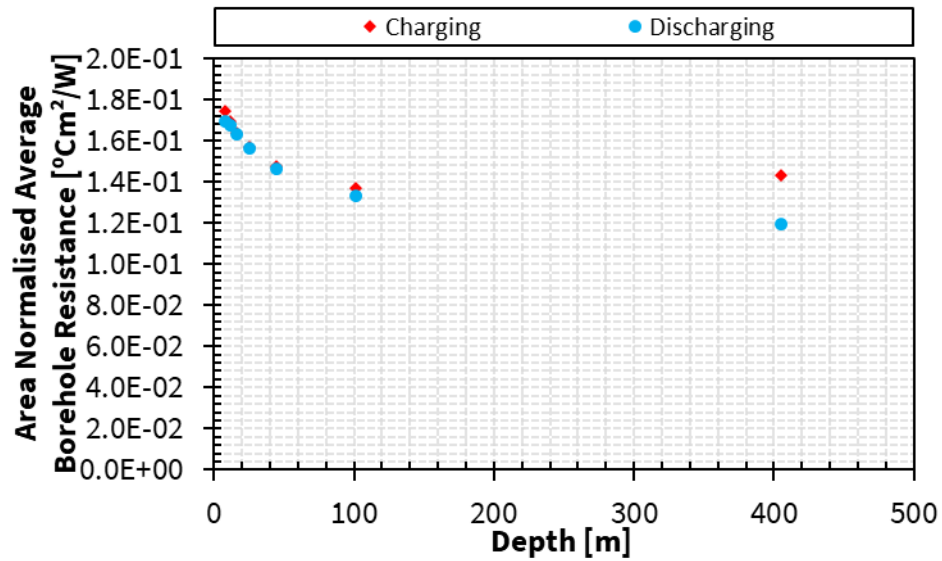
Figure C.16: Borehole heat exchanger thermal resistance of periodic steady state BTES operation normalized against total borehole area with respect to depth. Spacing and depth are the variable parameters. Number of boreholes and volume are held constant. Soil 3.
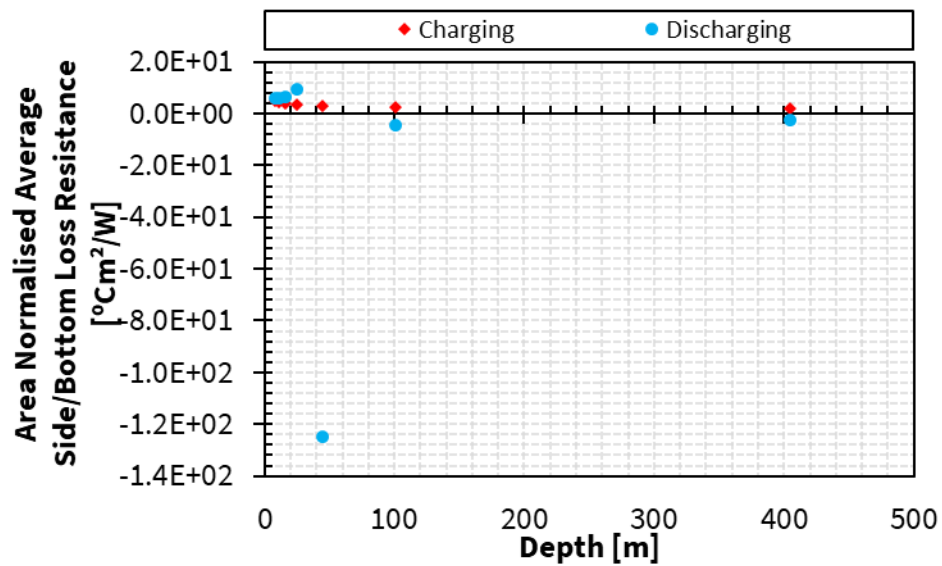
Figure C.17: Sides and bottom loss resistance of periodic steady state BTES operation normalized against storage volume side and bottom area with respect to depth. The negative discharging resistance values are a result of the change in heat transfer direction that occurs for periodic steady state side/bottom loss heat transfer rate. Spacing and depth are the variable parameters. Number of boreholes and volume are held constant. Soil 3.
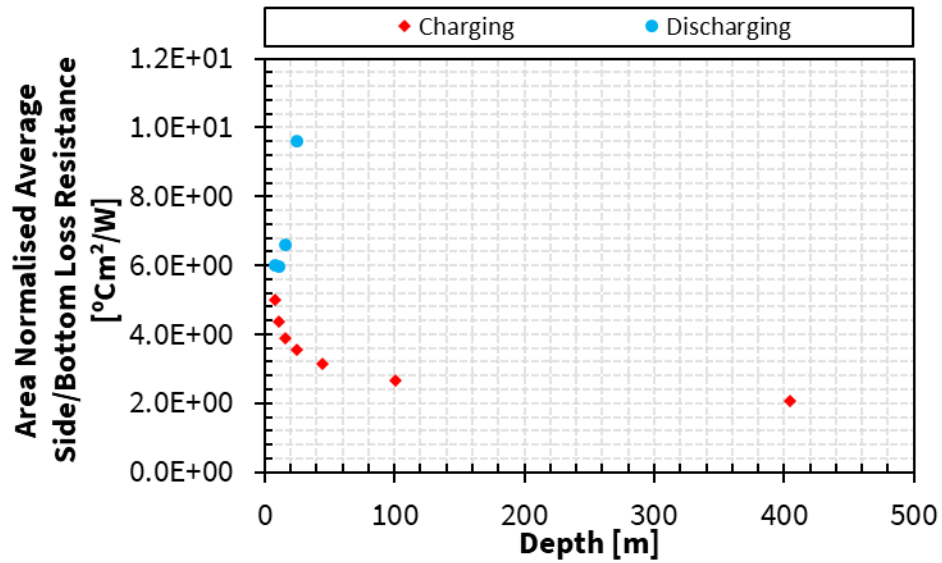
Figure C.18: Sides and bottom loss resistance of periodic steady state BTES operation normalized against storage volume side and bottom area with respect to depth. The figure's y-axis is reduced to omit discharging resistance outliers and better display charging resistance values. Spacing and depth are the variable parameters. Number of boreholes and volume are held constant. Soil 3.
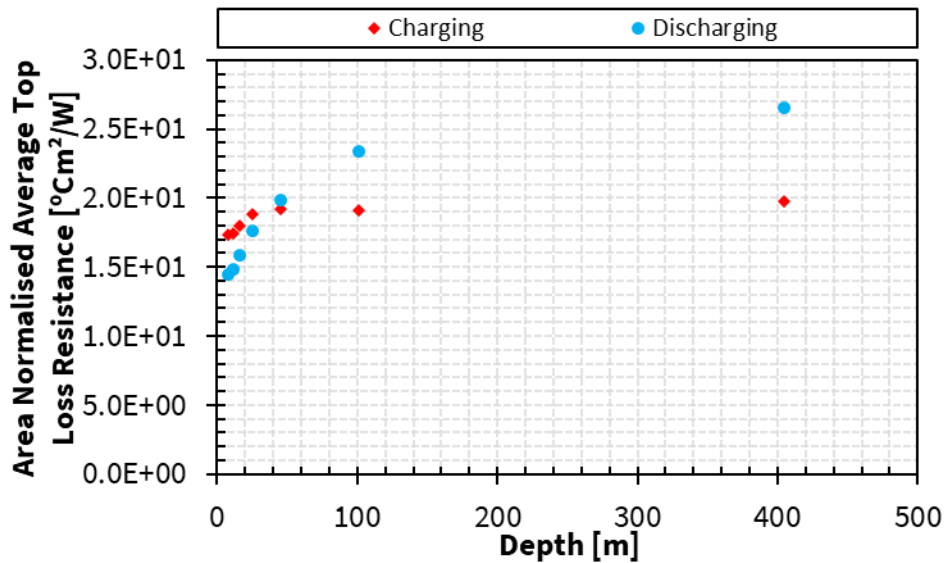
Figure C.19: Top loss resistance of periodic steady state BTES operation normalized against storage volume top area with respect to depth. Spacing and depth are the variable parameters. Number of boreholes and volume are held constant. Soil 3.
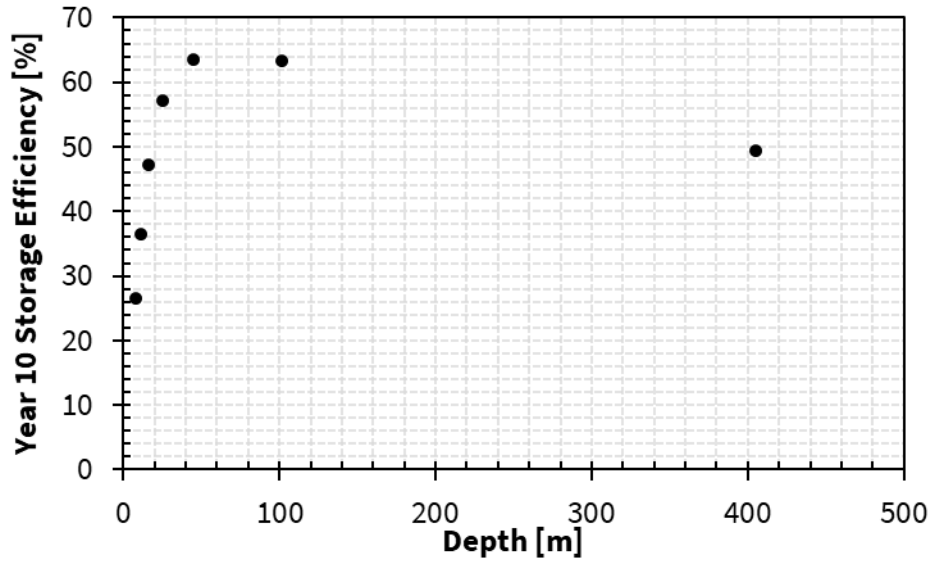
Figure C.20: Periodic steady state BTES thermal storage efficiency with respect to depth. BTES thermal storage efficiency is defined as the ratio of the total energy extracted during discharging timestep to the total energy injected during charging timestep for a simulation charging and discharging cycle. Spacing and depth are the variable parameters. Number of boreholes and volume are held constant. The inlet temperature setpoint of BTES charging is 95°C and BTES discharging is 20°C. Soil 3.

s [m]	#BH	H [m]	V [m³]	A_{TBA} [m²]	$A_{SV\_s,b}$ [m²]	A_{SV_t} [m²]	R_{hx} (charge) [°Cm²/W]	R_{hx} (discharge) [°Cm²/W]	$R_{loss\_s,b}$ (charge) [°Cm²/W]	$R_{loss\_s,b}$ (discharge) [°Cm²/W]	R_{loss_t} (charge) [°Cm²/W]	R_{loss_t} (discharge) [°Cm²/W]	Efficiency [%]
1	432	45	16833	9161	3459	374	1.32E-01	1.07E-01	2.25E+00	-1.76E+00	1.69E+01	2.18E+01	69.8
1.5	192	45	16833	4072	3459	374	1.31E-01	1.21E-01	2.43E+00	-2.63E+00	1.74E+01	2.13E+01	69.3
2	108	45	16833	2290	3459	374	1.37E-01	1.32E-01	2.64E+00	-4.61E+00	1.79E+01	2.09E+01	68.2
3	48	45	16833	1018	3459	374	1.48E-01	1.46E-01	3.16E+00	-1.25E+02	1.92E+01	1.99E+01	63.6
4	27	45	16833	573	3459	374	1.57E-01	1.56E-01	3.72E+00	1.21E+01	2.03E+01	1.97E+01	56.2
5	17	45	16833	360	3459	374	1.64E-01	1.63E-01	4.29E+00	7.92E+00	2.17E+01	1.99E+01	47.1
6	12	45	16833	254	3459	374	1.69E-01	1.67E-01	4.75E+00	6.80E+00	2.27E+01	2.02E+01	39.0
7	9	45	16833	191	3459	374	1.74E-01	1.70E-01	5.15E+00	6.27E+00	2.38E+01	2.05E+01	31.9

Table C.3: Design parameters, heat transfer areas, periodic steady state thermal resistances, and periodic steady state storage efficiencies for the soil 3 parameter sweep with variable parameters: spacing and number of boreholes and constant parameters: depth and volume. The periodic steady state thermal resistances of charging and discharging and the periodic steady state storage efficiency are presented in Figure C.21 to Figure C.30 with respect to the variable parameters.
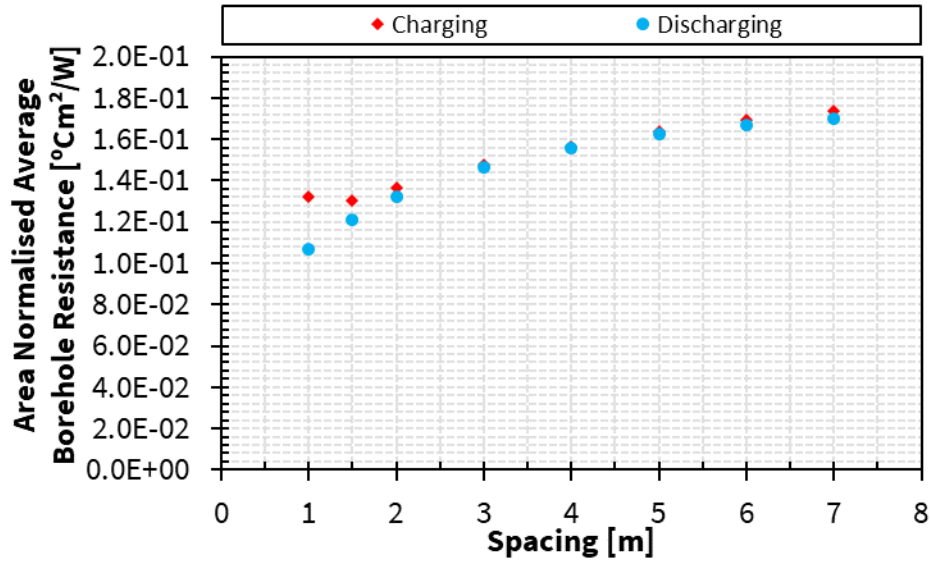
Figure C.21: Borehole heat exchanger thermal resistance of periodic steady state BTES operation normalized against total borehole area with respect to borehole spacing. Spacing and number of boreholes are the variable parameters. Depth and volume are held constant. Soil 3.
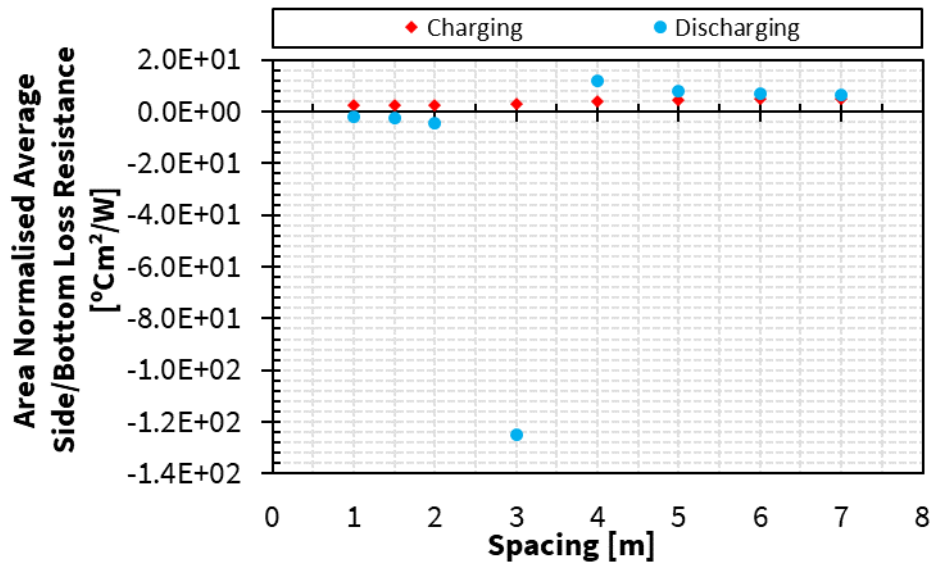
Figure C.22: Sides and bottom loss resistance of periodic steady state BTES operation normalized against storage volume side and bottom area with respect to borehole spacing. The negative discharging resistance values are a result of the change in heat transfer direction that occurs for periodic steady state side/bottom loss heat transfer rate. Spacing and number of boreholes are the variable parameters. Depth and volume are held constant. Soil 3.
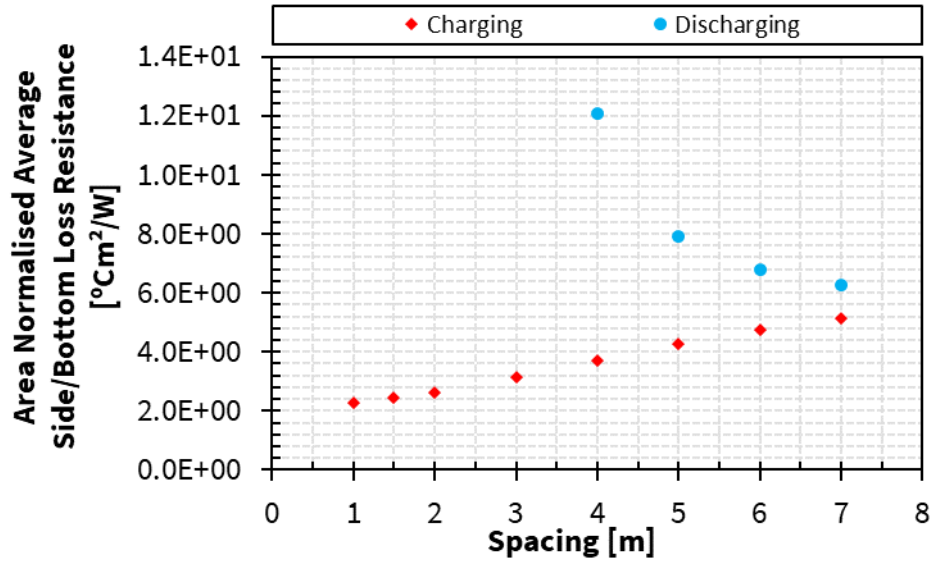
Figure C.23: Sides and bottom loss resistance of periodic steady state BTES operation normalized against storage volume side and bottom area with respect to borehole spacing. The figure's y-axis is reduced to omit discharging resistance outliers and better display charging resistance values. Spacing and number of boreholes are the variable parameters. Depth and volume are held constant. Soil 3.
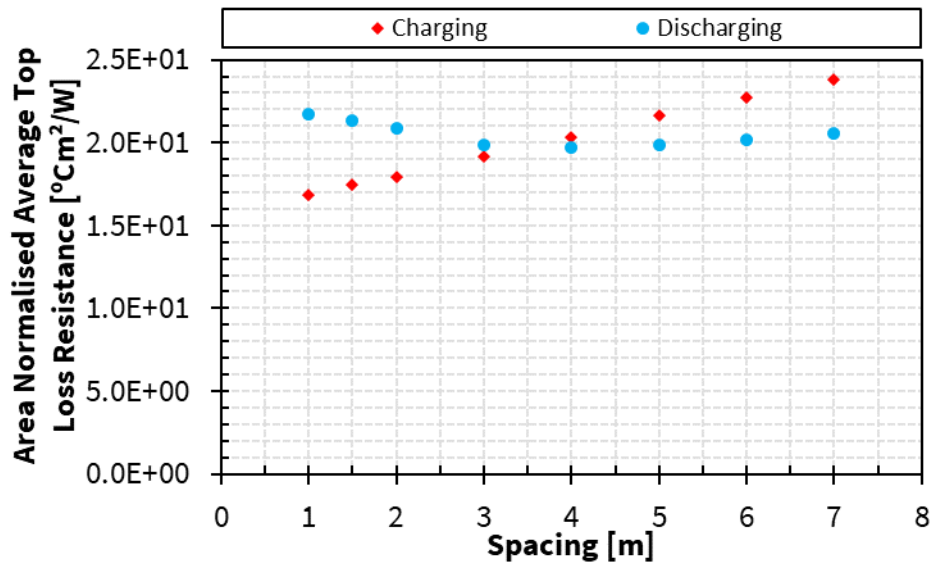
Figure C.24: Top loss resistance of periodic steady state BTES operation normalized against storage volume top area with respect to borehole spacing. Spacing and number of boreholes are the variable parameters. Depth and volume are held constant. Soil 3.
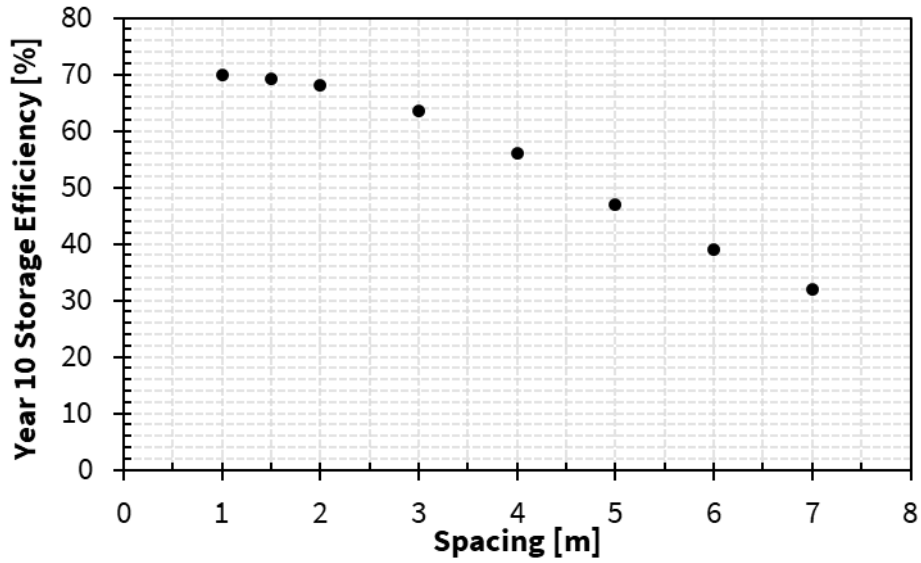
Figure C.25: Periodic steady state BTES thermal storage efficiency with respect to borehole spacing. BTES thermal storage efficiency is defined as the ratio of the total energy extracted during discharging timestep to the total energy injected during charging timestep for a simulation charging and discharging cycle. Spacing and number of boreholes are the variable parameters. Depth and volume are held constant. The inlet temperature setpoint of BTES charging is 95°C and BTES discharging is 20°C. Soil 3.
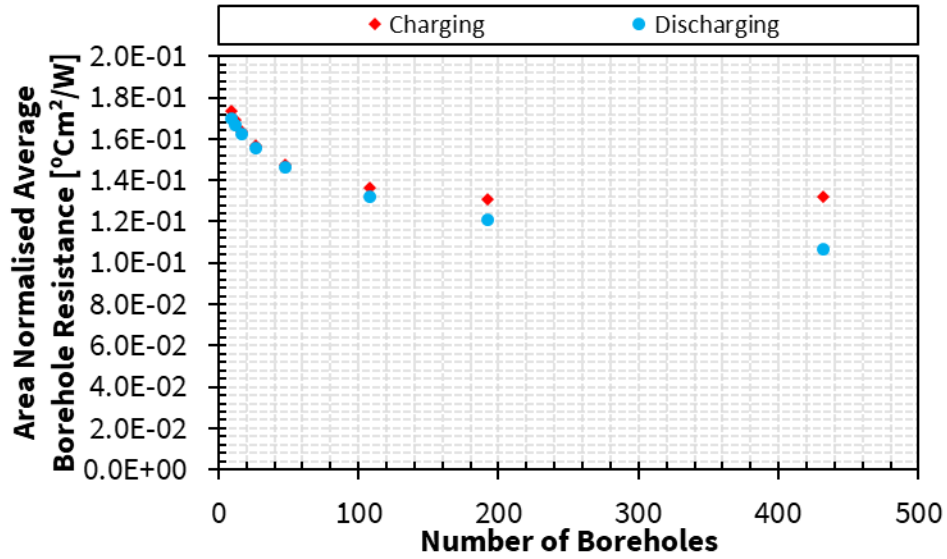
Figure C.26: Borehole heat exchanger thermal resistance of periodic steady state BTES operation normalized against total borehole area with respect to number of boreholes. Spacing and number of boreholes are the variable parameters. Depth and volume are held constant. Soil 3.
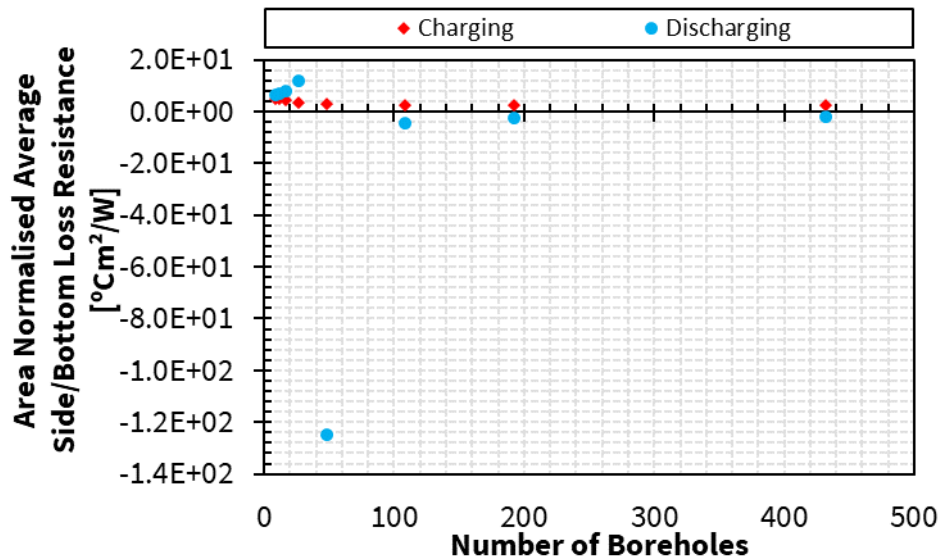
Figure C.27: Sides and bottom loss resistance of periodic steady state BTES operation normalized against storage volume side and bottom area with respect to number of boreholes. The negative discharging resistance values are a result of the change in heat transfer direction that occurs for periodic steady state side/bottom loss heat transfer rate. Spacing and number of boreholes are the variable parameters. Depth and volume are held constant. Soil 3.
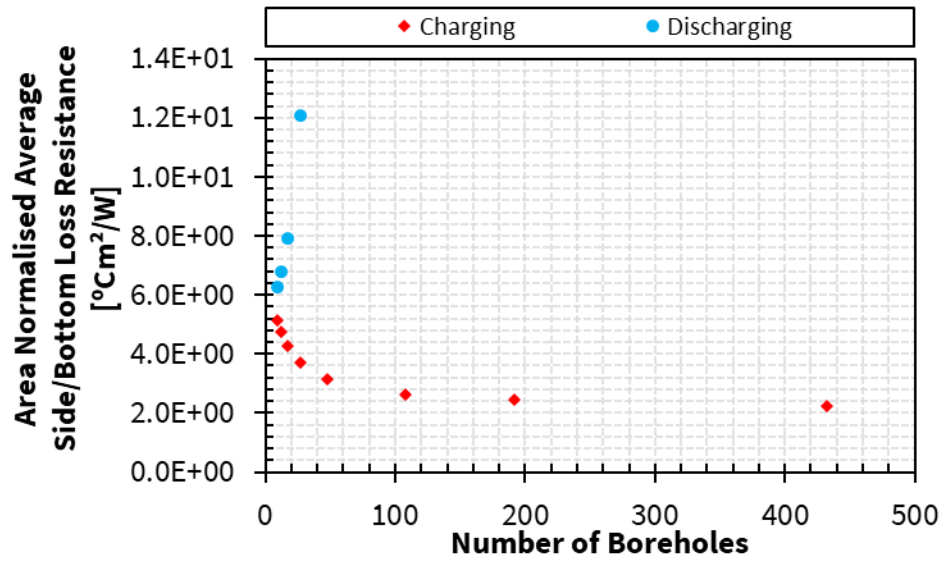
Figure C.28: Sides and bottom loss resistance of periodic steady state BTES operation normalized against storage volume side and bottom area with respect to number of boreholes. The figure's y-axis is reduced to omit discharging resistance outliers and better display charging resistance values. Spacing and number of boreholes are the variable parameters. Depth and volume are held constant. Soil 3.
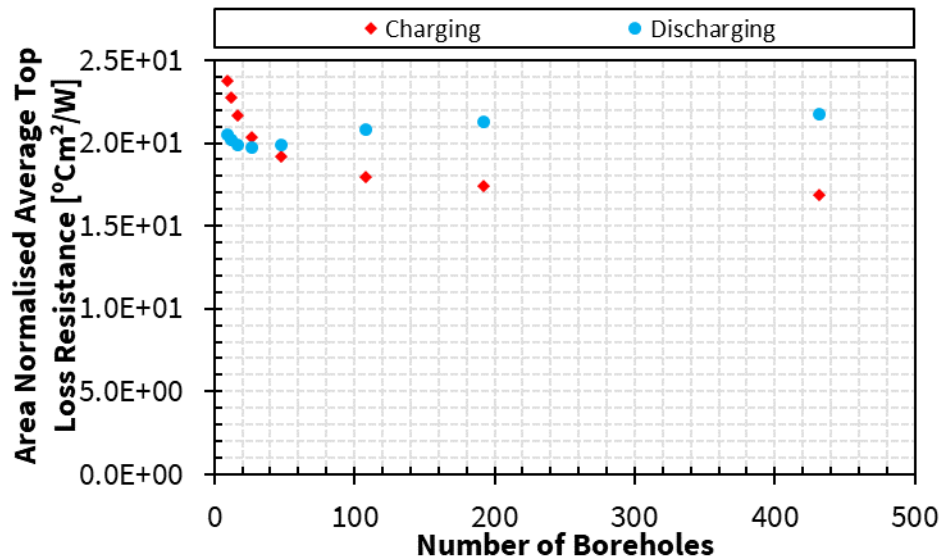
Figure C.29: Top loss resistance of periodic steady state BTES operation normalized against storage volume top area with respect to number of boreholes. Spacing and number of boreholes are the variable parameters. Depth and volume are held constant. Soil 3.
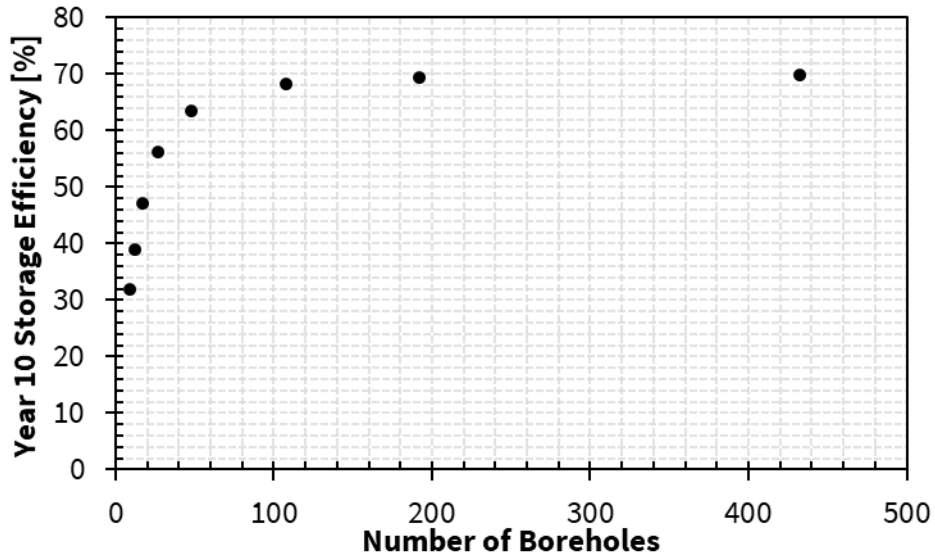
Figure C.30: Periodic steady state BTES thermal storage efficiency with respect to number of boreholes. BTES thermal storage efficiency is defined as the ratio of the total energy extracted during discharging timestep to the total energy injected during charging timestep for a simulation charging and discharging cycle. Spacing and number of boreholes are the variable parameters. Depth and volume are held constant. The inlet temperature setpoint of BTES charging is 95°C and BTES discharging is 20°C. Soil 3.

#BH	V [m^3]	s [m]	H [m]	A_{TBA} [m^2]	$A_{SV\_s,b}$ [m^2]	A_{SV_t} [m^2]	R_{hx} (charge) [°Cm^2/W]	R_{hx} (discharge) [°Cm^2/W]	$R_{loss\_s,b}$ (charge) [°Cm^2/W]	$R_{loss\_s,b}$ (discharge) [°Cm^2/W]	R_{loss_t} (charge) [°Cm^2/W]	R_{loss_t} (discharge) [°Cm^2/W]	Efficiency [%]
10	3507	3	45	212	1486	78	1.47E-01	1.46E-01	2.53E+00	4.01E+01	2.06E+01	2.32E+01	37.0
25	8767	3	45	530	2421	195	1.47E-01	1.46E-01	2.90E+00	-4.50E+02	1.93E+01	2.04E+01	53.9
48	16833	3	45	1018	3459	374	1.48E-01	1.46E-01	3.16E+00	-1.25E+02	1.92E+01	1.99E+01	63.6
75	26302	3	45	1590	4441	584	1.49E-01	1.46E-01	3.36E+00	-6.61E+02	1.95E+01	2.02E+01	68.9
100	35069	3	45	2121	5233	779	1.50E-01	1.47E-01	3.50E+00	2.11E+02	2.00E+01	2.07E+01	71.6
150	52604	3	45	3181	6623	1169	1.52E-01	1.48E-01	3.75E+00	4.60E+01	2.11E+01	2.21E+01	74.6
200	70138	3	45	4241	7856	1559	1.56E-01	1.49E-01	3.96E+00	2.79E+01	2.23E+01	2.34E+01	76.0
500	175345	3	45	10603	13854	3897	1.95E-01	1.65E-01	4.84E+00	1.31E+01	2.80E+01	2.96E+01	75.8

Table C.4: Design parameters, heat transfer areas, periodic steady state thermal resistances, and periodic steady state storage efficiencies for the soil 3 parameter sweep with variable parameters: number of boreholes and volume and constant parameters: spacing and depth. The periodic steady state thermal resistances of charging and discharging and the periodic steady state storage efficiency are presented in Figure C.31 to Figure C.40 with respect to the variable parameters.
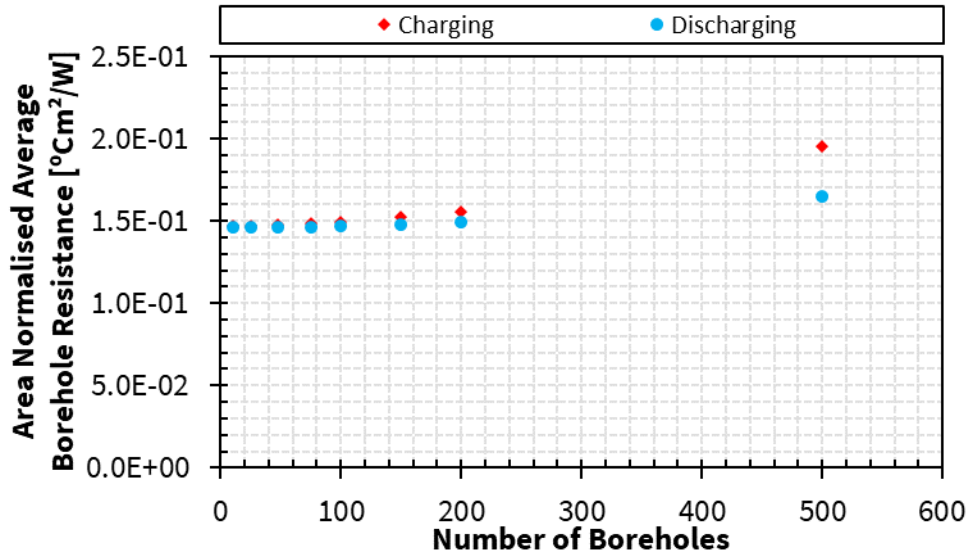
Figure C.31: Borehole heat exchanger thermal resistance of periodic steady state BTES operation normalized against total borehole area with respect to number of boreholes. Number of boreholes and volume are the variable parameters. Spacing and depth are held constant. Soil 3.
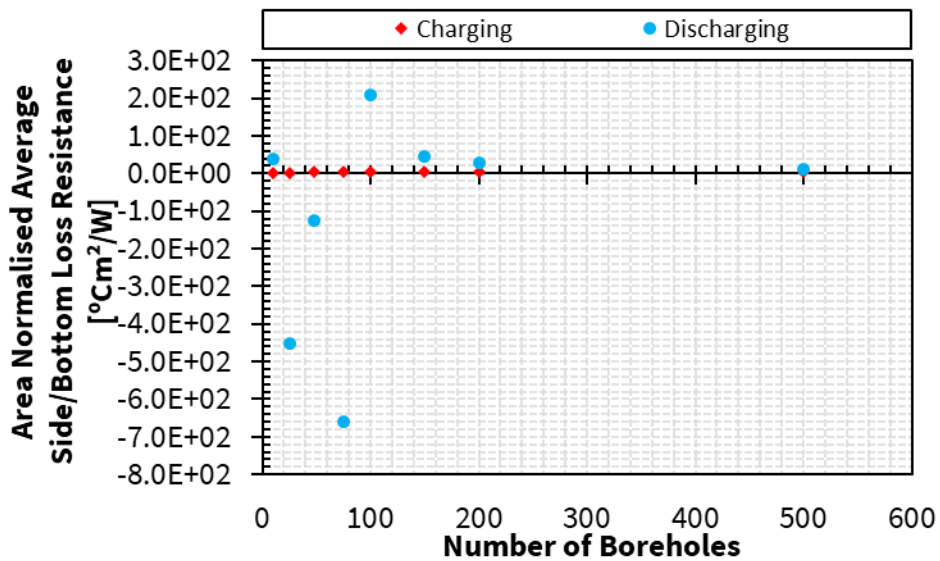
Figure C.32: Sides and bottom loss resistance of periodic steady state BTES operation normalized against storage volume side and bottom area with respect to number of boreholes. The negative and large magnitude discharging resistance are a result of the change in heat transfer direction that occurs for periodic steady state side/bottom loss heat transfer rate. Number of boreholes and volume are the variable parameters. Spacing and depth are held constant. Soil 3.
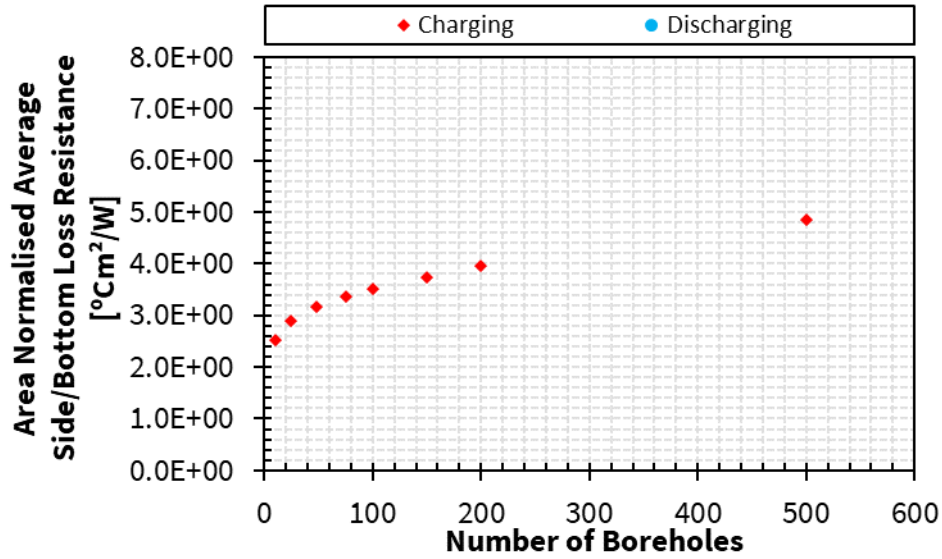
Figure C.33: Sides and bottom loss resistance of periodic steady state BTES operation normalized against storage volume side and bottom area with respect to number of boreholes. The figure's y-axis is reduced to omit negative and large magnitude discharging resistance outliers and better display charging resistance values. Number of boreholes and volume are the variable parameters. Spacing and depth are held constant. Soil 3.
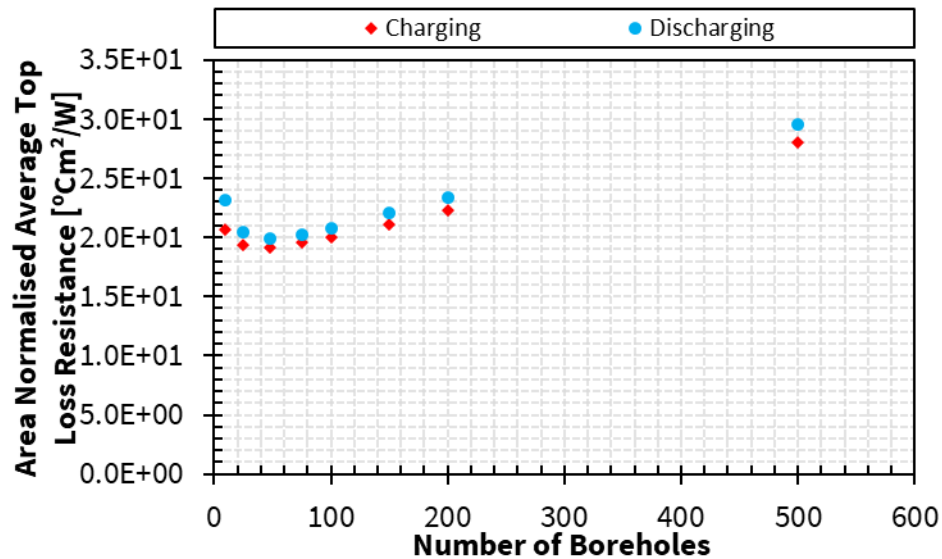
Figure C.34: Top loss resistance of periodic steady state BTES operation normalized against storage volume top area with respect to number of boreholes. Number of boreholes and volume are the variable parameters. Spacing and depth are held constant. Soil 3.
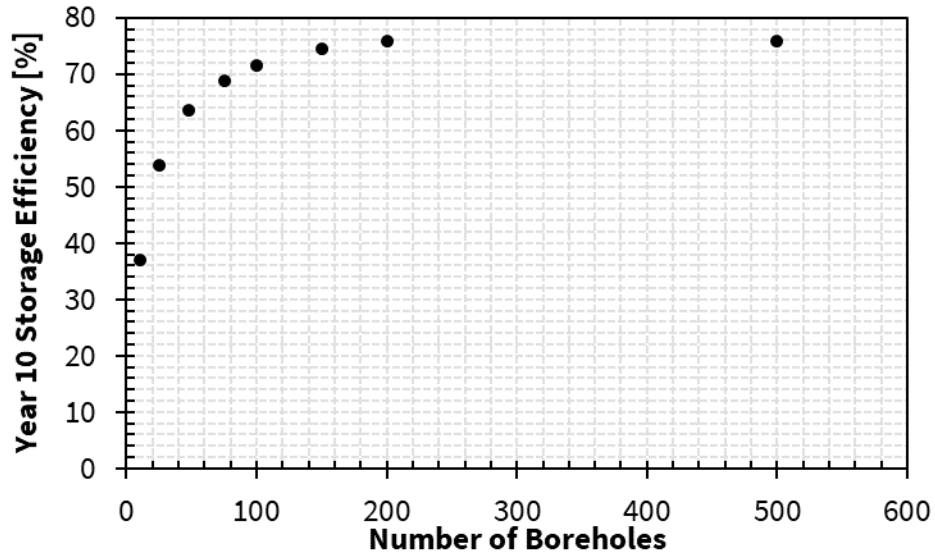
Figure C.35: Periodic steady state BTES thermal storage efficiency with respect to number of boreholes. BTES thermal storage efficiency is defined as the ratio of the total energy extracted during discharging timestep to the total energy injected during charging timestep for a simulation charging and discharging cycle. Number of boreholes and volume are the variable parameters. Spacing and depth are held constant. The inlet temperature setpoint of BTES charging is 95°C and BTES discharging is 20°C. Soil 3.
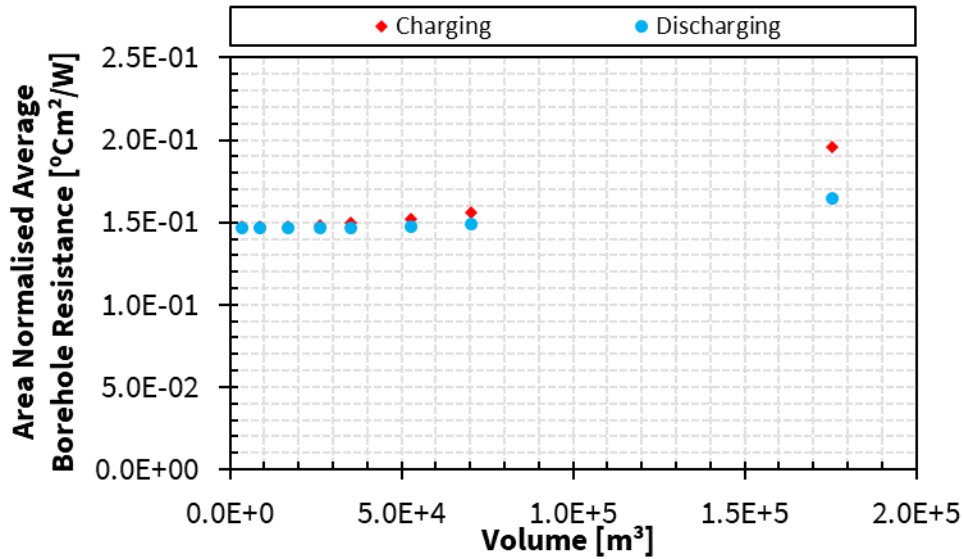
Figure C.36: Borehole heat exchanger thermal resistance of periodic steady state BTES operation normalized against total borehole area with respect to storage volume. Number of boreholes and volume are the variable parameters. Spacing and depth are held constant. Soil 3.
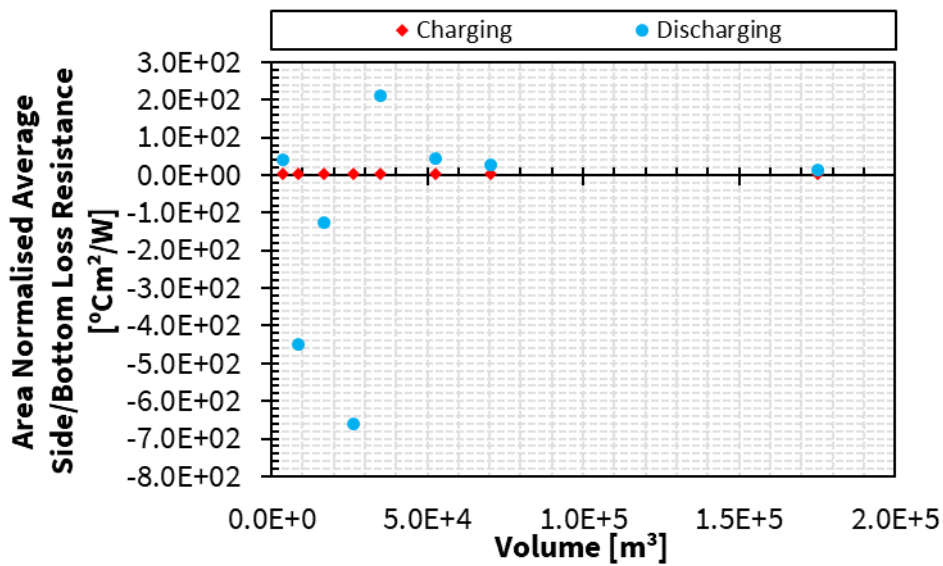
Figure C.37: Sides and bottom loss resistance of periodic steady state BTES operation normalized against storage volume side and bottom area with respect to storage volume. The negative and large magnitude discharging resistances are a result of the change in heat transfer direction that occurs for periodic steady state side/bottom loss heat transfer rate. Number of boreholes and volume are the variable parameters. Spacing and depth are held constant. Soil 3.
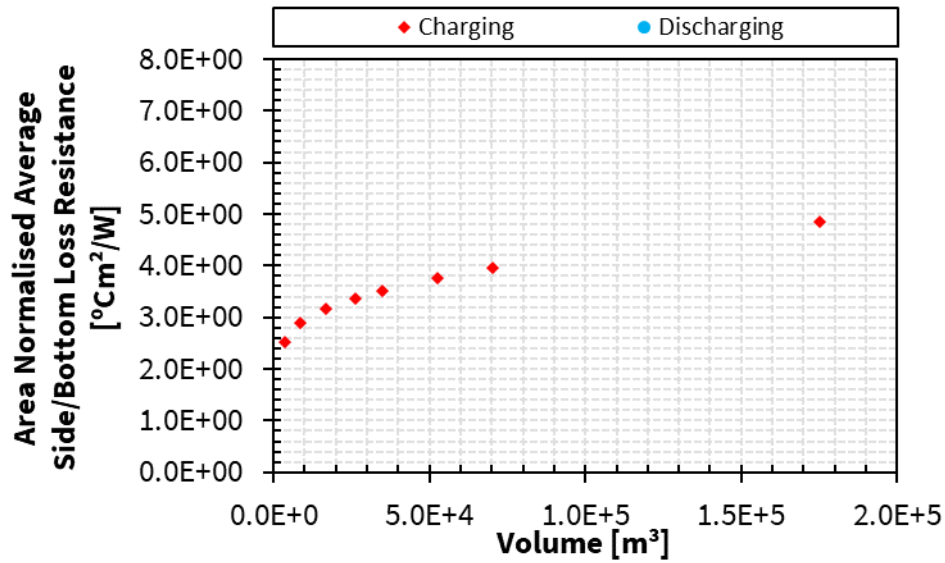
Figure C.38: Sides and bottom loss resistance of periodic steady state BTES operation normalized against storage volume side and bottom area with respect to storage volume. The figure's y-axis is reduced to omit negative and large magnitude discharging resistance outliers and better display charging resistance values. Number of boreholes and volume are the variable parameters. Spacing and depth are held constant. Soil 3.
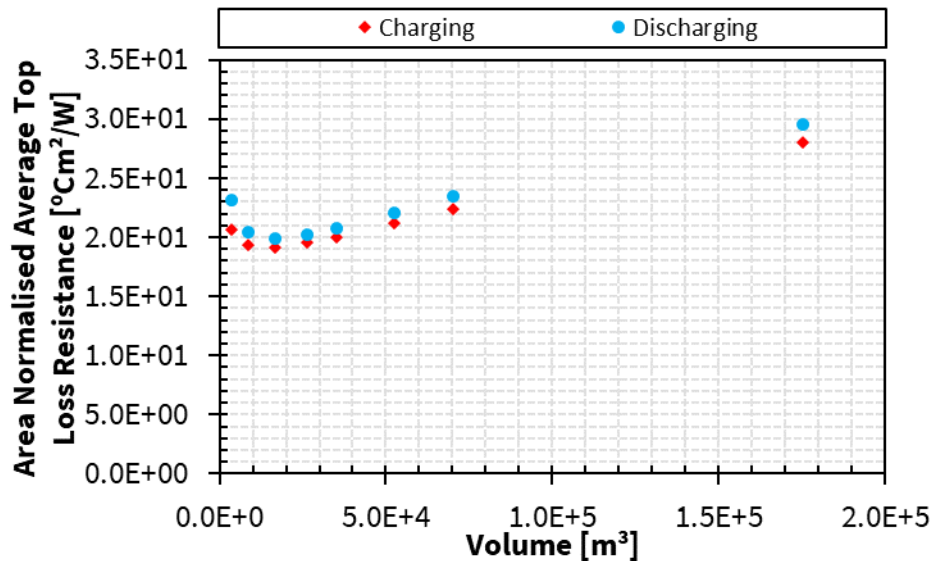
Figure C.39: Top loss resistance of periodic steady state BTES operation normalized against storage volume top area with respect to storage volume. Number of boreholes and volume are the variable parameters. Spacing and depth are held constant. Soil 3.
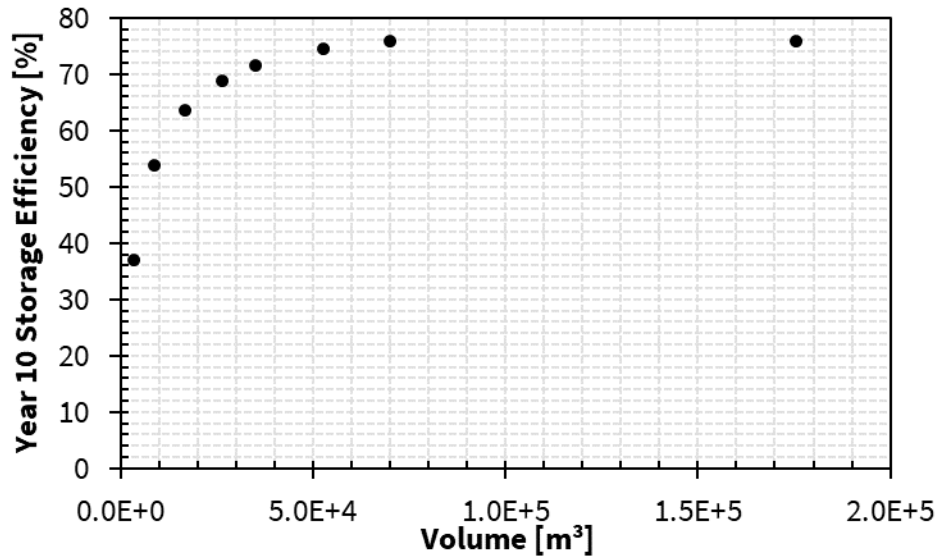
Figure C.40: Periodic steady state BTES thermal storage efficiency with respect to storage volume. BTES thermal storage efficiency is defined as the ratio of the total energy extracted during discharging timestep to the total energy injected during charging timestep for a simulation charging and discharging cycle. Number of boreholes and volume are the variable parameters. Spacing and depth are held constant. The inlet temperature setpoint of BTES charging is 95°C and BTES discharging is 20°C. Soil 3.

H [m]	V [m³]	s [m]	#BH	A_{TBA} [m²]	$A_{SV\_s,b}$ [m²]	A_{SV_t} [m²]	R_{hx} (charge) [°Cm²/W]	R_{hx} (discharge) [°Cm²/W]	$R_{loss\_s,b}$ (charge) [°Cm²/W]	$R_{loss\_s,b}$ (discharge) [°Cm²/W]	R_{loss_t} (charge) [°Cm²/W]	R_{loss_t} (discharge) [°Cm²/W]	Efficiency [%]
5	1870	3	48	113	717	374	1.47E-01	1.47E-01	2.13E+00	5.75E+00	1.55E+01	1.46E+01	25.9
10	3741	3	48	226	1060	374	1.47E-01	1.47E-01	2.36E+00	7.59E+00	1.64E+01	1.56E+01	39.8
25	9352	3	48	565	2088	374	1.47E-01	1.46E-01	2.82E+00	3.24E+01	1.80E+01	1.80E+01	56.5
45	16833	3	48	1018	3459	374	1.48E-01	1.46E-01	3.16E+00	-1.25E+02	1.92E+01	1.99E+01	63.6
75	28055	3	48	1696	5516	374	1.48E-01	1.46E-01	3.45E+00	-6.30E+01	2.06E+01	2.19E+01	67.0
100	37407	3	48	2262	7230	374	1.50E-01	1.47E-01	3.62E+00	-1.04E+02	2.16E+01	2.34E+01	67.8
150	56110	3	48	3393	10658	374	1.53E-01	1.46E-01	3.87E+00	1.92E+02	2.38E+01	2.60E+01	67.7
250	93517	3	48	5655	17514	374	1.64E-01	1.45E-01	4.26E+00	2.83E+01	2.78E+01	3.06E+01	65.1
300	112221	3	48	6786	20943	374	1.71E-01	1.41E-01	4.40E+00	2.19E+01	2.98E+01	3.25E+01	63.5

Table C.5: Design parameters, heat transfer areas, periodic steady state thermal resistances, and periodic steady state storage efficiencies for the soil 3 parameter sweep with variable parameters: depth and volume and constant parameters: spacing and number of boreholes. The periodic steady state thermal resistances of charging and discharging and the periodic steady state storage efficiency are presented in Figure C.41 to Figure C.50 with respect to the variable parameters.
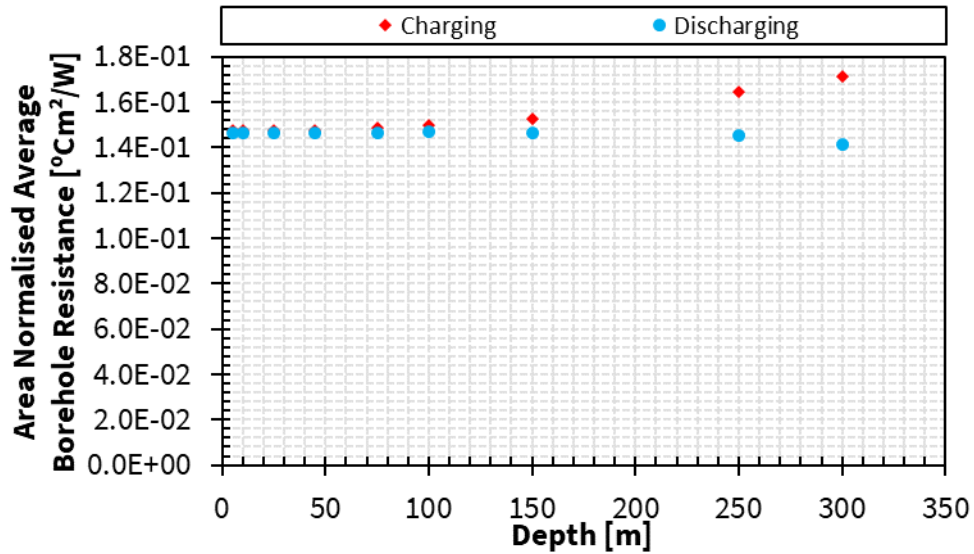
Figure C.41: Borehole heat exchanger thermal resistance of periodic steady state BTES operation normalized against total borehole area with respect to depth. Depth and volume are the variable parameters. Spacing and number of boreholes are held constant. Soil 3.
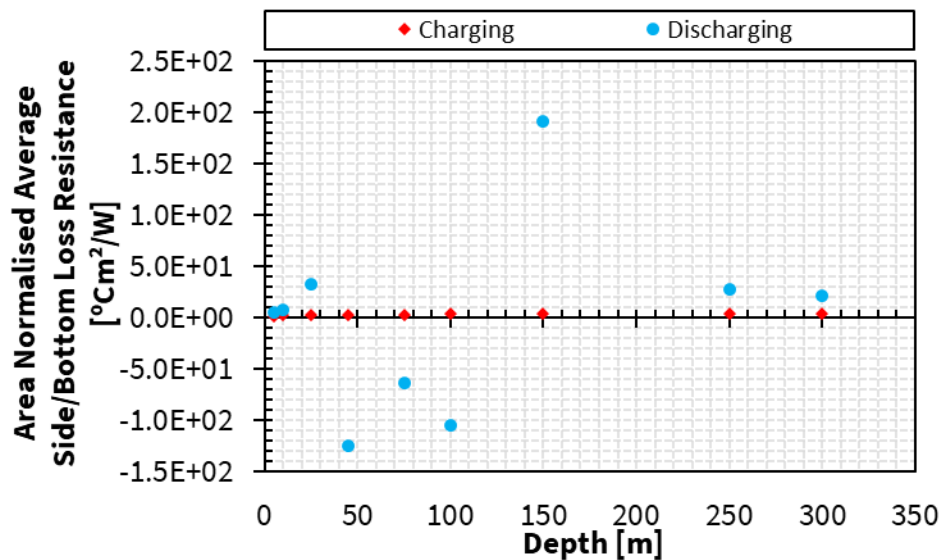
Figure C.42: Sides and bottom loss resistance of periodic steady state BTES operation normalized against storage volume side and bottom area with respect to depth. The negative and larger magnitudes of discharging resistances are a result of the change in heat transfer direction that occurs for periodic steady state side/bottom loss heat transfer rate. Depth and volume are the variable parameters. Spacing and number of boreholes are held constant. Soil 3.
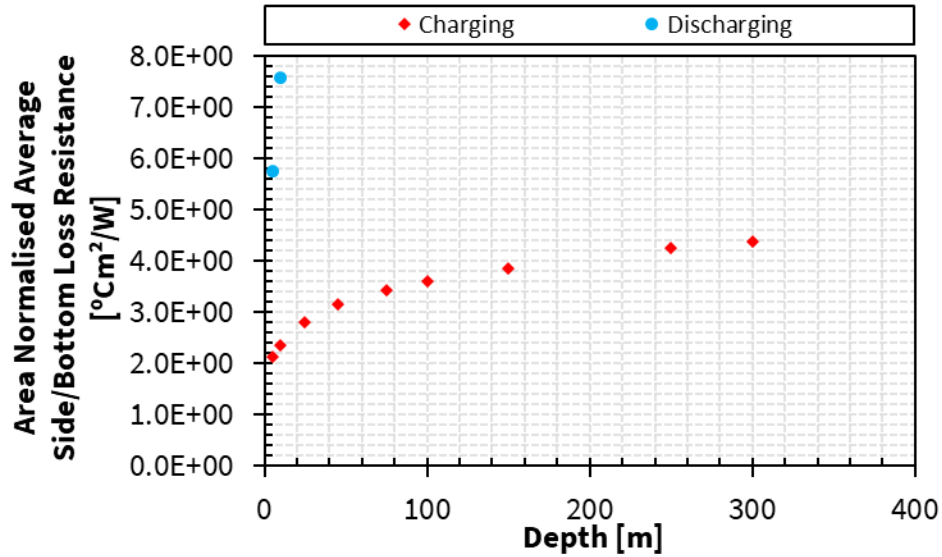
Figure C.43: Sides and bottom loss resistance of periodic steady state BTES operation normalized against storage volume side and bottom area with respect to depth. The figure's y-axis is reduced to omit negative and most large discharging resistances and better display charging resistance values. Depth and volume are the variable parameters. Spacing and number of boreholes are held constant. Soil 3.
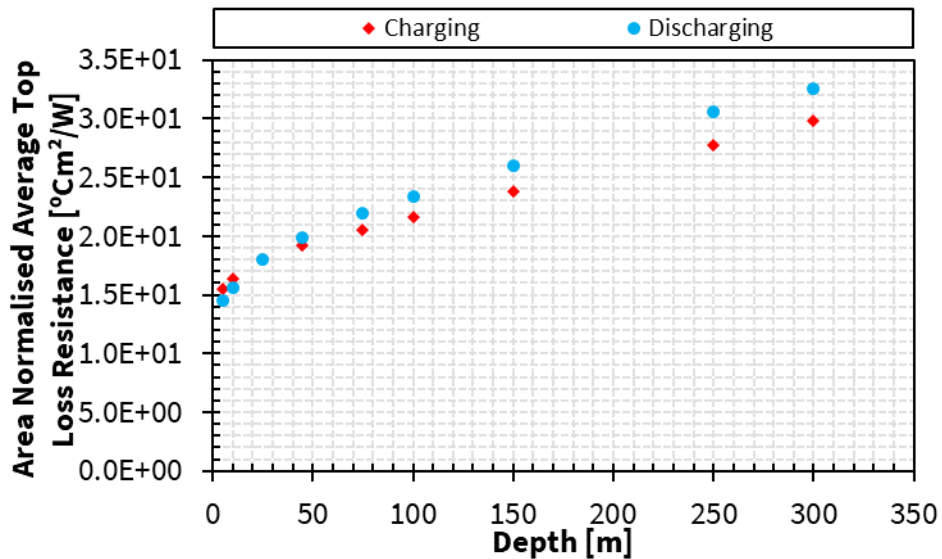
Figure C.44: Top loss resistance of periodic steady state BTES operation normalized against storage volume top area with respect to depth. Depth and volume are the variable parameters. Spacing and number of boreholes are held constant. Soil 3.
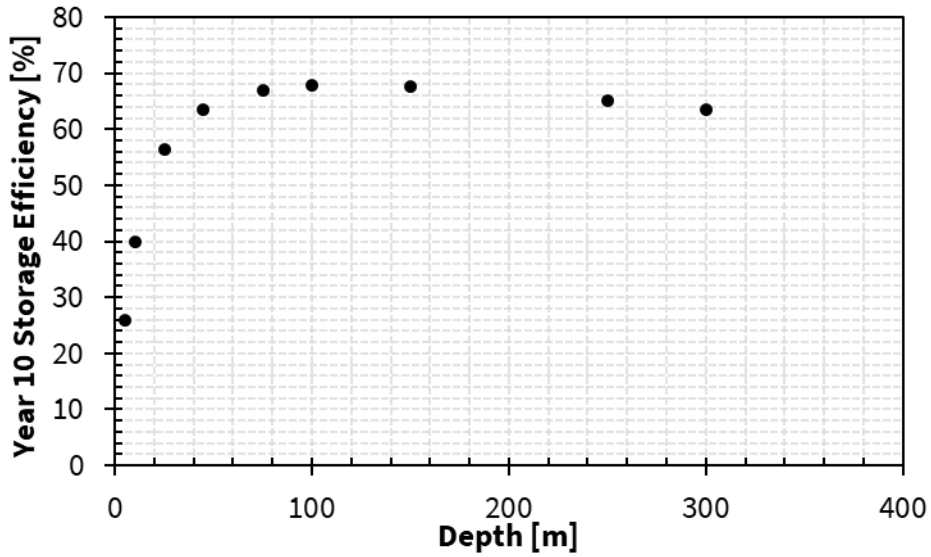
Figure C.45: Periodic steady state BTES thermal storage efficiency with respect to depth. BTES thermal storage efficiency is defined as the ratio of the total energy extracted during discharging timestep to the total energy injected during charging timestep for a simulation charging and discharging cycle. Depth and volume are the variable parameters. Spacing and number of boreholes are held constant. The inlet temperature setpoint of BTES charging is 95°C and BTES discharging is 20°C. Soil 3.
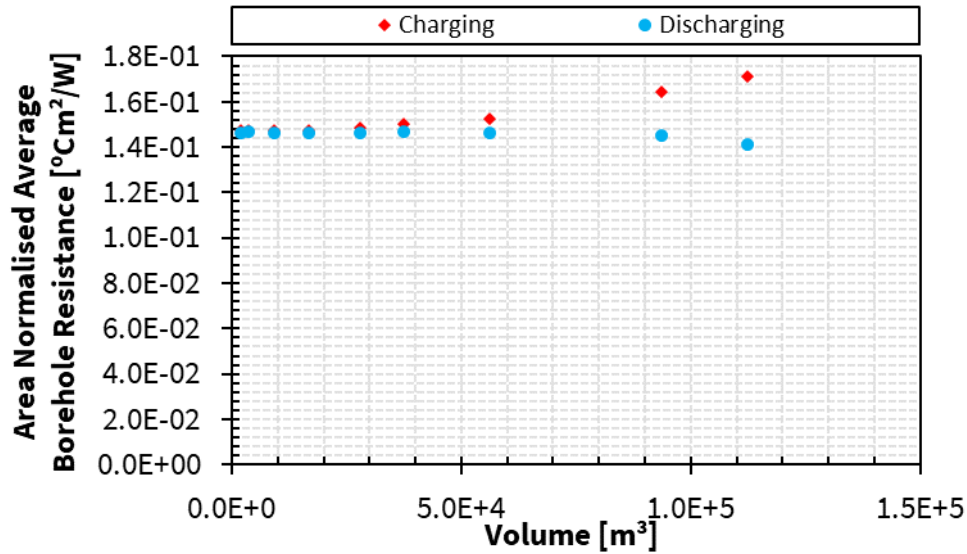
Figure C.46: Borehole heat exchanger thermal resistance of periodic steady state BTES operation normalized against total borehole area with respect to storage volume. Depth and volume are the variable parameters. Spacing and number of boreholes are held constant. Soil 3.

Figure C.47: Sides and bottom loss resistance of periodic steady state BTES operation normalized against storage volume side and bottom area with respect to storage volume. The negative and larger magnitudes of discharging resistances are a result of the change in heat transfer direction that occurs for periodic steady state side/bottom loss heat transfer rate. Depth
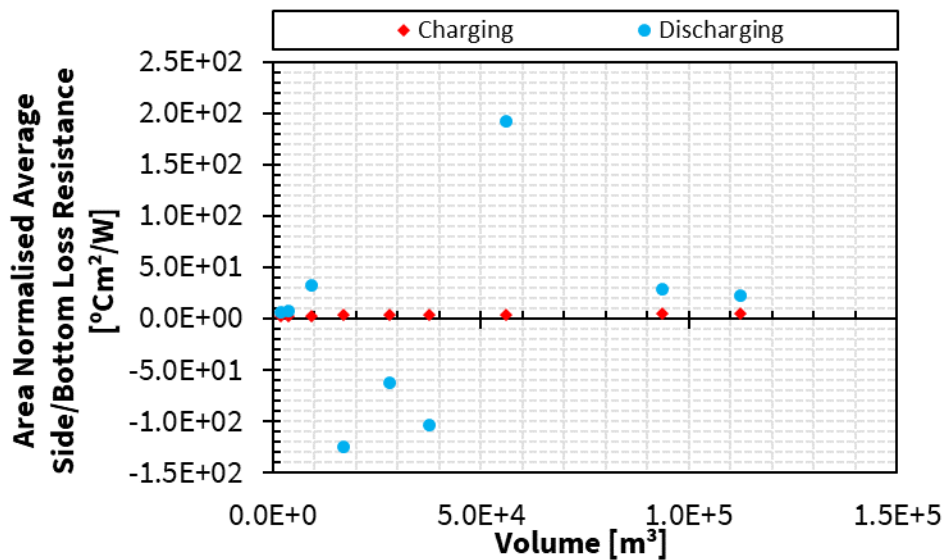
and volume are the variable parameters. Spacing and number of boreholes are held constant. Soil 3.
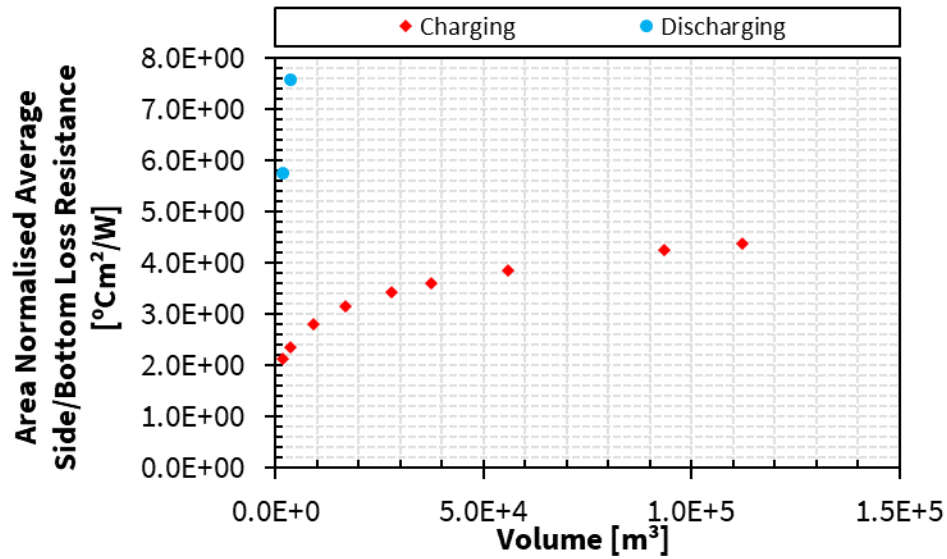
Figure C.48: Sides and bottom loss resistance of periodic steady state BTES operation normalized against storage volume side and bottom area with respect to storage volume. The figure's y-axis is reduced to omit negative and most large discharging resistances and better display charging resistance values. Depth and volume are the variable parameters. Spacing and number of boreholes are held constant. Soil 3.
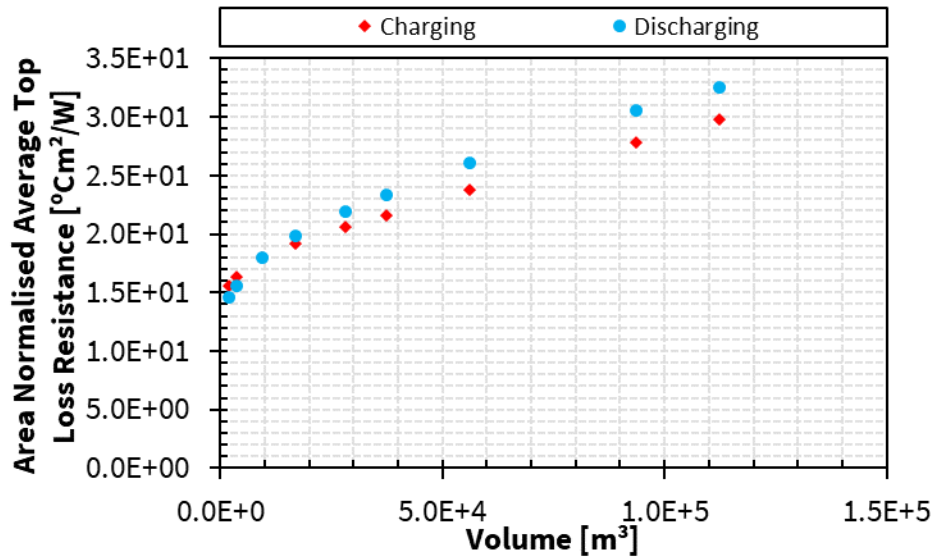
Figure C.49: Top loss resistance of periodic steady state BTES operation normalized against storage volume top area with respect to storage volume. Depth and volume are the variable parameters. Spacing and number of boreholes are held constant. Soil 3.
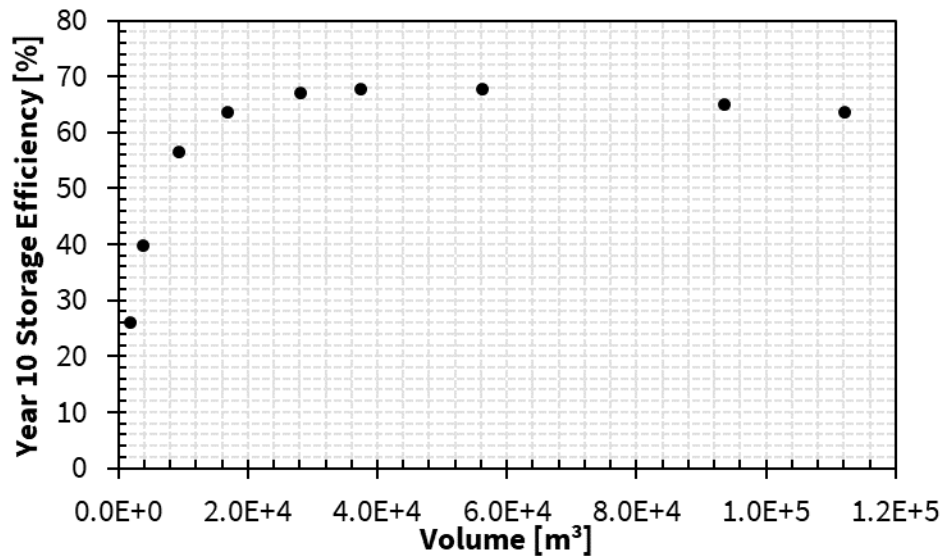
Figure C.50: Periodic steady state BTES thermal storage efficiency with respect to storage volume. BTES thermal storage efficiency is defined as the ratio of the total energy extracted during discharging timestep to the total energy injected during charging timestep for a simulation charging and discharging cycle. Depth and volume are the variable parameters. Spacing and

number of boreholes are held constant. The inlet temperature setpoint of BTES charging is 95°C and BTES discharging is 20°C. Soil 3.